

MULLER, CHANTÉ. Ph.D. *In silico* investigations of the ionotropic cannabinoid receptor TRPV1. (2022)  
Directed by Dr. Patricia H. Reggio. 176 pp.

Whether caused by inflammation or dysfunctional nerves, chronic pain affects nearly 10% of the world's population. Since there are few treatments that are effective while being non-invasive and non-addictive, new targets are being explored. Found in the peripheral nervous system, the transient receptor potential subfamily vanilloid type 1 (TRPV1) ion channel can be activated by a plethora of exogenous and endogenous stimuli including the spicy compound found in chili peppers, capsaicin, as well as temperatures above 43°C and acidic conditions. TRPV1, having the ability to be modulated by cannabinoid ligands, acts as an ionotropic cannabinoid receptor (ICR). Chapter II reviews cannabinoid ligands that can modulate ionotropic cannabinoid receptors, including TRPV1.

The endocannabinoid anandamide has been shown to have a similar binding affinity to TRPV1 as capsaicin and can rapidly desensitize the channel producing an analgesic effect. Models of the open and closed structures of TRPV1 were constructed for use in molecular dynamics simulations. Chapter III details the construction of the models, as well as observed interactions between the endogenous ligand anandamide and TRPV1 in a novel location across 10+  $\mu$ s of simulation time.

TRPV2, a close cousin of TRPV1 and another ICR, was recently resolved with the phytogenic cannabinoid cannabidiol (CBD). From Chapter II, CBD is shown to modulate some, though not all, ICRs. Chapter IV focuses on the cryo-EM structure of TRPV2 resolved with CBD (PDB: 6U88) and analyzes the putative binding site via sequence alignment and structural analyses, comparing these features to the comparable site among the other ICRs, lending credence to this novel CBD binding site in other ICRs.

Chapter V focuses on the results of additional long timescale MD simulations of TRPV1 in the presence of anandamide. In two independent runs, anandamide was observed to activate TRPV1 in a novel location between helices S1-S4.

The colocalization of canonical cannabinoid receptor CB2 and TRPV1 presents an interesting dynamic, especially when considering the crosstalk of the two receptors presumed to exist. CB2 and TRPV1 are implicated various disorders, making them prime targets for the identification and development of dual modulators. Chapter VI describes a virtual screening protocol used to screen ChEMBL indexed CB2 and TRPV1 agonists at the opposing receptor, leading to the identification of moieties that may be relevant in dual modulatory ligands.

*IN SILICO* INVESTIGATIONS OF THE IONOTROPIC CANNABINOID RECEPTOR TRPV1

by

Chanté Muller

A Dissertation

Submitted to

the Faculty of The Graduate School at

The University of North Carolina at Greensboro

in Partial Fulfillment

of the Requirements for the Degree

Doctor of Philosophy

Greensboro

2022

Approved by

---

Dr. Mitchell P. Croatt  
Committee Chair

## DEDICATION

*To Dad. I still can't hold a flashlight, but I can earn a PhD.*



## APPROVAL PAGE

This dissertation written by Chanté Muller has been approved by the following committee of the Faculty of The Graduate School at The University of North Carolina at Greensboro.

Committee Chair

---

Dr. Mitchell P. Croatt

Committee Members

---

Dr. Nicholas Oberlies

---

Dr. Jason Reddick

---

Dr. E. Will Taylor

June 9, 2022

Date of Acceptance by Committee

June 9, 2022

Date of Final Oral Examination

## ACKNOWLEDGMENTS

I would first like to acknowledge my advisor, Dr. Patricia H. Reggio, for the opportunity to work in her lab which has afforded me so much knowledge and so many opportunities.

For Dow Hurst and Dr. Diane Lynch, who have guided me with care to find resolutions to problems I have come across and pushed me to expand out of my research comfort zone.

For Dr. Paula Morales, who has taught me how to think differently, how to approach problems in a way I hadn't before, how to brainstorm more efficiently and effectively, who has always been there to mentor me, who has always been willing to be a sounding board for my ideas, and who is such a joy to work with. I am lucky to call her a colleague and friend.

For Dr. Nicholas Oberlies, a man that I consider a mentor, who has always made time to help me through any hurdles I came across and encouraged me when I needed it and who has helped me through some of the most difficult moments of my doctoral studies.

For my committee members, Dr. Mitchell Croatt, Jason Reddick, and Will Taylor who have shown me nothing but support throughout my PhD. It has been both an honor and a pleasure to have you all on my committee.

For Drs. Oberlies and Croatt... thank you.

For Dr. Vincenzo Di Marzo, who allowed me to intern in his lab at Université Laval in Quebec City for four months. The relationships I built there and the science I learned is truly a highlight of my PhD, and I am grateful to have had the opportunity. Special thanks to Enzo and all of his TRPV1 work that beautifully set up the project which my dissertation is based upon.

For Drs. Nicolas Flamand and Cristoforo Silvestri – You're both OK, but I love you guys, I guess.

To all of the instructors I had the privilege of TA-ing for and all of the students I have had the honor of guiding and teaching, thank you for challenging me to think and teach differently.

For the NIH and NIDA who awarded me with the NRSA F31 predoctoral fellowship award which allowed me to pursue my research.

For my mom, brother, and cousin who have offered their love and support, regardless of distance.

And finally, to my own little family: Brian, Moose, and Maisie – you have kept me sane on a daily basis and I love you endlessly.

## TABLE OF CONTENTS

LIST OF TABLES.....	vi
LIST OF FIGURES .....	xi
CHAPTER I. INTRODUCTION.....	1
CHAPTER II. CANNABINOID LIGANDS TARGETING TRP CHANNELS .....	3
Abstract .....	3
Introduction .....	4
TRPV1.....	14
TRPV2.....	20
TRPV3.....	24
TRPV4.....	27
TRPA1.....	31
TRPM8.....	36
Final Remarks .....	40
CHAPTER III. A CLOSER LOOK AT ANANDAMIDE INTERACTION AT TRPV1.....	44
Abstract .....	44
Introduction .....	45
Methods and Materials .....	47
Model of inactive TRPV1 .....	47
Unbiased molecular dynamics simulations.....	48
Predocked anandamide in TRPV1 .....	50
Production simulations on Anton2.....	50
Results .....	51
Unbiased anandamide entry into TRPV1 .....	51
Increased gate flexibility with predocked anandamide .....	51
ANTON2 simulations show more spontaneous binding.....	51
Discussion .....	55
Supplementary Material .....	58

CHAPTER IV. AN ANALYSIS OF THE PUTATIVE CBD BINDING SITE IN THE  
IONOTROPIC CANNABINOID RECEPTORS .....62

Abstract .....	62
Introduction .....	62
Cannabinoids and the modulation of pain .....	64
Location, location, location .....	65
Differences in the putative CBD binding site of the ionotropic cannabinoid receptors.....	65
TRPV1 .....	69
TRPV2 .....	69
TRPV3 .....	71
TRPV4 .....	71
TRPA1 .....	72
TRPM8 .....	73
Concluding remarks and future directions .....	74
Supplementary Material .....	76

CHAPTER V. TRPV1 ACTIVATION BY ANANDAMIDE VIA A UNIQUE LIPID  
PATHWAY

Abstract .....	77
Introduction .....	77
Results and Discussion .....	80
Conclusions .....	86
Supporting Information .....	87
Methods .....	87
Previous Work .....	89

CHAPTER VI. TARGETING CB2 AND TRPV1: COMPUTATIONAL APPROACHES  
FOR THE IDENTIFICATION OF DUAL MODULATORS .....108

Abstract .....	108
Introduction .....	108
Methods and Materials .....	111
Receptor structures .....	111
Grid generation.....	111

Curation of chemical libraries .....	112
CB2.....	112
TRPV1 .....	112
Internal standard ligands .....	112
JWH133.....	113
High-throughput virtual screening workflow .....	113
Ligand preparation .....	113
HTVS.....	113
XP screening.....	114
Additional criteria.....	114
Manual docking identification of potential PAINS off-targets evaluation .....	114
<i>In silico</i> calculation of ADME properties .....	115
Identification of potential PAINS .....	115
Off-targets evaluation .....	115
Results and Discussion .....	115
Structural understanding of compounds with reported activity at both targets.....	116
Towards the identification of potential dual ligands .....	119
Virtual Screening of JWH133 structurally related chemical databases .....	119
Cross-agonist virtual screening .....	126
Off-target evaluation .....	132
Conclusion.....	133
Supplementary Material .....	135
REFERENCES .....	166

## LIST OF TABLES

Table 1. Functionality of phytogenic, endogenous, and synthetic cannabinoid ligands at TRPV1. ....	18
Table 2. Functionality of phytogenic, endogenous, and synthetic cannabinoid ligands at TRPV2. ....	22
Table 3. Functionality of phytogenic, endogenous, and synthetic cannabinoid ligands at TRPV3. ....	26
Table 4. Functionality of phytogenic, endogenous, and synthetic cannabinoid ligands at TRPV4. ....	29
Table 5. Functionality of phytogenic, endogenous, and synthetic cannabinoid ligands at TRPA1. ....	34
Table 6. Functionality of phytogenic, endogenous, and synthetic cannabinoid ligands at TRPM8. ....	38
Table 7. The names of each MD system, ligands present, starting conformation, and length of time. ....	61
Table 8. I680 C $\alpha$ distances between bonds A-B, B-C, C-D, and D-A as shown in Figures S1 and S2. The distances of 5IRZ and 5IRX are used to gauge the level of openness of the lower gate. Since these values come from cryo-EM structures and are static, we use them as reference points rather than strict definitions of “closed” and “open”. The “MD start” values are listed as the closed structure from which runs 2a and 2b were started. These values are used as the dynamic reference of the closed state. ....	93
Table 9. I680 C $\alpha$ distances between bonds A-B, B-C, C-D, and D-A as shown in Figures S1, and represented in S15 and S16. The distances of 5IRZ and 5IRX are used to gauge the level of openness of the lower gate. Since these values come from cryo-EM structures and are static, we use them as reference points rather than strict definitions of “closed” and “open”. The “MD start” values are listed as the closed structure from which runs 2a and 2b were started. These values are used as the dynamic reference of the closed state. ....	106
Table 10. Potential dual CB2/TRPV1 candidates obtained upon screening of a JWH133 structurally related chemical database. Selected hits have been classified according to common structural moieties. ....	122

Table 11. Potential dual CB2/TRPV1 candidates obtained through the crossed-agonist strategy.....	128
Table 12. Functionality of reported cannabinoid ligands at TRPV1 and CB2. ....	136
Table 13. Physicochemical descriptors for potential CB2/TRPV1 modulators identified upon screening of a JWH133-related chemical library.....	141
Table 14. Physicochemical descriptors for potential CB2/TRPV1 modulators identified using the crossed-agonist strategy. ....	142
Table 15. Off-target evaluation at cannabinoid-related TRPs of selected dual hits 59824268, 1288208, 1288239, 1508577 and 1508215.....	144
Table 16. Off-target evaluation at cannabinoid-related GPCRs of selected dual hits 59824268, 1288208, 1288239, 1508577 and 1508215.....	146



## LIST OF FIGURES

Figure 1. General topology of the transient receptor potential (TRP) channels discussed in this review: TRPV1–4, TRPA1 and TRPM8.....	8
Figure 2. The lipid view of TRPV1 adapted from PDB: 3J5P. Ankyrin repeat domain (ARD) shown in red, transmembrane helices shown in yellow, TRP domain shown in purple, and intracellular regions (ICRs) and extracellular regions (ECRs) shown in green. Sections have been omitted for clarity. ....	9
Figure 3. (A) The lipid view of TRPA1 adapted from PDB: 3J9P. ARD shown in red, transmembrane region (TMR) shown in yellow, TRP-like domain shown in purple, ICRs- and ECRs shown in green and coiled-coil shown in pink. Sections have been omitted for clarity. (B) The intracellular view of TRPA1 adapted from PDB: 3J9P. Coiled-coil shown in pink. Sections have been omitted for clarity.....	10
Figure 4. Structure of selected endocannabinoids that target TRP channels. ....	11
Figure 5. Structure of selected plant cannabinoid ligands that target TRP channels. ....	12
Figure 6. Structure of selected synthetic cannabinoid ligands that target TRP channels: (A) aminoalkylindole derivatives; (B) arylpyrazole derivatives; (C) synthetic phytocannabinoids analogues. 13	
Figure 7. The equilibrated structure of TRPV1 in a POPC lipid bilayer. ....	49
Figure 8. (A) Spontaneous entry of two AEA ligands (gray licorice) into one tunnel of TRPV1 at 246 ns. One AEA interacts with both Y554 and Y555 (pink licorice) while the second interacts with Y487 (pink licorice) near the entrance of the tunnel. (B) Another instance of spontaneous entry where AEA (yellow licorice) enters the tunnel and interacts with S512 (pink), near the VBP at 315 ns. (C) The pore between the upper (G644, green VDW) and lower (I680, yellow VDW) gates with sodium atoms (gray VDW) and water molecules present. ....	52
Figure 9. (A) The starting point of Build 2 with AEA (yellow) docked in each tunnel with the headgroup interacting with Y554 (pink). (B) An intracellular view of partial opening of the lower gate (I680 in yellow surface) with water molecules passing through. ....	52
Figure 10. (A) AEA (yellow) backing into the VBP while interacting with Y511 and I573. (B) The upper gate (G644 in green) of TRPV1 significantly opened. Sodium ions (gray) and water molecules have entered the pore region between G644 and I680 (yellow). (C) A second AEA ligand (orange) in the VBP, pushing the first (yellow) back farther into the lipophilic region of the VBP and interacting with Y511. ....	54
Figure 11. The RMSD of apo-TRPV1 structure over the course of 500ns to show the stability of the model. The top panel shows the RMSD the transmembrane (TM) region (residues 430 to 455, 474 to 497, 510 to 532, 536 to 551, 576 to 597, and 656 to 687), the pore helix (residues 633 to 643), and the TRP box (residues 892 to 711). The middle panels shows the RMSD of the TM helices and pore helix. The last panel shows the RMSD of the TM helices only.....	59

Figure 12. A top-down view of TRPV1.....	60
Figure 13. The RMSD of the upper gate, G644, of the control shown in black with the average shown in yellow against the RMSD of the upper gate, G644, of Build 1 shown in magenta with the average shown in blue. ....	61
Figure 14. Upper panel shows the RMSD of the upper gate, G644, in the control run (G644-apo) with the average RMSD shown in yellow. The RMSD of the upper gate from Build 2 is shown in magenta with the average RMSD shown in blue. Lower panel shows the RMSD of the lower gate, I680, in the control run (I680-apo) with the average RMSD shown in yellow. The RMSD of the lower gate from Build 2 is shown in magenta with the average RMSD shown in blue.....	62
Figure 15. A truncated version of the human sequence alignment of six ionotropic cannabinoid receptors and rTRPV2. CBD has been resolved in rTRPV2 in two separate states and residues within 10 Å of the putative binding site of CBD have been highlighted and are shown here as a reference (yellow row). Comparable regions within the human ionotropic cannabinoid receptors have been aligned. Residues within hTRPV1 (red row), hTRPV2 (orange row), hTRPV3 (green row), hTRPV4 (blue row), hTRPA1 (purple row), and hTRPM8 (pink row) that are the same as the reference (rTRPV2) are shown in pale green. Residues that are of a similar type to the reference are shown in orange, and divergent residues are shown in red. The double starred residues, L537 and Y634, indicate the two residues that were noted to have rotameric changes from the apo to the CBD-bound structure of rTRPV2 and are visualized in Figure 2. Single starred residues are within 5 Å of bound CBD and are marked for easy vertical comparison across the ionotropic cannabinoid receptors. ....	68
Figure 16. (A) A close up of CBD (pink) bound in rTRPV2 (adapted from PDB: 6U88) with Y634 and L537 in cyan. Helices S1–S4 and S6 are shown as cartoon tubes with S5, the pore helix, and the TRP domain shown as cartoon ribbons. (B) A close up of hTRPV3 (adapted from PDB: 6MHO) with comparable residues F666 and V587 shown in cyan. Helices S1–S4 are shown as cartoon tubes and S5-TRP domain are shown as cartoon ribbons. (C) A close up of <i>Xenopus tropicalis</i> TRPV4 (adapted from PDB: 6BBJ) which shares 78% sequence homology with human TRPV4. F703 and L610 are shown in cyan. Helices S1–S4 are shown as cartoon tubes, and S5-TRP domain are shown as cartoon ribbons. ....	69
Figure 17. Panel A) A cartoon image of one monomer of a TRP channel. S1 is shown in red, S2 in orange, S3 in yellow, S4 in light green, the S4-5 linker in dark green, S5 in light blue, S6 in dark blue, and the TRP domain (present in TRPV1-4 and TRPM8, comparable to TRP-like domain present in TRPA1). Panel B displays the same monomer with CBD, shown as a pink oval, in one-half of the putative binding site. Panel C displays a second monomer, with the same color-coding as panels A and B, pivoted at a 90°-degree angle to complete the putative binding site of CBD with S6 of the first monomer (Panel B) shown “behind” the CBD molecule and S5 of the second monomer (Panel C) shown “in front” of the CBD molecule, forming the putative binding site.....	77
Figure 18. A graphical scheme of one monomer of TRPV1 with reported and putative locations of channel stimuli indicated as shown. V indicates voltage – activates via S1-S4 helices, DkTx shown for only one half of the bidentate structure and H <sup>+</sup> indicating protons – activate via extracellular region, °C indicating heat – activates via pore domain, caps representing capsaicin – activates via vanilloid binding	

pocket (VBP), while AEA represents the possible location of TRPV1 binding. Helices S5\* and S6\* refer to the S5 and S6 helices of the adjacent monomer, included to complete the VBP. .... 80

Figure 19. The S4-S5 linker, S5, and S6 (combined) RMSD from 8.00-12.00 microseconds. Peak 1 represents the region where the increased RMSD of the central helical structures begins to maintain its movements, peak 2 indicates the first location of partial opening, peak 3 indicates where the split opening occurred, and peak 4 indicates an instance where the channel allows a water molecule to pass while in a partially open state. .... 82

Figure 20. An extracellular view of TRPV1 with each monomer in a different color. Helices S1-S4 are shown as cartoon tubes and S4-TRP domain are shown as helical ribbons. The lower gate (I680, orange surface) shows a partial opening with AEA (yellow VDW) occupying one of the four equivalent tunnels and interacting with Y554 (cyan licorice). Figure 3b shows a close-up side view from the lipid bilayer of the AEA (yellow) headgroup interacting with Y554 (cyan). .... 83

Figure 21. An extracellular view of TRPV1 down the central pore. The lower gate (I680, orange) shown to be in a split opening while AEA (yellow) maintains its occupancy in the S1-S4 tunnel and maintaining interaction with Y554 (cyan). .... 85

Figure 22. The I680 C $\alpha$  atom distances of the apo TRPV1 structure (PDB: 5IRZ, A) and with I680 rendered as a surface (orange, B). The open TRPV1 structure (PDB: 5IRX) is shown in panel C with a surface rendering of I680 (orange) in panel D. Each S6 helix is labeled, each monomer is colored separately with the I680 shown in orange with monomer labels (A, B, C, D). .... 91

Figure 23. The I680 C $\alpha$  atom distances of the starting TRPV1 structure (frame 18,822 from run1) for runs 2a and 2b (left), the split structure (center), and the partial open structure where water passage was observed (right). Each S6 helix is labeled, each monomer is colored separately with I680 C $\alpha$  atoms shown in orange with monomer labels (A, B, C, D). .... 92

Figure 24. The measurements of adjacent I680 C $\alpha$  atoms for the trajectory of run 2a. The black line indicates each individual measurement for every 50<sup>th</sup> frame of the trajectory (equivalent to one frame every 12 ns, again, due to large datasets from Anton2). The red line represents the running average. The yellow horizontal line roughly translates to the I680 C $\alpha$  distances found in the static apo/closed (PDB: 5IRZ) state, while the pink horizontal line is the maximum I680 C $\alpha$  atom distance for the closed state from our MD where water or ions cannot pass through. Blue arrows indicate locations where the split opening occurred, around 10.8  $\mu$ s, and the green vertical lines indicate the location where the partial opening described in Figure 6 occurred, around 11.6  $\mu$ s. .... 94

Figure 25. A close-up view of the two residues that are thought to form an ionic lock, R557 and E570 in yellow licorice. Helix S4, the S4-S5 linker, and the TRP domain are shown in pink and labeled. .... 95

Figure 26. A graph of the distances between R557 and E570 for the trajectory of run 2a. The black line indicates each individual measurement for every 50<sup>th</sup> frame (equivalent to one frame every 12 ns) of the trajectory. The red line represents the running average, while the yellow horizontal line is placed at 4 Å, the distance between heteroatoms needed to form an ionic lock. .... 96

Figure 27. The RMSD of the central structures of TRPV1, the S4-S5 linker, S5, and S6. This plot shows the RMSD for every 50<sup>th</sup> frame of the trajectory, equivalent to one frame every 12 ns. The black line is the individual measurement for each frame and the red line is the running average. As shown, the first microsecond or so of this plot shows a noticeable increase in RMSD. This can be attributed to the equilibration of the system when moved from local GPUs to Anton 2. Peak 1 indicates the region where the split opening occurred and peak two indicates the location of the partial split where water was still able to pass through the channel as seen in Figure 34. .... 97

Figure 28. A graph of AEA contacts with Y554 from 8.00 to 12.00  $\mu$ s for each monomer. A value of -1 indicates no AEA/Y554 contact where a value of 1 or 2 indicates how many unique AEA ligands are interacting with Y554. Monomer B shows AEA contact with Y554 for nearly the entirety of the 8.00 to 12.00  $\mu$ s trajectory analyzed here. .... 98

Figure 29. Three sequential frames of lower gate (I680, orange) opening that occurred at 11.00  $\mu$ s in panel A, 11.24  $\mu$ s in panel B, and 11.48  $\mu$ s in panel C. .... 99

Figure 30. A lipid view of the central pore of TRPV1 with upper (G644 orange) and lower (I680 orange) gates present. As a sample representation, five water molecules within the pore (panel A) and are labeled and tracked as they exit the pore region and move to the intracellular side of the cell (panel B). .... 99

Figure 31. The solvent accessible surface area of I680 for the course of trajectory 2a. Because of the large data sets generated by Anton2, every 50<sup>th</sup> frame was used for this plot, equivalent to one frame every 12 ns. The black line shows the measurement of each point while the red line shows the running average. Peak 1 indicates the region where lower gate flexibility was more frequent, Peak 2 indicates the first point of partial opening, Peak 3 is indicative of the split opening, and Peak 4 indicates where the channel activity was starting to lessen, but a water molecule was still able to pass through a partial opening of I680. .... 100

Figure 32. A graph of the number of water molecules located in the region from G644 and I680 for run 2a for the limited segment of the trajectory. Peaks 1 and 2 indicate regions where the lower gate flexibility was observed to increase and the first instance of partial lower gate opening, respectively. Peak 3 indicates where the split channel opening occurred. We hypothesize that the decrease in water molecules is likely due to water being able to exit more quickly to reach a more manageable amount of water. Peak 4 is indicative of the region where the partial opening occurred, but still allowed for water to pass through the lower gate. The cylinder used for quantification (Figure 33A and 33B) extended 2 Å above G644 and 2 Å below I680 in order to accommodate for gate fluctuations. .... 101

Figure 33. A visual representation of the region used to collect the quantification of water molecules within the pore. Panel A shows the top-down view (extra- to intra- cellular view) of the cylinder with G644 and I680 shown in orange (G644 on top, I680 on bottom) with water molecules shown (red spheres). Each monomer is colored separately. Panel B shows a lipid view of the same cylinder (transparent orange) with the upper and lower gates shown as an orange surface. Water molecules are colored as red spheres. .... 102

Figure 34. An extracellular view in panels A and B shows a single water molecule (red) moving through a smaller opening in the lower gate (I680, orange). Panel A shows the water inside the pore and panel B shows the water molecule just as it passes I680 into the intracellular region. .... 102

Figure 35. The RMSD of the S1-S4 tunnel. This plot shows the RMSD for every 50<sup>th</sup> frame of the trajectory, equivalent to one frame every 12 ns. The black line is the individual measurement for each frame and the red line is the running average. As shown, the first microsecond or so of this plot shows a noticeable increase in RMSD. This can be attributed to the equilibration of the system when moved from local GPUs to Anton 2. Peak 1 indicates the region where the split opening occurred and peak two indicates the location of the partial split where water was still able to pass through the channel as seen in Figure 6. The movement of the S1-S4 helices provides information on how AEA interaction within these tunnels may influence their arrangement in TRPV1. .... 103

Figure 36. An instance of lower gate opening (I680, orange) that occurred in Build 1 run 2b at 9.6  $\mu$ s with AEA (yellow VDW) interacting with Y554 (cyan) (panel A). Measurements of the I680 C $\alpha$  atoms can be seen in panel B. The S6 helices are labeled, and each monomer is a different color. I680 is shown in orange. .... 104

Figure 37. An instance of a water molecule (red) passing through the lower gate (I680, orange) in Build 1 run 2b at 10.6  $\mu$ s. AEA (yellow VDW) interacting with Y554 (cyan) (panel A). Measurements of the I680 C $\alpha$  atoms can be seen in panel B. The S6 helices are labeled, and each monomer is a different color. I680 is shown in orange. .... 104

Figure 38. The measurements of adjacent I680 C $\alpha$  atoms for the trajectory of run 2b. The black line indicates each individual measurement for every 50<sup>th</sup> frame of the trajectory (equivalent to one frame every 12 ns, again, due to large datasets from Anton2). The red line represents the running average. The yellow horizontal line roughly translates to the I680 C $\alpha$  distances found in the static apo/closed (PDB: 5IRZ) state, while the pink horizontal line is the maximum I680 C $\alpha$  atom distance for the closed state from our MD where water or ions cannot pass through. Blue arrows indicate locations where the first split opening occurred, around 9.7  $\mu$ s, and the green vertical lines indicates the location where the second split opening occurred, around 10.7  $\mu$ s ..... 105

Figure 39. The solvent accessible surface area of I680 for the course of trajectory 2b. Because of the large data sets generated by Anton2, every 50<sup>th</sup> frame was used for this plot, equivalent to one frame every 12 ns. The black line shows the measurement of each point while the red line shows the running average. Peak 1 indicates the first split opening of I680 ~9.  $\mu$ s and peak 2 indicates the second split opening of I680 where a water molecule was seen passing through the pore ~10.7  $\mu$ s. .... 107

Figure 40. AEA contact with Y554 for run 2b. Because of the large data sets generated by Anton2, every 50<sup>th</sup> frame was used for this plot, equivalent to one frame every 12 ns. The black line shows the measurement of each point while the red line shows the running average. A value of -1 indicates there was no AEA contact with Y554. A value of 1 or 2 indicates that number of AEA ligands interacting with Y554. Similar to run 2a, monomer B has a significant portion of the trajectory occupied by AEA. Monomer C is shown to have a comparable level of AEA occupation with some instances of two AEA ligands working their way into the S1-S4 tunnel. .... 108

Figure 41. Selected compound 59824268 docked in CB2 (A) and TRPV1 (B). EC2: Extracellular loop 2; TMH, transmembrane helix. .... 126

Figure 42. Docks of selected potential dual candidates: TRPV1 in purple cartoon ribbons (Panels A-C) and CB2 in cyan cartoon ribbons (Panels D and E). Molecules are displayed in pink tubes; all interactions are shown via dashed lines and each helix and residue is labeled. Panel A shows 1288208 in the VBP. A portion of S3 is transparent to aid in visibility.; Panel B shows 1288208 in the tunnel. Helix S2 is shown completely transparent to aid in the visibility of the tunnel.; Panel C shows 1288239 in the tunnel with a portion of helix S2 transparent to aid in visibility. Panel D shows a lipid view of the 1508577/CB2 complex; Panel E shows a lipid view of the 1508215/CB2 complex; TMH6 and 7 are displayed with transparency for a clearer view of the binding site. .... 132

Figure 43. TRPV1 sites: A) RTX/TRPV1 complex in the VBP. The vanilloid binding pocket (VBP) is the location in TRPV1 in which capsaicin and resiniferatoxin (RTX) are shown to bind. RTX was used as the internal standard. The vanillyl moiety present in RTX binds deep in the VBP with the hydroxy group interacting with residues S512 and R557. Y511 interacts with one of the ester oxygens, providing stability from a key player in TRPV1 activation in response to vanilloid ligands.; B) AEA/TRPV1 complex in the S1-S4 tunnel. Previous MD results show AEA entering a novel region between the S1-S4 helices, separate from the VBP and where the putative CBD site has been reported in TRPV2.; C) CBD/TRPV1 complex between helices S5 and S6 of one monomer and S6 of another (S6\*). Ligands are shown in green VDW, helices S1-S4 are shown as purple cartoon tubes and labeled, helices S5, S6, S5\* and S6\* are shown as cartoon ribbons and labeled. S5\* and S6\* are helices from the adjacent monomer. A recently published cryo-EM structure shows CBD binding in a location separate from the VBP and the tunnel between helices S5 and S6 (double check) in TRPV2. Though TRPV1 and TRPV2 share some similar features with one another, they also have a fair share of differences as analyzed in Muller 2020. The central resorcinol ring found in CBD shows two pi-stacking interactions in this putative CBD site with Y584 and F639. .... 139

Figure 44. Workflows for the *in silico* identification of dual TRPV1/CB2 ligands. A) Virtual screening of JWH133 structurally related chemical databases; B) Cross-agonist HTVS. .... 140

Figure 45. Docking studies of JWH133 in CB2 and TRPV1. A) CB2/JWH133 complex; B) TRPV1/JWH133 complex. JWH133 is displayed in magenta while reference compounds AM12033 (for CB2) and CBD (for TRPV1) are displayed in green. EC2: Extracellular loop 2; TMH: transmembrane helix. .... 141

Figure 46. The docking output of AEA (pink) in the S1-S4 tunnel region of TRPV1. Headgroup interactions consist of H-bonds with N438, D708, Y487, Y554, and Y555 (all yellow). .... 143

Figure 47. Summary of selected hits. DS: docking scores in Kcal/mol. <sup>1</sup>Hit selected through the JWH133 structurally related chemical databases strategy; <sup>2</sup>Hit selected through the cross-agonist HTVS strategy. \*Low activity; \*\*Moderate activity. .... 148



## CHAPTER I: INTRODUCTION

Whether caused by inflammation or dysfunctional nerves, chronic pain affects nearly 10% of the world's population. Since there are few treatments that are effective while being non-invasive and non-addictive, new targets are being explored. The transient receptor potential ion channel vanilloid type 1 (TRPV1) channel can be found in the peripheral nervous system and can be activated by a plethora of exogenous and endogenous stimuli including the spicy compound found in chili peppers, capsaicin, temperatures above 43°C, acidic conditions, and the endogenous cannabinoid (endocannabinoid, eCB) ligand anandamide (AEA). TRPV1, having this ability to be modulated by cannabinoid ligands, acts as an ionotropic cannabinoid receptor (ICR) compared to metabotropic cannabinoid receptors like the G protein-couple receptors (GPCRs) CB1 and CB2. Several phytogenic, endogenous, and synthetic cannabinoid ligands that can modulate ICRs, which include TRPV1, TRPV2, TRPV3, TRPV4, TRPA1, and TRPM8, and have been reviewed in the following chapter.

One endocannabinoid ligand, anandamide, has been shown to have a similar binding affinity to TRPV1 as capsaicin and can rapidly desensitize the channel producing an analgesic effect. Models of the open (active) and closed (inactive) structures of TRPV1 were constructed from previously published cryo-EM and crystal structures for use in molecular dynamics simulations. Chapter III details the construction of the models, the set-up of the molecular dynamics simulation systems, as well as observed interactions between anandamide and TRPV1 in a novel location across 10+  $\mu$ s of simulation time.

TRPV2, a close cousin of TRPV1 and another ICR, was recently resolved with the phytogenic cannabinoid cannabidiol (CBD) in a novel binding site. From Chapter II, CBD is

shown to modulate some, though not all, ICRs. Chapter IV focuses on the cryo-EM structure of TRPV2 resolved with CBD (PDB: 6U88) and analyzes the novel putative binding site via sequence alignment and structural analyses, comparing these features to the comparable site among the other ICRs, including TRPV1, providing additional structural information to help rationalize this novel site in other ICRs.

Chapter V focuses on the results of additional long timescale MD simulations of TRPV1 in the presence of anandamide. In two independent runs, anandamide was observed to enter the aforementioned novel binding site between helices S1-S4, maintain interactions in that site for several microseconds, and activate TRPV1, allowing the passage of water from the extracellular side to the intracellular side of the simulation system.

TRPV1 and a canonical cannabinoid receptor, CB2, have been implicated in various disease states. The colocalization of the two receptors, in addition to the crosstalk hypothesized to exist between them, make them prime targets for the development of dual modulators. An issue that arises with multi-drug therapies to treat diseases is the increased likelihood of off-target effects, which can lead to more undesirable side effects. If one ligand can be designed or identified that can modulate both target receptors, the likelihood of off-target effects can be decreased thus lowering the likelihood of side effects. Chapter VI describes a virtual screening protocol used to screen ChEMBL indexed CB2 and TRPV1 agonists at the opposing receptor, leading to the identification of moieties that may be relevant in dual modulatory ligands.



## CHAPTER II: CANNABINOID LIGANDS TARGETING TRP CHANNELS

**Chanté Muller, Paula Morales, and Patricia H. Reggio**

Frontiers in Molecular Neuroscience, 2019, 11:487.

Received: 05 October 2018; Accepted: 14 December 2018; Published: 15 January 2019

Department of Chemistry and Biochemistry, University of North Carolina at Greensboro, Greensboro, NC 27412, USA

### **Abstract**

Transient receptor potential (TRP) channels are a group of membrane proteins involved in the transduction of a plethora of chemical and physical stimuli. These channels modulate ion entry, mediating a variety of neural signaling processes implicated in the sensation of temperature, pressure, and pH, as well as smell, taste, vision, and pain perception. Many diseases involve TRP channel dysfunction, including neuropathic pain, inflammation, and respiratory disorders. In the pursuit of new treatments for these disorders, it was discovered that cannabinoids can modulate a certain subset of TRP channels. The TRP vanilloid (TRPV), TRP ankyrin (TRPA), and TRP melastatin (TRPM) subfamilies were all found to contain channels that can be modulated by several endogenous, phytogenic, and synthetic cannabinoids. To date, six TRP channels from the three subfamilies mentioned above have been reported to mediate cannabinoid activity: TRPV1, TRPV2, TRPV3, TRPV4, TRPA1, and TRPM8. The increasing data regarding cannabinoid interactions with these receptors has prompted some researchers to consider these TRP channels to be “ionotropic cannabinoid receptors.” Although CB1 and CB2 are considered to be the canonical cannabinoid receptors, there is significant overlap between cannabinoids and ligands of TRP receptors. The first endogenous agonist of TRPV1 to be discovered was the endocannabinoid, anandamide (AEA). Similarly, *N*-arachidonyl

dopamine (NADA) and AEA were the first endogenous TRPM8 antagonists discovered. Additionally,  $\Delta^9$ -tetrahydrocannabinol ( $\Delta^9$ -THC), the most abundant psychotropic compound in cannabis, acts most potently at TRPV2, moderately modulates TRPV3, TRPV4, TRPA1, and TRPM8, though  $\Delta^9$ -THC is not reported to modulate TRPV1. Moreover, TRP receptors may modulate effects of synthetic cannabinoids used in research. One common research tool is WIN55,212-2, a CB1 agonist that also exerts analgesic effects by desensitizing TRPA1 and TRPV1. In this review article, we aim to provide an overview and classification of the cannabinoid ligands that have been reported to modulate TRP channels and their therapeutic potential.

**Keywords:** cannabinoids, TRP channels, cannabidiol, TRPV1, TRPA1, TRPM8

## Introduction

Transient receptor potential (TRP) channels are a superfamily of trans-membrane ion channels involved in transduction in response to a plethora of chemical and physical stimuli. Comprised of four subunits with 6 trans-membrane helices (S1–S6) each, TRP channels can homo- or heterotetramerize to create a pore for cation permeation that is located between helices 5 and 6<sup>1</sup>. These channels are found in the plasma membrane and can gate several types of mono- and divalent cations, in single-file fashion, through the pore following exposure to a stimulus. TRP channels have also been implicated as sensors of many physiological and pathological processes including itch, temperature sensation, cancers, genetic disorders, and pain<sup>1–3</sup>.

*Cannabis Sativa* has been used for centuries to treat ailments including chronic pain, and extensive literature precedent supports the role of phytogenic and endogenous cannabinoids as pain modulators<sup>1</sup>. Chronic pain is a significant and complex problem that encompasses many

different conditions, symptoms, and pathways. Once nociceptors are stimulated, action potentials are generated and then propagated to the brain, resulting in a sensation of pain<sup>4</sup>. Currently, the most efficient way to treat chronic pain is with opioids, however the opioid system also influences the reward center and long-term opioid usage can lead to addictive behavior<sup>5</sup>. Since the etiologies related to pain and the mechanisms of action underlying hypersensitivity are diverse, targeting the ion channels that contribute to the detection of stimuli may be an effective approach in treating pain syndromes<sup>6</sup>. Since the cloning of TRPV1, at least five other TRP channels have been discovered in the dorsal root ganglia (DRG), that can also be found in primary somatosensory neurons. These channels have been identified as sensory transducers that may participate in the generation of painful sensations evoked by thermal, mechanical, or chemical stimuli making them a desirable target in the development of treatments for chronic pain syndromes<sup>6</sup>. One feature sought for exploitation from these TRP channels, especially TRPV1, is desensitization. TRPV1 becomes rapidly desensitized upon activation, rendering the channel refractory to further stimulation. This mechanism is thought to underlie the paradoxical analgesic effect of TRPV1 and may explain the reduced neuronal activity upon activation of other TRP channels<sup>7</sup>. This paradoxical analgesic effect is the basis of capsaicin-based creams for chronic pain<sup>8</sup>. However, the pungency of compounds like capsaicin can cause vascular and respiratory side effects when administered systemically<sup>9</sup>. For this reason, the use of non-pungent compounds to activate and therefore desensitize TRP channels is desired.

Targeting the endocannabinoid system has been shown to be a promising strategy for the modulation of pain<sup>10</sup>. In fact, activation of the cannabinoid receptors CB1 and CB2, as well as inhibition of endocannabinoid deactivation (blockade of endocannabinoid uptake or degradation) has shown antinociceptive responses<sup>11</sup>. Pharmacological evidence suggests that cannabinoids and

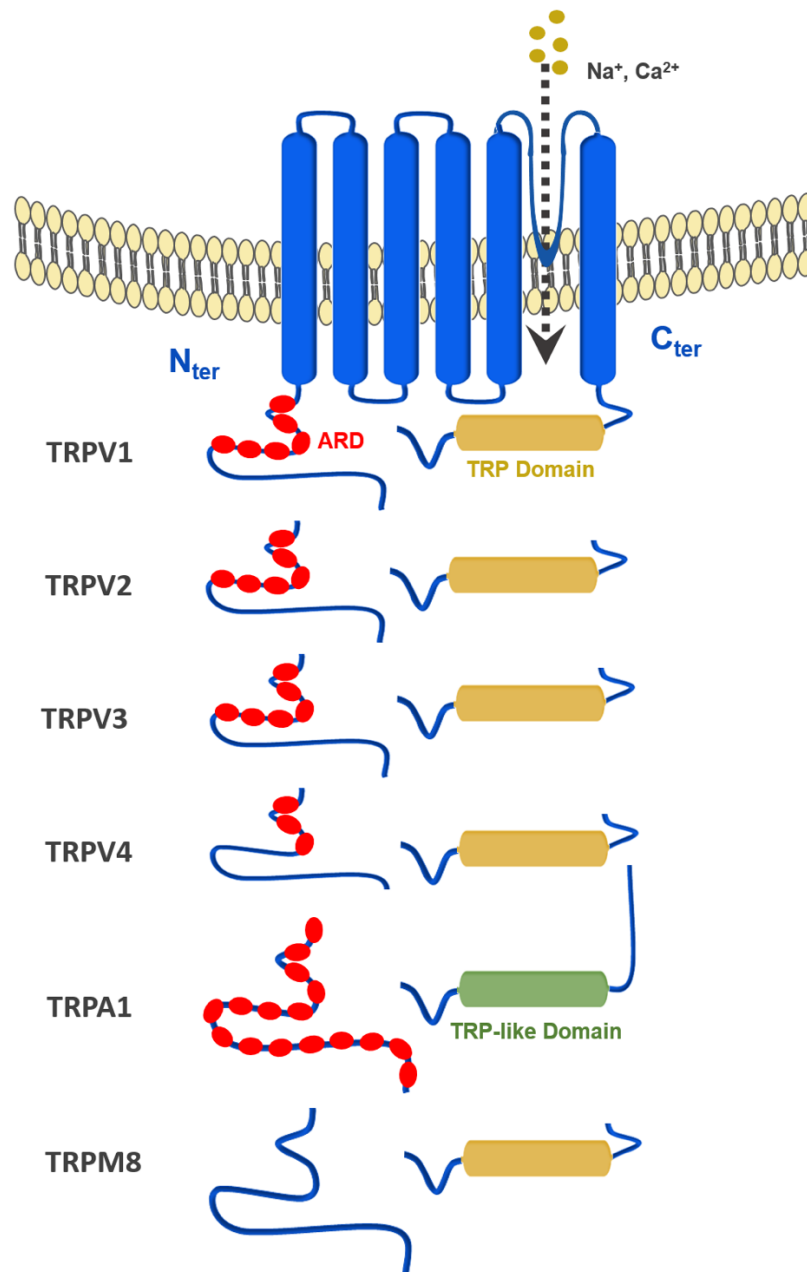
endocannabinoids target more than the canonical cannabinoid receptors<sup>12–14</sup>. There is evidence suggesting that some TRP channels (TRPV1–4, TRPA1, and TRPM8) can be modulated by cannabinoids, providing a promising multitarget approach for the treatment of pain. Interestingly, CB1 has been suggested to colocalize with TRP channels such as TRPV1 in sensory and brain neurons<sup>15–17</sup>, while CB2 colocalizes with this channel in sensory neurons and osteoclasts<sup>18,19</sup>. This expression pattern makes concerted actions possible to modulate nociceptive responses, as well as a synergistic functional effect of cannabinoid ligands.

The mammalian TRP superfamily consists of six subfamilies: canonical (TRPC), vanilloid (TRPV), polycystin (TRPP), mucolipin (TRPML), ankyrin (TRPA), and melastatin (TRPM<sup>20</sup>). There are 28 channels in the TRP superfamily. Six of these channels can be activated by a variety of endogenous, phytogenic, and synthetic cannabinoids, as well as other physical and chemical stimuli. These six channels, TRPV1-TRPV4, TRPA1, and TRPM8, are termed the *ionotropic cannabinoid receptors* and are the focus of this review.

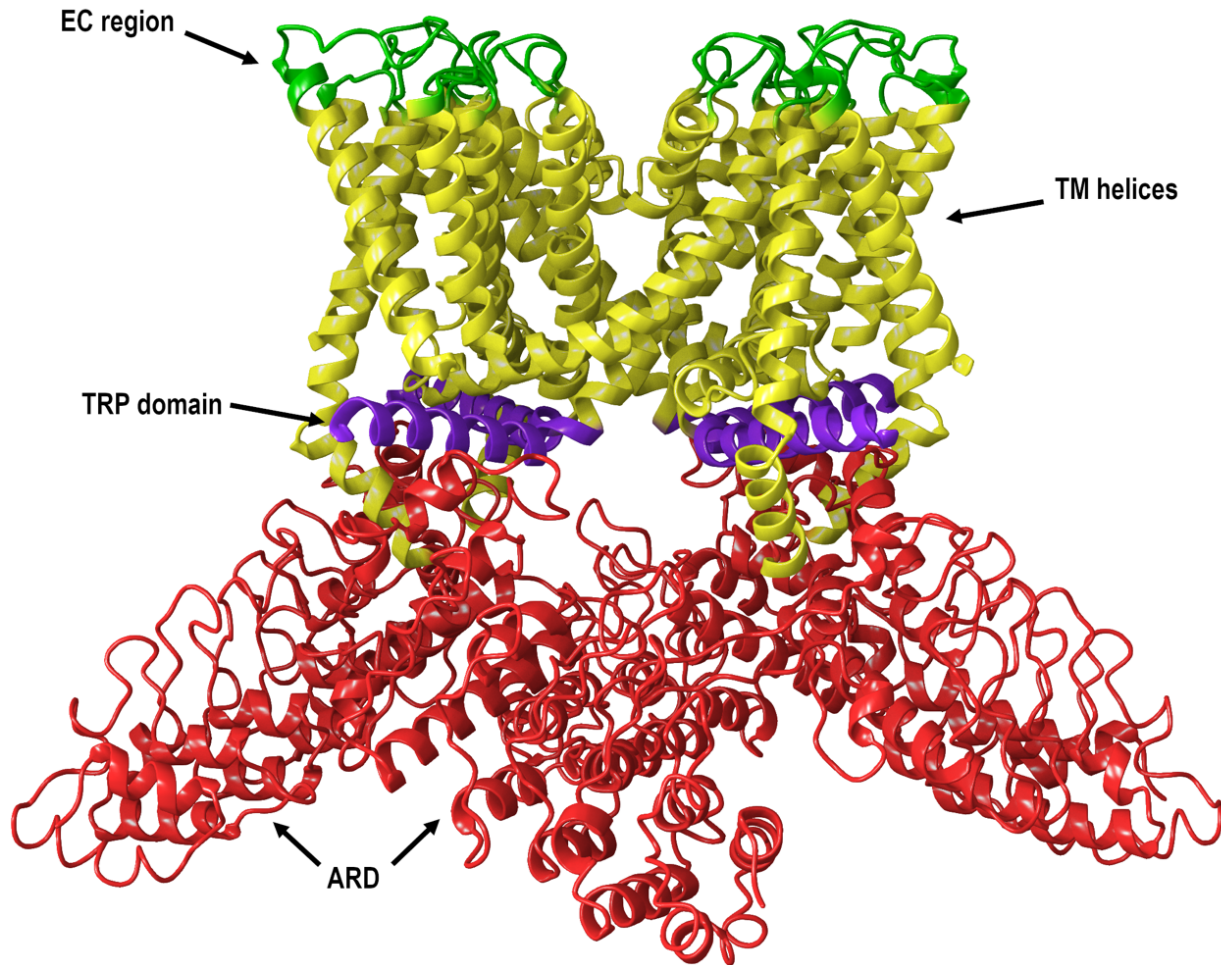
All TRP channels have a similar topological profile: six transmembrane helices, a short pore helix, and a pore loop. However, there are some structural divergences that characterize each class of TRP channels. The main difference among the three subfamilies discussed here is the variability in the number of ankyrin repeat domains (ARDs) located at the N-terminus of the receptor. Vanilloid-type channels bear a variable number of ankyrin repeats; the Ankyrin subfamily presents a high number of repeats; and the TRPM subfamily lacks ankyrin repeats. The topology of the channels reviewed here is depicted in Figure 1. For instance, on the N-terminal side of TRPV1 lies a series of ankyrin repeat units that form the ARD (Figure 2). Each unit contains two short anti-parallel alpha helices and a finger loop that extends out at a 90° angle from the axis of the helices<sup>21</sup>. TRPV1 specifically contains six of these repeat units on each

monomer that forms a concave surface used for interactions with other proteins like calmodulin (CaM) and phosphatidylinositol-3-kinase (PI3K<sup>22</sup>). Similarly, TRPA1 also contains an ARD and this class of ion channels was named for the unusually large number of ankyrin repeats it contains (Figure 3). One motif found in TRPA1 and TRPM8 that is not present in the vanilloid subfamily is a C-terminal tetrameric coiled-coil (Figures 3A,B) which mediates interactions between subunits and is important for trafficking and function<sup>23,24</sup>. Another large structural difference between the TRPV, TRPA, and TRPM subfamilies is the TRP box. The TRP box is a long helix that is parallel to the membrane, on the C-terminal side of the receptor, and can be found in both TRPV1 and TRPM8 (Figure 2). Though not canonically present in TRPA1 due to its location farther below the inner leaflet (Figure 3A), the  $\alpha$ -helix that extends off of the C-terminal side of the receptor is topologically and structurally analogous to a TRP box<sup>21,23</sup>. Despite the topological differences among TRPV1-V4, TRPA1, and TRPM8, all respond to select cannabinoids and are therefore classified as ionotropic cannabinoid receptors.

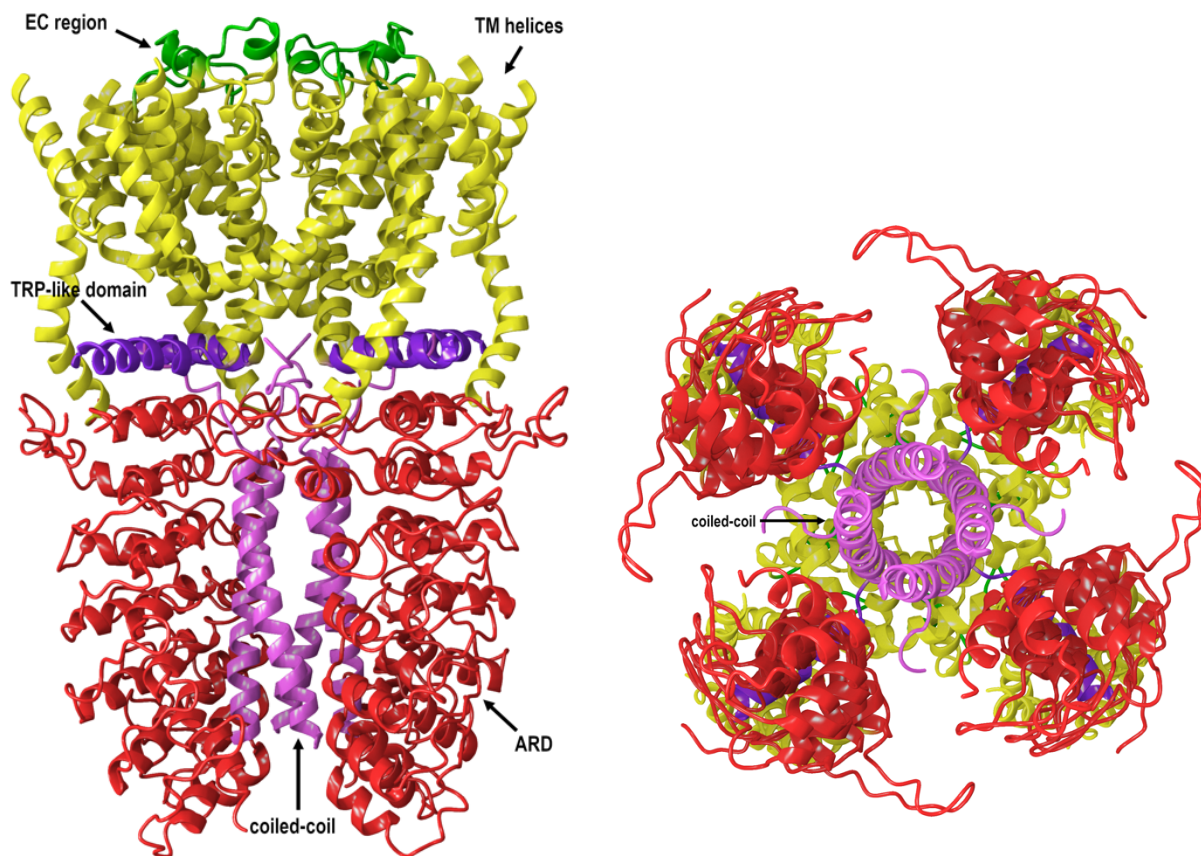
**Figure 1. General topology of the transient receptor potential (TRP) channels discussed in this review: TRPV1–4, TRPA1 and TRPM8.**



**Figure 2. The lipid view of TRPV1 adapted from PDB: 3J5P. Ankyrin repeat domain (ARD) shown in red, transmembrane helices shown in yellow, TRP domain shown in purple, and intracellular regions (ICRs) and extracellular regions (ECRs) shown in green. Sections have been omitted for clarity.**



**Figure 3. (A) The lipid view of TRPA1 adapted from PDB: 3J9P. ARD shown in red, transmembrane region (TMR) shown in yellow, TRP-like domain shown in purple, ICRs- and ECRs shown in green and coiled-coil shown in pink. Sections have been omitted for clarity. (B) The intracellular view of TRPA1 adapted from PDB: 3J9P. Coiled-coil shown in pink. Sections have been omitted for clarity.**



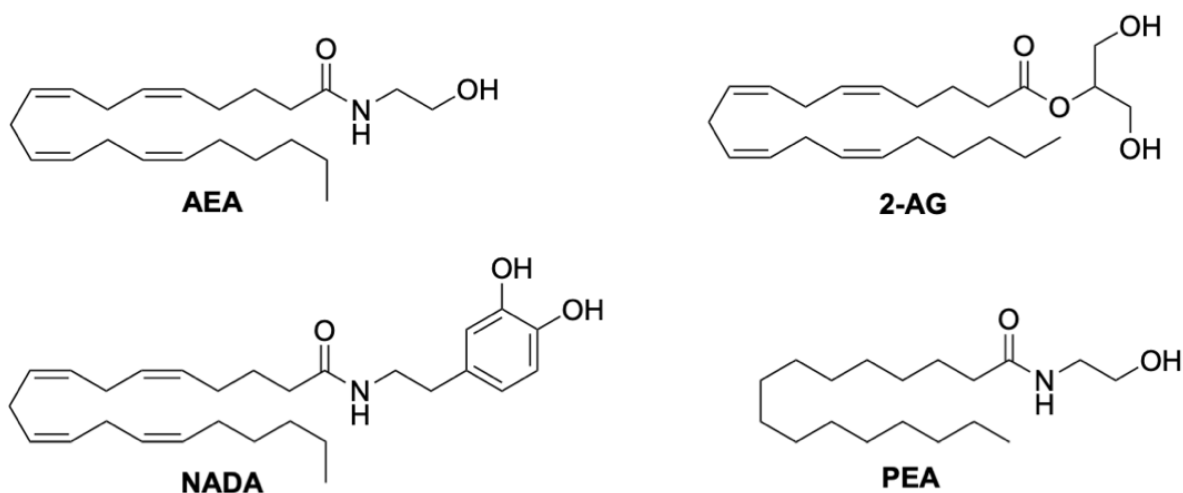
Many endogenous and exogenous compounds activate receptors found in the TRP superfamily. Natural, pungent compounds like capsaicin and allicin, from chili peppers and garlic respectively, can activate and gate specific TRP channels. In addition to these pungent compounds, the six TRP channels that make up the ionotropic cannabinoid receptors can also be modulated by endogenous, phytogenic, and synthetic cannabinoids. For example, the endocannabinoid anandamide (AEA, Figure 4) was the first endogenous TRPV1 agonist identified during a study of the vasodilator action of AEA<sup>25</sup>. *N*-arachidonyl dopamine (NADA,



Figure 4) and AEA were identified as the first endogenous antagonists of TRPM8<sup>26</sup>.  $\Delta^9$  -

tetrahydrocannabinol ( $\Delta^9$  -THC, Figure 5) acts most potently at TRPV2; moderately modulates TRPV3, TRPV4, TRPA1, and TRPM8; but, does not appear to modulate TRPV1<sup>27</sup>. Cannabidiol (CBD, Figure 5) has been shown to have many beneficial properties, including anti-inflammatory action. CBD has little affinity for the CB1 and CB2 receptors, but is reported to be most potent at TRPV1 and TRPM8 channels<sup>27</sup>. A common synthetic cannabinoid known for its use as a CB1 agonist, WIN55,212-2 (Figure 6), has been found to exert analgesic effects by desensitizing both TRPV1 and TRPA1<sup>28</sup>.

**Figure 4. Structure of selected endocannabinoids that target TRP channels.**



**Figure 5. Structure of selected plant cannabinoid ligands that target TRP channels.**

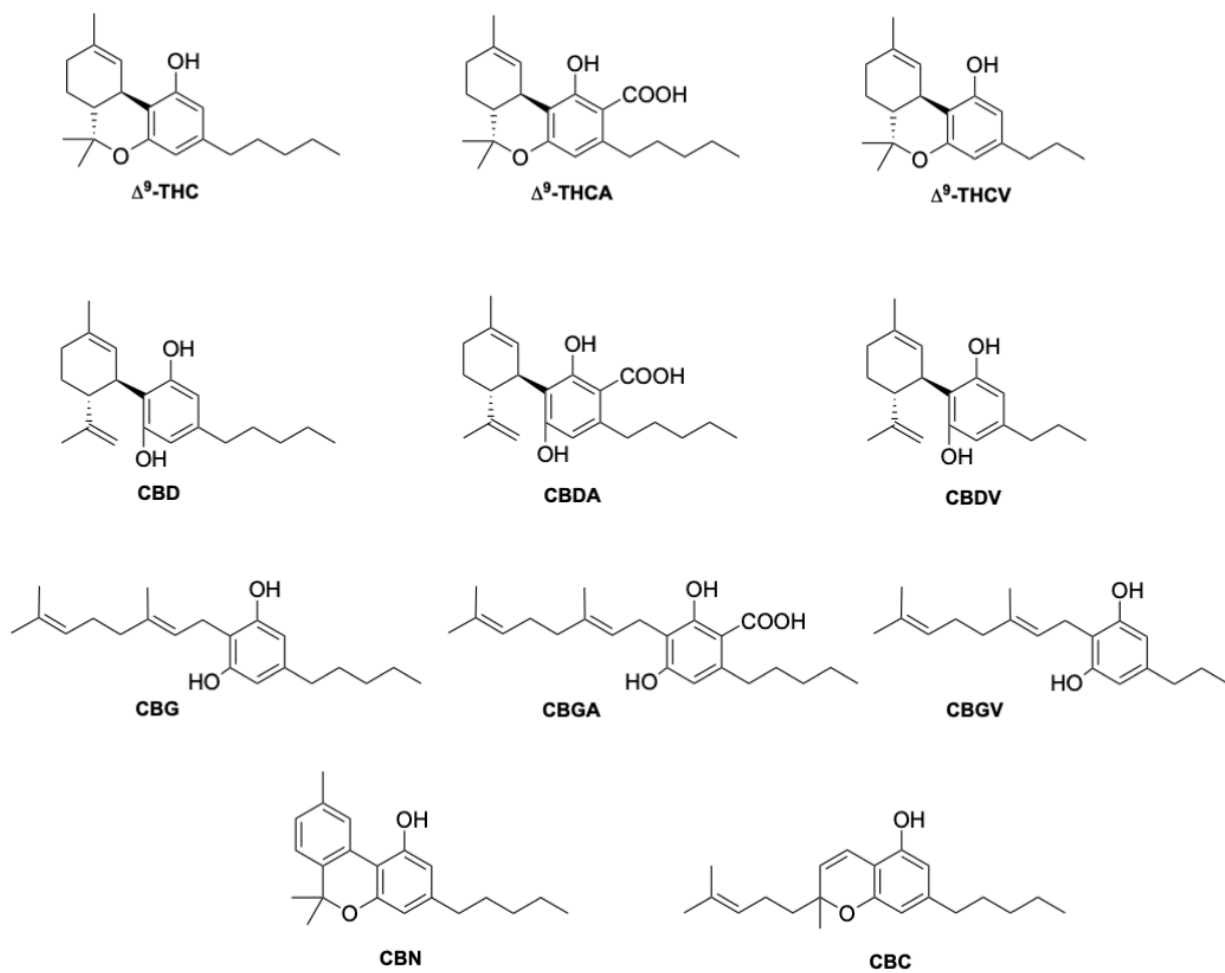
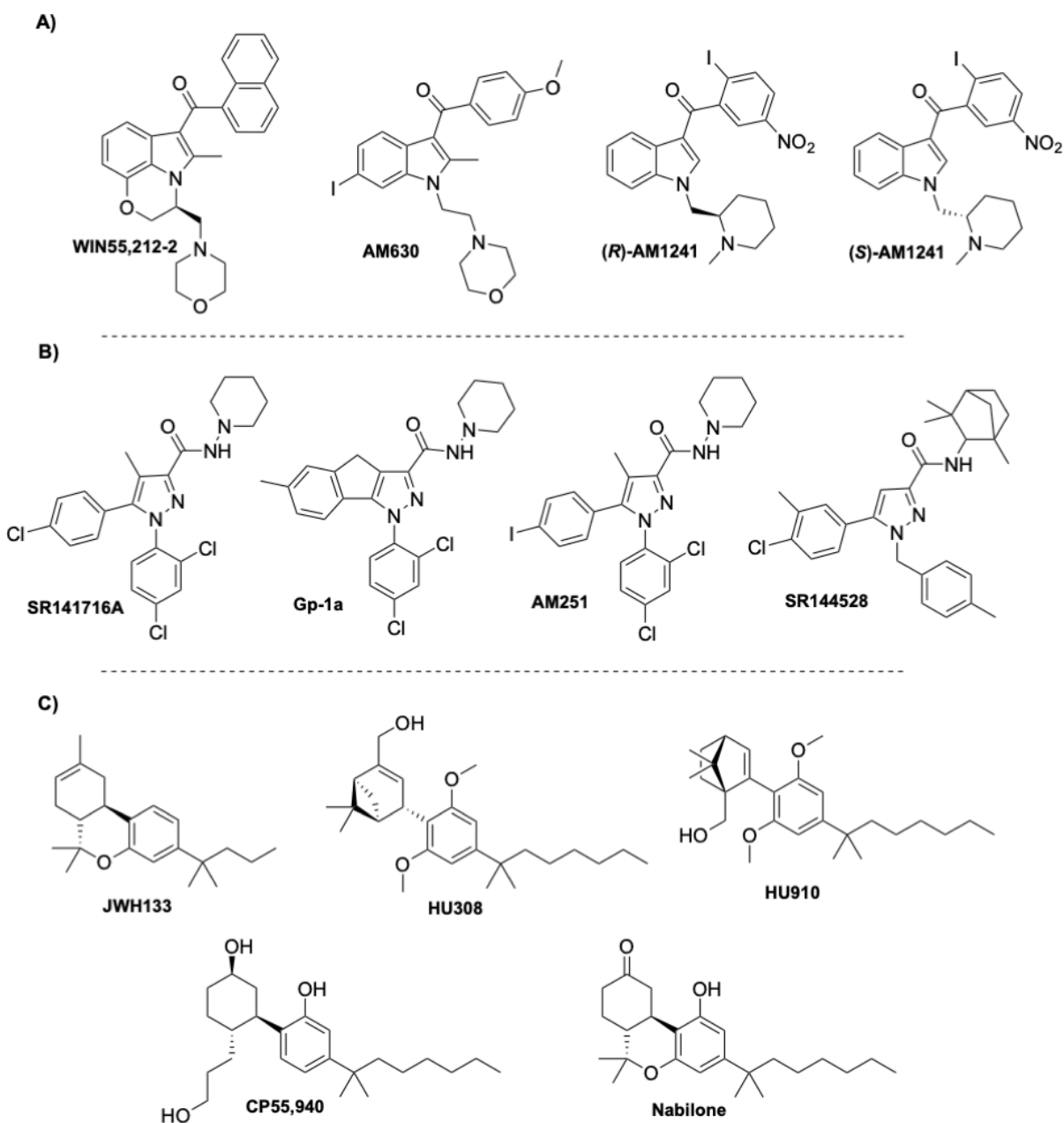


**Figure 6. Structure of selected synthetic cannabinoid ligands that target TRP channels: (A) aminoalkylindole derivatives; (B) arylpyrazole derivatives; (C) synthetic phytocannabinoids analogues.**



## TRPV1

TRPV1, also known as the capsaicin receptor, is a polymodal, nonselective cation channel expressed by all major classes of nociceptive neurons and is important for the detection of noxious stimuli<sup>1,4</sup>. Ion channels, including TRPV1, are typically found in the plasma membrane and form a passageway from one side of the membrane to the other<sup>29</sup>. Upon activation, the pore of TRPV1 opens and allows ions to pass from one side of the membrane to the other. TRPV1 can be activated by a number of endogenous and exogenous stimuli including heat, *N*-acyl amides, arachidonic acid (AA) derivatives, vanilloids, protons and cannabinoids<sup>29</sup>.

Two agonists, capsaicin and resiniferatoxin (RTX), potently activate TRPV1 and evoke strong burning sensations. Upon activation, calcium preferentially moves through the pore, enters the cell and stimulates a series of calcium-dependent processes that ultimately lead to desensitization of the channel. Upon desensitization, the channel enters a refractory period in which it can no longer respond to further stimulation, leading to the paradoxical analgesic effect of these compounds<sup>7</sup>. However, capsaicin and RTX can cause ablation of the nociceptive terminals. This, in turn, can cause a loss of the ability to identify potential tissue-damaging stimuli in the future<sup>30</sup>. Due to this, different avenues have been, and are currently, being explored to find ways to desensitize the channel without painful or ablative effects.

One avenue that has been explored is the modulation of TRP channels by cannabinoids. Endocannabinoids are the endogenous ligands that activate the CB1 and CB2 receptors, but they also activate the ionotropic cannabinoid receptors. AEA (Figure 4), an *N*-acyl amide, was the first endogenous agonist identified to activate TRPV1<sup>25</sup>. AEA has a similar binding affinity as capsaicin, although capsaicin is significantly more potent<sup>5</sup>. Palmitoylethanolamide (PEA, Figure

4), a congener of AEA, has low affinity for both CB1 and CB2 receptors, but activates TRPV1, albeit at very high concentrations<sup>31</sup>. However, Petrosino and colleagues have shown that PEA enhances the effects of AEA at both the cannabinoid receptors and TRPV1 by inhibiting the degradation of AEA<sup>31,32</sup>.

Other *N*-acyl amides have also shown activity at TRPV1. AEA analogs, such as NADA and *N*-oleoyl DA (OLDA), are structurally similar to both capsaicin and AEA and have been shown to activate TRPV1 and TRPV4 receptors<sup>33,34</sup>. *N*-acyl GABA (NGABA), *N*-acyl aspartic acid (NAsp), *N*-acyl glycine (NGly), and *N*-acyl serine (NSer) also have significant agonist activity at TRPV1<sup>34</sup>.

In addition to capsaicin and RTX, many other stimuli including heat, protons, and phytocannabinoids can activate TRPV1<sup>35,36</sup>. As reported by Bisogno and colleagues in 2001, CBD was shown to act as an agonist of TRPV1 in HEK—TRPV1 cells without the ablative effects of capsaicin and RTX<sup>27,37</sup>. Another study performed by Ligresti et al. (2006) suggests that CBD can induce apoptosis in breast carcinoma cells through either direct or indirect activation of CB2 and/or TRPV1. CBD and its phytocannabinoid analog cannabidivarin (CBDV, Figure 5) have been shown to act as negative allosteric modulators of CB1<sup>38</sup> or in a CB1-independent manner, respectively<sup>39</sup>. CBD has been reported to activate TRPV1 at low micromolar concentrations similar to CBDV, and although CBDV is a weaker TRPV1 agonist than capsaicin, it still retains a high potency at TRPV1<sup>7</sup>. In line with these findings, CBD has been proven to exert anti-hyperalgesic benefits that may result from underlying activation and desensitization of TRPV1 at the peripheral and spinal level. This suggests that CBD may have therapeutic potential against inflammatory and chronic pain<sup>27</sup>. While many other phytocannabinoids show very weak and often barely measurable efficacies, CBD and

cannabigerol (CBG, Figure 5) have been shown to be the most potent at TRPV1 and TRPM8<sup>27</sup>. Furthermore, in a study of the effects of cannabinoids and cannabinoid-enriched *Cannabis* extracts on ionotropic TRP channels, De Petrocellis et al. (2011b) found that  $\Delta^9$ -tetrahydrocannabivarin (THCV, Figure 5) and cannabigeravarin (CBGV, Figure 5) also stimulated TRPV1, while their acid analogs (CBDA, CBGA) stimulated TRPV1 to a lesser extent.  $\Delta^9$ -THC and its acid metabolite,  $\Delta^9$ -THCA, were not found to modulate the channel. Likewise, cannabichromene (CBC, Figure 5) and cannabitol (CBN, Figure 5) were shown to have very low efficacies at TRPV1<sup>27</sup>.

Synthetic cannabinoids can also modulate TRPV1. For instance, in a collaborative effort between academia and the pharmaceutical industry, Soethoudt et al. (2017) studied the pharmacology of diverse CB2 ligands. In this work, 11 synthetic cannabinoids were tested on the ionotropic cannabinoid receptors. Putative factors in synthetic cannabinoid ligand binding at TRPV1 seem to be different among classes of synthetic cannabinoids. While binding modes for these ligands remain unknown currently some structural features can be elucidated from the scarce SAR reported. The phytocannabinoid synthetic analogs HU308, HU910, and JWH133 (Figure 6), which activate CB2 receptors, were found to weakly modulate TRPV1.

Aminoalkylindole and arylpyrazole derivatives, well-known cannabinoid synthetic scaffolds, were also evaluated at these channels<sup>40</sup>. Among the aminoalkylindoles tested, the CB1/CB2 ligand WIN55,212-2 (Figure 6), was found to be the most efficacious TRPV1 ligand<sup>40</sup>. Both enantiomers of the aminoalkylindole AM1241 (*S* and *R*, Figure 6) had low efficacies at TRPV1, whereas AM630 did not appear to modulate TRPV1 at measurable values. This may indicate that the dihydro-oxazine indole core of WIN55,212-2 might be crucial for optimized TRPV1 activity,

while bulky aminoalkylindole substituents and electron withdrawing phenyl substituents may also play a role in this channel. Moreover, arylpyrazoles SR141716A, SR144528, AM251, and Gp-1a (Figure 6) were also assessed at these channels. SR141716A was found to be a partial agonist of TRPV1, while Gp-1a was able to desensitize TRPV1 in the low micromolar range<sup>40,41</sup>. SR144528 and AM251 failed to modulate this channel. These results prompt us to speculate that the role of the chlorine in the chlorophenyl moiety of SR141716A, which is an iodine in AM251, is essential, the latter halogen being too bulky. Moreover, the rigidity conferred to the molecule by the tricycle in Gp-1a also decreases activity, while the bulkier pyrazole substituents of SR144528 totally abolished activity at this channel. Further studies need to be done to see how these structural changes affect the binding mode within the TRPV1 pocket.

Table 1 below summarizes all these data on endo-, phyto-, and synthetic cannabinoids that have been tested at TRPV1, along with their potencies, efficacies, and desensitization values.

**Table 1. Functionality of phytogenic, endogenous, and synthetic cannabinoid ligands at TRPV1.**

Compound	Functionality	Efficacy* ( $\mu\text{M}$ )	Potency $\text{EC}_{50}$ ( $\mu\text{M}$ )	Desensitization** ( $\mu\text{M}$ )	Cell type	References
2-AG	Agonist	$59.1 \pm 0.3$	$0.85 \pm 0.6$	$0.75 \pm 0.03$	TRPV1-HEK-293	42,43
AEA	Agonist	$53.8 \pm 0.2$	$0.27 \pm 0.01$	$0.21 \pm 0.06$	TRPV1-HEK-293	42,43
NADA	Agonist	$73.1 \pm 6.4$	$0.040 \pm 0.006$	$1.5 \pm 0.3$	TRPV1-HEK-293	33
OLDA	Agonist	$62.1 \pm 5.5$	$36.0 \pm 0.9$	-	TRPV1-HEK-293	44
PEA	Agonist (entourage effect)	-	>10	-	TRPV1-CHO	45
NGABA	Agonist	$153.08 \pm 10.25$	-	-	TRPV1-HEK-293	34
NGly	Agonist	$85.61 \pm 16.80$	-	-	TRPV1-HEK-293	34
NAsp	Agonist	$95.13 \pm 10.24$	-	-	TRPV1-HEK-293	34
NSer	Agonist	$128.76 \pm 29.90$	-	-	TRPV1-HEK-293	34
CBD	Agonist	$44.7 \pm 0.02$	$1.0 \pm 0.1$	$0.6 \pm 0.05$	TRPV1-HEK-293	27
CBDA	Agonist	<10	$19.7 \pm 3.9$	$89.0 \pm 0.3$	TRPV1-HEK-293	27
CBDV	Agonist	$21.4 \pm 0.6$	$3.6 \pm 0.7$	$10.0 \pm 0.5$	TRPV1-HEK-293	27
CBG	Agonist	$33.8 \pm 2.3$	$1.3 \pm 0.5$	$2.6 \pm 0.2$	TRPV1-HEK-293	27
CBGA	Agonist	$72.8 \pm 2.0$	$21.0 \pm 1.25$	$20.6 \pm 0.5$	TRPV1-HEK-293	27
CBGV	Agonist	$58.8 \pm 0.9$	$2.0 \pm 0.1$	$2.3 \pm 0.3$	TRPV1-HEK-293	27
THC	-	<10	ND	ND	TRPV1-HEK-293	27
THCA	-	<10	ND	$19.2 \pm 5.3$	TRPV1-HEK-293	27
THCV	Agonist	$68.0 \pm 1.6$	$1.5 \pm 0.2$	$1.3 \pm 0.1$	TRPV1-HEK-293	27



THCVA	Agonist	20.0 ± 0.5	25.6 ± 1.1	>50	TRPV1-HEK-293	27
CBC	-	<10	24.2 ± 3.1	>50	TRPV1-HEK-293	27
CBN	-	<10	6.2 ± 3.7	81.7 ± 9.0	TRPV1-HEK-293	27
SR141716A	Agonist	17.5 ± 1.5	12.0 ± 0.6	33.7 ± 6.6	TRPV1-HEK-293	40
SR144528	Agonist	<10	NA	>100	TRPV1-HEK-293	40
AM251	Agonist	<10	NA	>50	TRPV1-HEK-293	40
Gp-1a	Agonist	<10	NA	3.0 ± 0.1	TRPV1-HEK-293	40
WIN55,212-2	Agonist	44.4 ± 0.9	19.2 ± 1.3	35.8 ± 2.2	TRPV1-HEK-293	40
(R)-AM1241	Agonist	10.7 ± 1.5	>50	>50	TRPV1-HEK-293	40
(S)-AM1241	Agonist	12.0 ± 1.2	>50	>50	TRPV1-HEK-293	40
AM630	-	<10	NA	>100	TRPV1-HEK-293	40
HU308	Agonist	<10	NA	69.0 ± 5.7	TRPV1-HEK-293	40
HU910	-	<10	NA	>100	TRPV1-HEK-293	40
JWH133	Agonist	24.6 ± 0.4	8.2 ± 0.7	77.7 ± 3.0	TRPV1-HEK-293	40

*\*Efficacy as % of ionomycin 4 μM. \*\*Desensitization vs. standardized agonist (0.1 μM capsaicin) at IC<sub>50</sub> concentrations. NA, No activity; ND, Not determined.*

## TRPV2

The second member of the vanilloid subfamily, TRPV2, shares 50% sequence identity with TRPV1. TRPV2 is widely expressed in a subpopulation of medium and large diameter sensory neurons<sup>1,4</sup>. TRPV2 is insensitive to protons and capsaicin, but can be activated by high temperatures and inflammation<sup>29</sup>. Similar to TRPV1, the activation and desensitization of TRPV2 is deeply involved in inflammatory and chronic pain<sup>6</sup>. Therefore, finding cannabinoid ligands that can activate and subsequently desensitize TRPV2 may be a desirable therapeutic strategy.

While TRPV1 is activated by endogenous, phytogenic, and synthetic cannabinoids, TRPV2 is mainly activated by phytocannabinoids<sup>29,40</sup>. Two *N*-acyl amides, *N*-acyl proline (NPro) and *N*-acyl tyrosine (NTyr), are the only *N*-acyl amides that have been shown to activate TRPV2 with any significance<sup>34</sup>. Endogenous ligands such as AEA, 2-arachidonoylglycerol (2-AG, Figure 4), and NADA barely elicit a response from TRPV2<sup>46</sup>.

CBD has been found to be the most potent and efficacious phytocannabinoid that activates TRPV2, although at slightly lower values than at TRPV1<sup>27,46</sup>. CBC (Figure 5) and the carboxylic acid derivatives CBGA and CBDA (Figure 5) are inactive at TRPV2, while the acid metabolite of  $\Delta^9$ -THC,  $\Delta^9$ -THCA (Figure 5), has a weaker potency<sup>27</sup>.  $\Delta^9$ -THC has been identified as the most potent phytocannabinoid at TRPV2, although it is not selective, as it also activates TRPA1<sup>46</sup>. Conversely, an analog of  $\Delta^9$ -THC, 11-OH- $\Delta^9$ -THC was found to have a low response at TRPV2, suggesting the hydroxy group somehow disrupts the activation and/or binding mode of  $\Delta^9$ -THC. However, THCV, containing a shortened alkyl side chain (propyl vs. pentyl), and  $\Delta^9$ -THCA, both act as agonists at TRPV2 with the best desensitizing ligand being THCV<sup>27</sup>. This suggests that the THC scaffold is robust enough to withstand moderate changes

and still maintain activity at TRPV2. Further structure-activity relationships on this chemotype may allow fine-tuning of phytocannabinoid activity at this channel.

Wanting to expand on the identity of cannabinoids that activate TRPV2, Qin et al. (2008) tested a variety of synthetic cannabinoids including the THC mimics, nabilone and CP55940 (Figure 6, Table 2). Both had comparable response rates at 58% and 42%, respectively, and were the most responsive of the synthetic cannabinoids tested. The synthetic phytocannabinoid analog JWH133 (Figure 6), a potent and selective CB2 agonist, was also determined to have a very low response rate at rat TRPV2<sup>46</sup>. The more commonly used aminoalkylindole derivative, WIN55,212-2, was shown to have no, or very weak, response in rat TRPV2, but maintained a relatively high response rate in rat TRPA1<sup>46</sup>.

**Table 2. Functionality of phytogenic, endogenous, and synthetic cannabinoid ligands at TRPV2.**

Compound	Functionality	Efficacy* ( $\mu\text{M}$ )	Potency $\text{EC}_{50}$ ( $\mu\text{M}$ )	Desensitization** ( $\mu\text{M}$ )	Cell type	References
AEA	Agonist	NA	-	-	TRPV2-HEK-293	46
2-AG	Agonist	29	-	-	TRPV2-HEK-293	46
NPro	Agonist	$73.35 \pm 2.20$	-	-	TRPV2-HEK-293	34
NTyr	Agonist	$74.78 \pm 15.21$	-	-	TRPV2-HEK-293	34
CBD	Agonist	$40.5 \pm 1.6$	$1.25 \pm 0.23$	$4.5 \pm 0.7$	TRPV2-HEK-293	27
CBDA	-	<10	ND	$114.0 \pm 18.0$	TRPV2-HEK-293	27
CBDV	Agonist	$49.9 \pm 0.9$	$7.3 \pm 0.4$	$31.1 \pm 0.2$	TRPV2-HEK-293	27
CBG	Agonist	$73.6 \pm 1.2$	$1.72 \pm 0.08$	$1.5 \pm 0.2$	TRPV2-HEK-293	27
CBGA	-	<10	ND	$87.3 \pm 1.2$	TRPV2-HEK-293	27
CBGV	Agonist	$75.4 \pm 2.4$	$1.41 \pm 0.36$	$0.7 \pm 0.06$	TRPV2-HEK-293	27
CBC	-	<10	ND	$6.5 \pm 1.6$	TRPV2-HEK-293	27
CBN	Agonist	$39.9 \pm 2.1$	$19.0 \pm 3.7$	$15.7 \pm 2.1$	TRPV2-HEK-293	27
THC	Agonist	$53.0 \pm 1.4$	$0.65 \pm 0.05$	$0.8 \pm 0.1$	TRPV2-HEK-293	27
		98	15.5	-		46
11-OH-THC	-	57	-	-	TRPV2-HEK-293	46
THCV	Agonist	$73.8 \pm 1.0$	$4.11 \pm 0.11$	$0.8 \pm 0.5$	TRPV2-HEK-293	27
THCA	Agonist	$68.2 \pm 1.0$	$18.4 \pm 0.9$	$9.8 \pm 2.6$	TRPV2-HEK-293	27
SR141716A	-	<10	NA	>100	TRPV2-HEK-293	40
SR144528	-	<10	NA	>50	TRPV2-HEK-293	40
AM251	-	<10	NA	$18.4 \pm 3.5$	TRPV2-HEK-293	40

Gp-1a	-	<10	NA	11.9 ± 0.7	TRPV2-HEK-293	40
WIN55,212-2	-	NA	-	-	TRPV2-HEK-293	46
(R)-AM1241	Agonist	14.5 ± 0.3	12.0 ± 3.1	35.5 ± 1.5	TRPV2-HEK-293	40
(S)-AM1241	Agonist	11.6 ± 0.1	5.0 ± 0.1	20.6 ± 3.1	TRPV2-HEK-293	40
AM630	-	<10	NA	35.6 ± 1.4	TRPV2-HEK-293	40
HU308	-	<10	NA	>100	TRPV2-HEK-293	40
HU910	-	<10	NA	>100	TRPV2-HEK-293	40
JWH133	-	4	-	-	TRPV2-HEK-293	46
CP55940	Agonist	42	-	-	TRPV2-HEK-293	46
Nabilone	Agonist	58	-	-	TRPV2-HEK-293	46

*\*Efficacy as % ionomycin 4 μM. \*\*Desensitization vs. standardized agonist (3 μM lysophosphatidylcholine) at IC<sub>50</sub> concentrations. NA, No activity; ND, Not determined.*

In summary, the data reported thus far (see Table 2) indicates that  $\Delta^9$ -THC, its mimics, and derivatives, have the best efficacies at TRPV2, with the exception of 11-OH- $\Delta^9$ -THC. These results could be further expanded upon and utilized to develop new and highly selective TRPV2 agonists.

### TRPV3

The third member of the vanilloid subfamily, TRPV3, shares a 43% sequence homology with TRPV1 and is predominantly expressed in the DRG, trigeminal ganglia, and in the brain, as well as, several peripheral tissues such as testis, skin and tongue<sup>47</sup>. The role of this channel is directly related to the perception of pain and itch. TRPV3 also acts as a thermosensor of innocuous warm temperatures (33–39°C)<sup>48</sup>. In addition to being activated by innocuous warm temperatures, the cooling-agent camphor and carvacrol, found in the oil of oregano and thyme, can also activate this channel<sup>1</sup>.

In contrast to TRPV1, only a few studies have demonstrated the activity of cannabinoids in this thermosensitive channel. So far, no canonical endocannabinoid has been reported to target TRPV3. However, in a recent study using endogenous lipids structurally related to AEA, *N*-acyl valine (NVal) mixtures were shown to exhibit antagonistic activity at this channel<sup>34</sup>. In particular, *N*-docosahexaenoyl, *N*-linoleoyl, *N*-oleoyl, and *N*-stearoyl valine were identified as individual hit antagonists, whereas no agonist was discovered among the lipids tested<sup>34</sup>.

When De Petrocellis et al. (2012a) tested 12 phytocannabinoids against TRPV3, they found that 10 of them exerted significant elevation of intracellular calcium, but that CBD and THCV were able to modulate TRPV3 with an efficacy similar to that of its typical agonist, carvacrol (Table 3). The authors reported that while these two phytocannabinoids potently activate TRPV3, cannabigerovarin (CBGV) and CBG acid (CBGA) were significantly more

efficacious at desensitizing this channel to subsequent carvacrol activation, suggesting that the CBG scaffold may serve as a structural basis to develop TRPV3 desensitizers<sup>49</sup>.

**Table 3. Functionality of phytogenic, endogenous, and synthetic cannabinoid ligands at TRPV3.**

Compound	Functionality	Efficacy* ( $\mu\text{M}$ )	Potency $\text{EC}_{50}$ ( $\mu\text{M}$ )	Desensitization** ( $\mu\text{M}$ )	Cell type	References
NVal	Antagonist	-	-	$39.73 \pm 4.16$	TRPV3-HEK-293	34
CBD	Agonist	$50.1 \pm 4.8$	$3.7 \pm 1.6$	$0.9 \pm 0.3$	TRPV3-HEK-293	49
THCV	Agonist	$72.4 \pm 2.4$	$3.8 \pm 0.4$	$3.0 \pm 0.2$	TRPV3-HEK-293	49
CBGA	Agonist	$17.5 \pm 1.3$	$12.6 \pm 0.2$	$7.4 \pm 1.2$	TRPV3-HEK-293	49
CBGV	Agonist	$23.5 \pm 1.7$	$2.4 \pm 0.8$	$0.8 \pm 0.04$	TRPV3-HEK-293	49
SR141716A	Agonist	$38.9 \pm 2.1$	$0.85 \pm 0.15$	$3.4 \pm 0.4$	TRPV3-HEK-293	40
SR144528	-	<10	NA	>100	TRPV3-HEK-293	40
AM251	Agonist	$25.9 \pm 1.3$	$0.6 \pm 0.1$	>50	TRPV3-HEK-293	40
Gp-1a	-	<10	NA	$22.6 \pm 3.9$	TRPV3-HEK-293	40
WIN55,212-2	Agonist	$22.9 \pm 0.6$	$6.5 \pm 0.9$	>100	TRPV3-HEK-293	40
(R)-AM1241	Agonist	$12.9 \pm 0.1$	$10.0 \pm 0.1$	>50	TRPV3-HEK-293	40
(S)-AM1241	Agonist	$16.2 \pm 0.1$	$9.0 \pm 0.1$	>50	TRPV3-HEK-293	40
AM630	-	<10	NA	>100	TRPV3-HEK-293	40
HU308	-	<10	NA	>100	TRPV3-HEK-293	40
HU910	Agonist	$31.3 \pm 2.2$	$0.12 \pm 0.05$	$12.9 \pm 4.2$	TRPV3-HEK-293	40
JWH133	-	<10	NA	$80.6 \pm 1.4$	TRPV3-HEK-293	40

*\*Efficacy as % ionomycin 4  $\mu\text{M}$ . \*\*Desensitization vs. standardized agonist (carvacrol) at  $\text{EC}_{50}$  concentrations or  $\text{IC}_{50}$  for antagonism. NA, No activity.*



Synthetic cannabinoids have only recently been tested at TRPV3<sup>47</sup>. The 1,1-dimethylheptyl phytocannabinoid derivative HU-910 was shown to activate TRPV3 with submicromolar potency. Interestingly, this compound does not modulate any other TRP channel tested. Other compounds such as the arylpyrazoles SR141716A and AM251 showed agonist activity at TRPV3, however, they are not selective since they also exhibited activity at other TRP channels. Since studies of TRPV3 and its interactions with cannabinoids are limited, further investigation is required to aid in the elucidation of key structural features within each cannabinoid ligand subclass. These discoveries could be used to develop new synthetic cannabinoids that lead to more potent compounds that act at this channel. However, unlike TRPV1, TRPV3 has been shown to exhibit sensitization in response to repetitive heat stimuli<sup>50</sup>. Due to this, studies should be performed to determine if ligand activation of TRPV3 causes a similar sensitization effect as heat activation, in which case, antagonists would be better suited for this channel.

#### **TRPV4**

The fourth and final member of the vanilloid subfamily discussed here shares over 40% sequence homology with TRPV1<sup>51</sup>. This receptor is widely expressed throughout the body and can be found in the central nervous system, epithelial cells, osteoblasts, blood vessels, and many other tissues including those of the heart, liver, and kidney<sup>52</sup>. TRPV4 is involved in the regulation of systemic osmotic pressure in the brain, and plays a role in vascular function, skin barrier function and nociception<sup>52-54</sup>. Similar to TRPV3, this channel responds to warm thermal changes, being activated by temperatures from 25° C to 34° C. In addition to diverse exogenous and endogenous ligands, TRPV4 is also activated by mechanical and osmotic stimuli<sup>55,56</sup>.

In 2003, Watanabe and coworkers reported the first experiments that linked endogenous cannabinoids to TRPV4 modulation. The authors proposed that the most abundant endocannabinoids, AEA and 2-AG, are able to activate this channel. This robust activation of TRPV4 is suggested to be due to AA metabolites formed by cytochrome P450, such as epoxyeicosatrienoic acids<sup>57</sup>. Though further research is needed to unravel structural determinants of ligand-receptor interactions, the epoxy group generated upon epoxxygenase metabolism of the polyunsaturated fatty acids found in endocannabinoids may be essential for ligand activity. Moreover, in the previously mentioned study of endogenous lipids, certain *N*-acyl amides were identified as TRPV4 modulators<sup>34</sup>. Among them, NTyr and *N*-acyl tryptophan (NTrp) mixtures stand out because of their agonist activity at TRPV4.

Concerning plant-derived cannabinoids, De Petrocellis et al. (2012a) discovered that specific compounds are also able to evoke intracellular  $\text{Ca}^{2+}$  response in cells expressing TRPV4. As depicted in Table 4, phytogenic analogs of CBD and  $\Delta^9$ -THC bearing a propyl side chain, CBDV and THCV, showed the highest efficacy and potency among the phytocannabinoids tested. These results may prompt consideration of the structural importance of cannabinoid lipophilic side chains and their interactions at TRPV4.

**Table 4. Functionality of phytogenic, endogenous, and synthetic cannabinoid ligands at TRPV4.**

Compound	Functionality	Efficacy* ( $\mu\text{M}$ )	Potency $\text{EC}_{50}$ ( $\mu\text{M}$ )	Desensitization** ( $\mu\text{M}$ )	Cell type	References
AEA	Agonist (indirect activation)	-	-	-	TRPV4-HEK-293	57
2-AG	Agonist (indirect activation)	-	-	-	TRPV4-HEK-293	57
NTyr	Agonist	-	$55.59 \pm 7.79$	-	TRPV4-HEK-293	34
NTrp	Agonist	-	$75.59 \pm 7.79$	-	TRPV4-HEK-293	34
CBDV	Agonist	$30.2 \pm 0.9$	$0.9 \pm 0.1$	$2.9 \pm 0.3$	TRPV4-HEK-293	49
THCV	Agonist	$59.8 \pm 1.7$	$6.4 \pm 0.7$	$3.2 \pm 0.2$	TRPV4-HEK-293	49
CBG	Agonist	$23.7 \pm 1.8$	$5.1 \pm 1.6$	$1.3 \pm 0.1$	TRPV4-HEK-293	49
CBGA	Agonist	$36.5 \pm 1.9$	$28.8 \pm 0.6$	$3.6 \pm 0.3$	TRPV4-HEK-293	49
CBGV	Agonist	$26.1 \pm 1.7$	$22.2 \pm 3.7$	$1.8 \pm 0.1$	TRPV4-HEK-293	49
CBN	Agonist	$15.3 \pm 1.5$	$16.1 \pm 4.5$	$5.4 \pm 0.8$	TRPV4-HEK-293	49
SR141716A	-	<10	NA	$2.0 \pm 0.1$	TRPV4-HEK-293	40
SR144528	-	<10	NA	>100	TRPV4-HEK-293	40
AM251	-	<10	NA	$1.2 \pm 0.1$	TRPV4-HEK-293	40
Gp-1a	-	<10	NA	$2.2 \pm 0.1$	TRPV4-HEK-293	40
WIN55,212-2	-	<10	NA	$16.1 \pm 1.7$	TRPV4-HEK-293	40
(R)-AM1241	-	<10	NA	$8.7 \pm 0.5$	TRPV4-HEK-293	40
(S)-AM1241	-	<10	NA	$8.6 \pm 0.3$	TRPV4-HEK-293	40
AM630	-	<10	NA	$3.2 \pm 0.1$	TRPV4-HEK-293	40
HU308	-	<10	NA	>100	TRPV4-HEK-293	40
HU910	-	<10	NA	>100	TRPV4-HEK-293	40

JWH133	-	$13.6 \pm 0.8$	$12.0 \pm 3.0$	>100	TRPV4-HEK-293	<sup>40</sup>
*Efficacy as % ionomycin 4 $\mu$ M. **Desensitization vs. standardized agonist (4- $\alpha$ -phorbol-12,13-didecanoate, 4 $\alpha$ PDD) at EC <sub>50</sub> concentrations. NA, No activity.						

On the other hand, phytocannabinoids such as CBG, CBGA, CBGV, and CBN (Figure 5) were more readily able to desensitize this channel (after activation by 4- $\alpha$ -phorbol-12,13-didecanoate, 4 $\alpha$ -PDD), even though these phytocannabinoids exhibited low efficacy and/or potency as activators of this channel. It is interesting to highlight that CBC reduced TRPV4 expression in the jejunum and ileum of mice treated with a gastrointestinal inflammatory agent, but not in control mice<sup>49</sup>.

Synthetic cannabinoid derivatives from representative structural families, such as aminoalkylindoles or arylpyrazoles have also been tested at this channel<sup>47</sup>. These ligands, including the CB1/CB2 agonist WIN55212-2, the cannabinoid inverse agonists SR141716A and SR144528, and the CB2 selective agonists HU-308 and HU-910 all failed to stimulate TRPV4 in the reported assays (Table 4).

More cannabinoids remain to be tested at this channel to determine the relevance of TRPV4 within the cannabinoid system.

### **TRPA1**

The first and only member of the ankyrin family to be discussed in this review is TRPA1. Members of this family are named for their extensive ARDs. TRPA1 itself contains 16 ankyrin repeat units in comparison to the six that TRPV1 contains<sup>23</sup>. TRPA1 can be found co-expressed with TRPV1 in a subset of peripheral sensory neurons and is activated by pungent compounds found in mustard, garlic, and onion. These pungent compounds, called isothiocyanates, are electrophiles that covalently bind to cysteine or lysine residues found in the ARD<sup>1,23</sup>. TRPA1 channels have also been shown to mediate mechanical and bradykinin-evoked hyperalgesia, playing an important role in neuropathic and inflammatory pain<sup>58</sup>. In addition to these various

ligands, TRPA1 is also activated by temperatures below 17°C, putting it at the low end of the thermo-TRP scale<sup>4</sup>.

Very few endocannabinoids have shown activity at TRPA1. AEA was determined to have a very high efficacy (~159%) when compared to the typical TRPA1 agonist, mustard oil isothiocyanates (MO), and AEA and AA were both found to exhibit low micromolar potencies<sup>59,60</sup>. Currently, these are the only two endocannabinoids with reported activity at this channel, which leaves room to discover other endogenous ligands.

In contrast to the few endocannabinoids that act at TRPA1, many phyto- and synthetic cannabinoids have been reported to activate this channel. De Petrocellis et al. (2008) tested various phytocannabinoids in TRPA1-HEK-293 cells and found that CBC, CBD,  $\Delta^9$ -THCA, CBDA, and CBG all increased intracellular  $\text{Ca}^{2+}$  levels. When the efficacy of CBC,  $\Delta^9$ -THC, and CBG was tested, it was shown that these three phytocannabinoids are more efficacious than MO. However,  $\Delta^9$ -THCA and CBDA are considered to be partial agonists of TRPA1, since they were determined to have a slightly lower efficacy than MO<sup>61</sup>. The most potent of the phytocannabinoids initially tested were CBC, CBD, and CBN with EC50 values of 90 nM, 110 nM, and 180 nM respectively<sup>27</sup>. Later, De Petrocellis et al. (2011b) tested a wider variety of phytocannabinoids and, in agreement with their previous data, found that CBC and CBD exhibited the highest potency. However, the acid derivatives, CBGA, CBDA, and  $\Delta^9$ -THCA all showed weaker activation at TRPA1 in response to subsequent application of MO, confirming their role as partial agonists. This data shows that while the acid derivatives of phytocannabinoids can still agonize the channel, it is to a lesser extent than their decarboxylated analogs.

In addition to the phytocannabinoids that have been tested, many synthetic cannabinoids have been evaluated showing activity at TRPA1. The synthetic endocannabinoid and CB1 agonist, arachidonyl-2'-chloroethylamine (ACEA), was shown to have a potency similar to that of AEA at TRPA1<sup>28,62</sup> while the arylpyrazoles SR141716A, Gp-1a, and AM251, and the aminoalkylindoles WIN55,212-2 and AM630 were determined to activate this channel more potently than ACEA<sup>47</sup>. Furthermore, HU308, HU910, (*R*)-AM1241, and SR144528 all displayed low or no desensitization ability and slightly lower potencies than the previously mentioned synthetic cannabinoids. However, the phytocannabinoid analog JWH133 was found to be one of the most efficacious synthetic cannabinoids tested at this channel with an efficacy of ~76%. These data suggest that a wide-spanning variety of synthetic cannabinoids can activate TRPA1 with low micromolar potencies. Table 5 summarizes functional data for synthetic cannabinoids tested.

**Table 5. Functionality of phytogenic, endogenous, and synthetic cannabinoid ligands at TRPA1.**

Compound	Functionality	Efficacy* ( $\mu\text{M}$ )	Potency $\text{EC}_{50}$ ( $\mu\text{M}$ )	Desensitization** ( $\mu\text{M}$ )	Cell type	References
AEA	Agonist	$158.7 \pm 11.1$	$10.1 \pm 1.9$	$21.0 \pm 1.6$	TRPA1-HEK-293	59
AA	Agonist	-	$13 \pm 4$	-	TRPA1-HEK-293	63
ACEA	Agonist	-	$12 \pm 2.0$	NS	TRPA1-CHO	64
THC	Agonist	$117 \pm 12$	$0.23 \pm 0.03$	-	TRPA1-HEK-293	61
THCA	Agonist	$41.6 \pm 2.1$	$2.7 \pm 0.9$	$95.25 \pm 0.01$	TRPA1-HEK-293	27
THCV	Agonist	$234.0 \pm 16.5$	$1.5 \pm 0.6$	$3.07 \pm 0.24$	TRPA1-HEK-293	27
THCVA	Agonist	$170.2 \pm 15.9$	$16.4 \pm 2.4$	$13.14 \pm 0.85$	TRPA1-HEK-293	27
CBD	Agonist	$115.9 \pm 4.6$	$0.11 \pm 0.05$	$0.16 \pm 0.05$	TRPA1-HEK-293	27
CBDA	Agonist	$113.0 \pm 11$	$5.3 \pm 1.5$	$4.92 \pm 0.09$	TRPA1-HEK-293	27
CBDV	Agonist	$105.0 \pm 0.7$	$0.42 \pm 0.01$	$1.29 \pm 0.38$	TRPA1-HEK-293	27
CBC	Agonist	$119.4 \pm 3.1$	$0.09 \pm 0.01$	$0.37 \pm 0.05$	TRPA1-HEK-293	27
CBG	Agonist	$99.9 \pm 1.1$	$0.7 \pm 0.03$	$13.0 \pm 4.8$	TRPA1-HEK-293	27
CBGA	Agonist	$182.8 \pm 0.2$	$8.4 \pm 3.5$	$7.14 \pm 0.17$	TRPA1-HEK-293	27
CBGV	Agonist	$151.4 \pm 0.9$	$1.6 \pm 0.01$	$2.02 \pm 0.25$	TRPA1-HEK-293	27
CBN	Agonist	$83.3 \pm 4.0$	$0.18 \pm 0.02$	$0.40 \pm 0.04$	TRPA1-HEK-293	27
SR141716A	Agonist	$67.3 \pm 1.2$	$1.9 \pm 0.1$	$12.5 \pm 2.2$	TRPA1-HEK-293	40
SR144528	Agonist	$43.8 \pm 1.4$	$8.9 \pm 1.2$	>100	TRPA1-HEK-293	40
AM251	Agonist	$44.4 \pm 0.7$	$0.86 \pm 0.06$	$17.1 \pm 2.2$	TRPA1-HEK-293	40
Gp-1a	Agonist	$83.6 \pm 0.9$	$2.1 \pm 0.1$	$10.4 \pm 1.4$	TRPA1-HEK-293	40
WIN55,212-2	Agonist	$72.3 \pm 0.9$	$2.3 \pm 0.1$	$6.4 \pm 0.6$	TRPA1-HEK-293	40
(R)-AM1241	Agonist	$19.8 \pm 1.3$	$19.5 \pm 5.8$	>50	TRPA1-HEK-293	40



(S)-AM1241	Agonist	47.5 ± 0.8	5.8 ± 0.4	40.9 ± 5.9	TRPA1-HEK-293	40
AM630	Agonist	118.0 ± 2.0	1.9 ± 0.2	3.7 ± 0.5	TRPA1-HEK-293	40
HU910	Agonist	33.1 ± 0.1	53.1 ± 1.1	>100	TRPA1-HEK-293	40
HU308	Agonist	43.1 ± 2.2	18.5 ± 3.9	>100	TRPA1-HEK-293	40
JWH133	Agonist	76.8 ± 3.8	8.5 ± 2.3	20.0 ± 3.2	TRPA1-HEK-293	40

*\*Efficacy as % ionomycin 4 μM. \*\*Desensitization vs. standardized agonist (100 μM allyl isothiocyanate) at iC<sub>50</sub> concentrations. NS, Not significant.*

TRPA1 is suggested to play a role in many different disease states and may be involved in the mediation of the therapeutic effects of cannabinoids<sup>65,66</sup>. Therefore, more cannabinoids should be tested at this channel in order to better elucidate structure activity relationships.

### **TRPM8**

The final TRP channel that will be discussed in this review resides in the melastatin subfamily: TRPM8. TRPM8 is known for its activation at temperatures below 27°C and response to “cooling” compounds such as menthol, eucalyptol, and icilin<sup>26</sup>. Similar to TRPV1, TRPM8 is abundantly expressed in subpopulations of primary afferent neurons<sup>26</sup>. However, in stark contrast to the other five ionotropic cannabinoid receptors at which cannabinoids typically act as agonists, TRPM8 is antagonized by cannabinoids. The juxtaposition between TRPV1 and TRPM8 is interesting in that TRPV1 undergoes activation followed by desensitization via dephosphorylation, whereas TRPM8 is regulated by being inactivated via phosphorylation through protein kinases A and C in response to cannabinoids<sup>61</sup>.

Similar to TRPA1, there are few endocannabinoids that seem to modulate TRPM8. The endocannabinoids, AEA and NADA have been identified as the first endogenous antagonists of TRPM8 and have potencies in the submicromolar region<sup>26</sup>. Other *N*-acyl amides have yet to be tested at TRPM8, which leaves room for more endogenous antagonists to be identified.

De Petrocellis et al. (2008), who tested numerous phytocannabinoids on all of the ionotropic cannabinoid receptors, found that of the 12 cannabinoids tested, nearly all inhibited the effects of menthol or icilin on TRPM8 with potencies in the low- to submicromolar range. CBC was the only phytocannabinoid that was found to be completely inactive at TRPM8<sup>61</sup>. Interestingly, CBC was shown to be the most potent cannabinoid at TRPA1 with a potency of

$0.09 \pm 0.01 \mu\text{M}^{27}$ . Table 6 summarizes the potencies of the cannabinoids tested in comparison to either icilin or menthol.

**Table 6. Functionality of phytogenic, endogenous, and synthetic cannabinoid ligands at TRPM8.**

Compound	Functionality	Potency IC <sub>50</sub> (μM)	Cell type	References
AEA	Antagonist vs. icilin	0.15 ± 0.08	TRPM8-HEK-293	26
	Antagonist vs. menthol	3.09 ± 0.61	TRPM8-HEK-293	26
NADA	Antagonist vs. icilin	0.74 ± 0.35	TRPM8-HEK-293	26
	Antagonist vs. menthol	1.98 ± 0.38	TRPM8-HEK-293	26
THC	Antagonist vs. icilin	0.16 ± 0.01	TRPM8-HEK-293	67
	Antagonist vs. menthol	0.15 ± 0.02	TRPM8-HEK-293	67
THCA	Antagonist vs. icilin	0.14 ± 0.02	TRPM8-HEK-293	67
	Antagonist vs. menthol	0.07 ± 0.01	TRPM8-HEK-293	67
THCV	Antagonist vs. icilin	0.87 ± 0.01	TRPM8-HEK-293	27
THCVA	Antagonist vs. icilin	1.33 ± 0.02	TRPM8-HEK-293	27
CBD	Antagonist vs. icilin	0.08 ± 0.01	TRPM8-HEK-293	67
	Antagonist vs. menthol	0.14 ± 0.01	TRPM8-HEK-293	67
CBDA	Antagonist vs. icilin	0.9 ± 0.1	TRPM8-HEK-293	67
	Antagonist vs. menthol	1.6 ± 0.4	TRPM8-HEK-293	67
CBDV	Antagonist vs. icilin	0.90 ± 0.01	TRPM8-HEK-293	27
CBG	Antagonist vs. icilin	0.14 ± 0.01	TRPM8-HEK-293	67
	Antagonist vs. menthol	0.16 ± 0.03	TRPM8-HEK-293	67
CBGA	Antagonist vs. icilin	1.31 ± 0.09	TRPM8-HEK-293	27
CBGV	Antagonist vs. icilin	1.71 ± 0.04	TRPM8-HEK-293	27
CBC	Antagonist vs. icilin	40.7 ± 0.6	TRPM8-HEK-293	27
CBN	Antagonist vs. icilin	0.21 ± 0.05	TRPM8-HEK-293	27
SR141716A	Antagonist vs. icilin	0.052 ± 0.011	TRPM8-HEK-293	26
SR144528	Antagonist vs. icilin	0.017 ± 0.005	TRPM8-HEK-293	26
AM251	Antagonist vs. icilin	18.4 ± 3.5	TRPM8-HEK-293	40

Gp-1a	NA	>50	TRPM8-HEK-293	40
WIN55,212-2	Antagonist vs. icilin	$72.9 \pm 4.5$	TRPM8-HEK-293	40
(R)-AM1241	NA	>50	TRPM8-HEK-293	40
(S)-AM1241	NA	>50	TRPM8-HEK-293	40
AM630	Antagonist vs. icilin	$4.3 \pm 0.3$	TRPM8-HEK-293	40
HU308	NA	>100	TRPM8-HEK-293	40
HU910	NA	>100	TRPM8-HEK-293	40
JWH133	Antagonist vs. icilin	$48.4 \pm 3.5$	TRPM8-HEK-293	40

*\*Functionality determined against 0.25  $\mu$ M icilin or 50  $\mu$ M menthol. NA, No activity.*

Soethoudt et al. (2017) evaluated several synthetic cannabinoids at TRPM8. Aminoalkylindole derivatives, such as AM630 and AM1241, or phytocannabinoid analogs, such as HU308 or HU910, failed to modulate this channel. However, certain arylpyrazoles were able to modulate TRPM8. SR141716A and SR144528 were found to have potencies in the submicromolar range against icilin. Interestingly, SR141716A, showed activity in the nanomolar range, therefore potentially modulating three of the six channels discussed in this review.

Since data on cannabinoids at TRPM8 is still sparse, further studies on its interactions with cannabinoids and the mechanism of inactivation need to be performed to fully understand the relevance of this channel.

In general terms, as we can observe from the summarized data, channel selectivity remains a challenge among cannabinoid chemotypes. Therefore, further studies should aim at the identification of novel selective TRP cannabinoids that help reveal the therapeutic potential and the mechanism of action of these ligands in the ionotropic receptors.

### **Final Remarks**

It has been widely demonstrated that cannabinoid ligands exert numerous physiopathological functions by modulating TRP channels. These cannabinoid-related TRP channels include members from the vanilloid, ankyrin, and melastatin subfamilies. The six channels discussed in this review are also considered thermo-TRP channels, due to their location in sensory neurons and their ability to be activated by a wide range of temperatures. The modulation of these six channels by temperature and cannabinoids is complex, and the relationship between the channels and their activation in response to cannabinoids can be further explored for various therapeutic uses, including chronic pain and inflammation. Current knowledge on how and which cannabinoids target TRP channels is still scarce, but has largely

increased in the last decade. By classifying the cannabinoid structures able to modulate these receptors, we aim to provide an analysis that helps identifying key features involved in their activity at each particular channel.

Of the endocannabinoids tested at the vanilloid-type channels thus far, all act as agonists with the exception of the endogenous lipid NVal, which acts as an antagonist of TRPV4. Endogenous cannabinoids are also able to activate the ankyrin channel, TRPA1, whereas they exhibit antagonistic effects at the melastatin receptor, TRPM8. The endocannabinoid, AEA was found to be the first endogenous agonist at TRPV1 and has a submicromolar potency. AEA also acts as an agonist at TRPA1, an antagonist at TRPM8, and indirectly activates TRPV4 through its cytochrome-450 metabolites<sup>57</sup>.

Several phytocannabinoids have shown remarkable results at these channels. The active compounds identified tend to activate TRPV1–4 and TRPA1, while they antagonize the activation of icilin or menthol at TRPM8. Among the phytocannabinoids tested in these six channels, CBD and THCV are the more promiscuous since they are potent and efficacious modulators of all the TRP channels discussed here. CBD and CBG are reported to be the most potent ligands tested at TRPV1.  $\Delta^9$ -THC has been found to show no channel modulation, however,  $\Delta^9$ -THC has been shown to potently activate TRPV2.

Concerning synthetic cannabinoids, so far only a few, but from representative cannabinoid scaffolds, have been tested. Arylpyrazoles such as SR141716A, SR144528, or AM251 (**Figure 6**) are able to activate TRPA1, while acting as TRPM8 antagonists. Even though these compounds do not show activity at the vanilloid channels TRPV2 and TRPV4, SR141716A and AM251 can weakly modulate TRPV1 and TRPV3. The aminoalkylindole chemotype has also been explored at these six channels. For instance, the widely used member of

this class, WIN55,212-2, has been shown to exert some of its effects through activation of TRPV1 and TRPA1<sup>28</sup>. Moreover, phytocannabinoid synthetic derivatives such as HU308, HU910, and JWH133 have also been tested in the search of a better understanding of their pharmacological profile. While HU308 does not display potent modulation of any of the channels, other analogs in this class do. For example, JWH133 was shown to modulate TRPV1 and TRPA1 and antagonize the effects of icilin at TRPM8, while HU910 was shown to activate TRPV3. HU308 and HU910 share the dimethoxyphenyl core and the lipophilic side chain, mainly differing in the position of the aliphatic hydroxyl group. This feature may determine TRPV3 recognition. On the other hand, the tricyclic rigidity of JWH133 along with the lack of phenolic hydroxyl may define the ability of this compound to target TRPV1 and TRPA1. The structural differences highlighted here clearly effect the ability of the ligand to modulate their TRP channels, but how these changes affect the binding of the ligand in the channel has yet to be determined. A more inclusive investigation of the binding sites, as well as, the effects of changing moieties could provide insight on how to better design cannabinoid ligands for selectivity and potency.

In summary, we have shown here that a broad range of cannabinoids (endogenous, phytogenic, and synthetic cannabinoids) act at one or more of the following ionotropic channels: TRPV1, TRPV2, TRPV3, TRPV4, TRPA1 and TRPM8. This information is the first step in understanding the importance of ionotropic channels to cannabinoid effects, such as analgesia for chronic pain. However, there is much more that needs to be discovered. What residues are involved in the binding of these cannabinoids to the ionotropic cannabinoid receptors? How do these cannabinoids activate or inactivate the channels at which they act? What structural modifications will produce more potent cannabinoids at these channels? Pursuit of these research



directions should lead to a better understanding of the importance of TRP channels to the physiology of the endocannabinoid system.

### CHAPTER III: A CLOSER LOOK AT ANANDAMIDE INTERACTION WITH TRPV1

**Chanté Muller, Diane L. Lynch, Dow P. Hurst, and Patricia H. Reggio**

Frontiers in Molecular Biosciences, 2020, 10:3389.

Received: 13 April 2020; Accepted: 10 June 2020; Published: 21 July 2020

Department of Chemistry and Biochemistry, University of North Carolina at Greensboro, Greensboro, NC 27412, USA

#### **Abstract**

The transient receptor potential subfamily vanilloid type 1 ion channel (TRPV1), located in the peripheral nervous system has been implicated in the perception of pain and possesses the ability to be modulated by various cannabinoid ligands. Because of its location, TRPV1 is an ideal target for the development of novel pain therapeutics. Literature precedent suggests a wide range of cannabinoid ligands can activate TRPV1, but the location and mode of entry is not well understood. Understanding the modes in which cannabinoids can enter and bind to TRPV1 can aid in rational drug design. The first endogenous ligand identified for TRPV1 was the endocannabinoid, anandamide (AEA). The Molecular Dynamics (MD) studies discussed here investigate the entry mode of AEA into TRPV1. During the course of the 10+ microsecond MD simulations, two distinct binding modes were observed: AEA binding in the tunnel formed by the S1–S4 region, and AEA binding in the vanilloid binding pocket, with preference for the former. Unbiased MD simulations have revealed multiple spontaneous binding events into the S1–S4 region, with only one event of AEA binding the vanilloid binding pocket. These results suggest that AEA enters TRPV1 via a novel location between helices S1–S4 via the lipid bilayer.

**Keywords:** cannabinoids, TRP channels, anandamide, TRPV1, molecular dynamics

## Introduction

While CB1 and CB2 are the most commonly known cannabinoid receptors<sup>68</sup>, other receptors and channels have the ability to be modulated by cannabinoid ligands<sup>1,69</sup>. In fact, a subset of transient receptor potential (TRP) channels have been identified as such<sup>69</sup> and have been coined “ionotropic cannabinoid receptors”<sup>70</sup>. TRP channels are a superfamily of homo- and hetero-tetrameric, transmembrane ion channels involved in the transduction of chemical, mechanical, or physical stimuli to the nervous system<sup>4</sup>. Topologically, all TRP channels have similar profiles: a tetrameric structure where each monomer has six transmembrane helices, a short pore helix, and a pore loop, with some structural divergences that are characteristic to each class of TRP channels<sup>23,24,71</sup>. The pore for cation permeation is located through the center of the tetrameric units, with a surface formed by helices 5 and 6 of each monomer. This allows ions to flow from one side of the cell membrane to the other<sup>1,71</sup>. TRP channels found in the vanilloid (TRPV1-4), ankyrin (TRPA1), and melastatin (TRPM8) subfamilies can be modulated by various cannabinoid ligands<sup>72</sup> and have been located in primary somatosensory neurons<sup>4</sup> making them a desirable target for novel pain treatments.

One of these channels, TRPV1, also known as the capsaicin receptor, elicits a burning and tingling sensation upon activation that ultimately leads to desensitization. This process renders the channel refractory to further stimulation, causing a paradoxical analgesic effect. In order to exploit this analgesic effect caused by TRPV1, different avenues of TRPV1 activation and desensitization are being explored, namely by cannabinoid ligands. While vanilloid ligands have been shown via cryo-EM and mutation studies to reside in a binding pocket located between helices 3 and 4 of one monomer and 5 and 6 of an adjacent monomer<sup>73</sup>, termed the vanilloid binding pocket (VBP), the identity of where cannabinoid ligands bind remains

unknown. Due to the identified structural similarities between the endocannabinoid anandamide (AEA) and capsaicin, their similar binding affinities at TRPV1, and similar structural determinants required for sensitivity at TRPV1, it is plausible that AEA and capsaicin could bind in the same location<sup>74</sup>. Literature supports the hypothesis that capsaicin gains access to the VBP of TRPV1 by flipping from the extracellular to the intracellular leaflet<sup>75,76</sup>. However, previously published data shows that the endogenous cannabinoid 2-arachidonoylglycerol (2-AG) enters the cannabinoid CB2 receptor (a G protein- coupled receptor) via the lipid bilayer by passing between two transmembrane helices<sup>77</sup>.

A lipid bilayer entry for the endogenous cannabinoid, AEA, into TRPV1 may be different from the entry route for other TRPV1 ligands, such as capsaicin. The major goal of the work described here is to determine how the endogenous cannabinoid, AEA, enters and interacts with TRPV1, using all-atom molecular dynamics (MD) simulations of TRPV1 in a fully hydrated POPC lipid bilayer. Identifying the location of cannabinoid ligand binding to TRPV1 is not only crucial to understanding the mechanism of channel gating, but also provides relevant information that can be used to aid in rational drug design. Since AEA is an endogenous agonist of TRPV1 that can activate the channel, probing the mechanism of binding in a realistic lipid bilayer environment via molecular dynamics simulations is imperative to understanding its role with relation to TRPV1. We find here that there are two distinct binding modes: AEA entering TRPV1 via the tunnel formed by helices S1–S4, and AEA in the VBP. Our results suggest that the preferred mode of AEA entry into TRPV1 is via the tunnel formed by S1–S4 in each monomer of the tetramer.

## Methods and Materials

### Model of inactive TRPV1

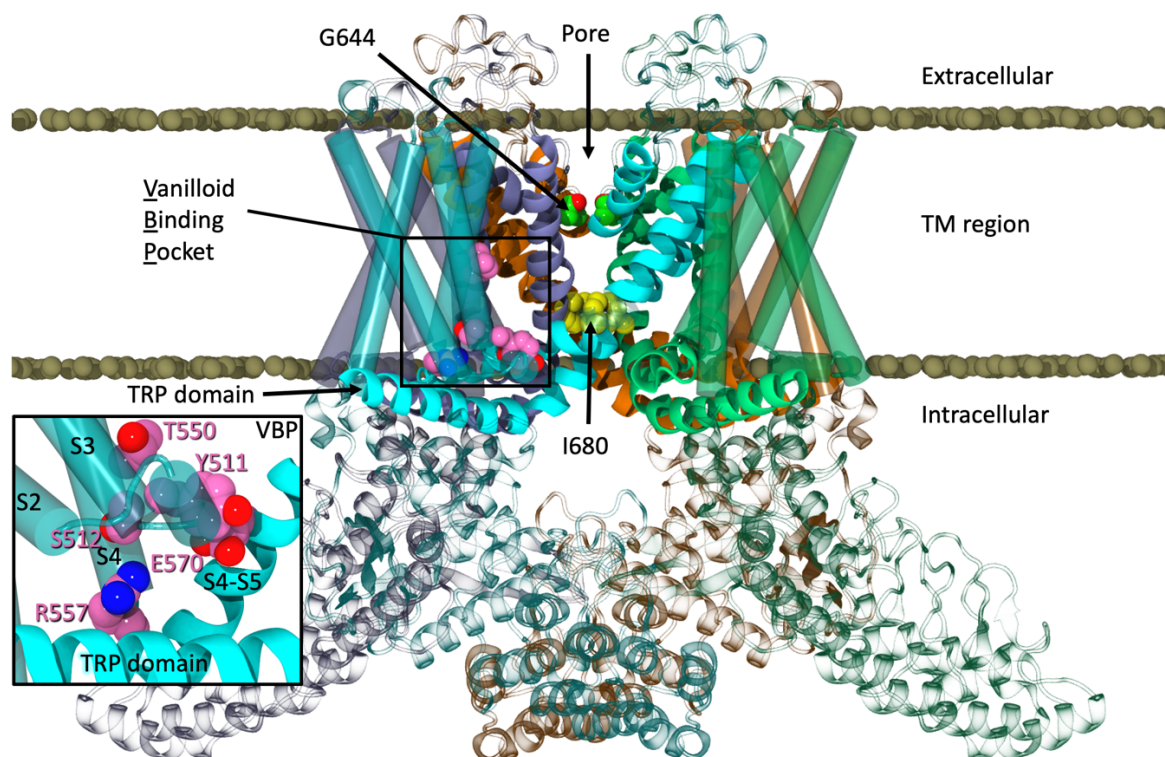
The previously published cryo-EM structure in lipid nanodiscs of TRPV1 in its apo state (PDB: 5IRZ) was used as the template for our model due to its high resolution (3.2 Å) and use of minimal rat sequencing for the transmembrane region of TRPV1<sup>73</sup>. The use of the lipid nanodiscs allows the channel to be in an amphipathic environment, largely without disturbing the transmembrane helical structures. A previously crystallized structure of the rat ankyrin repeat domain (ARD) was also used (PDB: 2PNN, 2.7 Å)<sup>78</sup>. The tetramerized structure of the minimal rat TRPV1 was deconstructed into monomeric subunits and aligned with one ARD. Prime Homology Modeling (Schrödinger, 2018) was utilized to combine these two structures and convert the sequence from rat to human TRPV1<sup>79</sup>. Due to the high sequence homology of rat and human TRPV1 channels (86%)<sup>80,81</sup> and the lack of bending or kinking residues being introduced into the transmembrane region of the channel, the two resolved structures were aligned and converted with relative ease<sup>82</sup>. Prime Homology Modeling also allowed for the fulfillment of residues that were absent in the preliminary model, including an extracellular loop of ~25 amino acid residues. A loop refinement was performed using Prime with the OPLS3 force field and VSGB solvation model<sup>83</sup> at a high dielectric constant to simulate the shape of the loop in an aqueous environment. The completed monomer was then tetramerized and minimized using an implicit membrane from the OPM database, the OPLS3 force field, and the VSGB solvation model to allow the subunits to relax with respect to one another. Note that within the cryo-EM structure(s) published by Gao and colleagues, a lipid headgroup was resolved between helices S1–S4 of the apo TRPV1 structure and was removed prior to the construction of the human TRPV1 model<sup>73</sup>. Additionally, the authors note a phosphatidylinositol lipid occupying the

vanilloid binding pocket of the apo structure. This lipid, suspected to tonically inhibit TRPV1 from constitutive activity, was also removed.

### **Unbiased molecular dynamics simulations**

For preliminary calculations, the TRPV1 model was embedded in a fully hydrated POPC lipid bilayer with neutralizing ions to bring the ionic strength to 0.15M NaCl. An initial relaxation of the channel was performed following the procedure of Lee et al. (2016)<sup>84</sup>. Unbiased NPT MD was performed using CHARMM36m<sup>85</sup> force fields for proteins and CHARMM36 for lipids<sup>86</sup> and ions<sup>87</sup> at physiological temperature (310 K) in the fully hydrated lipid bilayer. The CHARMM36 force field for lipids, rather than the OPLS3 force field was used because the CHARMM36 force field is more mature. In order to keep a homogenous force field environment, the CHARMM36 force field was also used for the protein and ligands. A simulation of this system was run using the pmemd.cuda version of AMBER18<sup>88</sup> for 500 ns in order to equilibrate the structure (Figure 7). The RMSD of the equilibrated structure and a top-down view of the structure can be found in Supplemental Information, Figures 11, 12, respectively.

**Figure 7. The equilibrated structure of TRPV1 in a POPC lipid bilayer.**



During equilibration, water was seen entering a lateral site of TRPV1 located between S1 and S4, which straddles the TRP domain. Further inspection revealed that many polar residues line this region. The cryo-EM structure modeled the density in this region as a lipid headgroup which was removed during hTRPV1 model construction. Additionally, this information, combined with the enhanced flexibility of arachidonic acid derivatives and their entry into CB2 via the lipid bilayer<sup>77,89</sup>, lead us to hypothesize that AEA would have the proper location and flexibility to enter TRPV1 via the tunnel formed by S1–S4, as well as potentially activate the channel from this lateral site.

In order to investigate this, a system was built using a frame from the equilibrated structure of TRPV1 at 50 ns in a 13.8 mol% AEA:POPC fully hydrated lipid bilayer (“Build 1”). Since the structure is homotetrameric, there are four equivalent tunnels that can be observed

while this simulation is underway. AEA ligands were randomly dispersed through the upper and lower leaflets of the lipid bilayer. In addition, AEA was placed outside of each tunnel ensuring no incidental contact or interaction occurred with TRPV1 prior to the start of the simulation. This system was run unbiased at 310K for 642 ns using the pmemd.cuda version of AMBER18.

### **Predocked anandamide in TRPV1**

Additional simulations were constructed based on Build 1. One of the noticeable interactions from Build 1 was the ethanolamine headgroup of the AEA interacting with Y554 inside the tunnel of TRPV1 during one of the spontaneous binding events. AEA was docked in all four tunnels, congruent to interactions observed in Build 1, in this second simulation (“Build 2”), and similarly the remainder of the 13.8 mol% AEA was dispersed randomly throughout the upper and lower leaflets of the lipid bilayer. The fully hydrated system was allowed to run unbiased at 310 K using the pmemd.cuda version of AMBER18 for a total of ~370 ns.

### **Production simulations on Anton2**

Producing simulations that are microseconds in length for these tetrameric channels embedded in a fully hydrated lipid bilayer is difficult due to their size and complexity. As such, we have continued production molecular dynamics runs on the special purpose supercomputer Anton2<sup>90</sup> at the Pittsburgh Supercomputing Center. These production simulations were run in the semi-isotropic NPT ensemble at 310 K and 1 bar using the Anton multigrator framework with a Nose-Hoover thermostat and Martyna, Tobias, Klein (MTK) barostat<sup>91–93</sup>. A timestep of 2.5 fs with default Anton settings for the long-range interactions was employed.



## Results

### Unbiased anandamide entry into TRPV1

During the unbiased simulation of Build 1, three spontaneous binding events were observed in the tunnels of TRPV1. At one point, two AEA ligands entered the same tunnel, with one AEA interacting with both Y555 and Y554 (Figure 8A). A second AEA enters and settles below the first with the amide oxygen interacting with Y487 near the entrance of the tunnel (Figure 8A). In a separate binding event, a third AEA propelled itself directly into another tunnel, with its headgroup -OH interacting with S512 near the VBP (Figure 8B). Although lower pore opening was not observed during these binding events, the upper pore showed great flexibility (Figure 13, Supplemental Information), allowing water and sodium ions to fill the pore between the two gates (Figure 8C). It is from these observations that we hypothesized the possibility of AEA entering TRPV1 through the tunnel, and directly or indirectly aiding in the formation of the ionic lock between R557 and E570 that is reported to facilitate gate opening<sup>73</sup>. This hypothesis was tested in Build 2 (Figure 9A) by docking AEA into each of the tunnels congruent to interactions that were observed during Build 1.

**Figure 8.** (A) Spontaneous entry of two AEA ligands (gray licorice) into one tunnel of TRPV1 at 246 ns. One AEA interacts with both Y554 and Y555 (pink licorice) while the second interacts with Y487 (pink licorice) near the entrance of the tunnel. (B) Another instance of spontaneous entry where AEA (yellow licorice) enters the tunnel and interacts with S512 (pink), near the VBP at 315 ns. (C) The pore between the upper (G644, green VDW) and lower (I680, yellow VDW) gates with sodium atoms (gray VDW) and water molecules present.

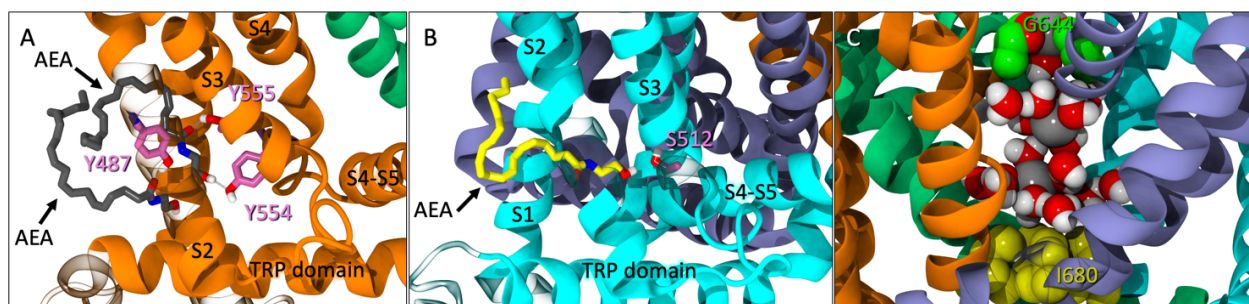
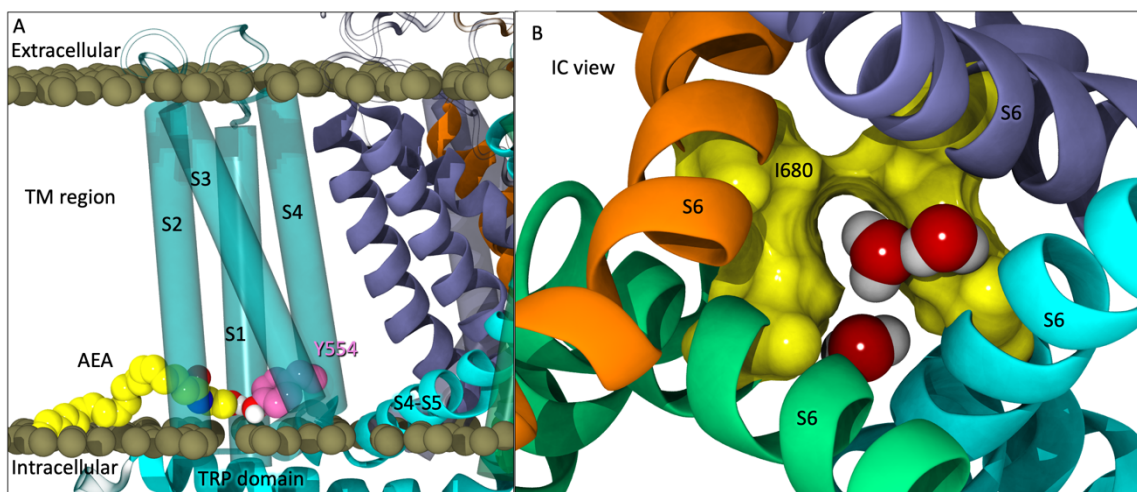


**Figure 9.** (A) The starting point of Build 2 with AEA (yellow) docked in each tunnel with the headgroup interacting with Y554 (pink). (B) An intracellular view of partial opening of the lower gate (I680 in yellow surface) with water molecules passing through.



### Increased gate flexibility with predocked anandamide

Partial opening of the lower gate (I680) was observed after ~125 ns (Figure 9B). At this point in the simulation, one of the four pre-docked AEA ligands have egressed into the lipid bilayer, two other pre-docked AEA ligands backed out of their respective tunnels but still maintain interactions at the entrance of the tunnel, and the final predocked AEA ligand remained stably within its tunnel. When observing the upper gate, G644, the RMSD increases dramatically

from 110 to 135 ns (For RMSD see Figure 14, Supplemental Information), opening at various points within this timeframe. After  $\sim 140$  ns, the upper gate returns to a closed state with small fluctuations. The lower gate undergoes increased fluctuations in the first 10 ns, however after the brief opening at  $\sim 127$  ns, the lower gate also returns to the closed conformation for the duration of the simulation (For RMSD see Figure S14, Supplemental Information).

In comparison to our apo simulation, which had no AEA present, no opening of the lower gate was observed. In fact, the lower gate showed incredible stability in comparison to the AEA-containing simulations. The upper gate showed some fluctuations throughout the trajectory allowing water and ions into the pore, however, as noted in Figures 13, 14 of the Supplementary Information, the frequency at which these events occurred were fewer than those in the presence of AEA.

During the initial simulations ( $\sim 1.7$   $\mu$ s total), AEA was not observed going into the VBP where vanilloids have been shown to bind. In order to efficiently achieve extended simulation lengths these trajectories were continued on Anton2.

### **ANTON2 simulations show more spontaneous binding**

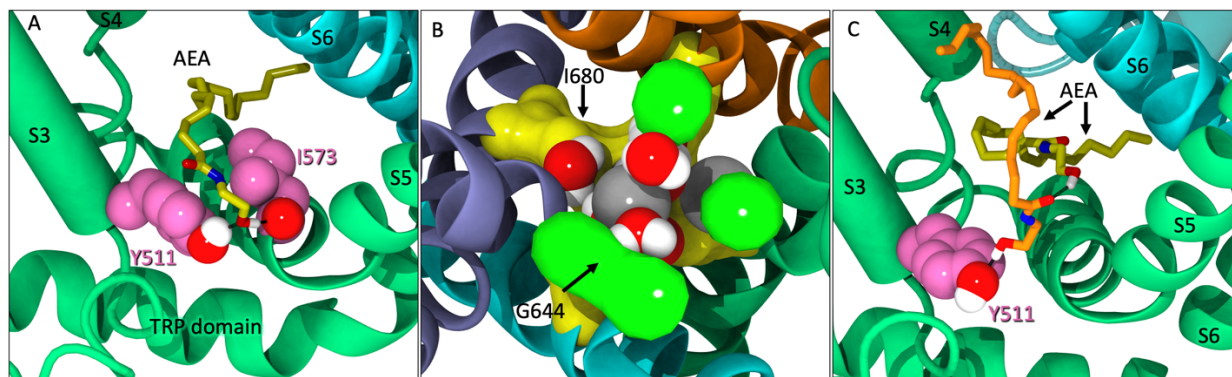
Starting points from Build 1 at 388 ns and Build 2 at 126 ns were selected from the previous simulations to be run on Anton2 for an additional 5.7 microseconds for Build 1 and 6.1 microseconds for Build 2 (Table 7, Supplemental Information).

During the additional microseconds of Build 1 on Anton2, additional spontaneous binding events in the tunnels of TRPV1 were observed throughout the course of the simulation. While the lower gate remained closed, the upper gate showed similar flexibility as observed in the pre-Anton2 builds. In one of the monomers, AEA was shown entering deep into the tunnel and once again interacting with Y544. Conversely, there are relatively few instances of POPC

headgroups entering the tunnels during this simulation. In addition, entry into the VBP was not observed.

Within the first microsecond of Build 2 on Anton2, AEA was observed entering the VBP, backing in tail-first, until the -OH headgroup began interacting with Y511 (Figure 10A). At the time of AEA entering the VBP, AEA was also observed occupying three of the four tunnels of TRPV1. The upper gate was significantly opened during this time (Figure 10B). In the microseconds that follow, a second AEA ligand accompanies the first in the lipophilic crevice of the VBP and adjusts itself to now interact with Y511 (Figure 10C). While both of these ligands are simultaneously occupying the same VBP, neither ligand seems to be facilitating the formation of the ionic lock between R557/E570, nor do their interactions appear to increase the flexibility of the lower gate during its occurrence. This might suggest that while AEA binding in the VBP does occur albeit at a lower frequency than in the tunnels, it may not cause activation of the channel.

**Figure 10. (A) AEA (yellow) backing into the VBP while interacting with Y511 and I573. (B) The upper gate (G644 in green) of TRPV1 significantly opened. Sodium ions (gray) and water molecules have entered the pore region between G644 and I680 (yellow). (C) A second AEA ligand (orange) in the VBP, pushing the first (yellow) back farther into the lipophilic region of the VBP and interacting with Y511.**



## Discussion

The complexities and etiologies of chronic pain encompasses many different conditions, symptoms, and pathways, making the condition notoriously difficult to treat. Since cannabis is well known for its analgesic properties, identifying ligands and receptors involved in nociception would greatly benefit the chronic pain population. In chronic pain conditions, action potentials are generated upon stimulation of a nociceptor, propagating the signal to the brain, ultimately resulting in the sensation of pain<sup>4</sup>. One of the most utilized ways to treat chronic pain conditions currently is with opioid medications. Since the opioid system can influence the reward center, long- and short-term usage can result in addictive behaviors and other unwanted side effects<sup>5</sup>. However, there is extensive literature precedent that supports the role of cannabinoid ligands, whether phytogenic, endogenous, or synthetic, as modulators of pain largely without the unwanted side effects of opioid medications<sup>94</sup>. This feature coupled with the location of the ionotropic cannabinoid receptors within the peripheral nervous system and their role as sensory transducers provides a potential new target for pain management therapies by targeting that which contributes to the detection of stimuli<sup>6</sup>.

A common example of the role of TRPV1 in pain management is that of capsaicin-based creams. Capsaicin, the pungent compound found in chili peppers, is known to activate TRPV1 and elicits a burning, tingling sensation upon application. However, upon activation, TRPV1 undergoes desensitization which renders the channel refractory to any further stimuli resulting in a paradoxical analgesic effect<sup>25,95,96</sup>. However, the use of capsaicin and other potent vanilloid agonists like resiniferatoxin (RTX) can have ablative effects on the axon terminals where TRPV1 is located, causing the loss of ability to detect future painful stimuli<sup>30</sup>. In order to exploit

the analgesic effect elicited by TRPV1, different avenues of TRPV1 activation and desensitization are being explored, namely by cannabinoid ligands.

While the binding modes of vanilloid ligands like capsaicin and resiniferatoxin have been well studied via cryo-EM and mutation data, the binding mode of cannabinoid ligands at TRPV1 has yet to be studied at the same level of detail. Throughout this series of MD simulations, totaling over a collective 10 microseconds, two distinct binding modes were observed: a novel point of entry in which AEA enters into the tunnel located between helices S1–S4, as well as AEA entering the putative VBP. Of these two modes, the binding pathway that was most prevalent in our simulations was that of AEA entering into the tunnels of TRPV1, formed by helices S1–S4, via the lipid bilayer. Additionally, the frequency at which AEA enters the tunnels of TRPV1 spontaneously far exceeds that of AEA entering the VBP. Thirteen unique AEA ligands were found to spontaneously enter into the tunnels of TRPV1 throughout the trajectory of Build 1, suggesting a low energy barrier for AEA entry at this location. In contrast, only one instance of AEA ligands entering the VBP directly was observed throughout the 10+ microseconds of simulation time. It is also worth noting that the system in which VBP binding occurred (Build 2), had all S1–S4 tunnels of TRPV1 occupied with AEA, whether fully inserted into the tunnel or interacting with residues near the entrance.

While the entrance of AEA into the tunnel region of TRPV1 is not the putative location, it is not unusual for TRPV channels to have several allosteric sites. In the cryo-EM structures published by Gao, et. al, a spider toxin called Double Knot Toxin was shown to bind to and activate TRPV1 via the extracellular side of the channel<sup>73</sup>. Recently, cannabidiol (CBD) has been resolved in TRPV2 between helix 5 of one monomer and helix 6 of an adjacent<sup>97</sup>. This region in TRPV2 has high sequence homology with other TRPV channels, potentially indicating that CBD

could interact with TRPV1 at the same location. These varieties to ligand binding at TRPV1 beyond the VBP lend credence to the idea that in addition to its many modes of activation, TRPV1 also has more than one site that can be occupied by a ligand. Additionally, previously published data which shows that the endogenous cannabinoid 2-arachidonoylglycerol (2-AG) enters the CB2 receptor between two transmembrane helices via the lipid bilayer<sup>77</sup> supports our finding that AEA entry into TRPV1 occurs in a similar fashion. Since both 2-AG and AEA contain an arachidonic acid tail, they both possess great flexibility, allowing it heightened mobility within the lipid bilayer, allowing it to reach regions of the protein that might be inaccessible to other ligands.

While sustained opening of the lower gate was not observed during these initial unbiased multi-microsecond simulations, opening of the upper gate was sampled frequently on multiple occasions, allowing water and ions to enter the pore. This was anticipated due to the location of the upper gate being in a loop region and formed by four glycine carbonyl oxygen atoms which appear to coordinate with a sodium ion. The opening of the upper gate allowed water and ions to enter the pore region between the two gates, and while complete opening of the lower gate has not yet been achieved, partial opening was observed in the predocked AEA system. In the apo build, the lower gate was very stable throughout the entirety of its trajectory, showing only mild flexibility. Additionally, the tunnels of the apo run remained largely unoccupied in the absence of AEA, while the AEA containing systems showed multiple binding events, including spontaneous binding from a completely unbiased system, as well as, the exit and re-entry of AEA ligands in the predocked system. The results of these simulations suggest that AEA prefers the lateral site of TRPV1 over the VBP. Due to the frequency of AEA interacting with Y554 and Y555 in the S1–S4 tunnel, it is possible that mutating these residues to phenylalanine to remove

hydrogen bonding capability, or mutating to alanine, to remove both hydrogen bonding and aromatic stacking interactions, may alter or ablate AEA binding in this location. While this is speculation, the data from these simulations suggest that both Y554 and Y555 play a role in AEA interaction with the S1–S4 tunnel.

Regardless of the structural similarities between capsaicin and AEA, our simulations suggest that AEA can enter TRPV1 via the S1–S4 tunnel with a higher probability than that of the VBP. The simulations discussed here are a promising start to better understanding the interactions between AEA and TRPV1 on a molecular level and introduces the idea that AEA enters and interacts with TRPV1 in a novel location between helices S1–S4.



## Supplementary Material

**Figure 11.** The RMSD of apo-TRPV1 structure over the course of 500ns to show the stability of the model. The top panel shows the RMSD the transmembrane (TM) region (residues 430 to 455, 474 to 497, 510 to 532, 536 to 551, 576 to 597, and 656 to 687), the pore helix (residues 633 to 643), and the TRP box (residues 892 to 711). The middle panels shows the RMSD of the TM helices and pore helix. The last panel shows the RMSD of the TM helices only.

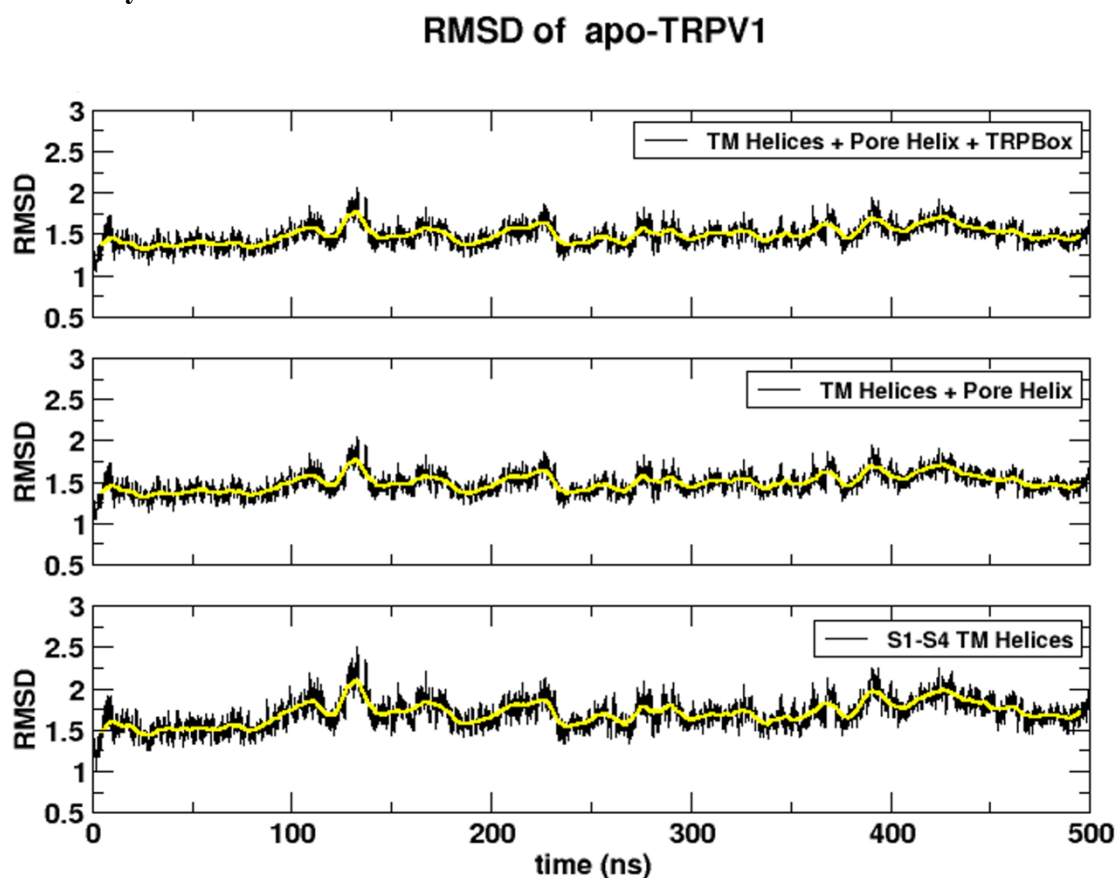


**Figure 12. A top-down view of TRPV1.**

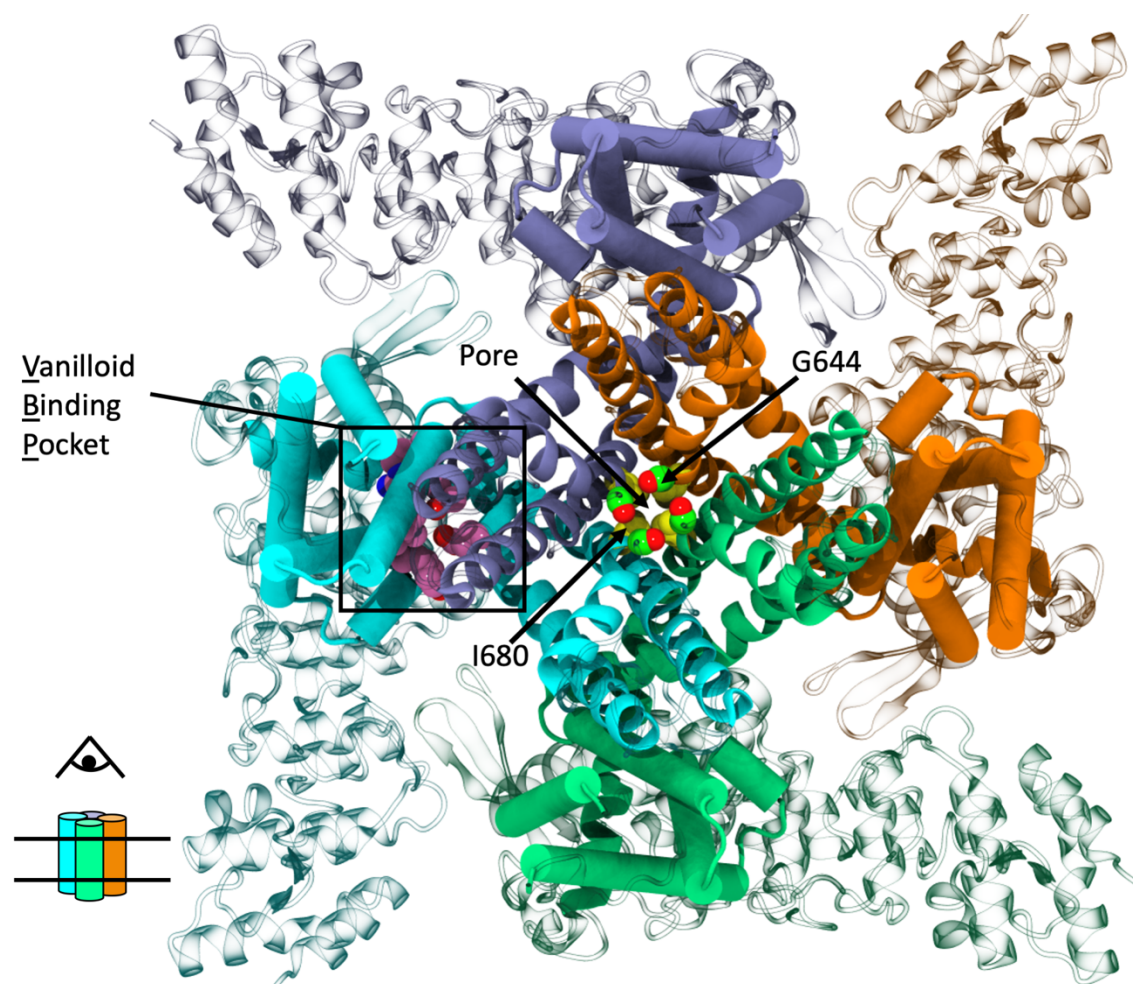


**Table 7.** The names of each MD system, ligands present, starting conformation, and length of time.

System	Ligand	Initial Conformation	Length
Apo	None	Human model from cryo-EM	500ns
Build_1	13mol% AEA	Human model from cryo-EM	642ns
Build_2	13mol% AEA	Human model from cryo-EM	370ns
Build_1 on ANTON2	13mol% AEA	388ns from Build_1	5.7 $\mu$ s
Build_2 on ANTON2	13mol% AEA	126ns from Build_2	6.1 $\mu$ s

**Figure 13.** The RMSD of the upper gate, G644, of the control shown in black with the average shown in yellow against the RMSD of the upper gate, G644, of Build 1 shown in magenta with the average shown in blue.

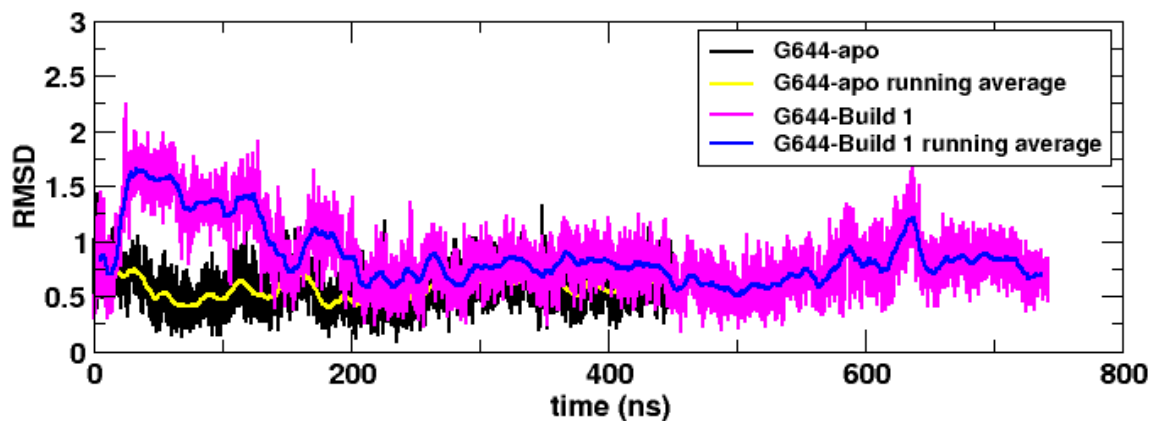
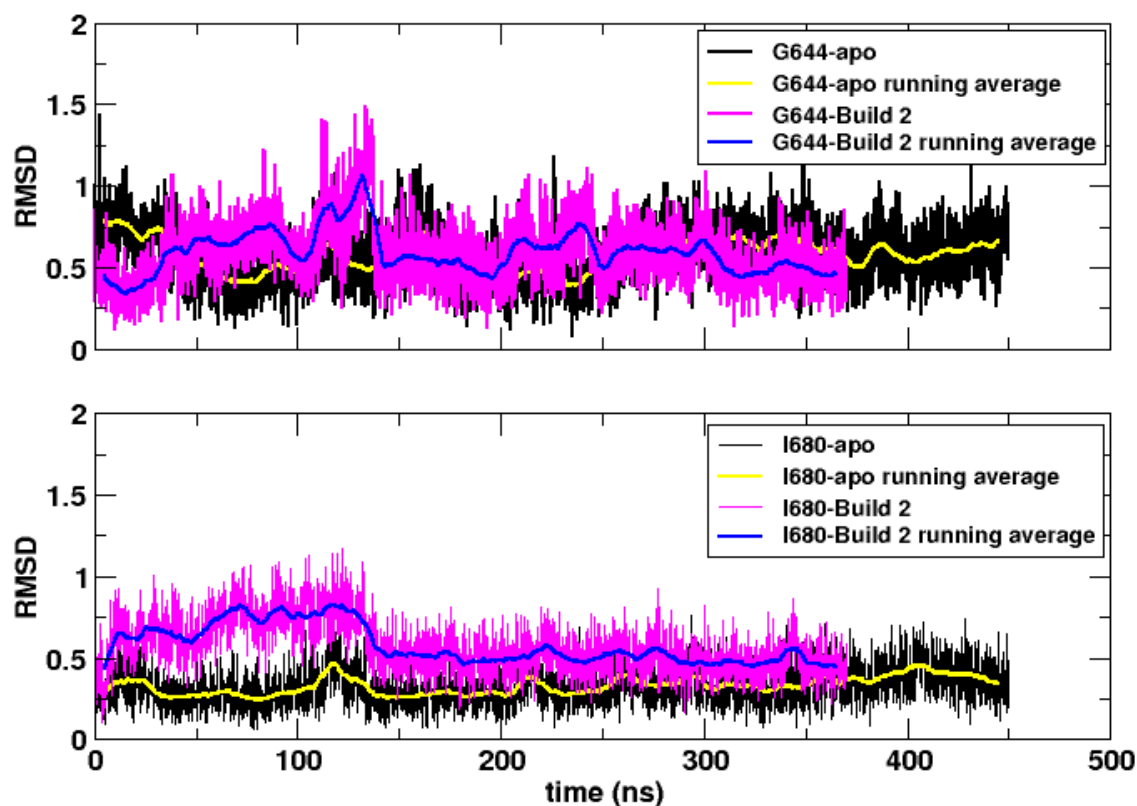


Figure 14. Upper panel shows the RMSD of the upper gate, G644, in the control run (G644-apo) with the average RMSD shown in yellow. The RMSD of the upper gate from Build 2 is shown in magenta with the average RMSD shown in blue. Lower panel shows the RMSD of the lower gate, I680, in the control run (I680-apo) with the average RMSD shown in yellow. The RMSD of the lower gate from Build 2 is shown in magenta with the average RMSD shown in blue.



## CHAPTER IV: AN ANALYSIS OF THE PUTATIVE CBD BINDING SITE IN THE IONOTROPIC CANNABINOID RECEPTORS

**Chanté Muller and Patricia H. Reggio**

Frontiers in Cellular Neuroscience, 2020, 10:3389.

Received: 10 October 2020; Accepted: 18 November 2020; Published: 9 December 2020

Department of Chemistry and Biochemistry, University of North Carolina at Greensboro, Greensboro, NC 27412, USA

### **Abstract**

Cannabinoids have been long studied for their therapeutic properties, particularly for their use in the treatment of pain. As new therapies are sought after to treat conditions of chronic pain, so is a better understanding of the ligands and their target receptors or channels. A recently published cryo-EM structure showed the putative binding location of a well-known cannabinoid ligand, cannabidiol (CBD), in TRPV2, a channel that has been implicated in inflammation and chronic pain. TRPV2, along with TRPV1, TRPV3, TRPV4, TRPA1, and TRPM8 all have the capability to be modulated by cannabinoid ligands and are located in the peripheral nervous system. Here, we analyze the putative CBD binding site in each of these channels and compare structural and sequential information with experimental data.

**Keywords:** cannabidiol, TRP channels, TRPV1, TRPV2, TRPV3, TRPV4, TRPA1, TRPM8

### **Introduction**

Transient receptor potential (TRP) ion channels are membrane-spanning channels that are formed by the homo- or hetero-tetramerization of TRP subunits. Each subunit contains six transmembrane helices (S1–S6), which, when tetramerized together, form a central pore, allowing for cation permeation<sup>6</sup>. These channels, located in the plasma membrane, are capable of

gating several mono- and di-valent cations through this pore in response to a stimulus. In mammals, six main subfamilies of TRP channels have been identified: ankyrin (TRPA), vanilloid (TRPV), melastatin (TRPM), canonical (TRPC), mucolipin (TRPML), and polycystin (TRPP)<sup>20</sup>. Several of these channels have been implicated as sensors of many pathological and physiological processes including itch, temperature, genetic disorders, and pain related to cancers, AIDS, or other neuropathic conditions<sup>3,4,98</sup>.

Chronic pain conditions remain a significant and prominent problem in today's society, effecting millions of people worldwide<sup>99</sup>. The complex mechanisms and etiologies that underlie chronic pain are diverse and cover a range of symptoms, conditions, and pathways<sup>6</sup> that can be brought on by a variety of causes including diabetes<sup>95</sup>, stroke<sup>100</sup>, and treatments for other conditions. Often, other symptoms like depression, anxiety, fatigue, and limitation of activity co-occur leading to an overall reduced quality of life<sup>101</sup>. The current therapies to treat chronic pain conditions are considered to be relatively inadequate. NSAIDs, opioids, tricyclic antidepressants, local anesthetics, and antiepileptics can work to alleviate some chronic pain sufferers' experiences but don't often produce sustained relief<sup>6,102</sup>. With opioid medications, there are also dangers of dependence, tolerance, and addictive behaviors associated with their usage. In an effort to combat the overuse of opioid medications and resultant side effects, as well as find other meaningful therapies, different avenues of pain-related therapeutics are being investigated, notably the use of *Cannabis* in the treatment of chronic pain<sup>103</sup>.

This perspective aims to discuss the putative binding site of a well-known cannabinoid, cannabidiol (CBD) in a selection of six TRP channels that are located in primary somatosensory neurons. This selection of channels (TRPV1–TRPV4, TRPA1, and TRPM8) have been identified as thermoTRPs, responding to various thresholds of temperature activation, as well as ionotropic

cannabinoid receptors due to their ability to be modulated by cannabinoid ligands<sup>72</sup>. The putative binding site of CBD has been identified in TRPV2<sup>97</sup>, and in an effort to better understand CBD interaction at the ionotropic cannabinoid receptors, a sequential and structural analysis will be discussed herein.

### **Cannabinoids and the modulation of pain**

*Cannabis* has been used for millennia to treat pain caused by various situations, including uses in ameliorating pain caused by childbirth in ancient Israel, as a surgical anesthetic in China, and for various painful ailments in the West in the 1800s<sup>101,104</sup>. Today, one of the most commonly cited reasons for seeking medical marijuana is due to chronic pain<sup>105,106</sup>. There is extensive literature that supports the role of phytogenic and endogenous cannabinoid ligands as pain modulators<sup>100,107</sup>, and the identification of broader targets for cannabinoid ligands also works to support this hypothesis<sup>1</sup>. Canonically, CB1 and CB2 are most widely known as receptors for cannabinoid ligands<sup>14,68,108</sup>. Pharmacological evidence shows, however, that other G protein-coupled receptors (GPCRs)<sup>14</sup> and other receptor types, including a subset of TRP channels, also have the ability to be modulated by cannabinoid ligands. Of the subfamilies of TRP channels found in mammals, at least three subfamilies contain channels that have been identified as having this ability, earning the name “ionotropic cannabinoid receptors”<sup>69,109</sup>. Additionally, these channels, TRPV1–4, TRPA1, and TRPM8 can be found in primary somatosensory neurons, acting as sensory transducers that may participate in the generation of painful sensations evoked by thermal, mechanical, or chemical stimuli. These attributes make the ionotropic cannabinoid receptors a worthwhile target to investigate for the development of new pain therapies by targeting that which contributes to the detection of stimuli.

### **Location, location, location**

The location of the TRP channels assessed in this perspective covers many neuron types within the peripheral nervous system, ranging from small diameter peripheral sensory nerves (TRPM8)<sup>110</sup>, to small- to medium-diameter neurons (TRPV1)<sup>111–113</sup>, to medium- to large-diameter neurons that give rise to A $\delta$  and A $\beta$  fibers (TRPV2)<sup>114,115</sup>, to co-expression with TRPV1<sup>116</sup> in a subset of small- to medium-diameter neurons (TRPA1)<sup>117–119</sup>, and to predominant expression in keratinocytes (TRPV3 and TRPV4)<sup>120,121</sup>. These channels (TRPV1–4, TRPA1, and TRPM8), having a wide distribution throughout the peripheral nervous system, have been implicated in roles of conducting various sensations, some of which are familiar to many. The spiciness of chili peppers from capsaicin action at TRPV1, the pungency of garlic and wasabi produced by allicin and isothiocyanate modulation of TRPA1<sup>109,122</sup>, and the cool, minty sensation of toothpastes or candies brought upon by menthol modulation of TRPM8<sup>123</sup> are sought after as welcomed, albeit sometimes discomforting, sensations. However, in the case of chronic pain conditions, whether due to nerve injury or inflammation, ongoing painful stimulation leads to peripheral and central sensitization that can lead to painful sensations upon mild tactile stimulation (allodynia), greater than normal pain response to a stimulus (hyperalgesia), and spontaneous pain<sup>104,124</sup>.

### **Differences in the putative CBD binding site of the ionotropic cannabinoid receptors**

Recently, a cryo-EM structure of rTRPV2 interacting with CBD has been elucidated in two separate states<sup>97</sup>. The putative binding location of CBD was identified as the region between helix 6 of one monomer and helix 5 of the adjacent monomer (see Figure 17), a general schematic of which can be found in the Supplementary Material. By using the information provided from the cryo-EM structures, we can identify regions of sequential homology and

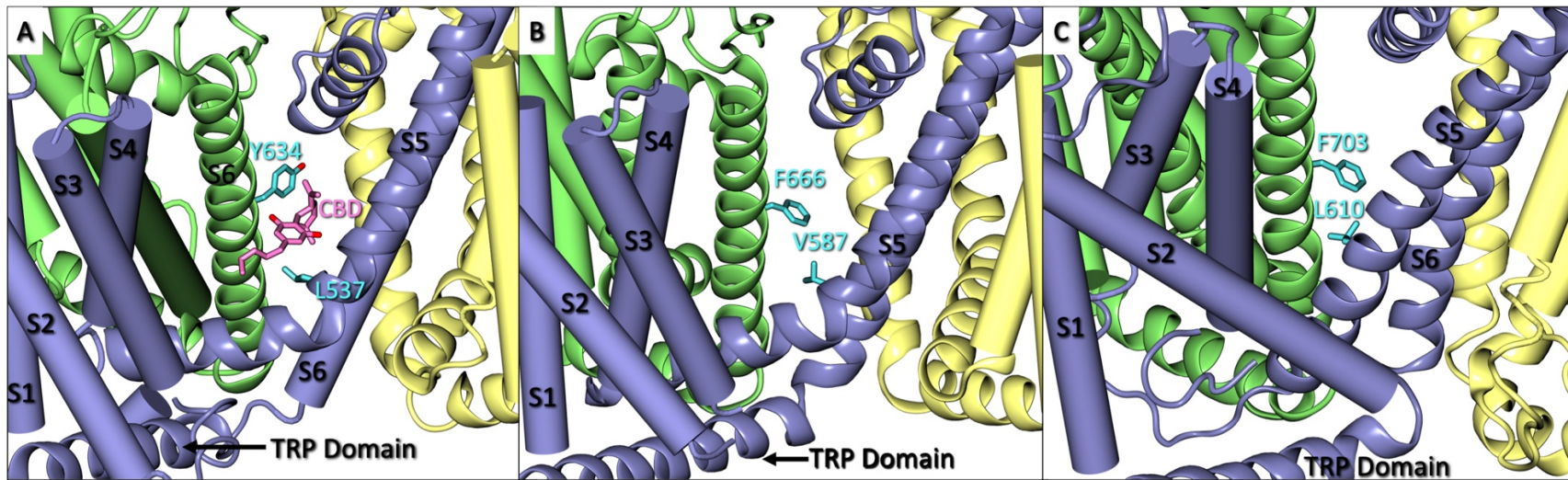


structural similarity in the putative CBD binding site across the ionotropic cannabinoid receptors. The sequence alignment (Figure 15) details the similarities between rTRPV2 and hTRPV2, as well as the human sequence of other ionotropic cannabinoid receptors TRPV1, TRPV3, TRPV4, TRPA1, and TRPM8. To get an idea of the binding site, residues within 10 Å of the putative CBD binding location in rTRPV2 these have been highlighted for analysis and directly compared to the other ionotropic cannabinoid receptors. A visual representation of the putative binding site(s) in three ionotropic cannabinoid receptors can be seen in Figure 16.

**Figure 15.** A truncated version of the human sequence alignment of six ionotropic cannabinoid receptors and rTRPV2. CBD has been resolved in rTRPV2 in two separate states and residues within 10 Å of the putative binding site of CBD have been highlighted and are shown here as a reference (yellow row). Comparable regions within the human ionotropic cannabinoid receptors have been aligned. Residues within hTRPV1 (red row), hTRPV2 (orange row), hTRPV3 (green row), hTRPV4 (blue row), hTRPA1 (purple row), and hTRPM8 (pink row) that are the same as the reference (rTRPV2) are shown in pale green. Residues that are of a similar type to the reference are shown in orange, and divergent residues are shown in red. The double starred residues, L537 and Y634, indicate the two residues that were noted to have rotameric changes from the apo to the CBD-bound structure of rTRPV2 and are visualized in Figure 2. Single starred residues are within 5 Å of bound CBD and are marked for easy vertical comparison across the ionotropic cannabinoid receptors.

<b>&gt;Q8NER1\</b>		<b>hTRPV1</b>	
...	569 570 571 572 573 574 575 576 577 578 579 580 581 582 583 584 585 586 587 588	...	635 636
I	E K M I L R D L C R F M F V Y I V F L	C L	
<b>&gt;Q9Y5S1\</b>		<b>hTRPV2</b>	
...	527 528 529 530 531 532 533 534 535 536 537 538 539 540 541 542 543 544 545 546	...	614 615
I	Q K V I L R D L L R F L L I Y L V F L	S L	
<b>&gt;Q9WUD2\</b>		<b>rTRPV2</b>	
...	529 530 531 532 533 534 535 536 537 538 539 540 541 542 543 544 545 546 547 548	...	597 598
I	Q K V I L R D L L R F L L V Y L V F L	S L	
<b>&gt;Q8NET8\</b>		<b>hTRPV3</b>	
...	579 580 581 582 583 584 585 586 587 588 589 590 591 592 593 594 595 596 597 598	...	629 630
I	Q K V I L R D V L K F L F V Y I V F L	V L	
<b>&gt;Q9HBA0\</b>		<b>hTRPV4</b>	
...	602 603 604 605 606 607 608 609 610 611 612 613 614 615 616 617 618 619 620 621	...	666 667
I	Q K I L F K D L F R F L L V Y L L F M	L L	
<b>&gt;O75762\</b>		<b>hTRPA1</b>	
...	862 863 864 865 866 867 868 869 870 871 872 873 874 875 876 877 878 879 880 881	...	- -
L	E - V I L K T L L R S T V V F I F L L	- -	
<b>&gt;Q7E2W7\</b>		<b>hTRPM8</b>	
...	859 860 861 862 - 863 864 865 866 867 868 869 870 871 872 873 874 875 876 877	...	941 942
L	Q R M - L I D V F F F L F L F A V W M	A H	

Figure 16. (A) A close up of CBD (pink) bound in rTRPV2 (adapted from PDB: 6U88) with Y634 and L537 in cyan. Helices S1–S4 and S6 are shown as cartoon tubes with S5, the pore helix, and the TRP domain shown as cartoon ribbons. (B) A close up of hTRPV3 (adapted from PDB: 6MHO) with comparable residues F666 and V587 shown in cyan. Helices S1–S4 are shown as cartoon tubes and S5-TRP domain are shown as cartoon ribbons. (C) A close up of *Xenopus tropicalis* TRPV4 (adapted from PDB: 6BBJ) which shares 78% sequence homology with human TRPV4. F703 and L610 are shown in cyan. Helices S1–S4 are shown as cartoon tubes, and S5-TRP domain are shown as cartoon ribbons.



## TRPV1

One of the most well-studied TRP channels is TRPV1, which shares an overall sequence identity of 50% with hTRPV2<sup>125</sup>. TRPV1 is primarily known for its activation via vanilloid agonists, like capsaicin, and the subsequent desensitization it undergoes leading to the paradoxical analgesic effect elicited<sup>126</sup>. This effect is sought after for its potential use in pain therapies and is the basis of how some current topical-based therapies work, like Capzasin cream. TRPV1 shares the highest sequence identity within the putative CBD binding site as described above at 79%, second only to TRPV2 itself. Additionally, CBD is reported to have the highest efficacy of the vanilloid subfamily at TRPV1 ( $\sim 78\%$ )<sup>127</sup>.

Two residues that have been identified for their involvement of CBD binding in TRPV2, L535, and Y634<sup>97</sup>, can also be found in TRPV1 as L577 and Y672. L577 and Y672 are in comparable sequential and physical locations to their TRPV2 counterpart in addition to fairly consistent sequence homology about the rest of the binding site as seen in Figure 15.

However, the tyrosine in either channel is unlikely to have a direct interaction with CBD in the putative binding site. Assuming the CBD binding site in TRPV1 is the same as that of TRPV2, this orientation of tyrosine would likely have minimal impact in the binding affinity of CBD, especially due to the reported role of Y634 in TRPV2 as a hydrophobic shield from water in the pore. Due to this, it is possible that Y672 in TRPV1 is still providing some degree of hydrophobic shielding for CBD should it bind in the same location, while the lipophilic interactions via L577 and surrounding lipophilic residues remain intact.

## TRPV2

TRPV2 is the thermoTRP with the highest temperature activation threshold among its subgroup with activation occurring above  $52^{\circ}\text{C}$ <sup>114</sup>. While TRPV2 is insensitive to capsaicin, it

undergoes similar desensitization following activation and is deeply involved in inflammation and chronic pain<sup>6</sup>. The cryo-EM structure of CBD in rTRPV2 was published in 2019 by Pumroy et al. and this structure allows us to delve deeper into how CBD interacts with TRPV2 specifically<sup>97</sup>, but also hypothesize on the binding of CBD in other TRP channels that can be modulated by this cannabinoid ligand via sequential comparison and computational exploration.

A comparison of the rTRPV2 and hTRPV2 putative binding site of CBD shows 96% sequence homology with few instances of changes between hydrophobic residues, such as valine (rTRPV2) to isoleucine (hTRPV2). Beyond this, the polarity and aromaticity of residues within the binding site between rTRPV2 and hTRPV2 remains consistent (see Figure 15). Rotameric comparisons between the apo (PDB: 6U84 and 6U86) and CBD-bound (PDB: 6U8A and 6U88) cryo-EM structures for rTRPV2 revealed several rotameric changes throughout. Though most rotameric changes were peripheral and not within the defined scope of the CBD binding site, two rotameric changes were located within this scope. In the apo structure, Y634 takes on a g<sup>+</sup> conformation while the CBD-bound structure shows Y634 adapting a trans conformation (Figure 16A). This movement shifts the hydroxyl group of the tyrosine toward the pore, believed to create some hydrophobic shielding for CBD from ions and water found there<sup>97</sup>. Additionally, L537 shows a rotameric change, going from trans in the apo structure to g<sup>+</sup> in the CBD-bound structure which is reported to allow accommodation for the aromatic ring of CBD. With two CBD-bound cryo-EM structures identifying CBD in the same general location<sup>97</sup> and a reported efficacy of ~67% at TRPV2<sup>127</sup>, exploring this region should provide insight on the binding mode of CBD.

### TRPV3

TRPV3 is predominantly expressed in the brain<sup>128</sup> as well as several peripheral tissues like the skin and tongue<sup>129</sup>. Additionally, TRPV3 acts as a thermosensor for innocuous warm temperatures, activating between 33 and 39°C<sup>95</sup>. During a screen with a variety of phytocannabinoids, CBD was observed to have a potency similar to that of its typical agonist<sup>49</sup>, carvacrol, though the efficacy of CBD at TRPV3 is poorer than that of TRPV1 and TRPV2 (~54 vs. ~78, ~67%, respectively). With 77% sequence homology in the CBD putative binding site, some small differences in sequence might be responsible for the low efficacy.

In TRPV2, Y634 is said to provide hydrophobic shielding for CBD by shifting to point the polar hydroxyl group toward the pore of the channel, preventing solvation of the location where CBD is proposed to bind. In TRPV3, this tyrosine is replaced by F666, losing the polar hydroxyl group which could lessen the shielding effect, but also occlude the binding site due to not being able to twist and point to the pore. Another sequential change that could impact the efficacy of CBD at TRPV3 is the change of leucine (L537, TRPV2) to valine (V587, TRPV3). While both hydrophobic, the shorter chain of the valine might affect the extent of the lipophilic interactions within TRPV3 (Figure 16B). While the efficacy of CBD at TRPV3 is generally considered poor, it still retains a submicromolar potency of around 0.51  $\mu\text{M}$ <sup>127</sup>.

### TRPV4

The final vanilloid subfamily member discussed in this perspective is TRPV4. Similar to TRPV3, TRPV4 responds to warm thermal changes of temperatures ranging from 25 to 34°C<sup>4</sup>. Additionally, this channel, located in cutaneous A and C fibers<sup>130</sup>, plays a role in skin barrier function and nociception<sup>131</sup>.

Initially, it appears that there are only moderate differences in the putative CBD binding site in TRPV4 and TRPV2 due to the 68% sequence homology of this region. However, CBD is the least efficacious at TRPV4 with a mere 15% efficacy<sup>127</sup>. The aspect that likely has the largest effect on CBD binding is the structurally different helical arrangement that TRPV4 takes in comparison to its family members. TRP channels in this subgroup typically adopt a “straddling” formation of S1–S4 over the TRP domain where S1 and S4 reside on one side of the TRP domain and S2 and S3 reside on the other. TRPV4, however, does not appear to follow suit. In a series of recently published cryo- EM structures of *Xenopus tropicalis* TRPV4, which maintains 78% sequence homology with hTRPV4<sup>132</sup>, helical packing of S1–S4 against S5–S6 was observed to be different from that of other resolved TRPV channels, such as TRPV1, TRPV2, and TRPV3<sup>132</sup>. Helices S1, S3, and S4 all appear on one side of the TRP domain, leaving S2 on the other. This differentiation in helical arrangement, as well as the angle at which S2 takes on in TRPV4, alters the shape of the S1–S4 bundle (see Figure 16C), affecting the putative CBD binding site by altering the interaction between S5 and S6 of adjacent monomers. Deng et al. note that this unique S1–S4 packing arrangement may be due to truncation of TRPV4, though it is reported that only the unstructured N- and C-termini were truncated. Additionally, multiple TRPV4 structures with various cations were resolved, all maintaining this feature. The S4 helix obstructs the putative CBD binding site located in this channel, lending support that this strange arrangement of S1–S4 helices is plausible rather than an artifact of truncation and/or crystallization.

### **TRPA1**

The first member of the ankyrin subfamily, TRPA1, can be found co-expressed with TRPV1 in a subset of peripheral sensory neurons<sup>124</sup>. TRPA1 is activated by isothiocyanates,

pungent compounds found in mustard, garlic, and onions<sup>133</sup>, covalently binding to an internal cysteine or lysine residue located on its extensive ankyrin repeat domain. With regard to its role as a thermoTRP, TRPA1 can be found on the lowest end of the temperature scale, activating below temperatures of 17°C<sup>116</sup>. Additionally, TRPA1 plays an important role in neuropathic and inflammatory pain through the mediation of bradykinin-evoked and mechanical hyperalgesia<sup>109</sup>.

CBD has been shown to act as an agonist at TRPA1 with an efficacy of 108% compared to its usual agonist of allylisothiocyanate (100µM)<sup>127</sup>, and while the putative CBD binding site is structurally comparable to that of the TRPVs, there is low sequence homology within the binding site (~30%). Similar to the previous TRP channels discussed, TRPA1 maintains a leucine in the same position as in TRPV2 (L870 and L537, respectively). Looking at the sequence alignment (Figure 15), hydrophobic residues are readily present and are, in fact, pointing in the region where CBD is proposed to bind. However, since the efficacy of CBD at TRPA1 is considerably higher than TRPV2, the sequence homology with TRPV2 might be of little importance in this case.

### **TRPM8**

Finally, the last member of the ionotropic cannabinoid receptors that will be discussed here is TRPM8. TRPM8 is activated by temperatures below 27°C<sup>134</sup> as well as by compounds that elicit a “cooling” effect, such as menthol, eucalyptol, and icilin<sup>110,135,136</sup>. Compounds tested at TRPM8 are usually tested for their antagonism against both menthol and icilin as they are reported to activate the channel in slightly different locations<sup>24,136–138</sup>. For both ligands, CBD acts as an antagonist at submicromolar concentrations<sup>61</sup>.

Because of this, it is slightly more difficult to hypothesize if CBD binds in the same location in TRPM8 as it would in the TRPV or TRPA subfamilies. The binding site in TRPM8



has ~30% sequence homology with that of TRPV2, but because CBD acts as an antagonist, the location of binding as well as the movements required by the channel to become inactive, could require different mechanisms than activation of the other ionotropic cannabinoid receptors.

### **Concluding remarks and future directions**

Targeting the endocannabinoid system has been a promising strategy for the modulation of pain<sup>100,107,139,140</sup>. One in particular, CBD, has gained mainstream attention in recent years due to over the counter (OTC) uses in balms, creams, tinctures, and more for joint and muscle pain, neuroprotection, anti-nausea, anti-inflammation, and anxiolytic properties<sup>141</sup>, as well as pharmaceutical uses in drugs, such as Sativex, a 1:1 CBD:THC oromucosal spray has been approved for use in the UK to aid in the relief of multiple sclerosis (MS) related symptoms, and Epidiolex, an FDA-approved CBD-based drug used to treat two severe forms of pediatric epilepsy. Additionally, there is literature precedent to support the claims of CBD as a means to treat other conditions, such as arthritis<sup>142</sup>, anxiety<sup>143</sup>, and the potential for treatment in substance use disorders<sup>94,144</sup>. By seeking to understand the targets of cannabinoid ligands, and particularly where they bind, researchers will be better equipped to design drugs to treat chronic pain disorders.

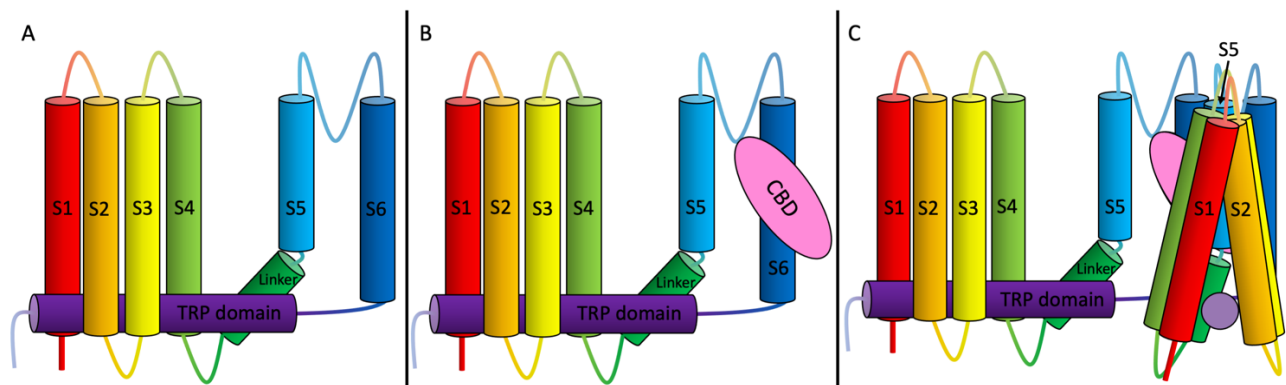
Recently, a dimerized version of CBD (CBDD or cannabitwinol) has been isolated, structurally characterized, and tested by Chianese et al. at the ionotropic cannabinoid receptors<sup>127</sup>. What was discovered was that CBDD was found to be nearly inactive at TRPV1 and TRPV2, in contrast to the good efficacies of CBD at these two channels, while exhibiting poor efficacy at TRPV3 and TRPV4, and retaining activity as a TRPA1 activator (~97% efficacy) and TRPM8 inhibitor against icilin ( $IC_{50} = 3.9 \pm 0.4 \mu M$ ). One structural factor that may play a role in how well CBDD interacts with TRPA1, despite its doubling in size, is the

TRP-like domain which lies lower in the intracellular region than a TRP domain<sup>23</sup>. The TRP domain found in TRPV1–4 and TRPM8 is nestled just below the lower leaflet in the intracellular region of the cell. In TRPV2, the S1–S4 domain straddles the TRP domain which acts as a “floor” to the putative CBD binding site. Since this feature is not present in TRPA1, instead having a TRP-like domain, more space is created in the putative binding region, potentially allowing for easier access by CBD and its dimerized sibling. If we hypothesize that CBDD binds in the same location as CBD in TRPA1, it is sensible to think that the increase in room from the TRP-like domain would allow more space for CBDD to fit, even if one-half of dimerized CBD were to bind, potentially leaving the other half “left out” of the binding site. Conversely, based on the features discussed here, CBDD would have limited space in TRPV1–TRPV4.

The comparison of the putative CBD binding site presented here is based on the sequence alignment of the ionotropic cannabinoid receptors and previously published crystal or cryo- EM structures from a molecular modeling perspective. Ideally, future work would combine cryo- EM/crystal structures of CBD interacting with the other TRP channels in addition to site-directed mutagenesis to further investigate these interactions.

## Supplementary Material

**Figure 17.** Panel A) A cartoon image of one monomer of a TRP channel. S1 is shown in red, S2 in orange, S3 in yellow, S4 in light green, the S4-5 linker in dark green, S5 in light blue, S6 in dark blue, and the TRP domain (present in TRPV1-4 and TRPM8, comparable to TRP-like domain present in TRPA1). Panel B displays the same monomer with CBD, shown as a pink oval, in one-half of the putative binding site. Panel C displays a second monomer, with the same color-coding as panels A and B, pivoted at a 90°-degree angle to complete the putative binding site of CBD with S6 of the first monomer (Panel B) shown “behind” the CBD molecule and S5 of the second monomer (Panel C) shown “in front” of the CBD molecule, forming the putative binding site.



## CHAPTER V: TRPV1 ACTIVATION BY ANANDAMIDE VIA A UNIQUE LIPID PATHWAY

**Chanté Muller, Diane L. Lynch, Dow P. Hurst, and Patricia H. Reggio**

Journal of Chemical Information and Modeling, 2021, 10.1021

Published: 15 November 2021

Department of Chemistry and Biochemistry, University of North Carolina at Greensboro, Greensboro, NC 27412, USA

### Abstract

The capsaicin receptor, transient receptor potential vanilloid type 1 (TRPV1), is a polymodal channel that has been implicated in the perception of pain and can be modulated by a variety of cannabinoid ligands. Here we report TRPV1 channel activation by the endocannabinoid, anandamide (AEA), in a unique, peripheral binding site via extended MD simulations. These results aim to expand the understanding of TRPV1 and assist in the development of new TRPV1 modulators.

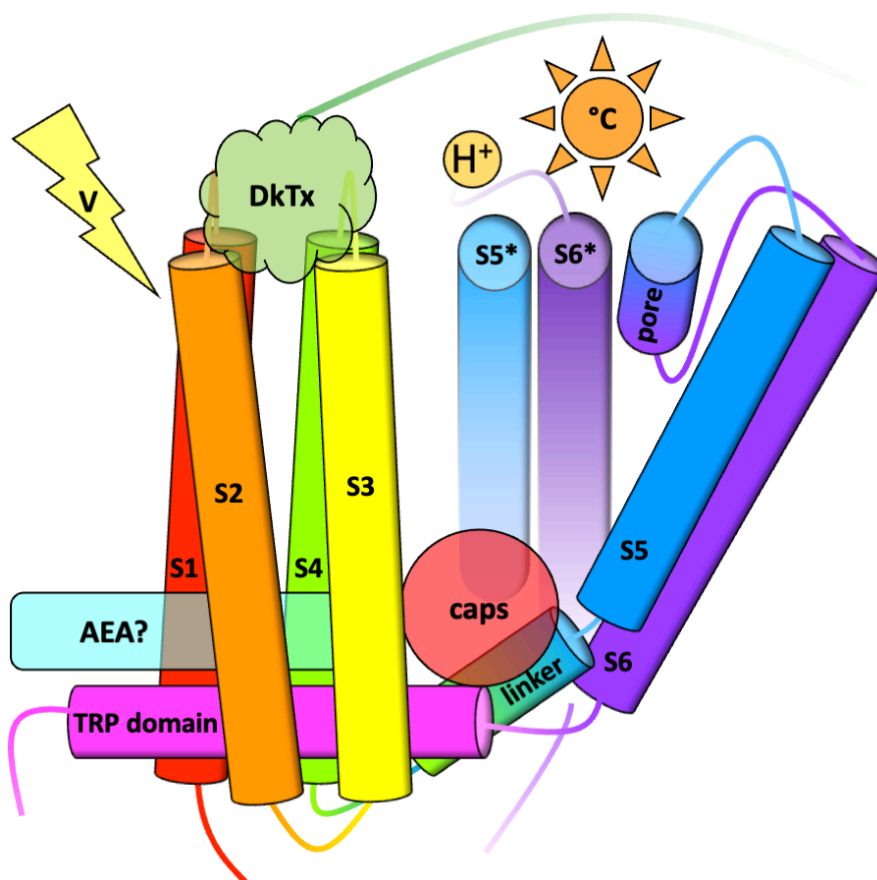
### Introduction

As the opioid epidemic progresses, the need and development of therapies to treat chronic pain conditions is becoming increasingly more relevant<sup>94</sup>. From alleviating pain in childbirth to surgical anesthesia<sup>104</sup>, Cannabis has a lengthy history dating back millennia for its use in pain management<sup>101,104,145</sup>. Ionotropic cannabinoid receptors (ICRs) are a subset of transient receptor potential (TRP) ion channels that can be modulated by cannabinoid ligands<sup>109,146,147</sup>. One of these, transient receptor potential ion channel vanilloid type 1 (TRPV1), also known as the capsaicin receptor, is the focus of this paper.

TRPV1 is a homotetrameric, polymodal ion channel located in the peripheral and central nervous systems<sup>148,149</sup> that spans the width of the lipid bilayer, acting as a passageway for ions

from one side of the cell to the other<sup>148</sup>. Each monomer is comprised of six transmembrane helices (S1–S6) with helices S5 and S6 forming a central pore gated by two sets of residues, G644 (upper) and I680 (lower), which open upon activation. TRPV1 is activated by a variety of stimuli<sup>72,78,111,150–153</sup> (Figure 18) including cannabinoid ligands<sup>72</sup>. Upon activation, the channel opens allowing cation permeation with a preference for calcium ions<sup>111</sup>, which elicits a burning, tingling sensation. Downstream effects eventually lead to channel desensitization, rendering the channel refractory to further stimulation<sup>154</sup>. This reduction in neuronal activity leads to paradoxical analgesia<sup>37</sup>, which is the basis behind TRPV1-mediated pain relief. This effect can potentially be exploited to aid in the development of new therapies to treat chronic pain conditions, making TRPV1 an ideal target to investigate with the hopes of developing new treatments to treat chronic pain conditions without the use of opioid medications.

**Figure 18. A graphical scheme of one monomer of TRPV1 with reported and putative locations of channel stimuli indicated as shown. V indicates voltage – activates via S1-S4 helices, DkTx shown for only one half of the bidentate structure and H<sup>+</sup> indicating protons – activate via extracellular region, °C indicating heat – activates via pore domain, caps representing capsaicin – activates via vanilloid binding pocket (VBP), while AEA represents the possible location of TRPV1 binding. Helices S5\* and S6\* refer to the S5 and S6 helices of the adjacent monomer, included to complete the VBP.**



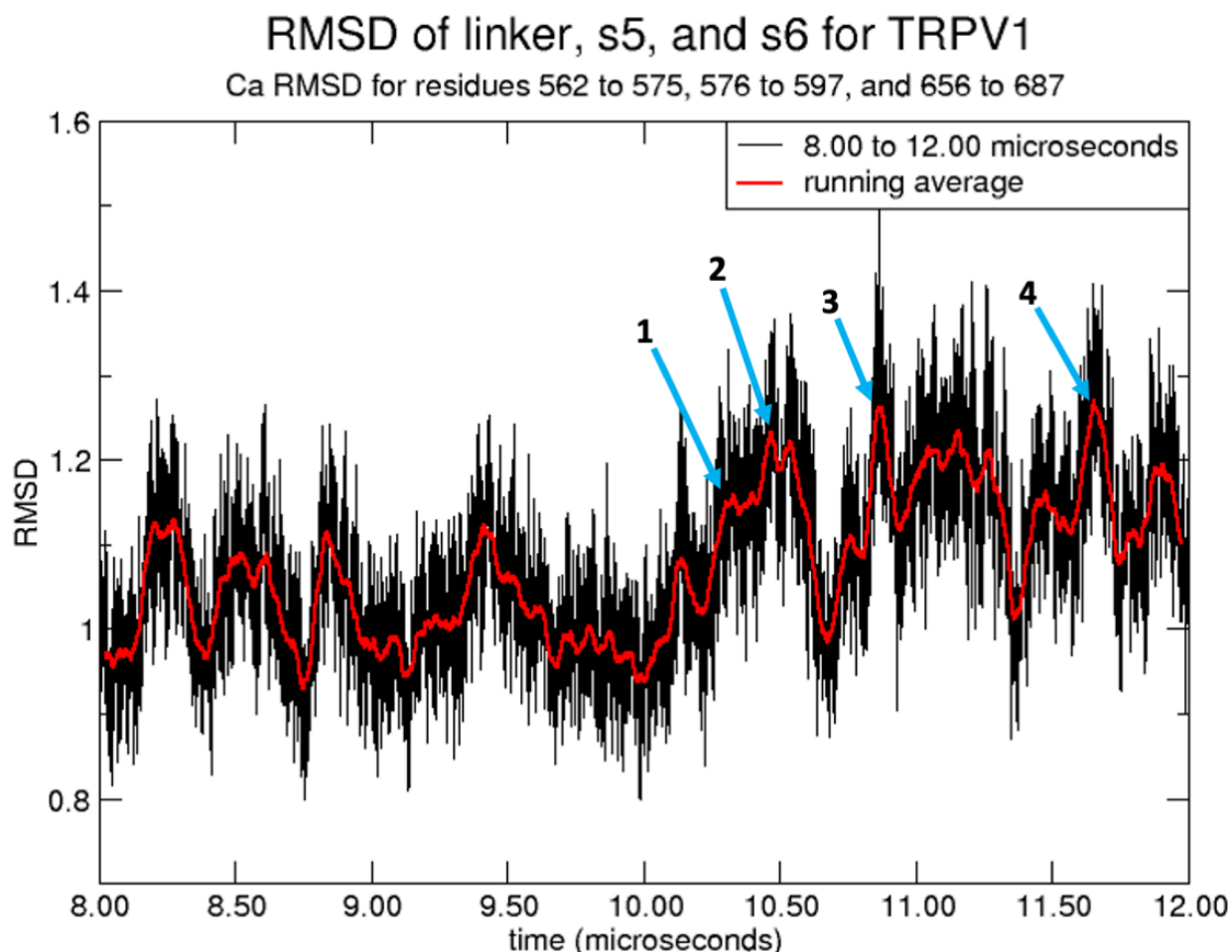
The location of cannabinoid ligand binding at TRPV1 has not been very well-studied, and several cannabinoid ligands are reported to activate TRPV1, including the endogenous cannabinoid ligand anandamide (AEA)<sup>41,155</sup>. Muller and colleagues previously reported AEA to enter a unique location formed between helices S1–S4 (termed the “tunnel”) at the periphery of the channel in early molecular dynamics (MD) simulations<sup>156</sup>, and it may activate TRPV1 from this location. Because of the involvement of both the endocannabinoid system and TRPV1 in chronic pain conditions, studying their interactions could provide a clearer image of how AEA

activates TRPV1. Here, we analyze and discuss the data collected from further MD simulations focusing on TRPV1 channel activation in response to AEA ligand binding.

## **Results and Discussion**

Several metrics were used to define, assess, and quantify states of interest. As a primary metric, the distance of adjacent I680 C $\alpha$  atoms were measured and compared to the apo (PDB: 5IRZ) and active TRPV1 structures (PDB: 5IRX) and the frame from which the simulation was started (Figures 22A–D, 23A–C, and Table 8). For a time-dependent measurement of I680 C $\alpha$  atoms in the full trajectory, see Figure 24. In addition to this metric, the RMSD of the components related to TRPV1 channel activation, the S4–S5 linker, S5, and S6, was measured (Figure 19). Helices S5 and S6 line the pore of TRPV1, moving outward upon activation, and it is believed that two residues located on the end of S4 and the S4–S5 linker, R557 and E570 (Figure 25), are responsible for this movement via the formation of an ionic lock<sup>156</sup>. Because of this, the RMSD of the S4–S5 linker, S5, and S6 was used to identify central channel movements while additionally tracking the R557–E570 distances as the trajectory progressed (Figure 26; see the SI for methods).

**Figure 19.** The S4-S5 linker, S5, and S6 (combined) RMSD from 8.00-12.00 microseconds. Peak 1 represents the region where the increased RMSD of the central helical structures begins to maintain its movements, peak 2 indicates the first location of partial opening, peak 3 indicates where the split opening occurred, and peak 4 indicates an instance where the channel allows a water molecule to pass while in a partially open state.

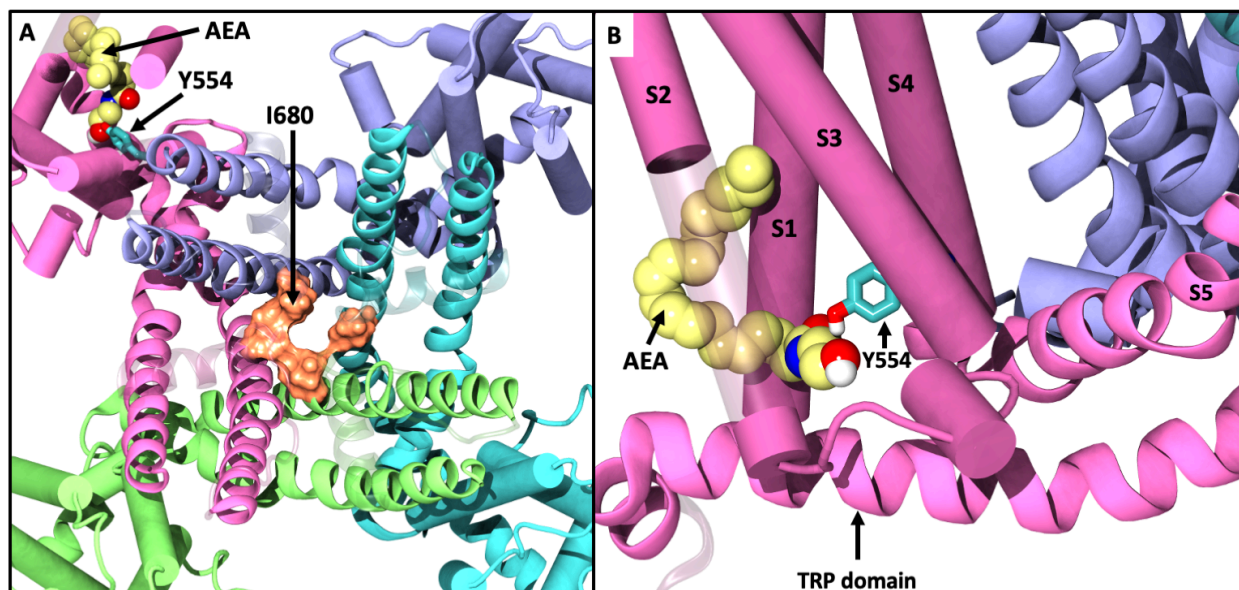


Runs 2a and 2b of the unbiased AEA/TRPV1 MD were started from frame 18,822, near the 4.7  $\mu$ s time point of run 1 (see the SI for previous work). In this frame, the S1-S4 tunnel of monomer B was occupied by an AEA ligand interacting with Y554. Trajectory 2a ran for a total simulation time of  $\sim 14$   $\mu$ s with channel activation occurring near 11  $\mu$ s. The RMSD of the S4-S5 linker, S5, and S6 was collected for the full trajectory (Figure 27), but due to the large data sets generated by Anton2, a subset of the RMSD is shown in Figure 19, where we bring attention to four representative areas.



Figure 19 shows several peaks indicating various shifts in RMSD of the central TRPV1 structures during 8.00–12.00  $\mu$ s. Peak 1 points where the RMSD begins to maintain its increase. Peak 2 indicates where the first instance of partial lower gate opening (Figure 20a) was observed in the trajectory, which shows that the AEA bound in monomer B maintained its occupancy in the S1–S4 tunnel, as well as its interaction with Y554 (Figure 20b). To measure the consistency of the AEA/ TRPV1 interaction, a full analysis of AEA contact with Y554 in each of the four tunnels (A–D) was performed (Figure 28).

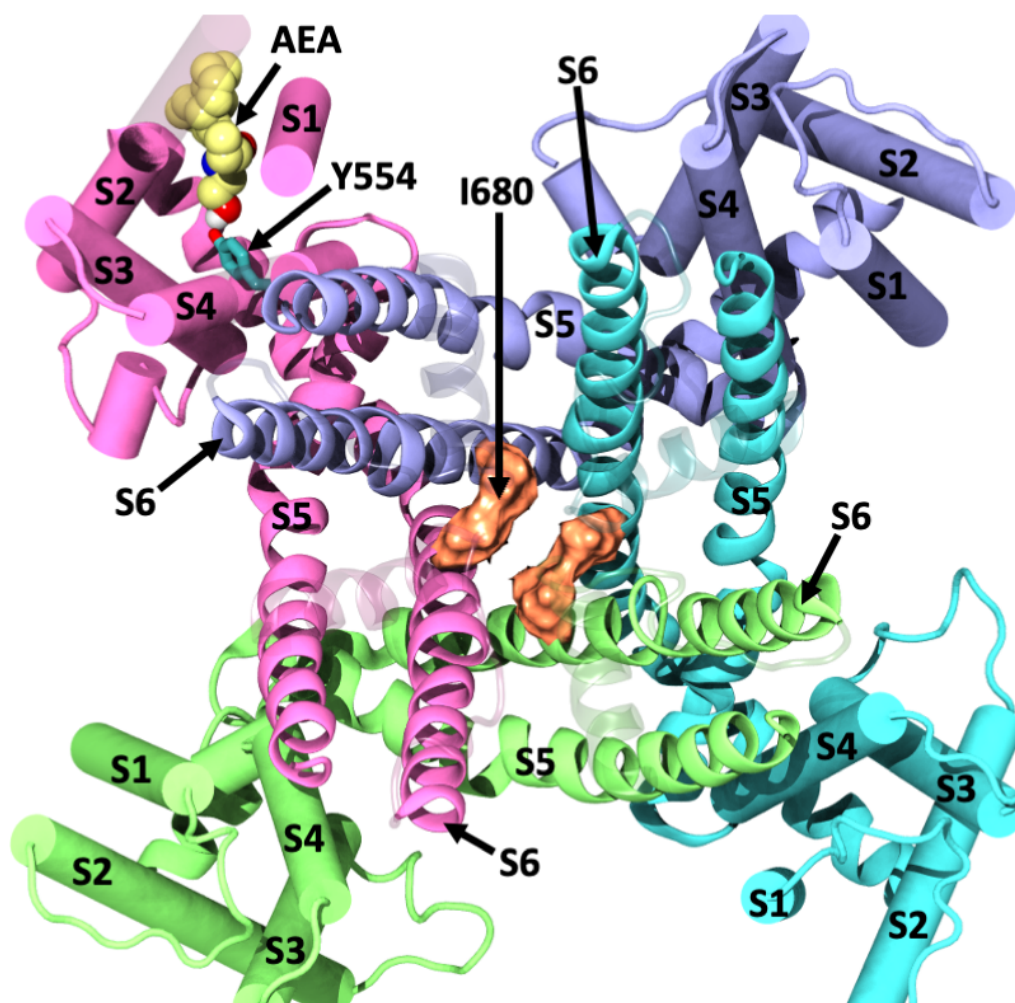
**Figure 20. An extracellular view of TRPV1 with each monomer in a different color. Helices S1–S4 are shown as cartoon tubes and S4–TRP domain are shown as helical ribbons. The lower gate (I680, orange surface) shows a partial opening with AEA (yellow VDW) occupying one of the four equivalent tunnels and interacting with Y554 (cyan licorice). Figure 3b shows a close-up side view from the lipid bilayer of the AEA (yellow) headgroup interacting with Y554 (cyan).**



Peak 3, near 10.8  $\mu$ s, indicates the highest change in RMSD of the S4–S5 linker, S5, and S6 thus far and correlates with occurrence of a “split” channel opening (Figure 21, additional sequential openings in Figure 29A–C). Typically, the four I680 residues that form the lower gate in TRPV1 maintain their interactions with each other via hydrophobic interactions, while the

four G644 residues that comprise the upper gate showed great lability in early MD simulations, allowing the pore between the two gates to fill with water and ions quickly. This suggests that the higher barrier to TRPV1 activation lies in the separation of the I680 residues from one another. This separation can be measured via the adjacent I680 C $\alpha$  atom distances from one another (Figure 24). In Figure 21, we see a split down the center of the I680 quartet and a reasonably symmetrical change in C $\alpha$  atoms distances (Figure 22C). The split opening lasted over 1 ns and allowed several water molecules to move from the pore region to the intracellular side of the cell (as represented in Figure 30).

**Figure 21.** An extracellular view of TRPV1 down the central pore. The lower gate (I680, orange) shown to be in a split opening while AEA (yellow) maintains its occupancy in the S1-S4 tunnel and maintaining interaction with Y554 (cyan).



While the trigger of downstream effects that leads to the analgesic properties of TRPV1 in a biological system is the passage of calcium ions not water, the vdW radii of water and  $\text{Ca}^{2+}$  ions are comparable (2.75 and 2.31 Å, respectively), and therefore highly relevant to this result. If it is possible for water molecules to flow through, then calcium ions would be able to as well. The observance of water molecules passing through the lower gate may provide indication that channel activation due to AEA binding has occurred. No cations were observed passing through the I680 gate in the simulation, but a sodium ion held residence in the pore for nearly the entire

trajectory. As an additional metric used to measure the I680 separation and thus level of pored openness, the solvent accessible surface area (SASA) of I680 was calculated (Figure 31). SASA provides a visual of solvation of I680—the more exposed I680 is, the more solvated the surface. Additionally, the number of water molecules occupying the pore (with a 2 Å buffer above G644 and below I680 to accommodate gate fluctuations) was quantified (see Figures 32 and 33A–B).

After ~1 ns of sustained split opening, the RMSD of the S4–S5 linker, S5, and S6 began to decrease, returning to a closed state. Smaller and shorter periods of RMSD increases still occurred after the split opening, with I680 fluctuating between closed and partial/split open states. During one instance of partial opening, indicated by peak 4 of Figure 19, a single water molecule was able to be tracked through I680, moving from the pore to the intracellular region (Figure 34). The passage of the single water molecule through this partially opened state suggests that ion passage is still possible even when the I680 residues are not in a split (Figure 21) or full (PDB 5IRX; see Figure 22C–D) opening. Comparing RMSD from Figure 19 with I680 SASA (Figure 31) revealed that increases in both occurred at the same time period. After peak 4, TRPV1 RMSD of the S4–S5 linker, S5, and S6 decreases and the I680 C $\alpha$  distances return to a closed state.

Since our data suggests that AEA binding in TRPV1 occurs through the S1–S4 tunnel, an additional plot of the S1–S4 helices RMSD was performed (see Figure 35). The time points of peaks present in the S1–S4 tunnel RMSD are similar to those observed in the S4–S5 linker, S5 and S6 as shown in Figure 19. Additionally, the ionic lock of monomer B was present throughout the majority of run 2a, suggesting that the AEA occupation in this tunnel helped to facilitate this formation (Figure 26). These data indicate that AEA binding likely directly affects the S1–S4

tunnel, which then indirectly affects the S4–S5 linker and other central structures via the formation of the ionic lock.

After the success of run 2a, where channel opening occurred, run 2b was performed to determine if the previous results could be independently replicated. Run 2b also yielded channel opening in response to AEA binding. Data can be found in Figures 36–40 and Table 9.

## Conclusions

Previous studies have used concatemeric constructs and mutagenesis to show that occupation of one TRPV1 binding site is sufficient for channel activation<sup>157,158</sup>. As previously reported from our early MD simulations, AEA has a higher probability to bind in the S1–S4 tunnel region than in the VBP in TRPV1<sup>156</sup>. In the extended Anton2 simulations described here, AEA occupies at least one of the four identical S1–S4 tunnels and triggers TRPV1 channel activation in two separate independent trajectories from this novel binding site. After the channel activation event, the channel begins to revert to a closed state, which is shown by the decrease of the S4–S5 linker, S5, and S6 RMSD (Figure 19), the decrease of water molecules quantified in the pore, the SASA of I680, and the decrease of C $\alpha$  distances of I680. (Figures 32, 31, and 24). The RMSD of the S1–S4 helices show structural movements that are comparable to those observed in the S4–S5 linker, S5, and S6 helical movements and are likely triggered by internal AEA ligand binding, which appear to influence the S4–S5 linker, S5, and S6 leading to channel activation.

Because of the concerted actions that TRPV1 undergoes during activation and the inherent complexity of the channel, it is difficult to determine from these simulations precisely what influences movement of the S1–S4 helices, triggering the movement of the central pore helices S5 and S6. However, the work presented here provides a foundation for further

exploration of the AEA novel S1–S4 binding site, including more in-depth simulation studies. Possible studies include investigating the pinwheel-like arrangement of the monomeric subunits and how the movement of one affects the movement of all. Additionally, unbiased TRPV1 simulations using other endocannabinoid ligands reported to activate TRPV1, like 2-arachidonoylglycerol (2-AG), could be performed to study how the changes in ligand structure could influence binding. Mutagenesis may also help identify the importance of Y554 for AEA binding at TRPV1 and provide experimental validation of these results. Throughout the course of our MD simulations, Y554 maintained consistent interaction with the AEA head- group. Mutation of Y554 to a nonpolar residue like phenylalanine would remove hydrogen bonding capability, while mutating to alanine would remove both hydrogen bonding and aromatic stacking capabilities, potentially reducing or ablating AEA activity at TRPV1.

The extended MD simulations discussed here show TRPV1 channel activation in response to AEA ligand binding in a unique non-VBP location in the S1–S4 tunnel in two independent simulations. The possibility of TRPV1 activation via the S1–S4 tunnel is a relatively new consideration which may help expand the current understanding of TRPV1 polymodality, allowing for more rational design of TRPV1 ligands.

## **Supporting Information**

### **Methods**

TRPV1 models were constructed from previously published crystal and cryo-EM structures (ARD PDB: 2PNN,<sup>78</sup> closed TRPV1 PDB: 5IRZ, and open TRPV1 PDB: 5IRX)<sup>73</sup> using Prime Homology Modeling, Schrödinger, Release 2018-4.<sup>159</sup> An initial relaxation of the TRPV1 model embedded in a fully hydrated POPC lipid bilayer with neutralizing ions at an ionic strength of 0.15 M NaCl (control) was performed by following the procedure of Lee et

al.<sup>160</sup> Unbiased NPT molecular dynamics (MD) simulations were performed using the CHARMM36m<sup>85</sup> force fields for protein and CHARMM36 force fields for lipids<sup>86</sup> and ions<sup>89,161</sup> at physiological temperature (310K). The CHARMM36 force fields were selected due to their maturity and to maintain consistency across all systems. The control system was equilibrated for 500 ns to ensure model stability and a frame from the equilibrated control (50 ns) was used to build the AEA/TRPV1 systems described below. All local simulations were run using the pmemd.cuda version of AMBER18,<sup>88</sup> with AMBER inputs generated using CHARMM-GUI.<sup>160</sup>

Build 1 was comprised of the equilibrated TRPV1 structure in a fully hydrated POPC lipid bilayer and 13.8 mol% AEA. During equilibration of the control system, water was observed entering the S1-S4 tunnel region. Upon closer inspection, several polar residues were found to line the tunnel. Because of this, an AEA ligand was placed outside of each tunnel (four ligands total), ensuring no incidental contact with TRPV1, with the remainder of the ligands dispersed randomly throughout the bilayer. Spontaneous entry of several AEA ligands into the tunnel region occurred with primary interactions occurring between the AEA headgroup and Y554 and Y555 of TRPV1. Build 1 was run for ~750 ns on local GPUs before being transferred to Anton2.

Build 2 was built with 13.8 mol% AEA as in Build 1, but with an AEA ligand pre-docked into each S1-S4 tunnel with AEA headgroup interactions with TRPV1 congruent to those observed in unbiased Build 1. Build 2 ran for ~370 ns on local GPUs before being transferred to Anton2.

Build 1 and Build 2 were transitioned to Anton2 and run for extended time periods using the semi-isotropic NPT ensemble at 310K and 1 bar, using the Anton multigrator framework with the Nosé-Hoover thermostat<sup>91,92</sup> and the Martyna, Tobias, Klein (MTK) barostat<sup>93</sup>. Default

Anton settings were used for the long-range interactions with a 2.5 fs timestep. All trajectories were analyzing using VMD from the University of Illinois at Urbana-Champaign.

### **Previous work**

Previously published work described two MD simulation builds that were constructed to better understand the interactions of AEA and TRPV1.<sup>156</sup> The unbiased system (Build 1) was constructed of 13.8 mol% AEA:POPC with one AEA ligand placed outside of each S1-S4 tunnel. The AEA placement outside of the tunnel was ensured to be devoid of any channel interactions with the remainder of the ligands dispersed randomly throughout the lipid bilayer. Build 2, the pre-docked AEA system, was constructed with one AEA placed inside each S1-S4 tunnel with interactions congruent to those observed during spontaneous AEA entry events from Build 1 (using methods above). Both simulations were run on local GPUs, during which time Build 2 had showed some indication of partial lower gate (I680) opening for a brief period (around 10 ps). Builds 1 and 2 were then extended for 6  $\mu$ s using the Anton2 supercomputer, but channel opening did not occur. The simulations were extended even further and the previously unreported results are discussed in the primary manuscript.



**Figure 22.** The I680 Ca atom distances of the apo TRPV1 structure (PDB: 5IRZ, A) and with I680 rendered as a surface (orange, B). The open TRPV1 structure (PDB: 5IRX) is shown in panel C with a surface rendering of I680 (orange) in panel D. Each S6 helix is labeled, each monomer is colored separately with the I680 shown in orange with monomer labels (A, B, C, D).

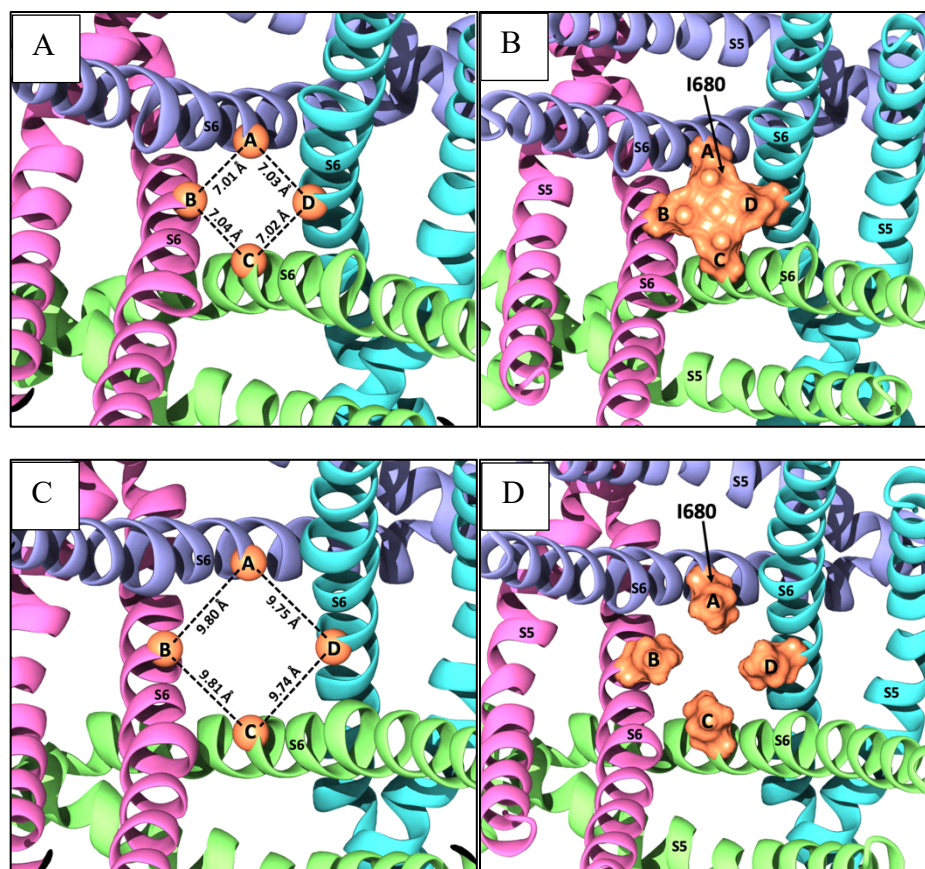


**Figure 23.** The I680 Ca atom distances of the starting TRPV1 structure (frame 18,822 from run1) for runs 2a and 2b (left), the split structure (center), and the partial open structure where water passage was observed (right). Each S6 helix is labeled, each monomer is colored separately with I680 Ca atoms shown in orange with monomer labels (A, B, C, D).

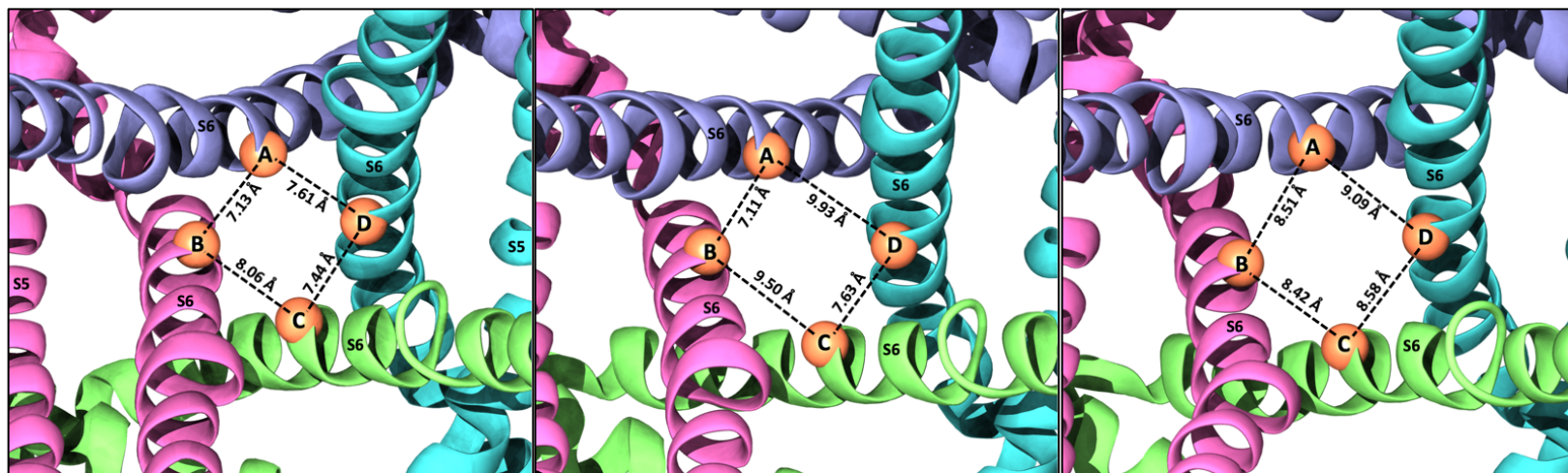


**Table 8. I680 Ca distances between bonds A-B, B-C, C-D, and D-A as shown in Figures 22 and 23. The distances of 5IRZ and 5IRX are used to gauge the level of openness of the lower gate. Since these values come from cryo-EM structures and are static, we use them as reference points rather than strict definitions of “closed” and “open”. The “MD start” values are listed as the closed structure from which runs 2a and 2b were started. These values are used as the dynamic reference of the closed state.**

<b>bonds</b>	<b>apo (5IRZ)</b>	<b>MD start</b>	<b>partial</b>	<b>split</b>	<b>open (5IRX)</b>
A-B	7.01 Å	7.13 Å	8.51 Å	7.11 Å	9.80 Å
B-C	7.04 Å	8.06 Å	8.42 Å	9.50 Å	9.81 Å
C-D	7.02 Å	7.44 Å	8.58 Å	7.63 Å	9.74 Å
D-A	7.03 Å	7.61 Å	9.90 Å	9.93 Å	9.75 Å

Figure 24. The measurements of adjacent I680 Ca atoms for the trajectory of run 2a. The black line indicates each individual measurement for every 50<sup>th</sup> frame of the trajectory (equivalent to one frame every 12 ns, again, due to large datasets from Anton2). The red line represents the running average. The yellow horizontal line roughly translates to the I680 Ca distances found in the static apo/closed (PDB: 5IRZ) state, while the pink horizontal line is the maximum I680 Ca atom distance for the closed state from our MD where water or ions cannot pass through. Blue arrows indicate locations where the split opening occurred, around 10.8  $\mu$ s, and the green vertical lines indicate the location where the partial opening described in Figure 6 occurred, around 11.6  $\mu$ s.

### 680 Ca distances

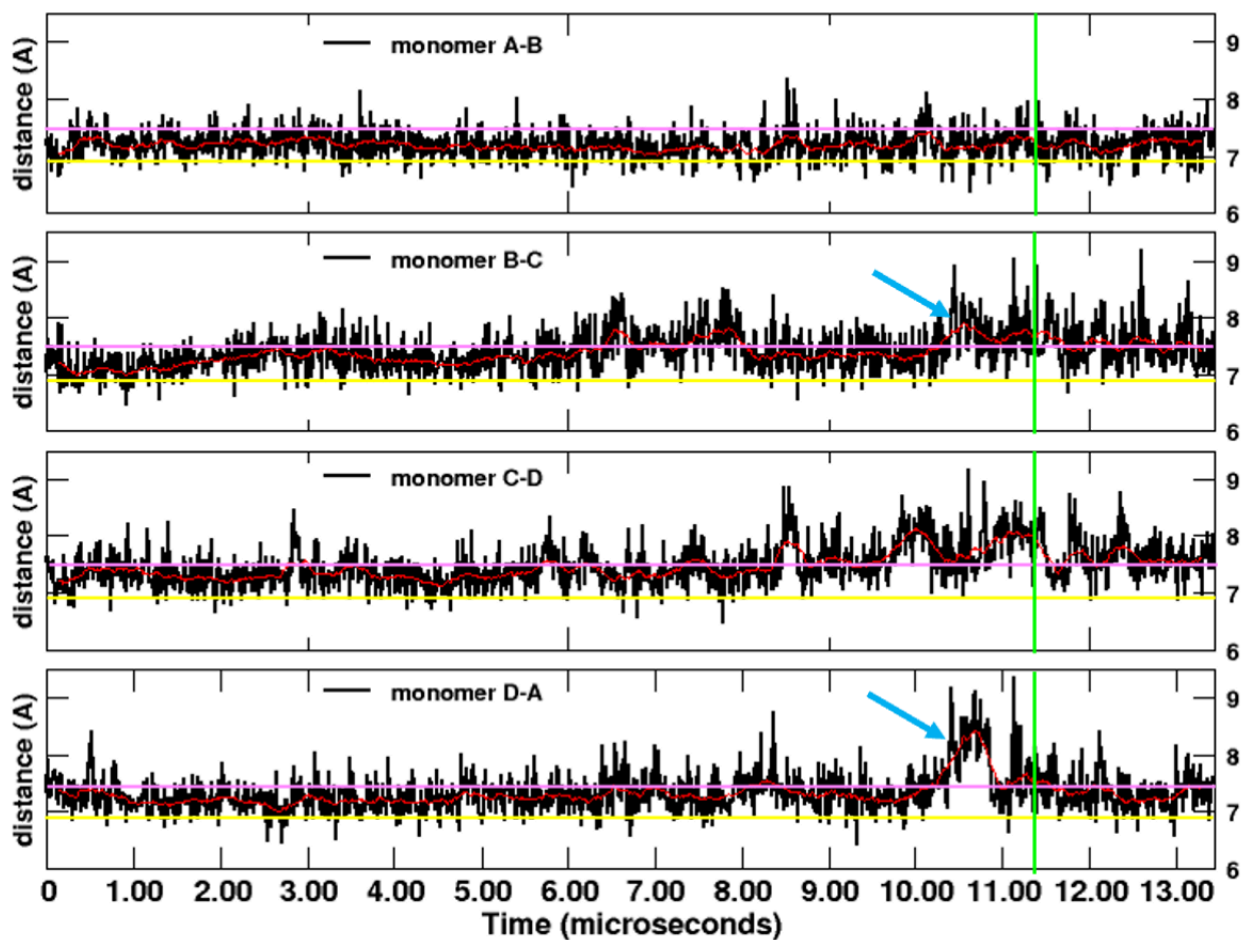


**Figure 25.** A close-up view of the two residues that are thought to form an ionic lock, R557 and E570 in yellow licorice. Helix S4, the S4-S5 linker, and the TRP domain are shown in pink and labeled.

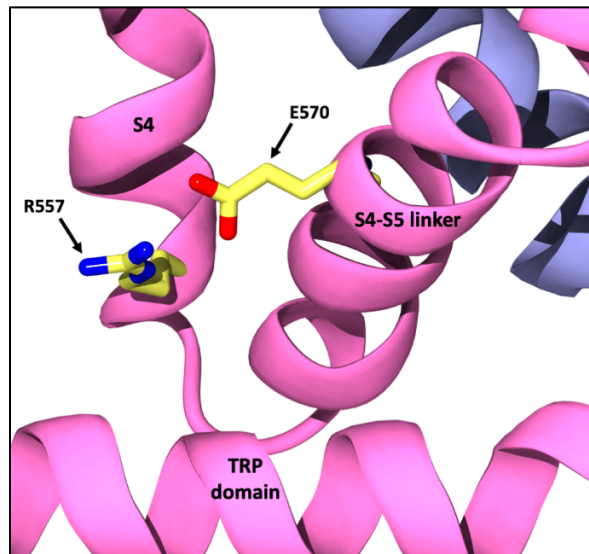
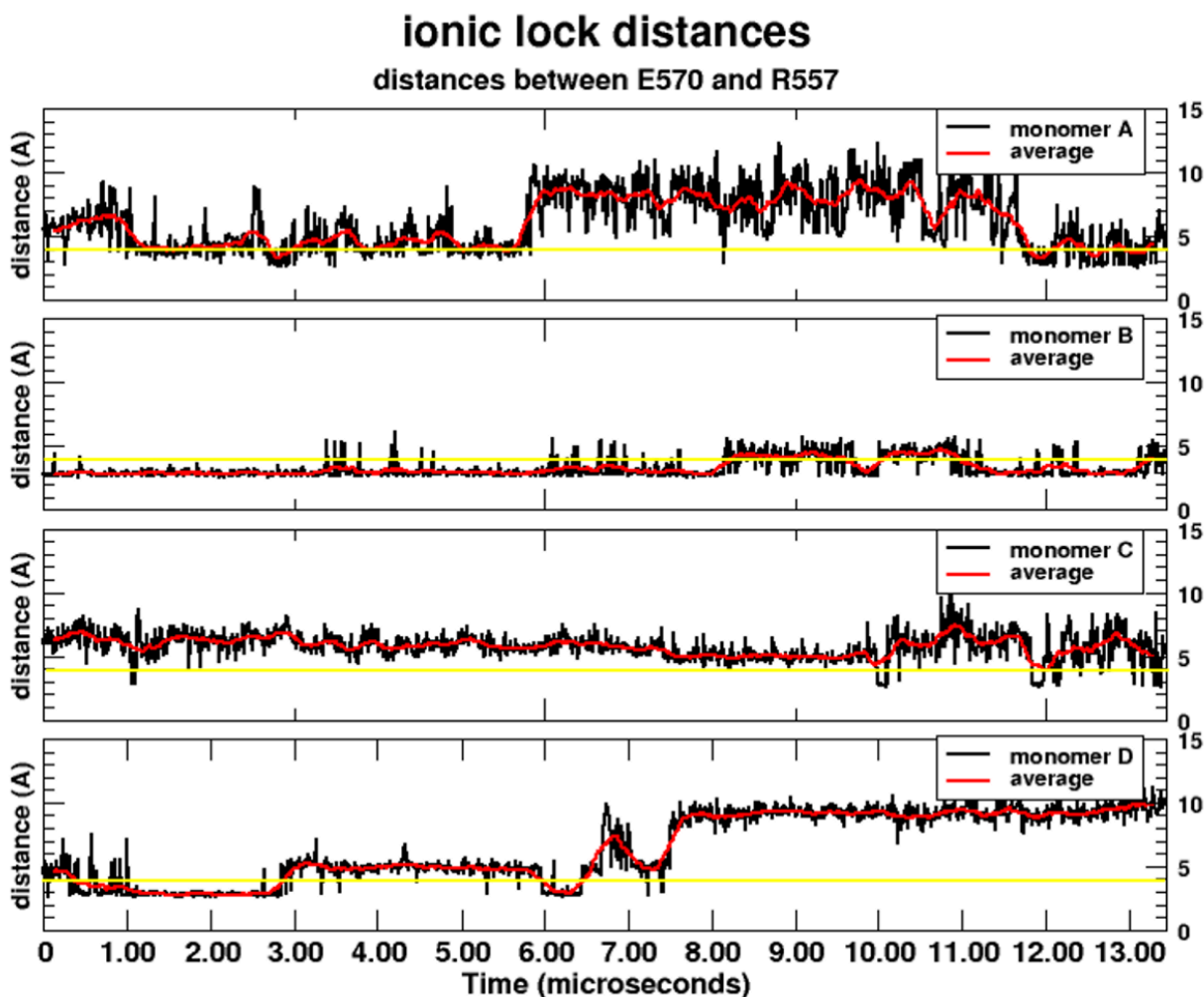
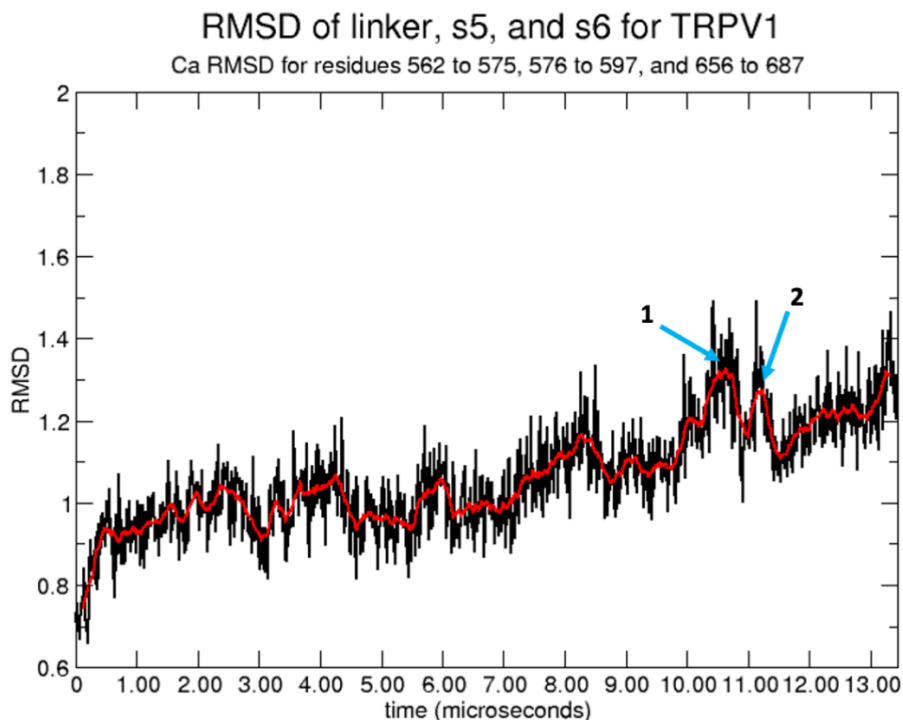


Figure 26. A graph of the distances between R557 and E570 for the trajectory of run 2a. The black line indicates each individual measurement for every 50<sup>th</sup> frame (equivalent to one frame every 12 ns) of the trajectory. The red line represents the running average, while the yellow horizontal line is placed at 4 Å, the distance between heteroatoms needed to form an ionic lock.



**Figure 27. The RMSD of the central structures of TRPV1, the S4-S5 linker, S5, and S6. This plot shows the RMSD for every 50<sup>th</sup> frame of the trajectory, equivalent to one frame every 12 ns. The black line is the individual measurement for each frame and the red line is the running average. As shown, the first microsecond or so of this plot shows a noticeable increase in RMSD. This can be attributed to the equilibration of the system when moved from local GPUs to Anton 2. Peak 1 indicates the region where the split opening occurred and peak two indicates the location of the partial split where water was still able to pass through the channel as seen in Figure 34.**



**Figure 28. A graph of AEA contacts with Y554 from 8.00 to 12.00  $\mu$ s for each monomer. A value of -1 indicates no AEA/Y554 contact where a value of 1 or 2 indicates how many unique AEA ligands are interacting with Y554. Monomer B shows AEA contact with Y554 for nearly the entirety of the 8.00 to 12.00  $\mu$ s trajectory analyzed here.**

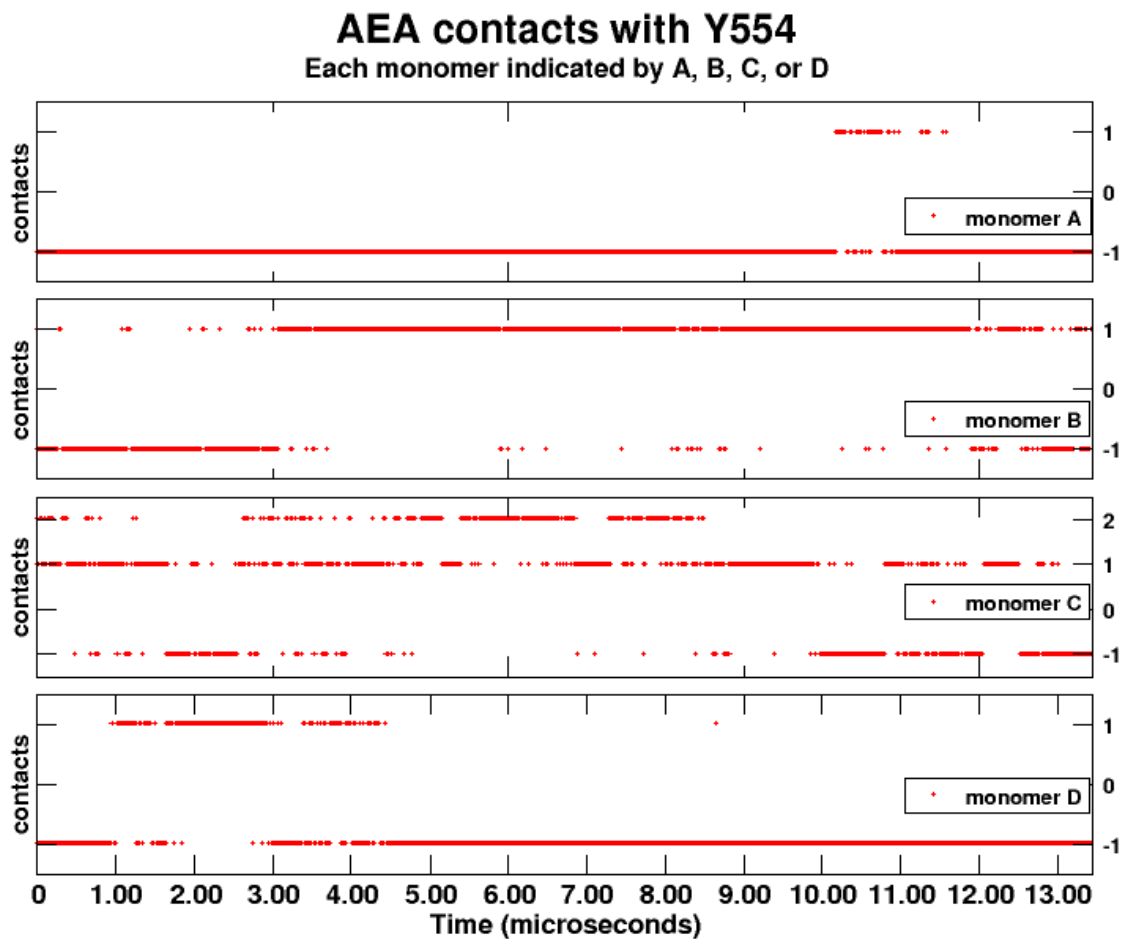




**Figure 29.** Three sequential frames of lower gate (I680, orange) opening that occurred at 11.00  $\mu$ s in panel A, 11.24  $\mu$ s in panel B, and 11.48  $\mu$ s in panel C.

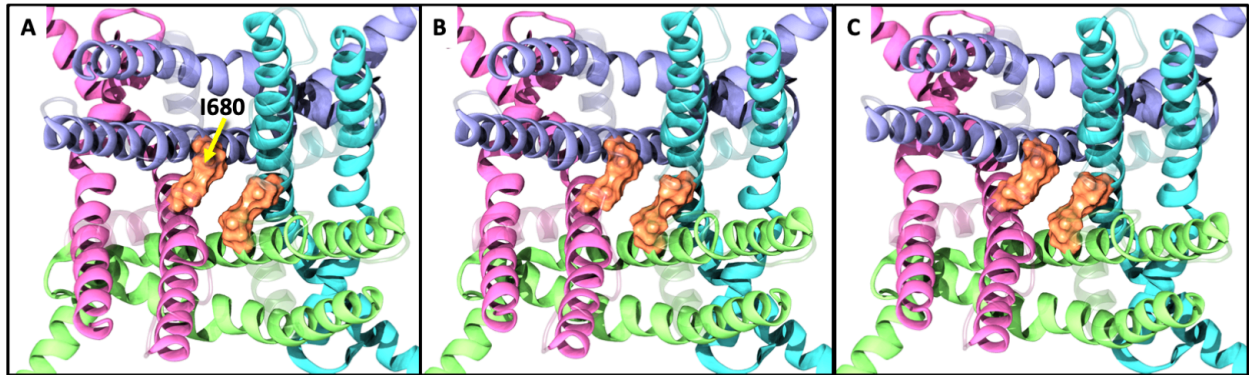


**Figure 30.** A lipid view of the central pore of TRPV1 with upper (G644 orange) and lower (I680 orange) gates present. As a sample representation, five water molecules within the pore (panel A) and are labeled and tracked as they exit the pore region and move to the intracellular side of the cell (panel B).

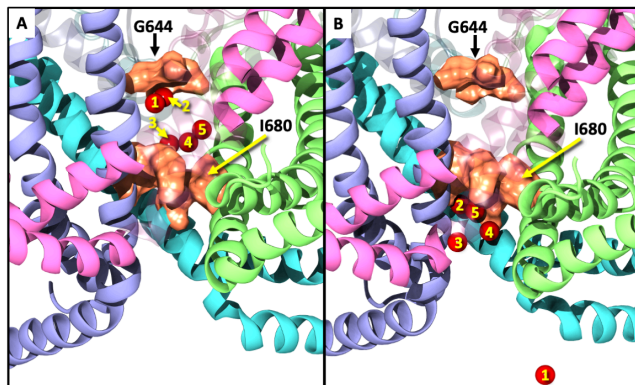


**Figure 31. The solvent accessible surface area of I680 for the course of trajectory 2a. Because of the large data sets generated by Anton2, every 50<sup>th</sup> frame was used for this plot, equivalent to one frame every 12 ns. The black line shows the measurement of each point while the red line shows the running average. Peak 1 indicates the region where lower gate flexibility was more frequent, Peak 2 indicates the first point of partial opening, Peak 3 is indicative of the split opening, and Peak 4 indicates where the channel activity was starting to lessen, but a water molecule was still able to pass through a partial opening of I680.**

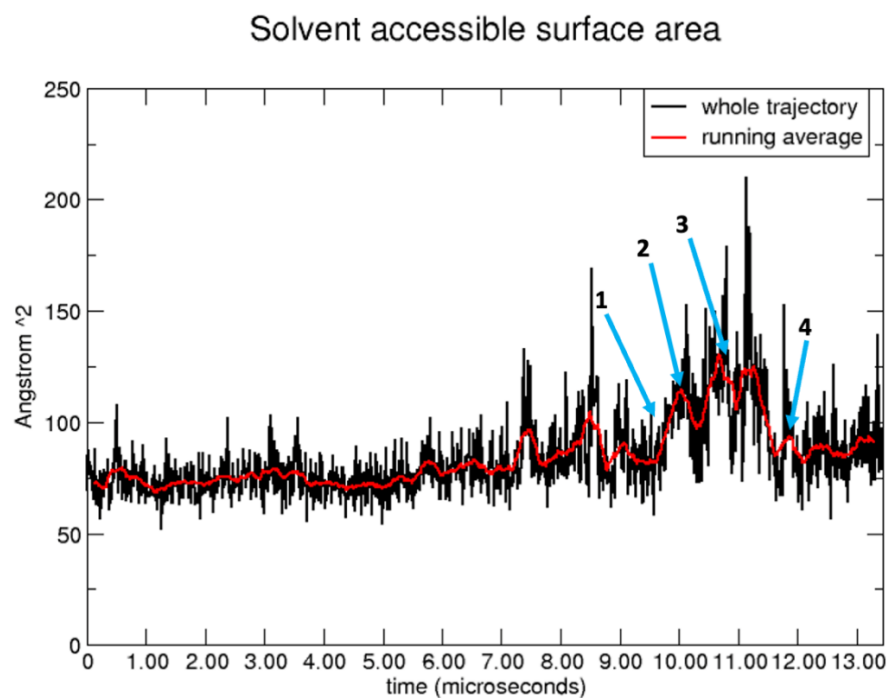
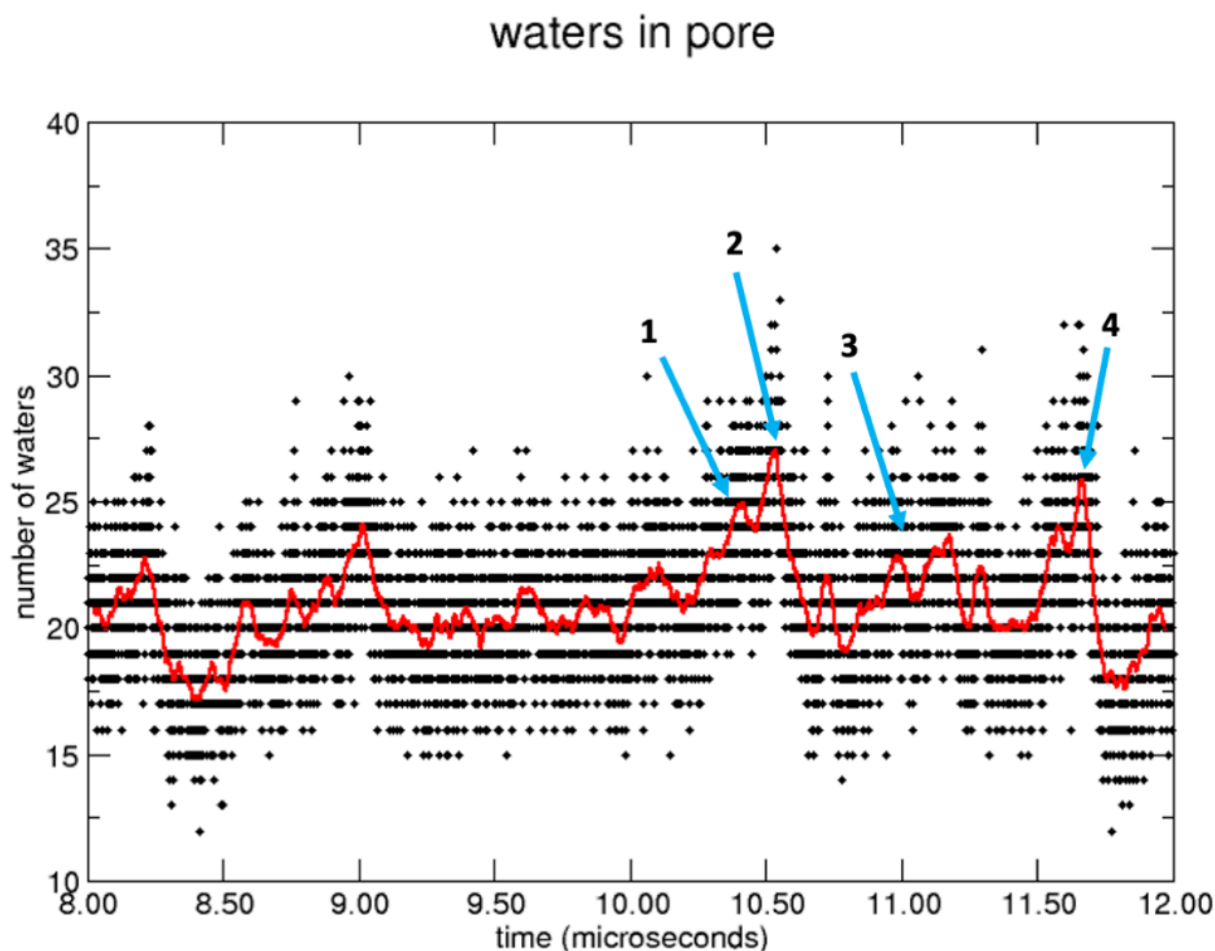
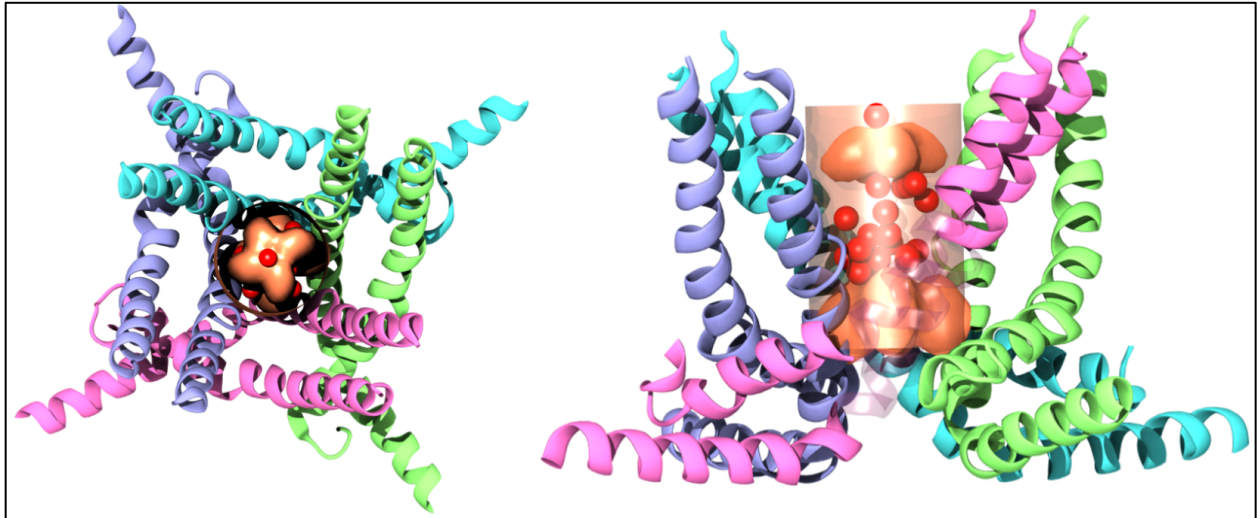


Figure 32. A graph of the number of water molecules located in the region from G644 and I680 for run 2a for the limited segment of the trajectory. Peaks 1 and 2 indicate regions where the lower gate flexibility was observed to increase and the first instance of partial lower gate opening, respectively. Peak 3 indicates where the split channel opening occurred. We hypothesize that the decrease in water molecules is likely due to water being able to exit more quickly to reach a more manageable amount of water. Peak 4 is indicative of the region where the partial opening occurred, but still allowed for water to pass through the lower gate. The cylinder used for quantification (Figure 33A and 33B) extended 2 Å above G644 and 2 Å below I680 in order to accommodate for gate fluctuations.



**Figure 33.** A visual representation of the region used to collect the quantification of water molecules within the pore. Panel A shows the top-down view (extra- to intra- cellular view) of the cylinder with G644 and I680 shown in orange (G644 on top, I680 on bottom) with water molecules shown (red spheres). Each monomer is colored separately. Panel B shows a lipid view of the same cylinder (transparent orange) with the upper and lower gates shown as an orange surface. Water molecules are colored as red spheres.



**Figure 34.** An extracellular view in panels A and B shows a single water molecule (red) moving through a smaller opening in the lower gate (I680, orange). Panel A shows the water inside the pore and panel B shows the water molecule just as it passes I680 into the intracellular region.

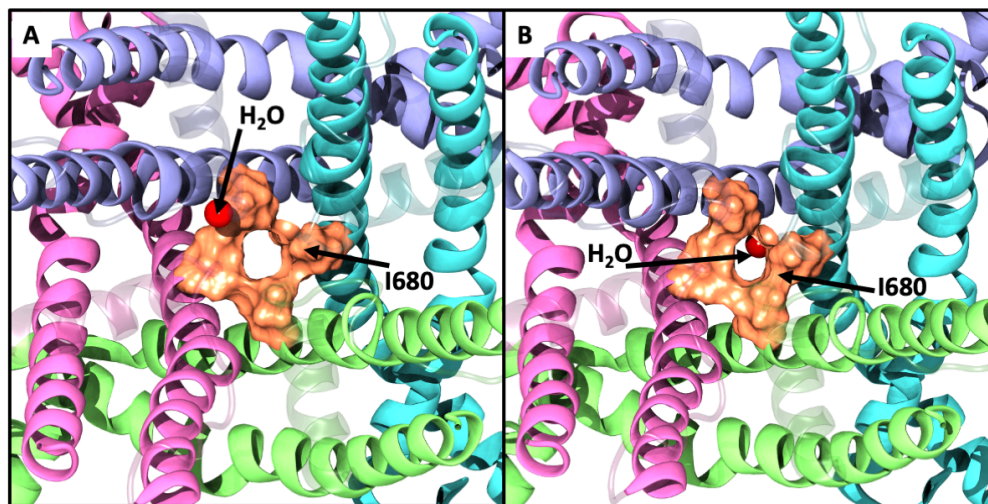


**Figure 35. The RMSD of the S1-S4 tunnel. This plot shows the RMSD for every 50<sup>th</sup> frame of the trajectory, equivalent to one frame every 12 ns. The black line is the individual measurement for each frame and the red line is the running average. As shown, the first microsecond or so of this plot shows a noticeable increase in RMSD. This can be attributed to the equilibration of the system when moved from local GPUs to Anton 2. Peak 1 indicates the region where the split opening occurred and peak two indicates the location of the partial split where water was still able to pass through the channel as seen in Figure 6. The movement of the S1-S4 helices provides information on how AEA interaction within these tunnels may influence their arrangement in TRPV1.**

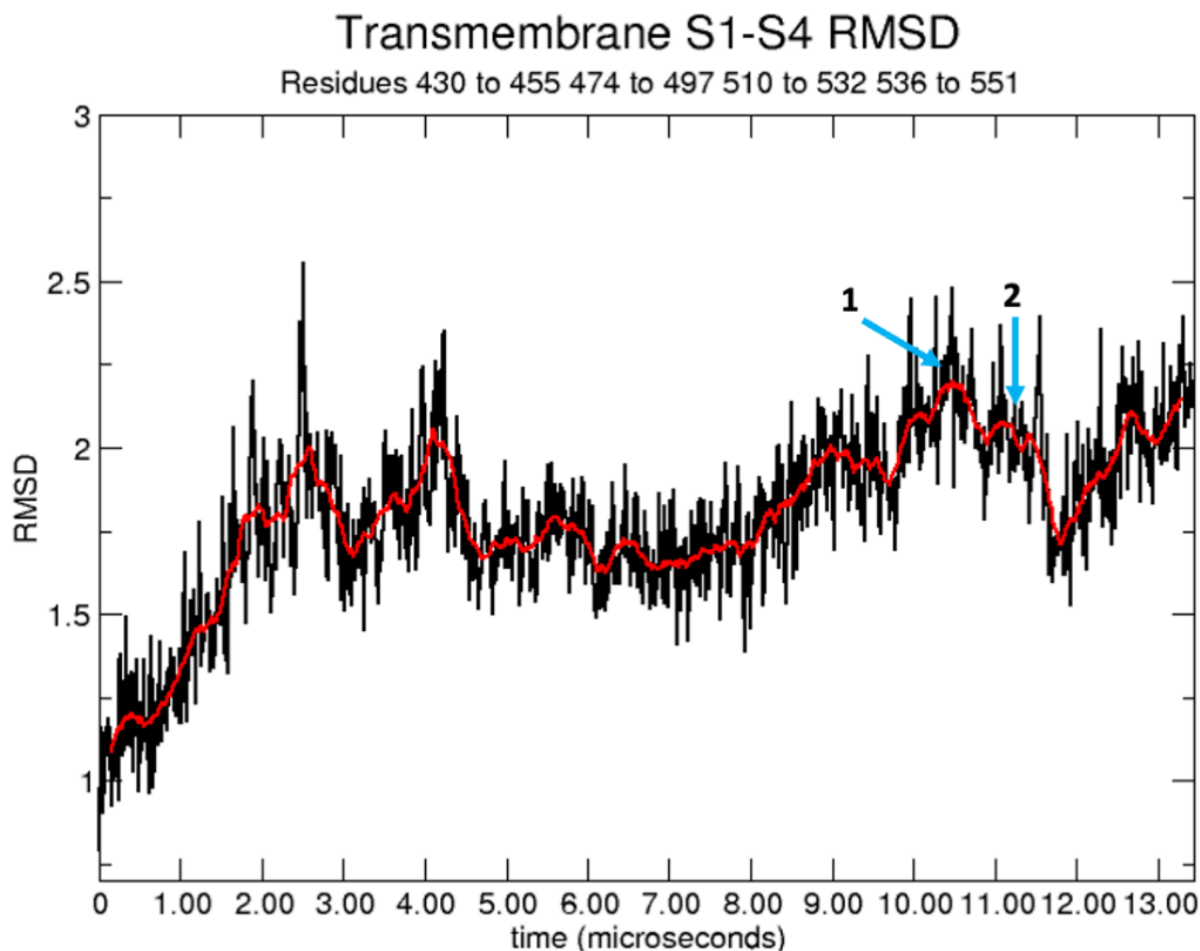




**Figure 36.** An instance of lower gate opening (I680, orange) that occurred in Build 1 run 2b at 9.6  $\mu$ s with AEA (yellow VDW) interacting with Y554 (cyan) (panel A). Measurements of the I680 C $\alpha$  atoms can be seen in panel B. The S6 helices are labeled, and each monomer is a different color. I680 is shown in orange.

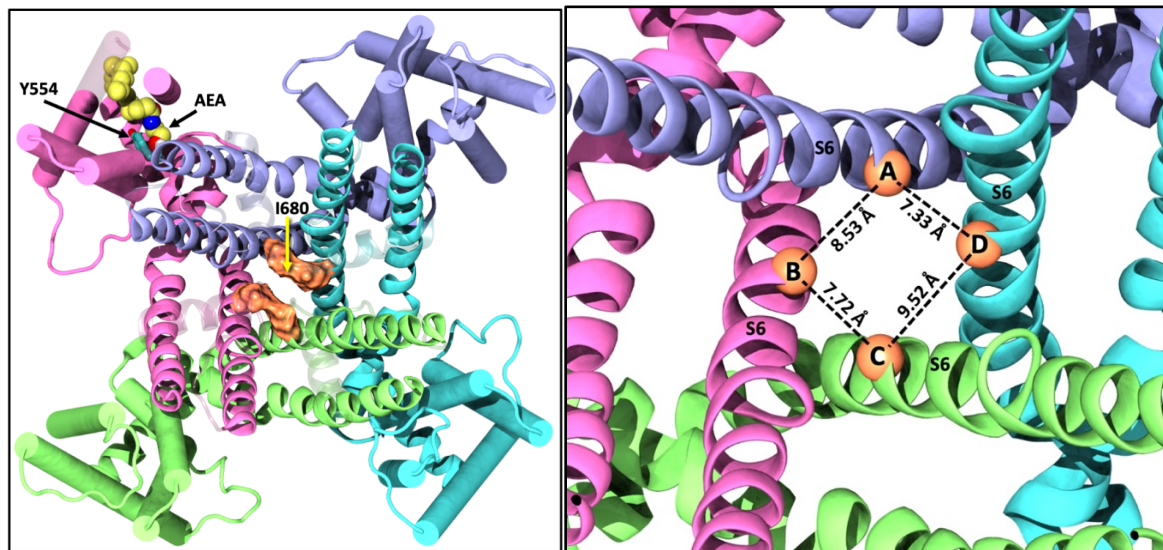


**Figure 37.** An instance of a water molecule (red) passing through the lower gate (I680, orange) in Build 1 run 2b at 10.6  $\mu$ s. AEA (yellow VDW) interacting with Y554 (cyan) (panel A). Measurements of the I680 C $\alpha$  atoms can be seen in panel B. The S6 helices are labeled, and each monomer is a different color. I680 is shown in orange.

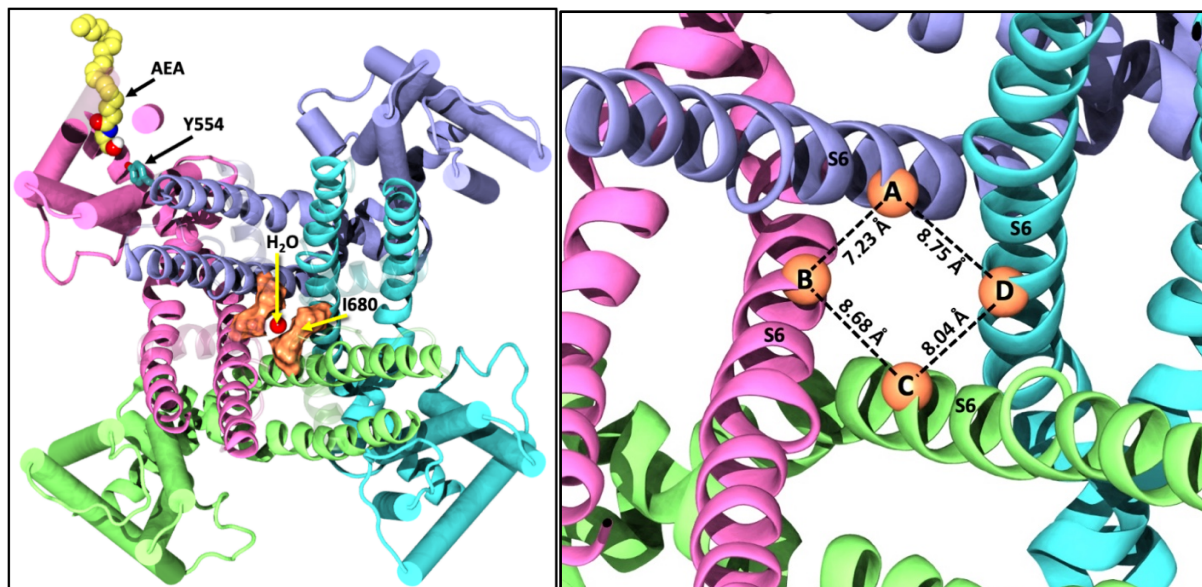
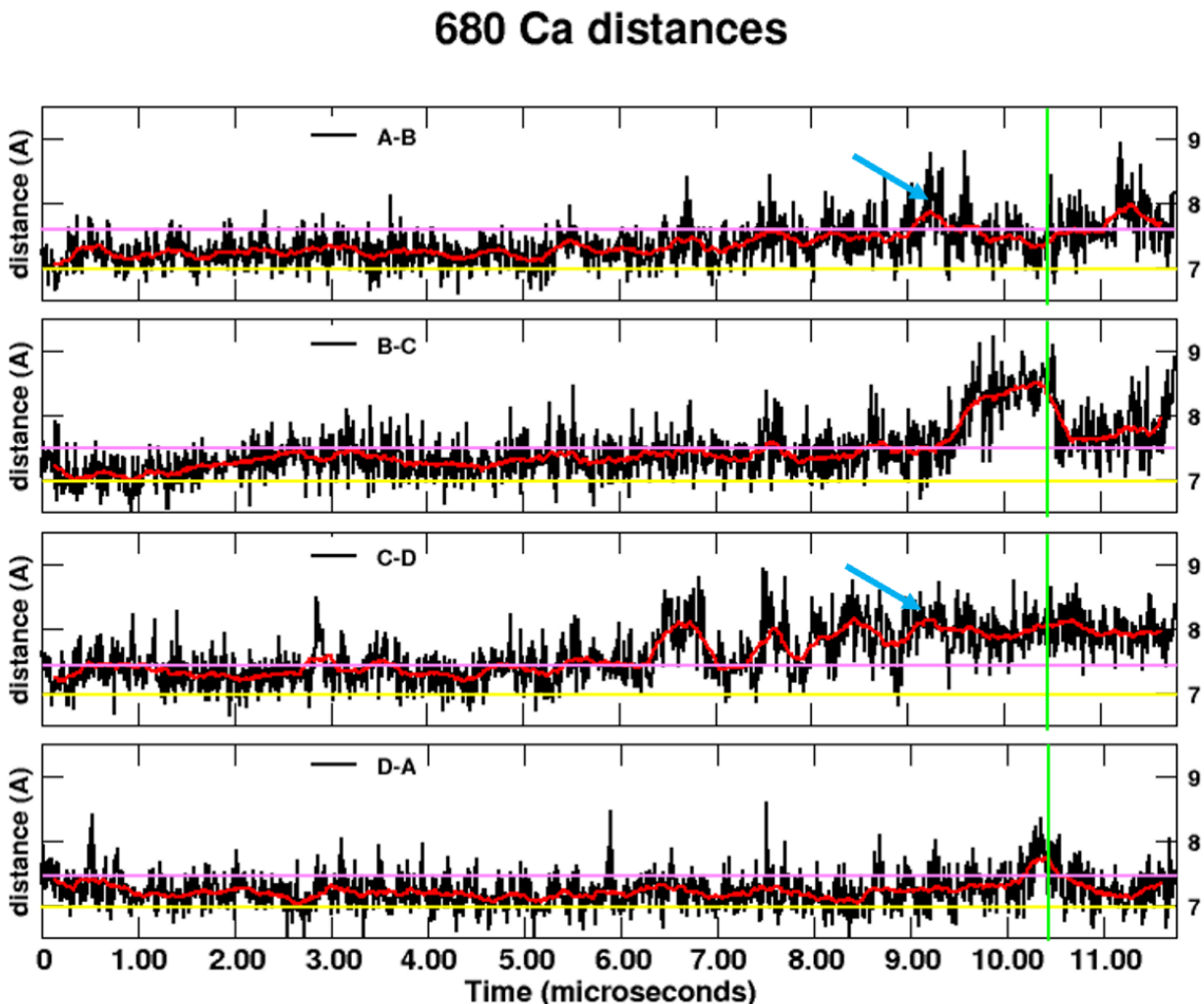


Figure 38. The measurements of adjacent I680 Ca atoms for the trajectory of run 2b. The black line indicates each individual measurement for every 50<sup>th</sup> frame of the trajectory (equivalent to one frame every 12 ns, again, due to large datasets from Anton2). The red line represents the running average. The yellow horizontal line roughly translates to the I680 Ca distances found in the static apo/closed (PDB: 5IRZ) state, while the pink horizontal line is the maximum I680 Ca atom distance for the closed state from our MD where water or ions cannot pass through. Blue arrows indicate locations where the first split opening occurred, around 9.7  $\mu$ s, and the green vertical lines indicates the location where the second split opening occurred, around 10.7  $\mu$ s



**Table 9. I680 C $\alpha$  distances between bonds A-B, B-C, C-D, and D-A as shown in Figures S1, and represented in S15 and S16. The distances of 5IRZ and 5IRX are used to gauge the level of openness of the lower gate. Since these values come from cryo-EM structures and are static, we use them as reference points rather than strict definitions of “closed” and “open”. The “MD start” values are listed as the closed structure from which runs 2a and 2b were started. These values are used as the dynamic reference of the closed state.**

<b>bonds</b>	<b>apo (5IRZ)</b>	<b>MD start</b>	<b>9.6 <math>\mu</math>s (S17)</b>	<b>10.6 <math>\mu</math>s (S18)</b>	<b>open (5IRX)</b>
A-B	7.01 Å	7.13 Å	8.53 Å	7.23 Å	9.80 Å
B-C	7.04 Å	8.06 Å	7.72 Å	8.68 Å	9.81 Å
C-D	7.02 Å	7.44 Å	9.52 Å	8.04 Å	9.74 Å
D-A	7.03 Å	7.61 Å	7.33 Å	8.75 Å	9.75 Å



**Figure 39.** The solvent accessible surface area of I680 for the course of trajectory 2b. Because of the large data sets generated by Anton2, every 50<sup>th</sup> frame was used for this plot, equivalent to one frame every 12 ns. The black line shows the measurement of each point while the red line shows the running average. Peak 1 indicates the first split opening of I680 ~9.  $\mu$ s and peak 2 indicates the second split opening of I680 where a water molecule was seen passing through the pore ~10.7  $\mu$ s.

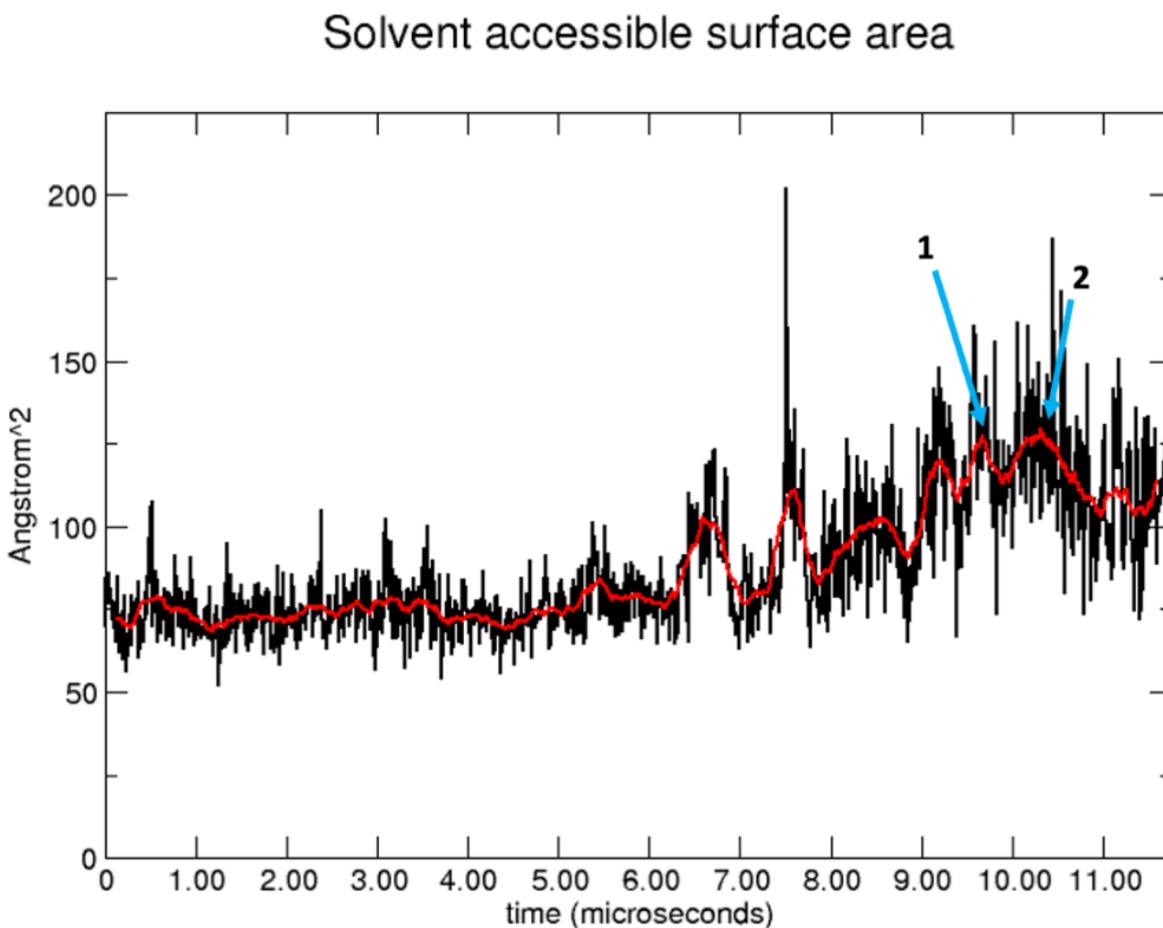
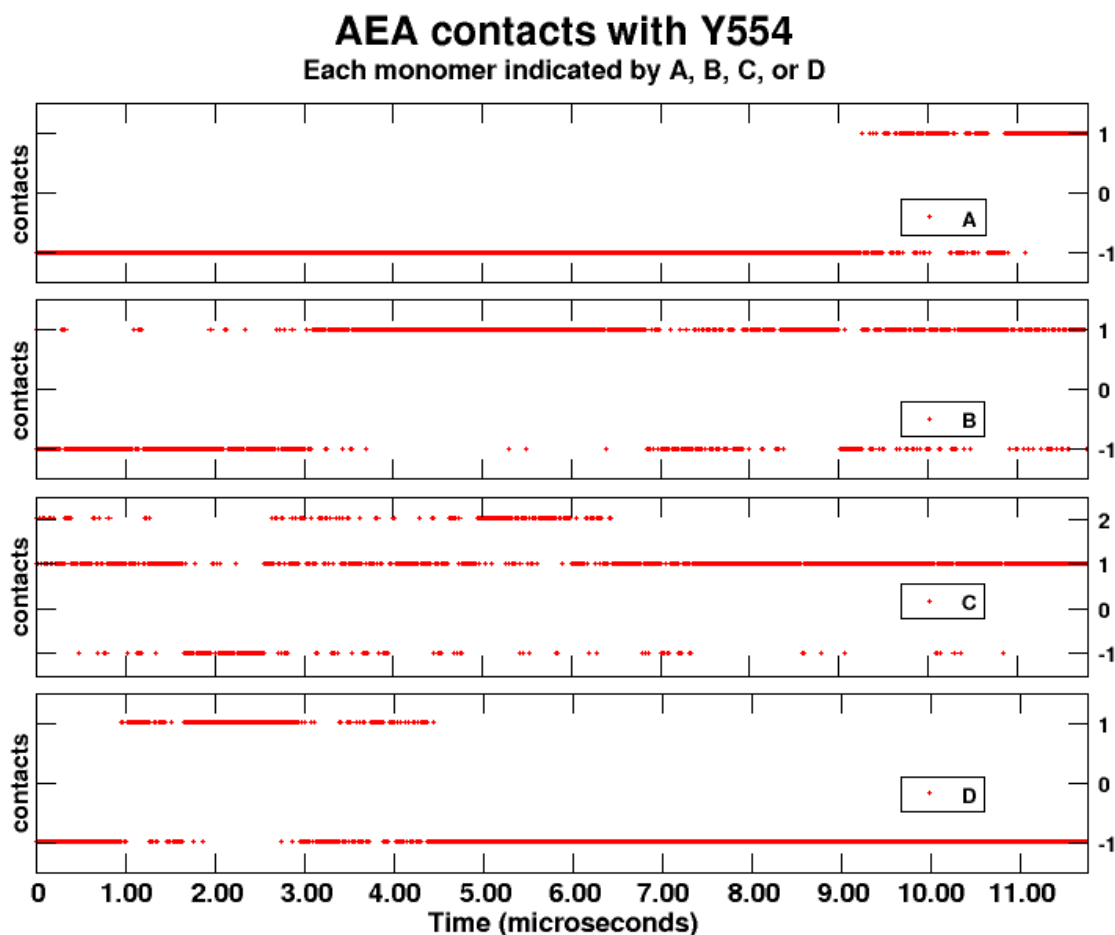


**Figure 40. AEA contact with Y554 for run 2b.** Because of the large data sets generated by Anton2, every 50<sup>th</sup> frame was used for this plot, equivalent to one frame every 12 ns. The black line shows the measurement of each point while the red line shows the running average. A value of -1 indicates there was no AEA contact with Y554. A value of 1 or 2 indicates that number of AEA ligands interacting with Y554. Similar to run 2a, monomer B has a significant portion of the trajectory occupied by AEA. Monomer C is shown to have a comparable level of AEA occupation with some instances of two AEA ligands working their way into the S1-S4 tunnel.



## CHAPTER VI: TARGETING CB2 AND TRPV1: COMPUTATIONAL APPROACHES FOR THE IDENTIFICATION OF DUAL MODULATORS

**Paula Morales<sup>1†</sup> & Chanté Muller<sup>2†</sup>, Nadine Jagerovic<sup>1</sup>, and Patricia H. Reggio<sup>2</sup>**

Frontiers in Molecular Biosciences, 2022, 10.3389

Submitted: 22 December 2021. Accepted: 03 February 2022. Published: 25 February 2022

<sup>1</sup>Medicinal Chemistry Institute, Spanish National Research Council, Madrid, Spain

<sup>2</sup>Department of Chemistry and Biochemistry, University of North Carolina at Greensboro, Greensboro, NC

<sup>†</sup>These authors contributed to this work equally

### Abstract

Both metabotropic (CBRs) and ionotropic cannabinoid receptors (ICRs) have implications in a range of neurological disorders. The metabotropic canonical CBRs CB1 and CB2 are highly implicated in these pathological events. However, selective targeting at CB2 versus CB1 offers optimized pharmacology due to the absence of psychoactive outcomes. The ICR transient receptor potential vanilloid type 1 (TRPV1) has also been reported to play a role in CNS disorders. Thus, activation of both targets, CB2 and TRPV1, offers a promising polypharmacological strategy for the treatment of neurological events including analgesia and neuroprotection. This brief research report aims to identify chemotypes with a potential dual CB2/TRPV1 profile. For this purpose, we have rationalized key structural features for activation and performed virtual screening at both targets using curated chemical libraries.

**Keywords:** cannabinoids, ionotropic receptors, CB2, TRPV1, dual ligands, multitargeting

### Introduction

Well documented pharmacological evidence supports functional crosstalk between the endocannabinoid system (ECS) and the endovanilloid system (EVS)<sup>42,151,162–175</sup>. Thus, these latest advances provide opportunities to develop innovative strategies for fighting disorders

where biological targets of both systems are involved. Here, we emphasize the cannabinoid receptor type 2 (CB2) and the transient receptor potential vanilloid type 1 (TRPV1) channel, both implicated in neurodegenerative diseases and pain.

CB2R is a G-protein-coupled receptor (GPCR) mainly present in the immune cells where they are expressed in lymphocytes, natural killer cells, macrophages, and neutrophils<sup>176</sup>. Thus, they are an attractive target for the treatment of inflammatory processes. The expression of CB2 is also detected in the central nervous system (CNS) under stressful conditions such as cytotoxic and neuroinflammatory injuries within the brainstem, microglia, and astrocytes, suggesting CB2 an interesting target for neuroprotection<sup>177</sup>. CB2 is also expressed in the blood brain barrier (BBB), and therefore could be beneficial in the brain and peripheral tissues at different stages of neurodegenerative processes<sup>178–183</sup>. CB2 selective agonists also represent an attractive approach for pain management among other therapeutic applications<sup>184</sup>. In animal models of chronic inflammation, CB2 agonists lead to beneficial outcomes for diverse pain managements such as neuropathic, osteoarthritic, postoperative, and human immunodeficiency virus (HIV) associated pain relief<sup>185–190</sup>.

TRPV1 is a nonselective cation channel mainly expressed in the sensory neurons of the peripheral nervous system<sup>111</sup>, acting as a detector of painful stimuli such as heat and pungent chemicals like capsaicin. TRPV1 modulators have attracted much attention as analgesics due to its implication in pathological pain such as inflammatory, visceral, neuropathic, and cancer-related pain<sup>162,191,192</sup>. TRPV1 has also been described in the CNS<sup>192–194</sup> with expression in neurons, microglia, and astrocytes<sup>195</sup>, and its level of expression can be up- or down-regulated according to age and pathophysiological conditions<sup>196</sup>. TRPV1 participates to the regulation of neuronal function and synaptic plasticity<sup>172,197,198</sup>, the control of motor behavior<sup>170,196,199</sup>, and the

regulation of neuroinflammation<sup>200</sup>. Therefore, TRPV1 has been suggested to be implicated in diseases associated with motor dysfunctions, such as Huntington's, Parkinson's, and multiple sclerosis, or with cognitive functions like Alzheimer's disease<sup>199,201–203</sup>.

Co-expression and crosstalk between TRPV1 and CB1<sup>147,163</sup> has been established primarily in the modulation of arthritic pain and inflammation<sup>42</sup>. In addition to CB1, CB2 is also co-expressed with TRPV1 in certain cells including osteoblasts<sup>175</sup>, osteoclasts<sup>164</sup>, and sensory neurons<sup>167</sup>. Moreover, CB2 and TRPV1 crosstalk has shown to be engaged diverse pathophysiological processes including pain<sup>167,204</sup>, bone disorders<sup>164,175</sup>, inflammatory processes<sup>205,206</sup>, cocaine-seeking behavior<sup>173</sup>, proliferation and apoptosis of T-lymphoblastic leukemia cells<sup>165</sup>, and multidrug resistance<sup>174</sup>. Benefits of the CBR/TRPV1 axis for neurodegenerative diseases has been suggested by some studies due to CBRs and TRPV1 inhibition of glial activation and expression of proinflammatory cytokines in a mouse model of Parkinson's disease<sup>167</sup>. Pharmacologically, strategies targeting CB1/TRPV1 have shown promising therapeutic results in models of pain, spasticity, arthritis, and dyskinesia<sup>42,168,170,207,208</sup>. For instance, arvanil, a CB1 agonist, TRPV1 activator, and potent inhibitor of anandamide (AEA) accumulation, alleviates hyperkinesia typical of Huntington's disease<sup>209</sup>. However, few reports have identified dual CB2/TRPV1 modulators thus far.

Current treatments for complex disorders based on selective- target drugs fail in their efficacy. As a consequence, a number of research studies have highlighted the importance of multiple- target strategies for the treatment of multifactorial disorders such as pain and neurodegenerative diseases<sup>210–212</sup>. Combinatorial therapies are generally associated with side effects derived from drug-drug interactions. Therefore, single dual-acting drugs should reduce side effects with unique pharmacokinetic or pharmacodynamic profiles. Cannabinoids have been

reported to directly modulate TRPV1<sup>72</sup>, and among them, few have shown selective CB2 vs CB1 activity. In this brief research report, we will primarily focus on the *in silico* identification of potential CB2/TRPV1 chemotypes, as well as rationalize reported dual modulators.

## **Methods and Materials**

### **Receptor Structures**

Structures of hCB2 and hTRPV1 were selected based on the reliability and stability of the structures. In a recent publication, an activated structure of hCB2 was resolved via cryo-EM at a resolution of 2.90Å (PDB: 6KPF)<sup>213</sup>. This structure was used for our docking screening upon treatment using the protein structure preparation wizard integrated in the Schrödinger software. A model of hTRPV1 was constructed using the cryo-EM structure PDB: 5IRZ congruent to the methods described in Muller et al. and was used for this work<sup>156</sup>.

### **Grid Generation**

Prior to using the Glide module high-throughput virtual screening (HTVS) and extra precise (XP) docking within the Schrödinger package (Schrödinger, LLC, New York, NY, 2019), docking grids were generated using the receptor grid generation tool within Glide to ensure ligand screening was performed in the appropriate sites within each receptor. Dimensions for the CB2 receptor grid were set at 20 Å in length along the x, y, and z axes and was centered on the ligand co-crystallized with the CB2 structure (the THC synthetic derivative AM12033).

Similarly, all three TRPV1 grids were generated to adhere to the same dimensions of 20 Å in length in the x, y, and z directions and were centered on residues that are believed and/or reported to be involved with ligand binding at each location. This resulted in three distinctly different grids for TRPV1 that will herein be referred to as “VBP” for the location that capsaicin binds, “tunnel” for the location where anandamide has been reported to interact with TRPV1 via

MD simulations, and “CBD-site” for the putative CBD interaction site reported in the TRPV2/CBD cryo-EM structure. Visual representations and further explanation of these TRPV1 sites can be found in Supplementary Figure 43. These grid specifications allow any ligand that is less than or equal to 20 Å in length to be docked within the specified region.

### **Curation of chemical libraries.**

**CB2.** From the CB2 indexed molecules, ligands showing EC<sub>50</sub>, E<sub>max</sub>, and activity data were selected (total of 6356) and retrieved from the ChEMBL webserver as a .csv file. The “activity” category includes compounds with not only agonist activity, but antagonist, inverse agonists, and allosteric modulators as well. DataWarrior, an open-source data visualization software, was used to further analyze the ligand output which included discarding ligands without an agonist profile (–568 ligands), removing duplicates (–2159 ligands), and eliminating ligands with low activity (–773 ligands). This resulted in a final CB2 library of 2856 unique molecules that included a variety of chemotypes.

**TRPV1.** Ligands that have been indexed for TRPV1 activity within the ChEMBL database were selected and filtered in search of agonists in accordance with the reported EC<sub>50</sub> and E<sub>max</sub> values and activity. The resulting 7,436 compounds were exported from the ChEMBL webserver as a .csv file and uploaded to DataWarrior. The selection of ligands with TRPV1 activity from the ChEMBL database included antagonists, inverse agonists, possible allosteric modulators, ligands with low activity, and duplicates which were all removed using DataWarrior. The final curated TRPV1 library contained 3,830 unique molecules with a variety of chemotypes.

**Internal standard ligands.** The CB2 agonist resolved with the active hCB2 structure (AM12033) was used as an internal standard for CB2 docking. Three internal standards were

used for hTRPV1: capsaicin in the VBP, AEA in the tunnel as observed from MD simulations, and CBD at the putative CBD site.

***JWH133 similarity library.*** JWH133, which acts as an agonist at both CB2 and TRPV1, was used as a molecular basis for this additional screen to explore more unique scaffold options that may not be present in the CB2 or TRPV1 curated libraries. A JWH133 similarity library was curated using PubChem Biosays, 2021 which included compounds that shared >0.85 Tanimoto similarity index with JWH133, while also following Lipinsky's rules of drug likeness (apart from xLogP values, which were set to -1 to 6 due to the lipophilicity of cannabinoid ligands). The JWH133 similarity library consisted of 5081 that were screened at all sites (CB2 and the three TRPV1 sites), and the output was analyzed to identify dual potential chemotypes.

### **High-throughput virtual screening workflow**

A general overview of the screening workflows is provided in Supplementary Figure 44.

***Ligand preparation.*** Each of the curated libraries were exported as .sdf files and their conformations were optimized using the LigPrep module of the Maestro suite (Schrödinger, LLC, New York, NY, 2019). The Epik software was employed to predict pKa values in the pH range of  $7.0 \pm 0.5$  and to return all chemically sensible structures in accordance with the Hammett and Taft methodology. All compounds were minimized using the OPLS3e force field as implemented in Maestro.

***HTVS.*** Molecular docking was performed using the HTVS Glide-dock module integrated in the Schrödinger package. The HTVS was conducted under the default setting, ensuring that high-energy ionization and tautomer states were removed, and the planarity of conjugated pi systems were enhanced. Ligands were docked flexibly, allowing for exploration of an arbitrary number of torsional degrees of freedom, in addition to the six spatial degrees of freedom spanned



by the translational and rotational parameters. Up to 10 poses per compound state were generated and ligand poses that were generated in this way were run through a series of hierarchical filters to evaluate ligand interactions with the receptor. Docking score, glide gscore, glide emodel, ionization penalty, and topological polar surface area (TPSA) were used to select the docking poses in the output. The output from the HTVS contained the top 10% of the best scoring compound states and were analyzed for use in the extra precise (XP) screen via their docking scores.

***XP screening.*** Top scoring compounds from the HTVS were then studied through high-precision docking calculations which was performed using the XP Glide module. As with the HTVS protocol, 10 poses of the short-listed ligands were docked flexibly in their respective receptor site within the generated grids. A post-docking minimization was performed and the top 20% of the best scoring ligands were retained. XP Glide uses two key features that impact the XP Glide scoring: the recognition of structural motifs that provide large contributions to binding affinity and the application of large desolvation penalties to ligand and protein polar and charged groups wherever appropriate. To accomplish this, the sampling algorithm and scoring functions have been simultaneously optimized in XP. Ligands making it through the XP screen were organized by their docking scores and analyzed for ligand/receptor interactions. Selected ligands for each receptor were investigated through manual docking based on the automatic docking score, binding mode, as well as reported activity.

### ***Additional criteria.***

**Manual docking identification of potential PAINS off-targets evaluation.** Selected compounds were subjected to manual docking at CB2 and TRPV1 for further investigation of key interactions. Docking at CB2 was performed following the protocols previously reported by us for cannabinoid and related GPCRs<sup>82</sup>. In the case of TRPV1, select ligands were positioned within the respective binding site with steric clashes being removed via ligand and/or receptor adjustment using a graphical interface. Minimization of the ligand and surrounding 6 Å of residues (due to complex size) was performed using Prime version 19.3 (Schrödinger Inc.) with the OPLS3e forcefield in an implicit membrane.

**In silico calculation of ADME properties.** A set of 34 physico- chemical descriptors was computed using QikProp version 3.5 integrated in Maestro (Schrödinger, LLC, New York, United States). The QikProp descriptors are shown in Supplementary Tables 13 and 14. The 3D conformations used in the calculation of QikProp descriptors were generated using LigPrep as previously detailed.

**Identification of potential PAINS.** In the search of potential candidates, it is crucial to avoid the presence of potential promiscuous moieties or PAINS (pan-assay interference compounds)<sup>214,215</sup>. Therefore, the selected molecules were subjected to a PAINS identification study using the swissADME webserver<sup>216</sup>.

**Off-targets evaluation.** XP Glide docks at potential off-target receptors including cannabinoid-related GPCRs such as CB1<sup>213,217</sup>, GPR55<sup>218,219</sup>, GPR18<sup>220</sup>, and TRP channels such as TRPV2<sup>221</sup>, TRPV3<sup>222,223</sup>, TRPA1<sup>224,225</sup>, and TRPM8<sup>226,227</sup>. For this purpose, the cited available structures, whether crystal, cryoEMs, or models previously developed in our group, have been used. Results of these additional dockings can be found in Supplementary Tables 15 and 16.

## Results and Discussion

Polypharmacological approaches targeting the ECS have already shown successful results in diverse disease models<sup>228–231</sup>. However, drug discovery strategies primarily targeting CB2 and TRPV1 have not yet been explored. As previously detailed, activation of these targets participates in diverse therapeutic effects including analgesia and neuroprotection, which both offer interesting polypharmacological prospects.

### Structural understanding of compounds with reported activity at both targets

To computationally identify promising chemotypes with a CB2/ TRPV1 dual agonist profile we have first analyzed reported compounds exhibiting activity at both receptors. As detailed in Supplementary Table 12, endocannabinoids, phytocannabinoids, and their respective synthetic derivatives have so far shown the best promise in this field.

The well-known endogenous ligands 2-arachidonoylglycerol (2-AG) and anandamide (AEA) exhibit agonist effects at both targets with low micromolar potency. As observed in diverse in vitro and in vivo models, these endocannabinoids also display activity at other cannabinoid-related GPCRs including CB1, GPR55, and GPR18<sup>13,232,233</sup> as well as other TRP channels including TRPA1 and TRPM8<sup>72</sup>.

Synthetic endocannabinoid-like derivatives have also shown dual activity (Supplementary Table 12). For instance, Appendino and coworkers reported a series of conformationally constrained fatty-acid ethanolamides with CB1, CB2, and TRPV1 activity<sup>234</sup>. An example from this series is ACPA-OH (Supplementary Table 12), which introduces a hydroxycyclopropyl in the amide head group forcing a specified stereochemistry and rigidity. This compound is a potent TRPV1 agonist that exerts low micromolar CB2 affinity and nanomolar binding at CB1<sup>234</sup>. Further synthetic efforts from Di Marzo's research group led to the

identification of hybrid cannabinoid-vanilloid ligands with a highly CB1 selective profile<sup>168,207,235,236</sup>. Among these fatty- acid derivatives, one of the few compounds that binds to CB2 is O-1811 (Supplementary Table 12), which presents a substituted dimethyl-hydroxyhexanyl tail<sup>207</sup>. Despite targeting CB2, O-1811 displays over 6-fold CB1 selectivity.

Interestingly, molecules combining the polyunsaturated fatty- acid chain with the vanillyl-amide head group of capsaicin behave as CB1/TRPV1 agonists that potently inhibit anandamide accumulation<sup>168,207,235,236</sup>. One such molecule, arvanil (Supplementary Table 12), has shown therapeutic potential in the treatment of dyskinesia associated to Huntington's disease<sup>209</sup> and inhibition of spasticity and persistent pain<sup>208</sup>.

Structural modifications in the long chain of endocannabinoid-like molecules led to the identification of the first series of CB2 selective/TRPV1 dual ligands<sup>237</sup>. Combination of non-polyunsaturated fatty acid-derived chains with 12-acylgroups yielded compounds such as 12-phenylacetylricinoleyl cyclopropylamide (PhAR derivative 12, Supplementary Table 12) which behaves as a potent TRPV1 agonist and CB2 inverse agonist.

Diverse phytocannabinoids have also shown activity at CB2 and TRPV1<sup>238,239</sup>. For instance, the main non-psychotropic component of *Cannabis sativa*, cannabidiol (CBD), is a CB2 partial agonist/TRPV1 agonist<sup>238,240</sup>. It is worth mentioning that at CB2, CBD has been reported to act as negative allosteric modulator in the presence of orthosteric full agonists<sup>241,242</sup>. The acidic CBD derivative, cannabidiolic acid (CBDA), and its propyl counterpart, cannabivarin (CBDV), also exhibited TRPV1 agonism while being CB2 partial agonists<sup>238,239</sup>. The phytogetic compound cannabigerol (CBG) presents the same functional profile at both targets<sup>238,239</sup>. On the other hand, the well-known psychoactive compound tetrahydrocannabinol (THC) is not active at TRPV1<sup>238</sup>, whereas its propyl derivative tetrahydrocannabivarin (THCV) behaves as a

TRPV1/CB2 agonist (Supplementary Table 12). It is important to note that all these phytocannabinoids also display activity at CB1 receptors.

Synthetic phytocannabinoid-like derivatives have also shown interesting dual activity. The CB2 selective agonists HU308 and JWH133 could be considered dual ligands due to their activity at TRPV1 being HU308 a weaker agonist at this channel<sup>47</sup>. The widely used aminoalkylindole WIN55212-2, which is a potent CB1/CB2 synthetic agonist, has also been reported to activate and desensitize TRPV1<sup>47</sup>.

In the search of novel structures with CB2/TRPV1 activity, we aim to minimize off-target effects at CB1 or related receptors. Therefore, considering the aforementioned reported activity, we selected JWH133 as a molecular basis for the identification of potential dual CB2/TRPV1 agonists. The therapeutic potential of this ligand has been recently reviewed elsewhere<sup>243</sup>. As a first step we rationalized its interactions at both receptors using molecular docking. At CB2 JWH133 sits in the orthosteric pocket with the same orientation as the CB2 agonist resolved in the cryoEM structure AM12033 (Supplementary Figure 45A). The tricycle establishes  $\pi$ - $\pi$  stacking with residues F2.61, F2.57 and F183 (extracellular loop 2) while residues I3.29, F2.64 and V3.32 stabilize the molecule through van der Waals interactions. The orientation of the distal aliphatic tail of JWH133 differs from that of AM12033 due to the lack of a functional group at the end. As in the case of AM12033 the so-called twin toggle switch residues F3.36 and W6.48<sup>213</sup> are stabilized in their active conformation as shown in Supplementary Figure 45A. In TRPV1, JWH133 cleared both HTVS and XP screening in what is thought to be the CBD binding site. CBD has yet to be co-resolved with TRPV1, though it has with TRPV2 and an analysis of the putative CBD binding site was performed across all ICRs<sup>244</sup>. The CBD structure in TRPV2 displays a different orientation than the CBD screen at TRPV1, though the differences

cited above could be responsible. CBD and JWH133 show similar  $\pi$ - $\pi$  stacking with Y584, though CBD is also stabilized by F639, likely due to the central constraint of JWH133 which angles the ligand slightly outward (Supplementary Figure 45B).

### **Towards the identification of potential dual ligands**

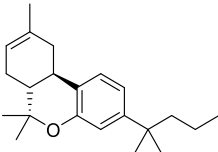
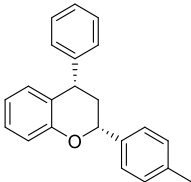
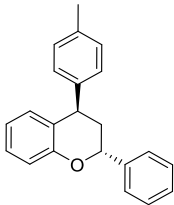
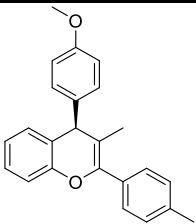
In order to identify potential chemotypes with a yet unexplored TRPV1/CB2 dual profile two different in silico approaches have been followed. These strategies are described in the following subsections and the workflows are depicted in Supplementary Figure 44.

#### **Virtual screening of JWH133 structurally related chemical databases**

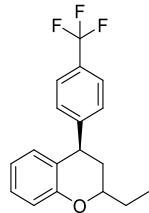
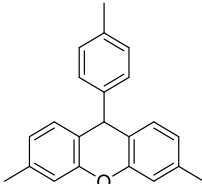
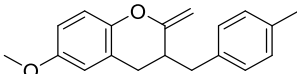
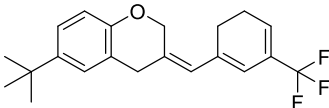
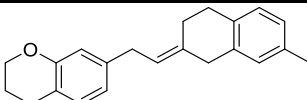
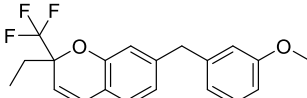
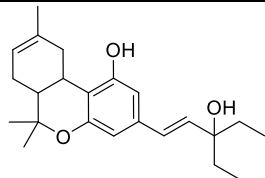
A chemical library of compounds with >0.85 Tanimoto similarity index with JWH133 was curated and screened at CB2 and TRPV1 using the methods described above (workflow depicted in Supplementary Figure 44A). Analysis of docking interactions of top-ranked XP results from the CB2 site and the TRPV1 sites revealed seventeen common ligands between the CB2 site and the VBP and CBD sites (Table 10). No common ligands were identified between the CB2 site and the TRPV1 tunnel. The selection of novel potential CB2/TRPV1 chemotypes includes key structural features and ligand-receptor site interactions at both targets, as well as the absence of previously reported activity at these receptors. This strategy allows for prioritization of molecularly diverse and novel compounds. To ensure the VBP and CBD sites were explored equally, two ligands were selected that targeted CB2 and the VBP (57756957 and 151332252), two ligands were selected that targeted CB2 and the CBD site (59824268 and 123533625), and one ligand was selected that targeted CB2, the VBP, and the CBD site (153641693), resulting in the selection of five ligands for further investigation via manual docking and pharmacokinetic profiling (Supplementary Table 13). The selected chemotypes have not been yet explored at

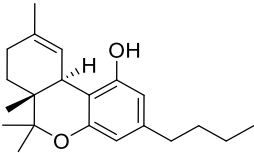
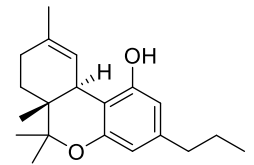
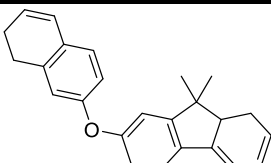
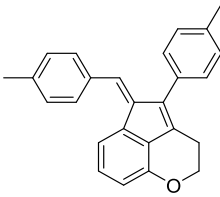
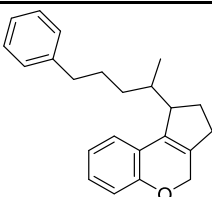
CB2/ TRPV1 and their reported activity is not significant, providing novel opportunities for the investigation of the endocannabinoid system.

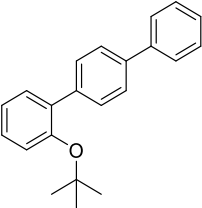
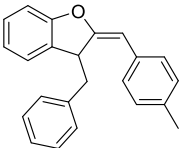
**Table 10. Potential dual CB2/TRPV1 candidates obtained upon screening of a JWH133 structurally related chemical database. Selected hits have been classified according to common structural moieties.**

PubChem ID	Structure	CB2 docking score	TRPV1 docking score		Reported biological activity	References
			VBP site	CBD site		
JWH133		-10.24	-7.05	-6.54	CB2/TRPV1 reference agonist	40,245
<i>4-Aryl chromanes</i>						
1238803		-10.35	-8.21	-	Synthetic methodology, no activity reported <sup>#</sup>	246
6577075		-10.49	-8.04	-	Synthetic methodology, no activity reported <sup>#</sup>	246
7066525		-10.13	-	-8.25	No activity reported <sup>#</sup>	Commercially available



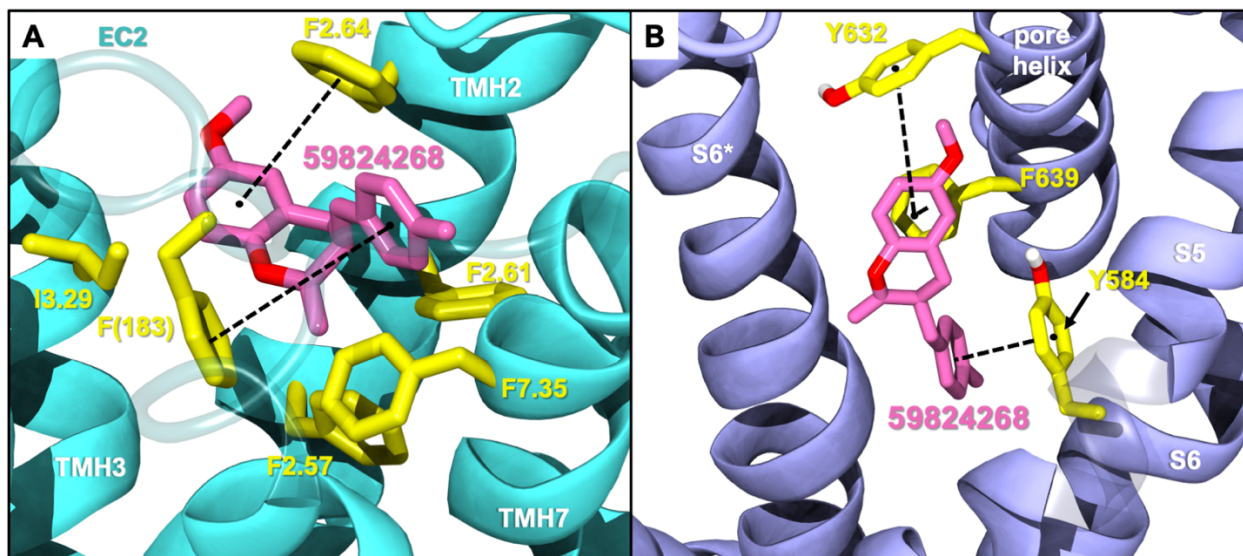
20560217		-10.03	-8.79	-	Anorexigenic activity in rats <sup>#</sup>	247
57756957*		-10.23	-8.73	-	Bactericide and antiviral activity <sup>#</sup>	248
<i>3- or 7-Methylene chromanes</i>						
59824268*		-9.78	-	-8.22	Ink composition <sup>#</sup>	249
148365500		-10.44	-	-8.81	Electrolyte composite for a fuel cell containing a fluorine ion-exchange resin <sup>#</sup>	250
91587558		-10.24	-8.18	-	Modulator of dopamine 3 receptor <sup>#</sup>	251
141098199		-10.28	-8.72	-	Anti-inflammatory properties <sup>#</sup>	252
<i>Phytocannabinoid-like molecules</i>						
68117155		-10.88	-8.99	-	Phytocannabinoid-like molecule claimed as tranquilizing and antidepressant agent	253

142557024		-10.30	-8.52	-	Phytocannabinoid-like molecule included in a cannabinoid preparation that contains $\alpha$ -tocopherol	254
148053384		-10.29	-8.29	-	Topical compositions comprising hydroxy acids and cannabinoids for skincare	255–257
<i>Other tricyclic structures</i>						
89342940		-10.69	-	-8.53	Organic luminescent material <sup>#</sup>	258
123533625*		-10.81	-	-9.50	Intermediate in the modular synthesis of graphene nanoribbons <sup>#</sup>	259,260
153641693*		-10.12	-8.49	-8.74	Synthesis of heterocyclic esters of benzopyrans, no activity reported <sup>#</sup>	261

<i>Miscellaneous chemotypes</i>						
140022260		-10.16	-8.75	-	Synthesis of new 4,4''-substituted oxy- <i>p</i> -terphenyl compounds, no activity reported <sup>#</sup>	262
151332252*		-10.35	-9.79	-	Synthesis of 2-substituted 3-arylmethylbenzofuran, no activity reported	263
*Molecules selected for further investigations through manual docking and ADMET profiling.						
<sup>#</sup> CB2 and TRPV1 activity has not been reported for these compounds. Docking scores are provided in Kcal/mol.						

Among the five selected candidates, 3-(4-methylbenzyl)- chromane 59824268 presented a better druggability profile (Supplementary Table 13) being therefore prioritized for future in vitro testing as CB2/TRPV1 dual modulator. As shown in Supplementary Table 13, candidates 57756957, 123533625, 153641693, and 151332252 exhibit HERG values that fall outside the range of approved drugs. Docking studies of 59824268 at CB2 and TRPV1 are shown in Figure 41. At CB2 this chromane sits a bit higher than JWH133 in the binding crevice being stabilized by hydrophobic and aromatic interactions with residues F2.64, F2.61, F2.57, F183 and F7.35. Regarding TRPV1, 59824268 orients itself in a way similar to JWH133 in the pocket maintaining overlap with the aromatic ring. While JWH133 appears to have primary interactions with Y584, 59824268 has interactions with Y584 in addition to Y632 and F639, further stabilizing the chromane in this pocket.

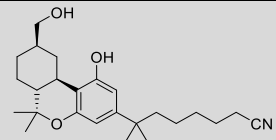
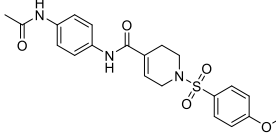
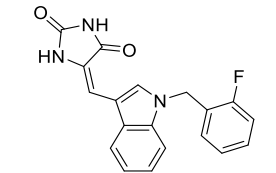
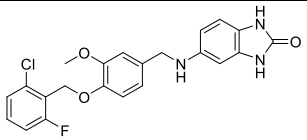
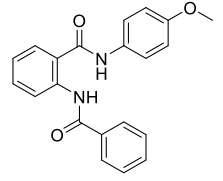
**Figure 41. Selected compound 59824268 docked in CB2 (A) and TRPV1 (B). EC2: Extracellular loop 2; TMH, transmembrane helix.**

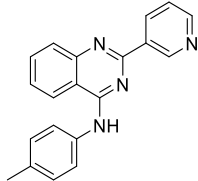
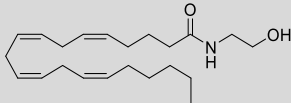
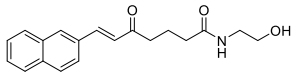
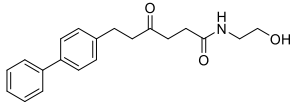
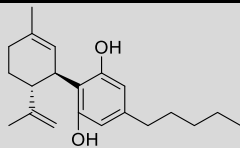
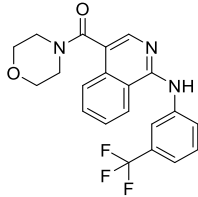


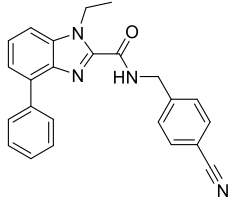
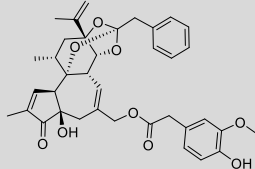
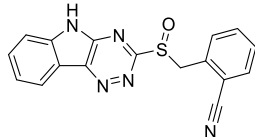
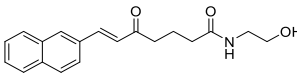
## Cross-agonist virtual screening

The second strategy for the identification of dual compounds is based on a HTVS of reported CB2 and TRPV1 agonists. CB2 agonists indexed in the ChEMBL database have been retrieved and studied in the three known TRPV1 binding sites as detailed in section 2.4. Likewise, TRPV1 ligands indexed in the ChEMBL database have been retrieved and studied in the CB2 binding site. Following the workflow depicted in Supplementary Figure 44B, five candidates were selected for further analysis at each receptor (Table 11). Reported activity at the known target, docking score (Table 11) and druggability profile (Supplementary Table 14) led us to select compounds 1288208, 1288239 (TRPV1 virtual screening) 1508577 and 1508215 (CB2 virtual screening). 1288208 passed the screening as a potential modulator of TRPV1 at two sites: the VBP and tunnel. While there is argument for the elimination of this ligand due to lack of site specificity, it was selected for exactly this reason. With the abundance of ligands reported to modulate TRPV1, and the variability in reported and putative binding locations, a ligand that shows the potential for interaction at multiple locations, both putative and confirmed, within the channel is worthy of further study to better understand why this is. In the VBP, the headgroup of 1288208 forms H-bonds with R557 and S512 via the backbone and hydroxy group, both reachable from within the tunnel. The  $\alpha,\beta$ -unsaturated ketone oxygen H-bonds with Y511, and the addition of the naphthyl moiety at the tail end of the ligand provides pi-stacking capabilities farther up in the VBP with F543 and F591 (Figure 42A).

Table 11. Potential dual CB2/TRPV1 candidates obtained through the crossed-agonist strategy.

ChEMBL ID	Structure	CB2 Docking score	TRPV1 reported activity	Other reported targets	References
AM12033		-12.61	NR	None reported	213
1508577		-11.81	EC <sub>50</sub> = 648.4 nM	Inhibitor of the malarial parasite plastid	PubChem bioassays <sup>#</sup>
1508215		-11.67	EC <sub>50</sub> = 23.0 nM	Aldehyde Dehydrogenase 1	PubChem bioassays <sup>#</sup>
1574712		-11.24	EC <sub>50</sub> = 2581.2 nM	None reported	PubChem bioassays
1383349		-11.18	EC <sub>50</sub> = 81623.2 nM	None reported	PubChem bioassays

1347563		-10.89	EC <sub>50</sub> = 1451.5 nM	Inhibitors of the malarial parasite plastid, tyrosyl-DNA phosphodiesterase 1 and TGF-β	PubChem bioassays
AEA		EC <sub>50</sub> = 0.43 μM K <sub>i</sub> = 0.44 μM <sup>##</sup>	-5.01 tunnel	CB1, PPARs, FAAH	40,264
1288208*		K <sub>i</sub> = 1.03 μM	-8.55 tunnel	No activity at CB1 No other target reported	265
1288239		K <sub>i</sub> = 2.25 μM	-8.32 tunnel	No activity at CB1 No other target reported	265
CBD		EC <sub>50</sub> = 0.05 μM K <sub>i</sub> = 0.02-0.56 μM <sup>##</sup>	-6.17 CBD	Several off targets	12,239,242
1644371		EC <sub>50</sub> = 15.8 nM	-9.45 CBD	Weak CB1 activity	266

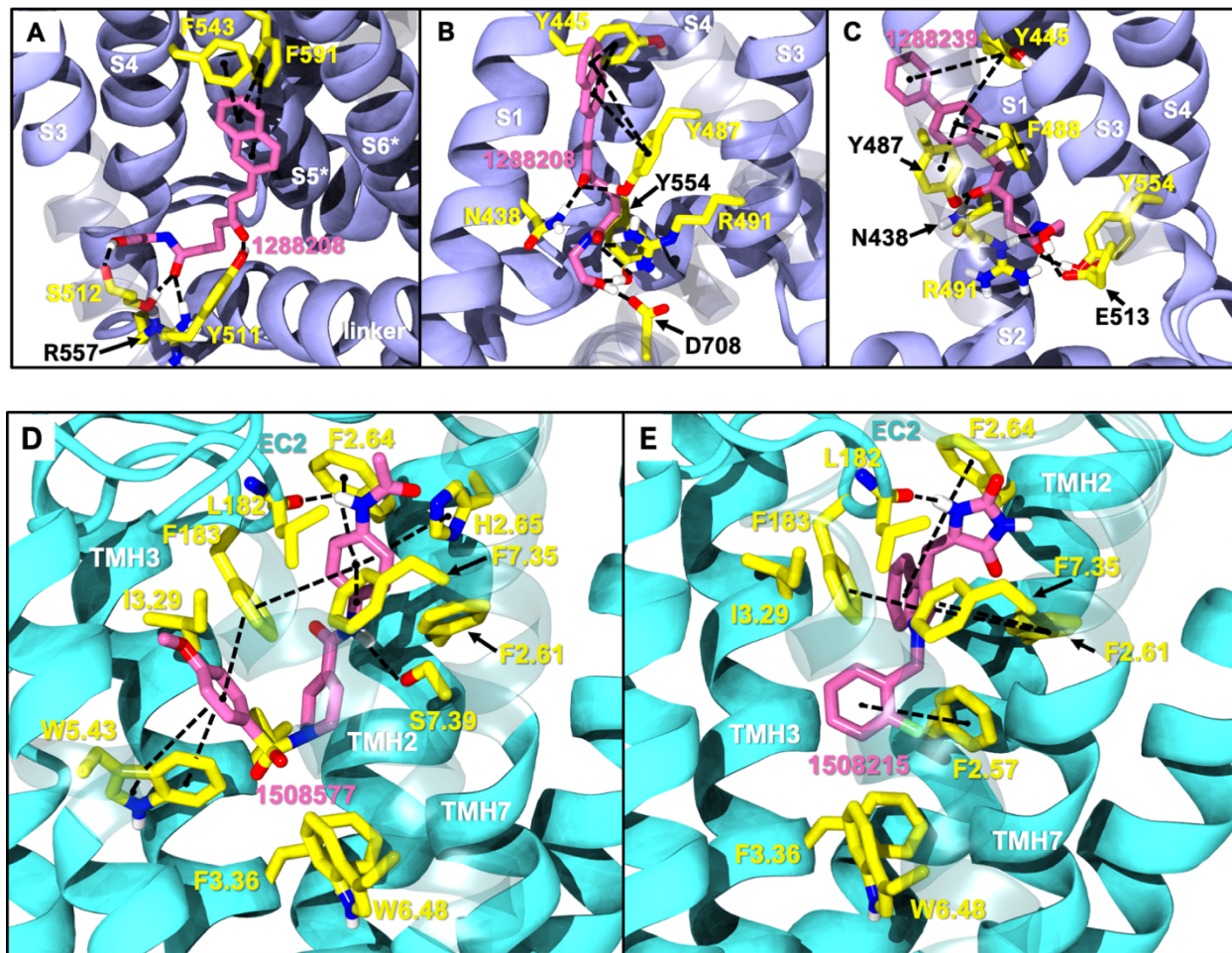
<b>3114522</b>		$EC_{50} = 84 \text{ nM}$	-9.56 CBD	No activity at CB1 No other target reported	267
<b>RTX</b>		NR	-7.62 VBP	Analgesic	73,268
<b>3353818</b>		$EC_{50} = 3.5 \text{ }\mu\text{M}$	-9.80 VBP	None reported	269
<b>1288208*</b>		$K_i = 1.03 \text{ }\mu\text{M}$	-9.97 VBP	No activity at CB1 No other target reported	265
# PubChem bioassays: qHTS Assay for Compounds that Act as Agonists of TRPV1: Hit Validation					
##See table 12 for further pharmacological information.					
NR: Not reported; *Compound selected for both tunnel and VBP docking.					



AEA docking in the tunnel shows headgroup interactions with several residues including Y554, Y555, Y487, D708, and N438 (Supplementary Figure 46). Like AEA, the hydroxyl portion of the headgroup of 1288208 maintains interactions with Y554 and D708, while additional H-bonding between R491 and the amide oxygen is present. The inclusion of an  $\alpha,\beta$ -unsaturated ketone mid-tail allows for more H-bonding via Y487 and N438 near the entrance of the tunnel. The naphthyl moiety at the end of the tail displays pi-pi interactions with both Y487 and Y445 (Figure 42B). The additional interactions of 1288208 could aid in the stability of the ligand in the tunnel from an external standpoint, allowing the headgroup more time in the tunnel, potentially triggering channel activation as previously hypothesized from MD simulations<sup>156,270</sup>

The other selected TRPV1 ligand, 1288239 (Figure 42C), shows headgroup interactions with R491 and Y554, like 1288208, with an additional interaction with E513. The ketone found midway down the tail of ligand H-bonds with N438 and Y487, again similar to 1288208. One feature that differentiates 1288239 from 1288208 is a biphenyl moiety in place of a naphthyl moiety. The lower ring of the biphenyl moiety has aromatic interactions with Y487 and F488, and both rings interact with Y445.

**Figure 42. Docks of selected potential dual candidates: TRPV1 in purple cartoon ribbons (Panels A-C) and CB2 in cyan cartoon ribbons (Panels D and E). Molecules are displayed in pink tubes; all interactions are shown via dashed lines and each helix and residue is labeled. Panel A shows 1288208 in the VBP. A portion of S3 is transparent to aid in visibility.; Panel B shows 1288208 in the tunnel. Helix S2 is shown completely transparent to aid in the visibility of the tunnel.; Panel C shows 1288239 in the tunnel with a portion of helix S2 transparent to aid in visibility. Panel D shows a lipid view of the 1508577/CB2 complex; Panel E shows a lipid view of the 1508215/CB2 complex; TMH6 and 7 are displayed with transparency for a clearer view of the binding site.**



Because of their high potency at TRPV1, their interaction pattern at the CB2 orthosteric pocket and their optimal drug-like properties, compounds 1508577 and 1508215 were selected as potential candidates in the in silico search of dual ligands. Compounds like ACPA-OH and JWH133 also ranked at the top, however, since we are looking for unexplored dual chemotypes, they were not selected in this in silico study. Consistent with the hydrophobic nature of the CB2

orthosteric pocket, compound 1508577 is mainly stabilized by aromatic and van der Waals interactions. As displayed in Figure 42D,  $\pi$ - $\pi$  stackings are established between the methoxybenzene group with W5.43 and F183 and the phenylacetamide group with F183, F7.35, F2.64 and H2.65. Moreover, the acetamide hydrogen engages with the backbone carbonyl oxygen of V182 in a H-bond while the central amide H-bonds with S7.39. Compound 1508215 (Figure 42E) orients similarly in the binding crevice establishing aromatic  $\pi$ - $\pi$  interactions between the central indole core and F183, F2.61 and F2.64, and the fluorobenzyl group with F2.57. In addition, the imidazolidinedione group H-bonds with the backbone carbonyl oxygen of V182.

In summation, from this approach, compounds 1288208, 1288239, 1508577, and 1508215 have been selected for future in vitro appraisal as dual CB2/TRPV1 agonists. Other compounds such as 1644371 could also be remarkable candidates for testing at TRPV1 due to its nanomolar agonist potency at CB2.

### **Off-target evaluation**

The selected hits (59824268, 1288208, 1288239, 1508577 and 1508215) have also been docked in related receptors in order to identify potential off-target effects. These molecules have been screened at CB1 and the cannabinoid-related GPCRs GPR55 and GPR18 in their active and inactive states. In addition, cannabinoid-related channels including TRPV2, TRPV3, TRPA1, and TRPM8 have also been assessed. As shown in Supplementary Table 16, by comparing docking scores to their reference orthosteric ligands we can conclude that at cannabinoid GPCRs compounds 1288208 and 1288239 might be more promiscuous showing high interaction energies at the GPR55 active and GPR18 inactive models. Moreover, compounds 1508577 and 1508215 may moderately act at CB1 whereas 1288208 and 1288239 were reported to lack

binding affinity<sup>265</sup>. 59824268 may be less selective with higher energies for the apo TRPV3 structure as well as both TRPA1 structures. 1288208 and 1288239 both show energies that are either comparable to or better than the reference ligand for each respective receptor, perhaps suggesting that the ethanolamide head group may be too promiscuous of a moiety to include when aiming to develop ligands for selective dual targeting. 1508577 shows variable activity across the TRP channels with comparable energies to the reference compounds of TRPV3 and TRPA1 in both states, with 1508215 displaying the potential for promiscuity at TRPA1. In light of these results, compounds 59824268, 1508577 and 1508215 could be prioritized as TRPV1/CB2 dual modulators. However, compounds with moderate activity at other cannabinoid targets could also be beneficial when targeting specific pathologies in which the ECS is involved or avoided when searching for more selective cannabinoid modulators.

Nonetheless, off-targets cannot be completely ruled out and not only cannabinoid-related but also other receptor families should be tested experimentally at further stages of this project.

### **Conclusion**

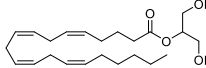
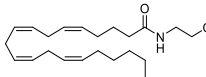
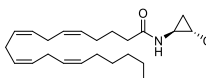
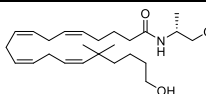
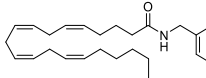
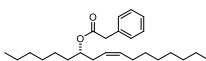
Three-dimensional crystal and cryo-EM structures of GPCRs and TRP channels are being resolved at a rapid pace in the last years. The resolution of these structures are showing great impact in the field of drug discovery facilitating the emergence of successful in silico strategies for the identification of potential drugs targeting complex physiopathological processes.

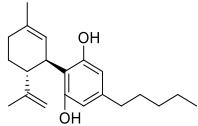
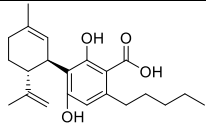
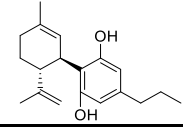
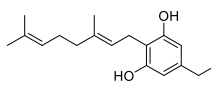
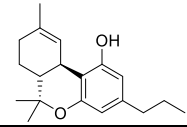
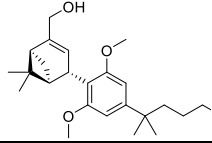
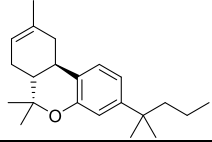
The ECS is composed by a variety of receptors including GPCRs, TRP channels, nuclear receptors such as the PPARs<sup>12</sup>. Polypharmacological approaches targeting this system have already shown successful results<sup>228–231</sup>. For instance, a PPAR $\gamma$ -CB2 molecule has entered clinical trials for the treatment of systemic and multiple sclerosis<sup>271,272</sup>.

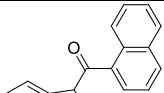
In this context, synergistic effects between TRPV1 and CBRs offer novel avenues for the management of pain or neurodegenerative pathologies among others. While CB1/ TRPV1 dual modulators have been further studied, CB2/ TRPV1 agonists have not been yet exploited. Therefore, this brief research article addresses the computational search of novel potential dual candidates for further in vitro and in vivo exploration.

Using two different virtual screening approaches we have identified hits with potential dual agonistic activity taking into account reported data and docking and druggability results. From this study, compounds 59824268, 1288208, 1288239, 1508577 and 1508215 (Supplementary Figure 47) are proposed as main candidates for future experimental appraisal. Other selected molecules reported in this article also present interesting profiles and might be worth exploring. These results provide insights into understudied scaffolds that potentially modulate CB2 and TRPV1 providing novel tools for further studies.

**Table 12. Functionality of reported cannabinoid ligands at TRPV1 and CB2.**

		TRPV1				CB <sub>2</sub>		
Compound	Structure	Efficacy* (%)	Functionality EC <sub>50</sub> (μM)	Desensitization** (μM)	Refs.	Binding <sup>s</sup> K <sub>i</sub> (nM)	Functionality EC <sub>50</sub> (nM)	Refs.
<i>Endocannabinoids and endocannabinoid-like molecules</i>								
<b>2-AG</b>		59.1 ± 0.3	Agonist	0.75 ± 0.03	31,42	1193.9 ± 327.7	Agonist	40,264
			0.85 ± 0.06				645.6 ± 0.4 <sup>#</sup>	
<b>AEA</b>		53.8 ± 0.2	Agonist	0.21 ± 0.06	31,42	439.6 ± 95.9	Agonist	40,264
			0.27 ± 0.01				426.6 ± 0.6 <sup>#</sup>	
<b>ACPA-OH</b> <b>(11a)</b>		75.7 ± 2.8	Agonist	ND	234	290 ± 6	ND	234
			0.047 ± 0.01					
<b>O-1811</b>		62.5 ± 0.8	Agonist	ND	207	800.1 ± 150.2	ND	207
			0.72 ± 0.1					
<b>Arvanil</b>		75.4 ± 4.7	Agonist	ND	168,235	ND	ND	168,235
			0.5 ± 0.2					
<b>PhAR</b> <b>derivative 12</b>		28.9 ± 2.3	Agonist	ND	237	22.0 ± 3.0	Inverse Agonist <sup>##</sup>	237
			0.063 ± 0.004					

<i>Phytocannabinoids and phytocannabinoid-like molecules</i>								
<b>CBD</b>		$44.7 \pm 0.02$	Agonist $1.0 \pm 0.1$	$0.6 \pm 0.05$	<sup>238</sup>	240 (24–560)	Partial Agonist and NAM	<sup>239,242</sup>
							$50.1 \pm 3.6^{###}$	
<b>CBDA</b>		<10	Agonist $19.7 \pm 3.9$	$89.1 \pm 0.3$	<sup>238</sup>	12 (4.9–77)	Partial Agonist 140 (29–310)	<sup>239</sup>
<b>CBDV</b>		$21.4 \pm 0.6$	Agonist $3.6 \pm 0.7$	$10.0 \pm 0.5$	<sup>238</sup>	140 (96–280)	Partial Agonist 5.0 (0.46–33)	<sup>239</sup>
<b>CBG</b>		$33.8 \pm 2.3$	Agonist $1.3 \pm 0.5$	$2.6 \pm 0.2$	<sup>238</sup>	490 (130–2500)	Partial Agonist 130 (30–550)	<sup>239</sup>
<b>THCV</b>		$68.0 \pm 1.6$	Agonist $1.5 \pm 0.2$	$1.3 \pm 0.1$	<sup>238</sup>	47 (21–270)	Agonist 280 (49–610)	<sup>239</sup>
<b>HU308</b>		<10	NA	$69.0 \pm 5.7$	<sup>40</sup>	$22.7 \pm 3.9$	Agonist $51.3 \pm 0.3^{\#}$	<sup>40,273</sup>
<b>JWH133</b>		$24.6 \pm 0.4$	Agonist $8.2 \pm 0.7$	$77.7 \pm 3.0$	<sup>40</sup>	$3.4 \pm 1.0$	Agonist $109.6 \pm 0.4^{\#}$	<sup>40,245</sup>

Aminoalkylindole							
<b>WIN55212-2</b> 	44.4 ± 0.9	Agonist	35.8 ± 2.2	40	3.7 ± 0.2	Agonist	40,232
		19.2 ± 1.3				10.9 ± 0.9 <sup>#</sup>	

\*Efficacy as % of ionomycin 4 μM; \*\*Desensitization vs standardized agonist (0.1 μM capsaicin) at IC<sub>50</sub> concentrations.

<sup>§</sup>[<sup>3</sup>H]CP55,940 displacement from hCB2R cell membranes.

<sup>#</sup>GTPγS assays; <sup>##</sup>GTPγS assays-IC<sub>50</sub> ≈ 3.2 nM (extracted from the graph); <sup>###</sup>cAMP assays

NA: No activity, ND: Not determined; NAM: Negative allosteric modulator.



**Figure 43. TRPV1 sites:** A) RTX/TRPV1 complex in the VBP. The vanilloid binding pocket (VBP) is the location in TRPV1 in which capsaicin and resiniferatoxin (RTX) are shown to bind. RTX was used as the internal standard. The vanillyl moiety present in RTX binds deep in the VBP with the hydroxy group interacting with residues S512 and R557. Y511 interacts with one of the ester oxygens, providing stability from a key player in TRPV1 activation in response to vanilloid ligands.; B) AEA/TRPV1 complex in the S1-S4 tunnel. Previous MD results show AEA entering a novel region between the S1-S4 helices, separate from the VBP and where the putative CBD site has been reported in TRPV2.; C) CBD/TRPV1 complex between helices S5 and S6 of one monomer and S6 of another (S6\*). Ligands are shown in green VDW, helices S1-S4 are shown as purple cartoon tubes and labeled, helices S5, S6, S5\* and S6\* are shown as cartoon ribbons and labeled. S5\* and S6\* are helices from the adjacent monomer. A recently published cryo-EM structure shows CBD binding in a location separate from the VBP and the tunnel between helices S5 and S6 (double check) in TRPV2. Though TRPV1 and TRPV2 share some similar features with one another, they also have a fair share of differences as analyzed in Muller 2020. The central resorcinol ring found in CBD shows two pi-stacking interactions in this putative CBD site with Y584 and F639.

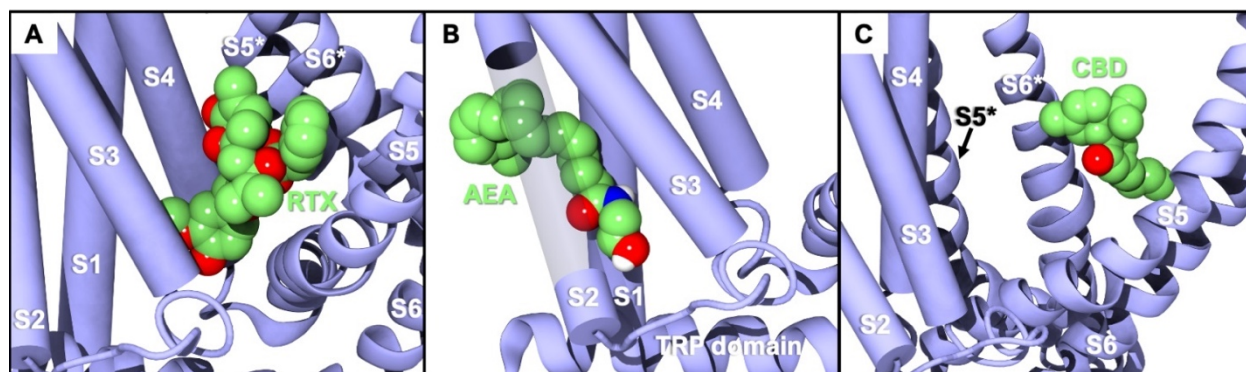
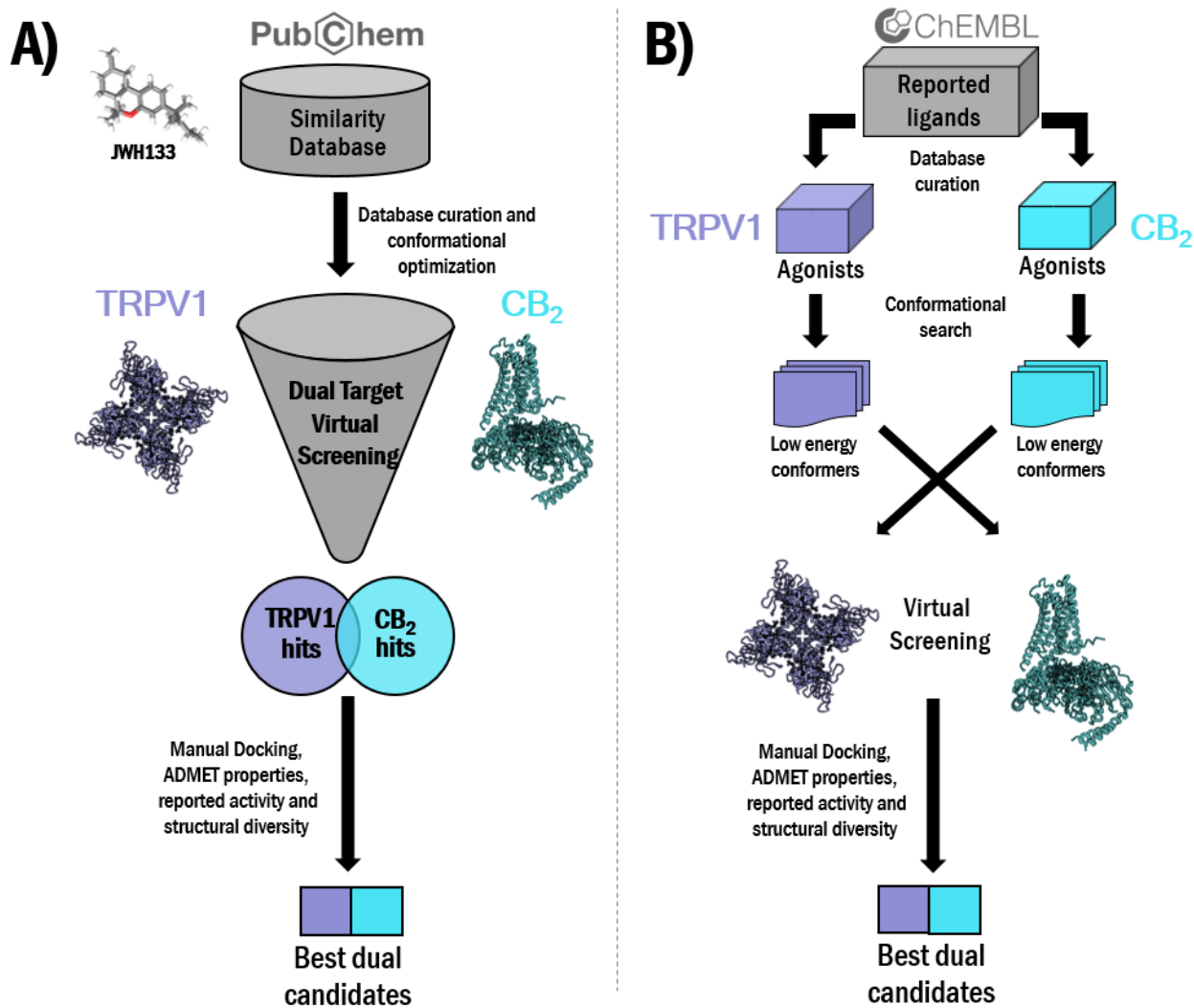
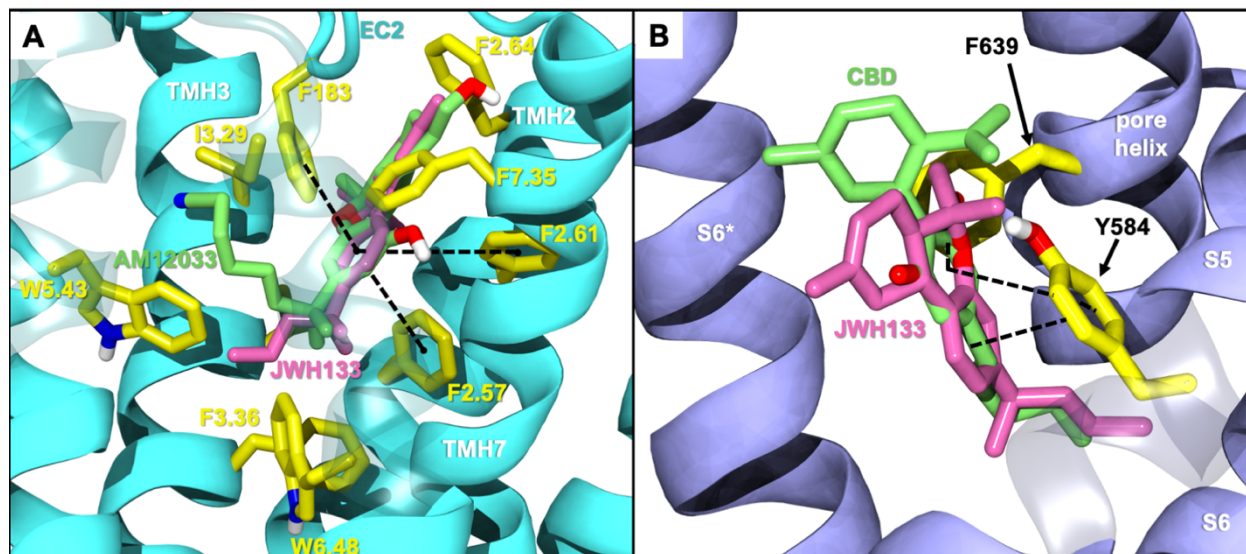


Figure 44. Workflows for the *in silico* identification of dual TRPV1/CB2 ligands. A) Virtual screening of JWH133 structurally related chemical databases; B) Cross-agonist HTVS.



**Figure 45. Docking studies of JWH133 in CB2 and TRPV1. A) CB2/JWH133 complex; B) TRPV1/JWH133 complex. JWH133 is displayed in magenta while reference compounds AM12033 (for CB2) and CBD (for TRPV1) are displayed in green. EC2: Extracellular loop 2; TMH: transmembrane helix.**



**Table 13. Physicochemical descriptors calculated by QikProp 3.5 integrated in Maestro (Schrödinger, LLC, New York, USA) for potential CB2/TRPV1 modulators identified upon screening of a JWH133-related chemical library.**

Compd	QPlogS <sup>a</sup>	QlogBB <sup>b</sup>	QPlogHERG <sup>c</sup>	QPPCaco <sup>d</sup>	%Human oral absorption GI <sup>e</sup>	PAINS <sup>#</sup>
<b>JWH133</b>	-9.13	0.92	-4.62	9906.04	100	0
<b>57756957</b>	-8.26	0.52	-5.82	9897.08	100	0
<b>59824268</b>	-6.38	0.22	-4.95	9902.03	100	0
<b>123533625</b>	-9.12	0.39	-5.98	9734.16	100	1
<b>153641693</b>	-8.79	0.38	-5.76	9938.04	100	0
<b>151332252</b>	-8.54	0.25	-6.45	8901.59	100	0

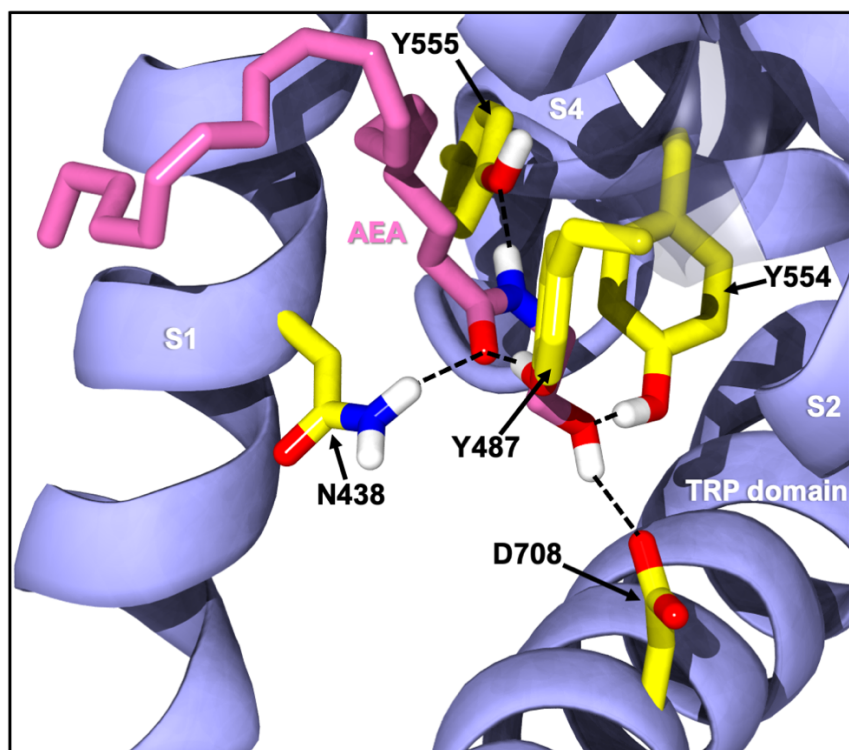
<sup>a</sup>Predicted aqueous solubility [-6.5/0.5]; <sup>b</sup>Predicted log of the brain/blood partition coefficient [-3.0/1.2]; <sup>c</sup>HERG K<sup>+</sup> Channel Blockage (log IC<sub>50</sub>) [concern below -5]; <sup>d</sup>Apparent Caco-2 cell permeability in nm/s [<25 poor, >500 excellent]; <sup>e</sup>Human Oral Absorption in GI [<25% is poor]. [range of 95% of drugs]. <sup>#</sup>Number of structural alerts as calculated using the swissADME webserver <sup>216</sup>.

**Table 14. Physicochemical descriptors calculated by QikProp 3.5 integrated in Maestro (Schrödinger, LLC, New York, USA) for potential CB2/TRPV1 modulators identified using the crossed-agonist strategy.**

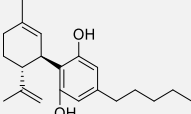
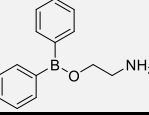
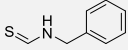
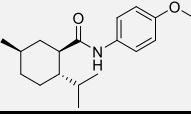
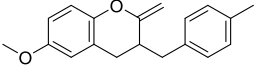
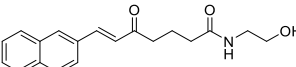
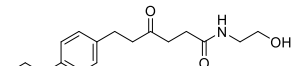
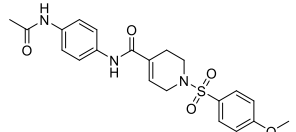
Compd	QPlogS <sup>a</sup>	QlogBB <sup>b</sup>	QPlogHERG <sup>c</sup>	QPPCaco <sup>d</sup>	%Human oral absorption GI <sup>e</sup>	PAINS <sup>#</sup>
AM12033	-7.38	-1.62	-4.95	353.08	100	0
1508577	-4.84	-1.56	-5.91	264.91	84	0
1508215	-4.86	-0.99	-5.07	376.21	93	0
1574712	-5.32	-0.99	-5.47	446.52	100	0
1383349	-5.49	-0.40	-7.00	2405.32	100	0
1347563	-5.46	-0.14	-6.73	3176.79	100	0
<b>TRPV1</b>						
Compd	QPlogS <sup>a</sup>	QlogBB <sup>b</sup>	QPlogHERG <sup>c</sup>	QPPCaco <sup>d</sup>	%Human oral absorption GI <sup>e</sup>	PAINS <sup>#</sup>
AEA	-6.02	-1.52	-4.69	994.90	100	0
1288208*	-3.04	-1.33	-4.58	395.41	86	0
1288239	-3.65	-1.51	-5.16	287.31	86	0
CBD	-5.92	-0.47	-4.87	2519.02	100	0
1644371	-5.42	0.15	-5.59	2986.65	100	0
3114522	-8.35	-1.19	-7.69	774.81	100	0
RTX	-8.81	-1.97	-7.17	289.99	81	1
3353818	-4.77	1.38	-6.10	7.99	51	0
1288208*	-3.04	-1.33	-4.58	395.41	86	0
1644673	-6.13	0.67	-8.15	1152.10	100	0

<sup>a</sup>Predicted aqueous solubility [-6.5/0.5]; <sup>b</sup>Predicted log of the brain/blood partition coefficient [-3.0/1.2]; <sup>c</sup>HERG K<sup>+</sup> Channel Blockage (log IC<sub>50</sub>) [concern below -5]; <sup>d</sup>Apparent Caco-2 cell permeability in nm/s [<25 poor, >500 excellent]; <sup>e</sup>Human Oral Absorption in GI [<25% is poor]. [range of 95% of drugs]; \*Compound selected for both tunnel and VBP docking. <sup>#</sup>Number of structural alerts as calculated using the swissADME webserver <sup>216</sup>.

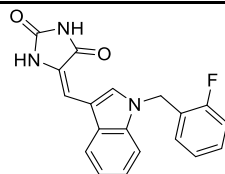
**Figure 46.** The docking output of AEA (pink) in the S1-S4 tunnel region of TRPV1. Headgroup interactions consist of H-bonds with N438, D708, Y487, Y554, and Y555 (all yellow).



**Table 15. Off-target evaluation at cannabinoid-related TRPs of selected dual hits 59824268, 1288208, 1288239, 1508577 and 1508215. The following compounds have been included as reference for each target: TRPV2 agonist (CBD), TRPV3 agonist (2-ABP), TRPA1 agonist (benzothioformamide), and TRPM8 agonist (WS-12).**

Compd	Structure	TRPV2 active <sup>a</sup>	TRPV2 apo <sup>ah</sup>	TRPV3 active <sup>b</sup>	TRPV3 apo <sup>ch</sup>	TRPA1 active <sup>dh</sup>	TRPA1 apo <sup>chi</sup>	TRPM8 active <sup>f,h</sup>	TRPM8 apo <sup>gh</sup>
<b>CBD<sup>a</sup></b>		-10.79	-8.71	-	-	-	-	-	-
<b>2-ABP<sup>c</sup></b>		-	-	-6.99	-4.08	-	-	-	-
<b>Benzothioformamide<sup>d</sup></b>		-	-	-	-	-7.98	-5.21	-	-
<b>WS-12<sup>f</sup></b>		-	-	-	-	-	-	-9.43	-4.56
<b>59824268</b>		-8.24	-7.60	-6.11	-5.11	-6.28	-6.48	-7.07	-4.53
<b>1288208</b>		-10.28	-9.13	-7.18	-6.42	-7.04	-7.60	-8.35	-6.96
		VBP	VBP	TNL	TNL	VBP	VBP	VBP	VBP
<b>1288239</b>		-9.83	-8.98	-8.76	-7.35	-7.98	-7.43	-9.43	-6.58
		VBP	TNL	TNL	TNL	VBP	VBP	VBP	VBP
<b>1508577</b>		-5.58	-6.50	-6.40	-3.92	-4.13	-4.56	-4.80	-3.87

---

**1508215**

-5.24

-8.77

-5.47

-5.94

-6.21

-6.88

-6.93

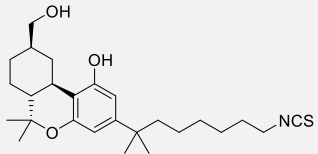
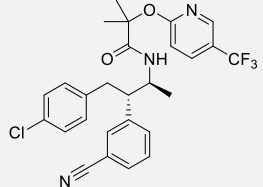
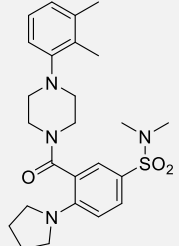
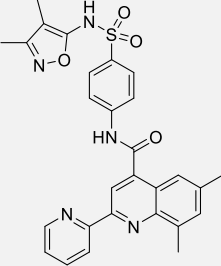
-2.90

---

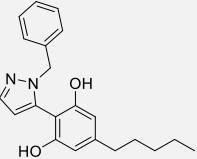
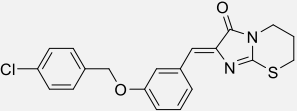
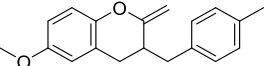
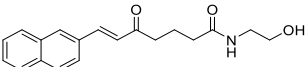
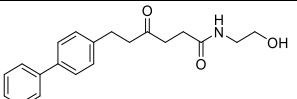
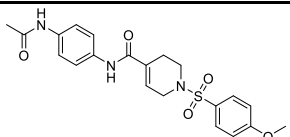
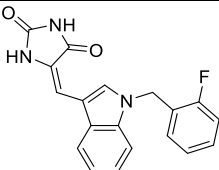
<sup>a</sup>221, <sup>b</sup> 223, <sup>c</sup>222, <sup>d</sup>224, <sup>e</sup>225, <sup>f</sup>227, <sup>g</sup>226226,227; <sup>h</sup>Reference ligands were tested at each apo structure to determine their docking score at the inactive structure. TRPV2, TRPV3, and TRPM8 showed decreases in the scoring. <sup>i</sup>The apo state in TRPA1 indicates a higher score than the active structure. Since benzothioformamide covalently binds intracellularly, the resolved lipid found in the transmembrane region was used as the inactive reference. Since the ligands tested are more lipophilic than the agonist used, this site was used to dock the selected ligands. <sup>\*</sup>These ligands were screened in the VBP and the tunnel of each channel due to their docking withing the tunnel of TRPV1. The best score of the two recorded and indicated here as “VBP” or “TNL”.

---

**Table 16. Off-target evaluation at cannabinoid-related GPCRs of selected dual hits 59824268, 1288208, 1288239, 1508577 and 1508215. The following compounds have been included as reference for each target: CB1 agonist (AM841), CB1 antagonist (Taranabant), GPR55 agonist (ML184), GPR55 antagonist (ML193), GPR18 agonist (S5), and GPR18 antagonist (PBS-CB5).**

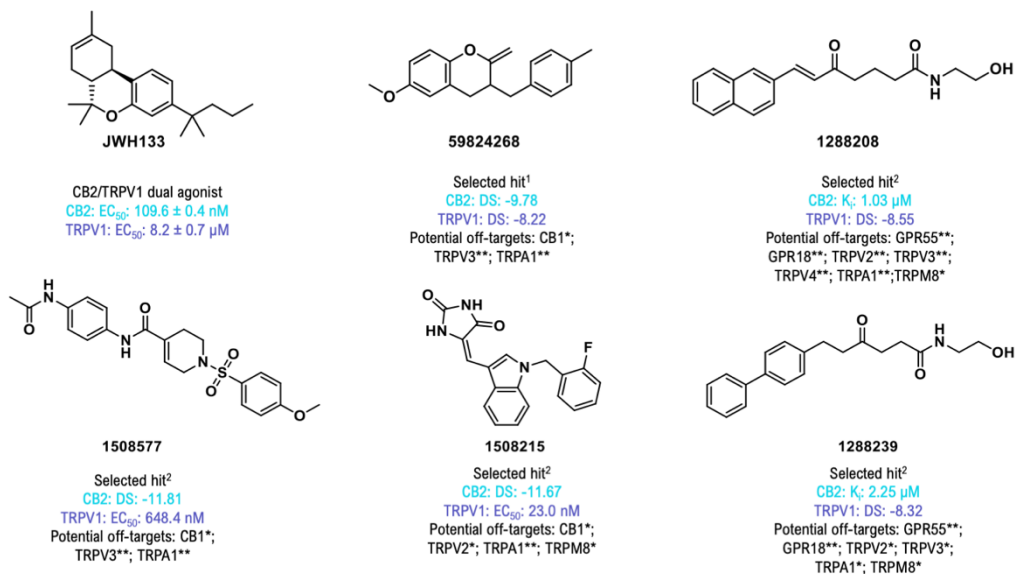
Compd	Structure	CB1 active <sup>a</sup>	CB1 inactive <sup>b</sup>	GPR55 active <sup>c</sup>	GPR55 Inactive <sup>d</sup>	GPR18 active <sup>e</sup>	GPR18 Inactive <sup>e</sup>
AM841 <sup>a</sup>		-12.07	-	-	-	-	-
Taranabant <sup>b</sup>		-	-14.89	-	-	-	-
ML184 <sup>c</sup>		-	-	-10.31	-	-	-
ML193 <sup>d</sup>		-	-	-	-6.98	-	-



<b>S5<sup>f</sup></b>		-	-	-	-	-7.19	-
<b>PSB-CB5<sup>g</sup></b>		-	-	-	-	-	-6.79
<b>59824268</b>		-7.19	-8.46	-7.85	-4.37	-4.40	-4.15
<b>1288208</b>		Inactive <sup>h</sup>	Inactive <sup>h</sup>	-10.51	-5.75	-3.20	-6.03
<b>1288239</b>		Inactive <sup>h</sup>	Inactive <sup>h</sup>	-10.16	-4.31	-5.56	-5.91
<b>1508577</b>		-7.85	-9.27	-8.03	-1.65	-2.40	-3.50
<b>1508215</b>		-8.03	-9.51	-7.49	-5.97	-3.18	-4.64

<sup>a</sup>PDB-ID: 6KPG <sup>213</sup>; <sup>b</sup>PDB-ID: 5U09 <sup>274</sup>; <sup>c</sup>219; <sup>d</sup>275; <sup>e</sup>220; <sup>f</sup>276; <sup>g</sup>277; <sup>h</sup>Reported binding assays indicate that these compounds do not show activity at CB1 [ $K_i > 10 \mu\text{M}$  <sup>265</sup>]

**Figure 47. Summary of selected hits. DS: docking scores in Kcal/mol. <sup>1</sup>Hit selected through the JWH133 structurally related chemical databases strategy; <sup>2</sup>Hit selected through the cross-agonist HTVS strategy. \*Low activity; \*\*Moderate activity.**



## REFERENCES

- (1) Caterina, M. J. TRP Channel Cannabinoid Receptors in Skin Sensation, Homeostasis, and Inflammation. *ACS Chemical Neuroscience*. American Chemical Society November 19, 2014, pp 1107–1116. <https://doi.org/10.1021/cn5000919>.
- (2) Vay, L.; Gu, C.; McNaughton, P. A. The Thermo-TRP Ion Channel Family: Properties and Therapeutic Implications. *British Journal of Pharmacology*. February 2012, pp 787–801. <https://doi.org/10.1111/j.1476-5381.2011.01601.x>.
- (3) Perálvarez-Marín, A.; Doñate-Macian, P.; Gaudet, R. What Do We Know about the Transient Receptor Potential Vanilloid 2 (TRPV2) Ion Channel? In *FEBS Journal*; 2013; Vol. 280, pp 5471–5487. <https://doi.org/10.1111/febs.12302>.
- (4) Vay, L.; Gu, C.; McNaughton, P. A. The Thermo-TRP Ion Channel Family: Properties and Therapeutic Implications. *British Journal of Pharmacology*. 2012. <https://doi.org/10.1111/j.1476-5381.2011.01601.x>.
- (5) Storozhuk, M. V.; Zholos, A. V. TRP Channels as Novel Targets for Endogenous Ligands: Focus on Endocannabinoids and Nociceptive Signalling. *Curr. Neuropharmacol.* **2017**, 15 (0). <https://doi.org/10.2174/1570159x15666170424120802>.
- (6) Levine, J. D.; Alessandri-Haber, N. TRP Channels: Targets for the Relief of Pain. *Biochimica et Biophysica Acta - Molecular Basis of Disease*. August 2007, pp 989–1003. <https://doi.org/10.1016/j.bbadis.2007.01.008>.
- (7) Iannotti, F. A.; Hill, C. L.; Leo, A.; Alhusaini, A.; Soubrane, C.; Mazzarella, E.; Russo, E.; Whalley, B. J.; Di Marzo, V.; Stephens, G. J. Nonpsychotropic Plant Cannabinoids, Cannabidiol (CBD) and Cannabidiol (CBD), Activate and Desensitize Transient Receptor Potential Vanilloid 1 (TRPV1) Channels in Vitro: Potential for the Treatment of Neuronal Hyperexcitability. *ACS Chem. Neurosci.* **2014**, 5 (11), 1131–1141. <https://doi.org/10.1021/cn5000524>.
- (8) De Petrocellis, L.; Guida, F.; Moriello, A. S.; De Chiaro, M.; Piscitelli, F.; De Novellis, V.; Maione, S.; Di Marzo, V. N-Palmitoyl-Vanillamide (Palvanil) Is a Non-Pungent Analogue of Capsaicin with Stronger Desensitizing Capability against the TRPV1 Receptor and Anti-Hyperalgesic Activity. *Pharmacol. Res.* **2011**, 63 (4), 294–299. <https://doi.org/10.1016/j.phrs.2010.12.019>.
- (9) Luongo, L.; Costa, B.; D'Agostino, B.; Guida, F.; Comelli, F.; Gatta, L.; Matteis, M.; Sullo, N.; De Petrocellis, L.; De Novellis, V.; Maione, S.; Di Marzo, V. Palvanil, a Non-Pungent Capsaicin Analogue, Inhibits Inflammatory and Neuropathic Pain with Little Effects on Bronchopulmonary Function and Body Temperature. *Pharmacol. Res.* **2012**. <https://doi.org/10.1016/j.phrs.2012.05.005>.

- (10) Woodhams, S. G.; Chapman, V.; Finn, D. P.; Hohmann, A. G.; Neugebauer, V. The Cannabinoid System and Pain. *Neuropharmacology* **2017**, *124*, 105–120. <https://doi.org/10.1016/j.neuropharm.2017.06.015>.
- (11) Guindon, J.; Hohmann, A. The Endocannabinoid System and Pain. *CNS Neurol. Disord. - Drug Targets* **2012**, *8* (6), 403–421. <https://doi.org/10.2174/187152709789824660>.
- (12) Morales, P.; Hurst, D. P.; Reggio, P. H. Molecular Targets of the Phytocannabinoids: A Complex Picture. *Progress in the chemistry of organic natural products*. January 1, 2017, pp 103–131. [https://doi.org/10.1007/978-3-319-45541-9\\_4](https://doi.org/10.1007/978-3-319-45541-9_4).
- (13) Morales, P.; Reggio, P. H. An Update on Non-CB1, Non-CB2 Cannabinoid Related G-Protein-Coupled Receptors. *Cannabis and cannabinoid research*. Mary Ann Liebert Inc January 2017, pp 265–273. <https://doi.org/10.1089/can.2017.0036>.
- (14) Morales, P.; Isawi, I.; Reggio, P. H. Towards a Better Understanding of the Cannabinoid-Related Orphan Receptors GPR3, GPR6, and GPR12. *Drug Metabolism Reviews*. Taylor and Francis Ltd January 2, 2018, pp 74–93. <https://doi.org/10.1080/03602532.2018.1428616>.
- (15) Ahluwalia, J.; Urban, L.; Bevan, S.; Nagy, I. Anandamide Regulates Neuropeptide Release from Capsaicin-Sensitive Primary Sensory Neurons by Activating Both the Cannabinoid 1 Receptor and the Vanilloid Receptor 1 in Vitro. *Eur. J. Neurosci.* **2003**, *17* (12), 2611–2618. <https://doi.org/10.1046/j.1460-9568.2003.02703.x>.
- (16) Price, T. J.; Patwardhan, A.; Akopian, A. N.; Hargreaves, K. M.; Flores, C. M. Modulation of Trigeminal Sensory Neuron Activity by the Dual Cannabinoid-Vanilloid Agonists Anandamide, N-Arachidonoyl-Dopamine and Arachidonoyl-2-Chloroethylamide. *Br. J. Pharmacol.* **2004**, *141* (7), 1118–1130. <https://doi.org/10.1038/sj.bjp.0705711>.
- (17) Cristino, L.; de Petrocellis, L.; Pryce, G.; Baker, D.; Guglielmotti, V.; Di Marzo, V. Immunohistochemical Localization of Cannabinoid Type 1 and Vanilloid Transient Receptor Potential Vanilloid Type 1 Receptors in the Mouse Brain. *Neuroscience* **2006**, *139* (4), 1405–1415. <https://doi.org/10.1016/j.neuroscience.2006.02.074>.
- (18) Anand, U.; Otto, W. R.; Sanchez-Herrera, D.; Facer, P.; Yiangou, Y.; Korchev, Y.; Birch, R.; Benham, C.; Bountra, C.; Chessell, I. P.; Anand, P. Cannabinoid Receptor CB2 Localisation and Agonist-Mediated Inhibition of Capsaicin Responses in Human Sensory Neurons. *Pain* **2008**, *138* (3), 667–680. <https://doi.org/10.1016/j.pain.2008.06.007>.
- (19) Rossi, F.; Siniscalco, D.; Luongo, L.; De Petrocellis, L.; Bellini, G.; Petrosino, S.; Torella, M.; Santoro, C.; Nobile, B.; Perrotta, S.; Di Marzo, V.; Maione, S. The Endovanilloid/Endocannabinoid System in Human Osteoclasts: Possible Involvement in Bone Formation and Resorption. *Bone* **2009**, *44* (3), 476–484. <https://doi.org/10.1016/j.bone.2008.10.056>.

- (20) Winter, Z.; Buhala, A.; Ötvös, F.; Jósvay, K.; Vizler, C.; Dombi, G.; Szakonyi, G.; Oláh, Z. Functionally Important Amino Acid Residues in the Transient Receptor Potential Vanilloid 1 (TRPV1) Ion Channel--an Overview of the Current Mutational Data. *Mol. Pain* **2013**, 9 (1), 30. <https://doi.org/10.1186/1744-8069-9-30>.
- (21) Hellmich, U. A.; Gaudet, R. High-Resolution Views of TRPV1 and Their Implications for the TRP Channel Superfamily. **2014**, 222, 991–1004. <https://doi.org/10.1007/978-3-642-54215-2>.
- (22) Nilius, B.; Szallasi, A. Transient Receptor Potential Channels as Drug Targets: From the Science of Basic Research to the Art of Medicine. *Pharmacol. Rev.* **2014**, 66 (3), 676–814. <https://doi.org/10.1124/pr.113.008268>.
- (23) Paulsen, C. E.; Armache, J. P.; Gao, Y.; Cheng, Y.; Julius, D. Structure of the TRPA1 Ion Channel Suggests Regulatory Mechanisms. *Nature* **2015**, 520 (7548), 511–517. <https://doi.org/10.1038/nature14367>.
- (24) Yin, Y.; Wu, M.; Zubcevic, L.; Borschel, W. F.; Lander, G. C.; Lee, S. Y. Structure of the Cold- And Menthol-Sensing Ion Channel TRPM8. *Science (80-. )*. **2018**, 359 (6372), 237–241. <https://doi.org/10.1126/science.aan4325>.
- (25) Zygmunt, P. M.; Petersson, J.; Andersson, D. A.; Chuang, H. H.; Sörgård, M.; Di Marzo, V.; Julius, D.; Högestätt, E. D. Vanilloid Receptors on Sensory Nerves Mediate the Vasodilator Action of Anandamide. *Nature* **1999**, 400 (6743), 452–457. <https://doi.org/10.1038/22761>.
- (26) De Petrocellis, L.; Starowicz, K.; Moriello, A. S.; Vivese, M.; Orlando, P.; Di Marzo, V. Regulation of Transient Receptor Potential Channels of Melastatin Type 8 (TRPM8): Effect of CAMP, Cannabinoid CB1receptors and Endovanilloids. *Exp. Cell Res.* **2007**, 313 (9), 1911–1920. <https://doi.org/10.1016/j.yexcr.2007.01.008>.
- (27) De Petrocellis, L.; Ligresti, A.; Moriello, A. S.; Allarà, M.; Bisogno, T.; Petrosino, S.; Stott, C. G.; Di Marzo, V. Effects of Cannabinoids and Cannabinoid-Enriched *Cannabis* Extracts on TRP Channels and Endocannabinoid Metabolic Enzymes. *Br. J. Pharmacol.* **2011**, 163 (7), 1479–1494. <https://doi.org/10.1111/j.1476-5381.2010.01166.x>.
- (28) Ruparel, N. B.; Patwardhan, A. M.; Akopian, A. N.; Hargreaves, K. M. Desensitization of Transient Receptor Potential Ankyrin 1 (TRPA1) by the TRP Vanilloid 1-Selective Cannabinoid Arachidonoyl-2 Chloroethanolamine. *Mol. Pharmacol.* **2011**, 80 (1), 117–123. <https://doi.org/10.1124/mol.110.068940>.
- (29) De Petrocellis, L.; Nabissi, M.; Santoni, G.; Ligresti, A. Actions and Regulation of Ionotropic Cannabinoid Receptors. In *Advances in Pharmacology*; Academic Press Inc., 2017; Vol. 80, pp 249–289. <https://doi.org/10.1016/bs.apha.2017.04.001>.

- (30) Chung, M. K.; Campbell, J. N. Use of Capsaicin to Treat Pain: Mechanistic and Therapeutic Considerations. *Pharmaceuticals* **2016**, *9* (66). <https://doi.org/10.3390/ph9040066>.
- (31) Petrosino, S.; Schiano Moriello, A.; Cerrato, S.; Fusco, M.; Puigdemont, A.; De Petrocellis, L.; Di Marzo, V. The Anti-Inflammatory Mediator Palmitoylethanolamide Enhances the Levels of 2-Arachidonoyl-Glycerol and Potentiates Its Actions at TRPV1 Cation Channels. *Br. J. Pharmacol.* **2016**, *173* (7), 1154–1162. <https://doi.org/10.1111/bph.13084>.
- (32) De Petrocellis, L.; Di Marzo, V. Lipids as Regulators of the Activity of Transient Receptor Potential Type V1 (TRPV1) Channels. *Life Sci.* **2005**, *77* (14), 1651–1666. <https://doi.org/10.1016/j.lfs.2005.05.021>.
- (33) Huang, S. M.; Bisogno, T.; Trevisani, M.; Al-Hayan, A.; De Petrocellis, L.; Fezza, F.; Tognetto, M.; Petros, T. J.; Krey, J. F.; Chu, C. J.; Miller, J. D.; Davies, S. N.; Geppetti, P.; Walker, J. M.; Di Marzo, V. An Endogenous Capsaicin-like Substance with High Potency at Recombinant and Native Vanilloid VR1 Receptors. *Proc. Natl. Acad. Sci.* **2002**, *99* (12), 8400–8405. <https://doi.org/10.1073/pnas>.
- (34) Raboune, S.; Stuart, J. M.; Leishman, E.; Takacs, S. M.; Rhodes, B.; Basnet, A.; Jameyfield, E.; McHugh, D.; Widlanski, T.; Bradshaw, H. B. Novel Endogenous N-Acyl Amides Activate TRPV1-4 Receptors, BV-2 Microglia, and Are Regulated in Brain in an Acute Model of Inflammation. *Front. Cell. Neurosci.* **2014**, *8* (AUG). <https://doi.org/10.3389/fncel.2014.00195>.
- (35) Millan, M. J. The Induction of Pain: An Integrative Review. *Prog. Neurobiol.* **1999**, *57* (1), 1–164. [https://doi.org/10.1016/S0301-0082\(98\)00048-3](https://doi.org/10.1016/S0301-0082(98)00048-3).
- (36) Vandewauw, I.; De Clercq, K.; Mulier, M.; Held, K.; Pinto, S.; Van Ranst, N.; Segal, A.; Voet, T.; Vennekens, R.; Zimmermann, K.; Vriens, J.; Voets, T. A TRP Channel Trio Mediates Acute Noxious Heat Sensing. *Nature* **2018**, *555* (7698), 662–666. <https://doi.org/10.1038/nature26137>.
- (37) Bisogno, T.; Hanusae, L. R.; De Petrocellis, L.; Tchilibon, S.; Ponde, D. E.; Brandi, I.; Moriello, A. S.; Davis, J. B.; Mechoulam, R.; Marzo, V. Di. Molecular Targets for Cannabidiol and Its Synthetic Analogues: Effect on Vanilloid VR1 Receptors and on the Cellular Uptake and Enzymatic Hydrolysis of Anandamide. *Br. J. Pharmacol.* **2001**, *134*, 845–852. <https://doi.org/10.1038/sj.bjp.0704327>.
- (38) Laprairie, R. B.; Bagher, A. M.; Kelly, M. E. M.; Denovan-Wright, E. M. Cannabidiol Is a Negative Allosteric Modulator of the Cannabinoid CB1 Receptor. *Br. J. Pharmacol.* **2015**, *172* (20), 4790–4805. <https://doi.org/10.1111/bph.13250>.
- (39) Hill, T. D. M.; Cascio, M. G.; Romano, B.; Duncan, M.; Pertwee, R. G.; Williams, C. M.; Whalley, B. J.; Hill, A. J. Cannabidivarin-Rich Cannabis Extracts Are Anticonvulsant in

- Mouse and Rat via a CB1 Receptor-Independent Mechanism. *Br. J. Pharmacol.* **2013**. <https://doi.org/10.1111/bph.12321>.
- (40) Soethoudt, M.; Grether, U.; Fingerle, J.; Grim, T. W.; Fezza, F.; De Petrocellis, L.; Ullmer, C.; Rothenhäusler, B.; Perret, C.; Van Gils, N.; Finlay, D.; Macdonald, C.; Chicca, A.; Gens, M. D.; Stuart, J.; De Vries, H.; Mastrangelo, N.; Xia, L.; Alachouzos, G.; Baggelaar, M. P.; Martella, A.; Mock, E. D.; Deng, H.; Heitman, L. H.; Connor, M.; Di Marzo, V.; Gertsch, J.; Lichtman, A. H.; Maccarrone, M.; Pacher, P.; Glass, M.; Van Der Stelt, M. Cannabinoid CB2 Receptor Ligand Profiling Reveals Biased Signalling and Off-Target Activity. *Nat. Commun.* **2017**, *8*. <https://doi.org/10.1038/ncomms13958>.
  - (41) De Petrocellis, L.; Bisogno, T.; Maccarrone, M.; Davis, J. B.; Finazzi-Agrò, A.; Di Marzo, V. The Activity of Anandamide at Vanilloid VR1 Receptors Requires Facilitated Transport across the Cell Membrane and Is Limited by Intracellular Metabolism. *J. Biol. Chem.* **2001**, *276* (16), 12856–12863. <https://doi.org/10.1074/jbc.M008555200>.
  - (42) Lowin, T.; Straub, R. H. Cannabinoid-Based Drugs Targeting CB1 and TRPV1, the Sympathetic Nervous System, and Arthritis. *Arthritis Res. Ther.* **2015**, *17* (1), 226. <https://doi.org/10.1186/s13075-015-0743-x>.
  - (43) Petrosino, S.; Schiano Moriello, A.; Cerrato, S.; Fusco, M.; Puigdemont, A.; De Petrocellis, L.; Di Marzo, V. The Anti-Inflammatory Mediator Palmitoylethanolamide Enhances the Levels of 2-Arachidonoyl-Glycerol and Potentiates Its Actions at TRPV1 Cation Channels. *Br. J. Pharmacol.* **2016**, *173* (7), 1154–1162. <https://doi.org/10.1111/bph.13084>.
  - (44) Chu, C. J.; Huang, S. M.; De Petrocellis, L.; Bisogno, T.; Ewing, S. A.; Miller, J. D.; Zipkin, R. E.; Daddario, N.; Appendino, G.; Di Marzo, V.; Walker, J. M. N-Oleoyldopamine, a Novel Endogenous Capsaicin-like Lipid That Produces Hyperalgesia. *J. Biol. Chem.* **2003**, *278* (16), 13633–13639. <https://doi.org/10.1074/jbc.M211231200>.
  - (45) Ambrosino, P.; Soldovieri, M. V.; Russo, C.; Taglialatela, M. Activation and Desensitization of TRPV1 Channels in Sensory Neurons by the PPAR $\alpha$  Agonist Palmitoylethanolamide. *Br. J. Pharmacol.* **2013**, *168* (6), 1430–1444. <https://doi.org/10.1111/bph.12029>.
  - (46) Qin, N.; Neeper, M. P.; Liu, Y.; Hutchinson, T. L.; Lubin, M. Lou; Flores, C. M. TRPV2 Is Activated by Cannabidiol and Mediates CGRP Release in Cultured Rat Dorsal Root Ganglion Neurons. *J. Neurosci.* **2008**, *28* (24), 6231–6238. <https://doi.org/10.1523/JNEUROSCI.0504-08.2008>.
  - (47) Soethoudt, M.; Grether, U.; Fingerle, J.; Grim, T. W.; Fezza, F.; De Petrocellis, L.; Ullmer, C.; Rothenhäusler, B.; Perret, C.; Van Gils, N.; Finlay, D.; Macdonald, C.; Chicca, A.; Gens, M. D.; Stuart, J.; De Vries, H.; Mastrangelo, N.; Xia, L.; Alachouzos, G.; Baggelaar, M. P.; Martella, A.; Mock, E. D.; Deng, H.; Heitman, L. H.; Connor, M.; Di Marzo, V.; Gertsch, J.; Lichtman, A. H.; Maccarrone, M.; Pacher, P.; Glass, M.; Van

- Der Stelt, M. Cannabinoid CB2 Receptor Ligand Profiling Reveals Biased Signalling and Off-Target Activity. *Nat. Commun.* **2017**, *8*. <https://doi.org/10.1038/ncomms13958>.
- (48) Pedersen, S. F.; Owsianik, G.; Nilius, B. TRP Channels: An Overview. *Cell Calcium* **2005**, *38* (3–4), 233–252. <https://doi.org/10.1016/j.ceca.2005.06.028>.
- (49) De Petrocellis, L.; Orlando, P.; Moriello, A. S.; Aviello, G.; Stott, C.; Izzo, A. A.; di Marzo, V. Cannabinoid Actions at TRPV Channels: Effects on TRPV3 and TRPV4 and Their Potential Relevance to Gastrointestinal Inflammation. *Acta Physiol.* **2012**, *204* (2), 255–266. <https://doi.org/10.1111/j.1748-1716.2011.02338.x>.
- (50) Chung, M. K.; Lee, H.; Mizuno, A.; Suzuki, M.; Caterina, M. J. TRPV3 and TRPV4 Mediate Warmth-Evoked Currents in Primary Mouse Keratinocytes. *J. Biol. Chem.* **2004**, *279* (20), 21569–21575. <https://doi.org/10.1074/jbc.M401872200>.
- (51) Nilius, B.; Vriens, J.; Prenen, J.; Droogmans, G.; Voets, T. TRPV4 Calcium Entry Channel: A Paradigm for Gating Diversity. *Am. J. Physiol. Physiol.* **2004**, *286* (2), C195–C205. <https://doi.org/10.1152/ajpcell.00365.2003>.
- (52) Nilius, B.; Owsianik, G. The Transient Receptor Potential Family of Ion Channels. *Genome Biol* **2011**, *12* (3), 218. <https://doi.org/10.1186/gb-2011-12-3-218>.
- (53) Strotmann, R.; Harteneck, C.; Nunnenmacher, K.; Schultz, G.; Plant, T. D. OTRPC4, a Nonspecific Cation Channel That Confers Sensitivity to Extracellular Osmolarity. *Nat. Cell Biol.* **2000**, *2* (10), 695–702. <https://doi.org/10.1038/35036318>.
- (54) Liedtke, W. TRPV4 Plays an Evolutionary Conserved Role in the Transduction of Osmotic and Mechanical Stimuli in Live Animals. *J. Physiol.* **2005**, *567* (1), 53–58. <https://doi.org/10.1113/jphysiol.2005.088963>.
- (55) Vincent, F.; Duncton, M. TRPV4 Agonists and Antagonists. *Curr. Top. Med. Chem.* **2011**, *11* (17), 2216–2226. <https://doi.org/10.2174/156802611796904861>.
- (56) Duncton, M. A. J. Small Molecule Agonists and Antagonists of TRPV4. In *TRP Channels as Therapeutic Targets: From Basic Science to Clinical Use*; Elsevier, 2015; pp 205–219. <https://doi.org/10.1016/B978-0-12-420024-1.00012-6>.
- (57) Watanabe, H.; Vriens, J.; Prenen, J.; Droogmans, G.; Voets, T.; Nilius, B. Anandamide and Arachidonic Acid Use Epoxyeicosatrienoic Acids to Activate TRPV4 Channels. *Nature* **2003**, *424* (6947), 434–438. <https://doi.org/10.1038/nature01807>.
- (58) Yekkiral, A. S. Two to Tango: GPCR Oligomers and GPCR-TRP Channel Interactions in Nociception. *Life Sci.* **2013**, *92* (8–9), 438–445. <https://doi.org/10.1016/j.lfs.2012.06.021>.
- (59) De Petrocellis, L.; Schiano Moriello, A.; Imperatore, R.; Cristino, L.; Starowicz, K.; Di Marzo, V. A Re-Evaluation of 9-HODE Activity at TRPV1 Channels in Comparison with



- Anandamide: Enantioselectivity and Effects at Other TRP Channels and in Sensory Neurons. *Br. J. Pharmacol.* **2012**, *167* (8), 1643–1651. <https://doi.org/10.1111/j.1476-5381.2012.02122.x>.
- (60) Redmond, W. J.; Gu, L.; Camo, M.; McIntyre, P.; Connor, M. Ligand Determinants of Fatty Acid Activation of the Pronociceptive Ion Channel TRPA1. *PeerJ* **2014**, *2*, e248. <https://doi.org/10.7717/peerj.248>.
  - (61) De Petrocellis, L.; Vellani, V.; Schiano-Moriello, A.; Marini, P.; Magherini, P. C.; Orlando, P.; Di Marzo, V. Plant-Derived Cannabinoids Modulate the Activity of Transient Receptor Potential Channels of Ankyrin Type-1 and Melastatin Type-8. *J. Pharmacol. Exp. Ther.* **2008**, *325* (3), 1007–1015. <https://doi.org/10.1124/jpet.107.134809>.
  - (62) Akopian, A. N.; Ruparel, N. B.; Patwardhan, A.; Hargreaves, K. M. Cannabinoids Desensitize Capsaicin and Mustard Oil Responses in Sensory Neurons via TRPA1 Activation. *J. Neurosci.* **2008**, *28* (5), 1064–1075. <https://doi.org/10.1523/JNEUROSCI.1565-06.2008>.
  - (63) Redmond, W. J.; Gu, L.; Camo, M.; McIntyre, P.; Connor, M. Ligand Determinants of Fatty Acid Activation of the Pronociceptive Ion Channel TRPA1. *PeerJ* **2014**. <https://doi.org/10.7717/peerj.248>.
  - (64) Akopian, A. N.; Ruparel, N. B.; Jeske, N. A.; Hargreaves, K. M. Transient Receptor Potential TRPA1 Channel Desensitization in Sensory Neurons Is Agonist Dependent and Regulated by TRPV1-Directed Internalization. *J. Physiol.* **2007**, *583* (1), 175–193. <https://doi.org/10.1113/jphysiol.2007.133231>.
  - (65) Romano, B.; Borrelli, F.; Fasolino, I.; Capasso, R.; Piscitelli, F.; Cascio, M. G.; Pertwee, R. G.; Coppola, D.; Vassallo, L.; Orlando, P.; Di Marzo, V.; Izzo, A. A. The Cannabinoid TRPA1 Agonist Cannabichromene Inhibits Nitric Oxide Production in Macrophages and Ameliorates Murine Colitis. *Br. J. Pharmacol.* **2013**, *169* (1), 213–229. <https://doi.org/10.1111/bph.12120>.
  - (66) Araújo, D. S. M.; Miya-Coreixas, V. S.; Pandolfo, P.; Calaza, K. C. Cannabinoid Receptors and TRPA1 on Neuroprotection in a Model of Retinal Ischemia. *Exp. Eye Res.* **2017**, *154*, 116–125. <https://doi.org/10.1016/j.exer.2016.11.015>.
  - (67) Vellani, V.; Petrosino, S.; De Petrocellis, L.; Valenti, M.; Prandini, M.; Magherini, P. C.; McNaughton, P. A.; Di Marzo, V. Functional Lipidomics. Calcium-Independent Activation of Endocannabinoid/Endovanilloid Lipid Signalling in Sensory Neurons by Protein Kinases C and A and Thrombin. *Neuropharmacology* **2008**, *55* (8), 1274–1279. <https://doi.org/10.1016/j.neuropharm.2008.01.010>.
  - (68) Howlett, A. C. The Cannabinoid Receptors. *Prostaglandins Other Lipid Mediat.* **2002**, *68–69*, 619–631. [https://doi.org/10.1016/S0090-6980\(02\)00060-6](https://doi.org/10.1016/S0090-6980(02)00060-6).

- (69) Akopian, A. N.; Ruparel, N. B.; Jeske, N. A.; Patwardhan, A.; Hargreaves, K. M. Role of Ionotropic Cannabinoid Receptors in Peripheral Antinociception and Antihyperalgesia. *Trends in Pharmacological Sciences*. February 2009, pp 79–84. <https://doi.org/10.1016/j.tips.2008.10.008>.
- (70) Di Marzo, V. Endovanilloid Signaling in Pain. *Curr. Opin. Neurobiol.* **2002**, *12* (4), 372–379. [https://doi.org/10.1016/S0959-4388\(02\)00340-9](https://doi.org/10.1016/S0959-4388(02)00340-9).
- (71) Gaudet, R. Divide and Conquer: High Resolution Structural Information on TRP Channel Fragments. *Journal of General Physiology*. March 2009, pp 231–237. <https://doi.org/10.1085/jgp.200810137>.
- (72) Muller, C.; Morales, P.; Reggio, P. H. Cannabinoid Ligands Targeting TRP Channels. *Front. Mol. Neurosci.* **2019**, *11*. <https://doi.org/10.3389/fnmol.2018.00487>.
- (73) Gao, Y.; Cao, E.; Julius, D.; Cheng, Y. TRPV1 Structures in Nanodiscs Reveal Mechanisms of Ligand and Lipid Action. *Nature* **2016**, *534* (7607), 347–351. <https://doi.org/10.1038/nature17964>.
- (74) Ross, R. A. Anandamide and Vanilloid TRPV1 Receptors. *British Journal of Pharmacology*. November 2003, pp 790–801. <https://doi.org/10.1038/sj.bjp.0705467>.
- (75) Hanson, S. M.; Newstead, S.; Swartz, K. J.; Sansom, M. S. P. Capsaicin Interaction with TRPV1 Channels in a Lipid Bilayer: Molecular Dynamics Simulation. *Biophys. J.* **2015**, *108* (6), 1425–1434. <https://doi.org/10.1016/j.bpj.2015.02.013>.
- (76) Yang, F.; Zheng, J. Understand Spiciness: Mechanism of TRPV1 Channel Activation by Capsaicin. *Protein Cell* **2017**, *8* (3), 169–177. <https://doi.org/10.1007/s13238-016-0353-7>.
- (77) Hurst, D. P.; Grossfield, A.; Lynch, D. L.; Feller, S.; Romo, T. D.; Gawrisch, K.; Pitman, M. C.; Reggio, P. H. A Lipid Pathway for Ligand Binding Is Necessary for a Cannabinoid G Protein-Coupled Receptor. *J. Biol. Chem.* **2010**, *285* (23), 17954–17964. <https://doi.org/10.1074/jbc.M109.041590>.
- (78) Liao, M.; Cao, E.; Julius, D.; Cheng, Y. Structure of the TRPV1 Ion Channel Determined by Electron Cryo-Microscopy. *Nature* **2013**, *504* (7478), 107–112. <https://doi.org/10.1038/nature12822>.
- (79) Jacobson, M. P.; Pincus, D. L.; Rapp, C. S.; Day, T. J. F.; Honig, B.; Shaw, D. E.; Friesner, R. A. A Hierarchical Approach to All-Atom Protein Loop Prediction. *Proteins Struct. Funct. Genet.* **2004**, *55* (2), 351–367. <https://doi.org/10.1002/prot.10613>.

- (80) Gavva, N. R.; Klionsky, L.; Qu, Y.; Shi, L.; Tamir, R.; Edenson, S.; Zhang, T. J.; Viswanadhan, V. N.; Toth, A.; Pearce, L. V.; Vanderah, T. W.; Porreca, F.; Blumberg, P. M.; Lile, J.; Sun, Y.; Wild, K.; Louis, J. C.; Treanor, J. J. S. Molecular Determinants of Vanilloid Sensitivity in TRPV1. *J. Biol. Chem.* **2004**, *279* (19), 20283–20295. <https://doi.org/10.1074/jbc.M312577200>.
- (81) Johnson, D. M.; Garrett, E. M.; Rutter, R.; Bonnert, T. P.; Gao, Y. D.; Middleton, R. E.; Sutton, K. G. Functional Mapping of the Transient Receptor Potential Vanilloid 1 Intracellular Binding Site. *Mol. Pharmacol.* **2006**, *70* (3), 1005–1012. <https://doi.org/10.1124/mol.106.023945>.
- (82) Morales, P.; Hurst, D. P.; Reggio, P. H. Methods for the Development of In Silico GPCR Models. In *Methods in Enzymology*; Academic Press Inc., 2017; Vol. 593, pp 405–448. <https://doi.org/10.1016/bs.mie.2017.05.005>.
- (83) Li, J.; Abel, R.; Zhu, K.; Cao, Y.; Zhao, S.; Friesner, R. A. The VSGB 2.0 Model: A next Generation Energy Model for High Resolution Protein Structure Modeling. *Proteins Struct. Funct. Bioinforma.* **2011**, *79* (10), 2794–2812. <https://doi.org/10.1002/prot.23106>.
- (84) Lee, J.; Cheng, X.; Swails, J. M.; Yeom, M. S.; Eastman, P. K.; Lemkul, J. A.; Wei, S.; Buckner, J.; Jeong, J. C.; Qi, Y.; Jo, S.; Pande, V. S.; Case, D. A.; Brooks, C. L.; MacKerell, A. D.; Klauda, J. B.; Im, W. CHARMM-GUI Input Generator for NAMD, GROMACS, AMBER, OpenMM, and CHARMM/OpenMM Simulations Using the CHARMM36 Additive Force Field. *J. Chem. Theory Comput.* **2016**, *12* (1), 405–413. <https://doi.org/10.1021/acs.jctc.5b00935>.
- (85) Huang, J.; Rauscher, S.; Nawrocki, G.; Ran, T.; Feig, M.; De Groot, B. L.; Grubmüller, H.; MacKerell, A. D. CHARMM36m: An Improved Force Field for Folded and Intrinsically Disordered Proteins. *Nat. Methods* **2016**, *14* (1), 71–73. <https://doi.org/10.1038/nmeth.4067>.
- (86) Klauda, J. B.; Venable, R. M.; Freites, J. A.; O'Connor, J. W.; Tobias, D. J.; Mondragon-Ramirez, C.; Vorobyov, I.; MacKerell, A. D.; Pastor, R. W. Update of the CHARMM All-Atom Additive Force Field for Lipids: Validation on Six Lipid Types. *J. Phys. Chem. B* **2010**, *114* (23), 7830–7843. <https://doi.org/10.1021/jp101759q>.
- (87) Venable, R. M.; Luo, Y.; Gawrisch, K.; Roux, B.; Pastor, R. W. Simulations of Anionic Lipid Membranes: Development of Interaction-Specific Ion Parameters and Validation Using NMR Data. *J. Phys. Chem. B* **2013**, *117* (35), 10183–10192. <https://doi.org/10.1021/jp401512z>.
- (88) Case, D. A.; Ben-Shalom, I. Y.; Brozell, S. R.; Cerutti, D. S.; Cheatham, T. E.; Cruzeiro, V. W. D.; Al., E. AMBER 2018. *San Fr. CA Univ. Calif.*
- (89) Barnett-Norris, J.; Guarnieri, F.; Hurst, D. P.; Reggio, P. H. Exploration of Biologically Relevant Conformations of Anandamide, 2- Arachidonylglycerol, and Their Analogues

- Using Conformational Memories. *J. Med. Chem.* **1998**, *41* (24), 4861–4872.  
<https://doi.org/10.1021/jm9803471>.
- (90) Shaw, D. E.; Grossman, J. P.; Bank, J. A.; Batson, B.; Butts, J. A.; Chao, J. C.; Deneroff, M. M.; Dror, R. O.; Even, A.; Fenton, C. H.; Forte, A.; Gagliardo, J.; Gill, G.; Greskamp, B.; Ho, C. R.; Ierardi, D. J.; Iserovich, L.; Kuskin, J. S.; Larson, R. H.; Layman, T.; Lee, L. S.; Lerer, A. K.; Li, C.; Killebrew, D.; Mackenzie, K. M.; Mok, S. Y. H.; Moraes, M. A.; Mueller, R.; Nociolo, L. J.; Peticolas, J. L.; Quan, T.; Ramot, D.; Salmon, J. K.; Scarpazza, D. P.; Ben Schafer, U.; Siddique, N.; Snyder, C. W.; Spengler, J.; Tang, P. T. P.; Theobald, M.; Toma, H.; Towles, B.; Vitale, B.; Wang, S. C.; Young, C. Anton 2: Raising the Bar for Performance and Programmability in a Special-Purpose Molecular Dynamics Supercomputer. In *International Conference for High Performance Computing, Networking, Storage and Analysis, SC*; IEEE Computer Society, 2014; Vol. 2015-January, pp 41–53. <https://doi.org/10.1109/SC.2014.9>.
  - (91) Nosé, S. A Unified Formulation of the Constant Temperature Molecular Dynamics Methods. *J. Chem. Phys.* **1984**, *81* (1), 511–519. <https://doi.org/10.1063/1.447334>.
  - (92) Hoover, W. G. *Canonical Dynamics: Equilibrium Phase-Space Distributions*; 1985; Vol. 31.
  - (93) Martyna, G. J.; Tobias, D. J.; Klein, M. L. Constant Pressure Molecular Dynamics Algorithms. *J. Chem. Phys.* **1994**, *101* (5), 4177–4189. <https://doi.org/10.1063/1.467468>.
  - (94) Wiese, B.; Wilson-Poe, A. R. Emerging Evidence for Cannabis’ Role in Opioid Use Disorder. *Cannabis Cannabinoid Res.* **2018**, *3* (1), 179–189.  
<https://doi.org/10.1089/can.2018.0022>.
  - (95) Szallasi, A.; Cortright, D. N.; Blum, C. A.; Eid, S. R. The Vanilloid Receptor TRPV1: 10 Years from Channel Cloning to Antagonist Proof-of-Concept. *Nat. Rev. Drug Discov.* **2007**, *6* (5), 357–372. <https://doi.org/10.1038/nrd2280>.
  - (96) Sanz-Salvador, L.; Andrés-Borderia, A.; Ferrer-Montiel, A.; Planells-Cases, R. Agonist- and Ca<sup>2+</sup>-Dependent Desensitization of TRPV1 Channel Targets the Receptor to Lysosomes for Degradation. *J. Biol. Chem.* **2012**, *287* (23), 19462–19471.  
<https://doi.org/10.1074/jbc.M111.289751>.
  - (97) Pumroy, R. A.; Samanta, A.; Liu, Y.; Hughes, T. E. T.; Zhao, S.; Yudin, Y.; Rohacs, T.; Han, S.; Moiseenkova-Bell, V. Y. Molecular Mechanism of TRPV2 Channel Modulation by Cannabidiol. *Elife* **2019**, *8*. <https://doi.org/10.7554/elife.48792>.
  - (98) Nilius, B.; Vennekens, R. TRP Channels and Human Diseases. In *Vanilloid Receptor TRPV1 in Drug Discovery: Targeting Pain and Other Pathological Disorders*; 2010; pp 1–67. <https://doi.org/10.1002/9780470588284.ch1>.
  - (99) Starkus, J.; Jansen, C.; Shimoda, L. M. N.; Stokes, A. J.; Small-Howard, A. L.; Turner, H.

- Diverse TRPV1 Responses to Cannabinoids. *Channels* **2019**, *13* (1), 172–191.  
<https://doi.org/10.1080/19336950.2019.1619436>.
- (100) Lau, B. K.; Vaughan, C. W. Targeting the Endogenous Cannabinoid System to Treat Neuropathic Pain. *Front. Pharmacol.* **2014**, *5*. <https://doi.org/10.3389/fphar.2014.00028>.
- (101) Ware, M. A.; Gamsa, A.; Persson, J.; Fitzcharles, M. A. Cannabis for Chronic Pain: Case Series and Implications for Clinicians. *Pain Res. Manag.* **2002**, *7* (2), 95–99.  
<https://doi.org/10.1155/2002/380509>.
- (102) Luongo, L.; Starowicz, K.; Maione, S.; Di Marzo, V. Allodynia Lowering Induced by Cannabinoids and Endocannabinoids (ALICE). *Pharmacol. Res.* **2017**, *119*, 272–277.  
<https://doi.org/10.1016/j.phrs.2017.02.019>.
- (103) Nielsen, S.; Sabioni, P.; Trigo, J. M.; Ware, M. A.; Betz-Stablein, B. D.; Murnion, B.; Lintzeris, N.; Khor, K. E.; Farrell, M.; Smith, A.; Le Foll, B. Opioid-Sparing Effect of Cannabinoids: A Systematic Review and Meta-Analysis. *Neuropsychopharmacology*. Nature Publishing Group August 1, 2017, pp 1752–1765.  
<https://doi.org/10.1038/npp.2017.51>.
- (104) Walker, J. M.; Huang, S. M. Cannabinoid Analgesia. *Pharmacology and Therapeutics*. 2002, pp 127–135. [https://doi.org/10.1016/S0163-7258\(02\)00252-8](https://doi.org/10.1016/S0163-7258(02)00252-8).
- (105) Ilgen, M. A.; Bohnert, K.; Kleinberg, F.; Jannausch, M.; Bohnert, A. S. B.; Walton, M.; Blow, F. C. Characteristics of Adults Seeking Medical Marijuana Certification. *Drug Alcohol Depend.* **2013**, *132* (3), 654–659.  
<https://doi.org/10.1016/j.drugalcdep.2013.04.019>.
- (106) Klimkiewicz, A.; Jasinska, A. The Health Effects of Cannabis and Cannabinoids. *Psychiatry* **2018**, *15* (2), 88–92. <https://doi.org/10.17226/24625>.
- (107) Maione, S.; Starowicz, K.; Palazzo, E.; Rossi, F.; Di Marzo, V. The Endocannabinoid and Endovanilloid Systems and Their Interactions in Neuropathic Pain. *Drug Development Research*. April 2006, pp 339–354. <https://doi.org/10.1002/ddr.20098>.
- (108) Pertwee, R. G.; Howlett, A. C.; Abood, M. E.; Alexander, S. P. H.; Di Marzo, V.; Elphick, M. R.; Greasley, P. J.; Hansen, H. S.; Kunos, G.; Mackie, K.; Mechoulam, R.; Ross, R. A. International Union of Basic and Clinical Pharmacology. LXXIX. Cannabinoid Receptors and Their Ligands: Beyond CB1 and CB2. *Pharmacological Reviews*. December 2010, pp 588–631. <https://doi.org/10.1124/pr.110.003004>.
- (109) Jordt, S. E.; Bautista, D. M.; Chuang, H. H.; McKemy, D. D.; Zygmunt, P. M.; Högestätt, E. D.; Meng, I. D.; Julius, D. Mustard Oils and Cannabinoids Excite Sensory Nerve Fibres through the TRP Channel ANKTM1. *Nature* **2004**, *427* (6971), 260–265.  
<https://doi.org/10.1038/nature02282>.

- (110) Peier, A. M.; Moqrich, A.; Hergarden, A. C.; Reeve, A. J.; Andersson, D. A.; Story, G. M.; Earley, T. J.; Dragoni, I.; McIntyre, P.; Bevan, S.; Patapoutian, A. A TRP Channel That Senses Cold Stimuli and Menthol. *Cell* **2002**, *108* (5), 705–715. [https://doi.org/10.1016/S0092-8674\(02\)00652-9](https://doi.org/10.1016/S0092-8674(02)00652-9).
- (111) Caterina, M. J.; Schumacher, M. A.; Tominaga, M.; Rosen, T. A.; Levine, J. D.; Julius, D. The Capsaicin Receptor: A Heat-Activated Ion Channel in the Pain Pathway. *Nature* **1997**, *389* (6653), 816–824. <https://doi.org/10.1038/39807>.
- (112) Tominaga, M.; Caterina, M. J.; Malmberg, A. B.; Rosen, T. A.; Gilbert, H.; Skinner, K.; Raumann, B. E.; Basbaum, A. I.; Julius, D. The Cloned Capsaicin Receptor Integrates Multiple Pain-Producing Stimuli. *Neuron* **1998**, *21* (3), 531–543. [https://doi.org/10.1016/S0896-6273\(00\)80564-4](https://doi.org/10.1016/S0896-6273(00)80564-4).
- (113) Sanchez, J. F.; Krause, J. E.; Cortright, D. N. The Distribution and Regulation of Vanilloid Receptor VR1 and VR1 5' Splice Variant RNA Expression in Rat. *Neuroscience* **2001**, *107* (3), 373–381. [https://doi.org/10.1016/s0306-4522\(01\)00373-6](https://doi.org/10.1016/s0306-4522(01)00373-6).
- (114) Caterina, M. J.; Rosen, T. A.; Tominaga, M.; Brake, A. J.; Julius, D. A Capsaicin-Receptor Homologue with a High Threshold for Noxious Heat. *Nature* **1999**, *398*, 436–441.
- (115) Bender, F.; Mederos y Schnitzler, M.; Li, Y.; Ji, A.; Weihe, E.; Gudermann, T.; Schäfer, M. The Temperature-Sensitive Ion Channel TRPV2 Is Endogenously Expressed and Functional in the Primary Sensory Cell Line F-11. *Cell. Physiol. Biochem.* **2005**, *15* (1–4), 183–194. <https://doi.org/10.1159/000083651>.
- (116) Story, G. M.; Peier, A. M.; Reeve, A. J.; Eid, S. R.; Mosbacher, J.; Hricik, T. R.; Earley, T. J.; Hergarden, A. C.; Andersson, D. A.; Hwang, S. W.; McIntyre, P.; Jegla, T.; Bevan, S.; Patapoutian, A. ANKTM1, a TRP-like Channel Expressed in Nociceptive Neurons, Is Activated by Cold Temperatures. *Cell* **2003**, *112* (6), 819–829. [https://doi.org/10.1016/S0092-8674\(03\)00158-2](https://doi.org/10.1016/S0092-8674(03)00158-2).
- (117) Bautista, D. M.; Movahed, P.; Hinman, A.; Axelsson, H. E.; Sterner, O.; Högestätt, E. D.; Julius, D.; Jordt, S. E.; Zygmunt, P. M. Pungent Products from Garlic Activate the Sensory Ion Channel TRPA1. *Proc. Natl. Acad. Sci. U. S. A.* **2005**, *102* (34), 12248–12252. <https://doi.org/10.1073/pnas.0505356102>.
- (118) Kobayashi, K.; Fukuoka, T.; Obata, K.; Yamanaka, H.; Dai, Y.; Tokunaga, A.; Noguchi, K. Distinct Expression of TRPM8, TRPA1, and TRPV1 MRNAs in Rat Primary Afferent Neurons with A $\delta$ /C-Fibers and Colocalization with Trk Receptors. *J. Comp. Neurol.* **2005**, *493* (4), 596–606. <https://doi.org/10.1002/cne.20794>.
- (119) Caterina, M. J. Transient Receptor Potential Ion Channels as Participants in Thermosensation and Thermoregulation. *Am. J. Physiol. - Regul. Integr. Comp. Physiol.* **2007**, *292* (1). <https://doi.org/10.1152/ajpregu.00446.2006>.

- (120) Peier, A. M.; Reeve, A. J.; Andersson, D. A.; Moqrich, A.; Earley, T. J.; Hergarden, A. C.; Story, G. M.; Colley, S.; Hogenesch, J. B.; McIntyre, P.; Bevan, S.; Patapoutian, A. A Heat-Sensitive TRP Channel Expressed in Keratinocytes. *Science* (80-. ). **2002**, *296* (5575), 2046–2049. <https://doi.org/10.1126/science.1073140>.
- (121) Mandadi, S.; Sokabe, T.; Shibasaki, K.; Katanosaka, K.; Mizuno, A.; Moqrich, A.; Patapoutian, A.; Fukumi-Tominaga, T.; Mizumura, K.; Tominaga, M. TRPV3 in Keratinocytes Transmits Temperature Information to Sensory Neurons via ATP. *Pflugers Arch. Eur. J. Physiol.* **2009**, *458* (6), 1093–1102. <https://doi.org/10.1007/s00424-009-0703-x>.
- (122) Macpherson, L. J.; Geierstanger, B. H.; Viswanath, V.; Bandell, M.; Eid, S. R.; Hwang, S. W.; Patapoutian, A. The Pungency of Garlic: Activation of TRPA1 and TRPV1 in Response to Allicin. *Curr. Biol.* **2005**, *15* (10), 929–934. <https://doi.org/10.1016/j.cub.2005.04.018>.
- (123) Moran, M. M. TRP Channels as Potential Drug Targets. *Annu. Rev. Pharmacol. Toxicol.* **2018**, *58*, 309–330. <https://doi.org/10.1146/annurev-pharmtox>.
- (124) Patapoutian, A.; Tate, S.; Woolf, C. J. Transient Receptor Potential Channels: Targeting Pain at the Source. *Nature Reviews Drug Discovery*. 2009, pp 55–68. <https://doi.org/10.1038/nrd2757>.
- (125) Bishnoi, M.; Premkumar, L. S. Changes in TRP Channels Expression in Painful Conditions. *Open Pain J.* **2013**, *6* (1), 10–22. <https://doi.org/10.2174/1876386301306010010>.
- (126) Wong, G. Y.; Gavva, N. R. Therapeutic Potential of Vanilloid Receptor TRPV1 Agonists and Antagonists as Analgesics: Recent Advances and Setbacks. *Brain Research Reviews*. April 2009, pp 267–277. <https://doi.org/10.1016/j.brainresrev.2008.12.006>.
- (127) Chianese, G.; Lopatriello, A.; Schiano-Moriello, A.; Caprioglio, D.; Mattoteia, D.; Benetti, E.; Ciceri, D.; Arnoldi, L.; De Combarieu, E.; Vitale, R. M.; Amodeo, P.; Appendino, G.; De Petrocellis, L.; Taglialatela-Scafati, O. Cannabitwinol, a Dimeric Phytocannabinoid from Hemp, Cannabis Sativa L., Is a Selective Thermo-TRP Modulator. *J. Nat. Prod.* **2020**, *83* (9), 2727–2736. <https://doi.org/10.1021/acs.jnatprod.0c00668>.
- (128) Xu, H.; Ramsey, I. S.; Kotecha, S. A.; Moran, M. M.; Chong, J. A.; Lawson, D.; Ge, P.; Lilly, J.; Silos-Santiago, I.; Xie, Y.; DiStefano, P. S.; Curtis, R.; Clapham, D. E. TRPV3 Is a Calcium-Permeable Temperature-Sensitive Cation Channel. *Nature* **2002**, *418* (6894), 181–186. <https://doi.org/10.1038/nature00882>.
- (129) Wang, B.; Danjo, A.; Kajiya, H.; Okabe, K.; Kido, M. A. Oral Epithelial Cells Are Activated via TRP Channels. *J. Dent. Res.* **2011**, *90* (2), 163–167. <https://doi.org/10.1177/0022034510385459>.

- (130) Suzuki, M.; Watanabe, Y.; Oyama, Y.; Mizuno, A.; Kusano, E.; Hirao, A.; Ookawara, S. Localization of Mechanosensitive Channel TRPV4 in Mouse Skin. *Neurosci. Lett.* **2003**, 353 (3), 189–192. <https://doi.org/10.1016/j.neulet.2003.09.041>.
- (131) Nilius, B.; Owsianik, G. Transient Receptor Potential Channelopathies. *Pflügers Arch. - Eur. J. Physiol.* **2010**, 460 (2), 437–450. <https://doi.org/10.1007/s00424-010-0788-2>.
- (132) Deng, Z.; Paknejad, N.; Makshev, G.; Sala-Rabanal, M.; Nichols, C. G.; Hite, R. K.; Yuan, P. Cryo-EM and X-Ray Structures of TRPV4 Reveal Insight into Ion Permeation and Gating Mechanisms. *Nat. Struct. Mol. Biol.* **2018**, 25 (3), 252–260. <https://doi.org/10.1038/s41594-018-0037-5>.
- (133) Niforatos, W.; Zhang, X.; Lake, M. R.; Walter, K. a; Neelands, T.; Holzman, T. F.; Scott, V. E.; Faltynek, C. R.; Moreland, R. B.; Chen, J. Activation of TRPA1 Channels by the Fatty Acid Amide Hydrolase Inhibitor 3 J -Carbamoylbiphenyl-3-Yl. *Mol. Pharmacol.* **2007**, 71 (5), 1209–1216. <https://doi.org/10.1124/mol.106.033621>.
- (134) de la Peña, E.; Mälkiä, A.; Cabedo, H.; Belmonte, C.; Viana, F. The Contribution of TRPM8 Channels to Cold Sensing in Mammalian Neurons. *J. Physiol.* **2005**, 567 (2), 415–426. <https://doi.org/10.1113/jphysiol.2005.086546>.
- (135) McKemy, D. D.; Neuhausser, W. M.; Julius, D. Identification of a Cold Receptor Reveals a General Role for TRP Channels in Thermosensation. *Nature* **2002**, 416 (6876), 52–58. <https://doi.org/10.1038/nature719>.
- (136) Chuang, H. H.; Neuhausser, W. M.; Julius, D. The Super-Cooling Agent Icilin Reveals a Mechanism of Coincidence Detection by a Temperature-Sensitive TRP Channel. *Neuron* **2004**, 43 (6), 859–869. <https://doi.org/10.1016/j.neuron.2004.08.038>.
- (137) Bandell, M.; Dubin, A. E.; Petrus, M. J.; Orth, A.; Mathur, J.; Sun, W. H.; Patapoutian, A. High-Throughput Random Mutagenesis Screen Reveals TRPM8 Residues Specifically Required for Activation by Menthol. *Nat. Neurosci.* **2006**, 9 (4), 493–500. <https://doi.org/10.1038/nn1665>.
- (138) Xu, L.; Han, Y.; Chen, X.; Aierken, A.; Wen, H.; Zheng, W.; Wang, H.; Lu, X.; Zhao, Z.; Ma, C.; Liang, P.; Yang, W.; Yang, S.; Yang, F. Molecular Mechanisms Underlying Menthol Binding and Activation of TRPM8 Ion Channel. *Nat. Commun.* **2020**, 11 (1). <https://doi.org/10.1038/s41467-020-17582-x>.
- (139) Aizpurua-Olaizola, O.; Elezgarai, I.; Rico-Barrio, I.; Zarandona, I.; Etzebarria, N.; Usobiaga, A. Targeting the Endocannabinoid System: Future Therapeutic Strategies. *Drug Discovery Today*. Elsevier Ltd January 1, 2017, pp 105–110. <https://doi.org/10.1016/j.drudis.2016.08.005>.
- (140) Chanda, D.; Neumann, D.; Glatz, J. F. C. The Endocannabinoid System: Overview of an Emerging Multi-Faceted Therapeutic Target. *Prostaglandins Leukotrienes and Essential*



- Fatty Acids*. Churchill Livingstone January 1, 2019, pp 51–56.  
<https://doi.org/10.1016/j.plefa.2018.11.016>.
- (141) Mechoulam, R.; Peters, M.; Murillo-Rodriguez, E.; Hanuš, L. O. Cannabidiol-Recent Advances. *Chem. Biodivers.* **2007**, *4*, 1678–1692.
  - (142) Malfait, A. M.; Gallily, R.; Sumariwalla, P. F.; Malik, A. S.; Andreaskos, E.; Mechoulam, R.; Feldmann, M. The Nonpsychoactive Cannabis Constituent Cannabidiol Is an Oral Anti-Arthritic Therapeutic in Murine Collagen-Induced Arthritis. *Proc. Natl. Acad. Sci. U. S. A.* **2000**, *97* (17), 9561–9566. <https://doi.org/10.1073/pnas.160105897>.
  - (143) Guimaraes, F. S.; de Aguiar, J. C.; Mechoulam, R.; Breuer, A. Anxiolytic Effect of Cannabidiol Derivatives in The. *Gen. Pharmacol.* **1994**, *25* (1), 161–164.
  - (144) Turna, J.; Syan, S. K.; Frey, B. N.; Rush, B.; Costello, M. J.; Weiss, M.; MacKillop, J. Cannabidiol as a Novel Candidate Alcohol Use Disorder Pharmacotherapy: A Systematic Review. *Alcoholism: Clinical and Experimental Research*. Blackwell Publishing Ltd April 1, 2019, pp 550–563. <https://doi.org/10.1111/acer.13964>.
  - (145) Russo, E. B.; Guy, G. W.; Robson, P. J. Cannabis, Pain, and Sleep: Lessons from Therapeutic Clinical Trials OfSativex®, a Cannabis-Based Medicine. *Chem. Biodivers.* **2007**, *4* (8), 1729–1743. <https://doi.org/10.1002/cbdv.200790150>.
  - (146) De Petrocellis, L.; Di Marzo, V. Non-CB1, Non-CB2 Receptors for Endocannabinoids, Plant Cannabinoids, and Synthetic Cannabimimetics: Focus on G-Protein-Coupled Receptors and Transient Receptor Potential Channels. *J. Neuroimmune Pharmacol.* **2010**, *5* (1), 103–121. <https://doi.org/10.1007/s11481-009-9177-z>.
  - (147) Cristino, L.; de Petrocellis, L.; Pryce, G.; Baker, D.; Guglielmotti, V.; Di Marzo, V. Immunohistochemical Localization of Cannabinoid Type 1 and Vanilloid Transient Receptor Potential Vanilloid Type 1 Receptors in the Mouse Brain. *Neuroscience* **2006**, *139* (4), 1405–1415. <https://doi.org/10.1016/j.neuroscience.2006.02.074>.
  - (148) Caterina, M. J.; Julius, D. The Vanilloid Receptor: A Molecular Gateway to the Pain Pathway. *Annu. Rev. Neurosci.* **2001**, *24* (1), 487–517.  
<https://doi.org/10.1146/annurev.neuro.24.1.487>.
  - (149) Caterina, M. J. Transient Receptor Potential Ion Channels as Participants in Thermosensation and Thermoregulation. *American Journal of Physiology - Regulatory Integrative and Comparative Physiology*. 2007, pp 64–76.  
<https://doi.org/10.1152/ajpregu.00446.2006>.
  - (150) Rosenbaum, T.; Gordon-Shaag, A.; Munari, M.; Gordon, S. E. Ca<sup>2+</sup>/Calmodulin Modulates TRPV1 Activation by Capsaicin. *J. Gen. Physiol.* **2004**, *123* (1), 53–62.  
<https://doi.org/10.1085/jgp.200308906>.

- (151) Zhang, M.; Chi, M.; Zou, H.; Tian, S.; Zhang, Z.; Wang, G. Effects of Coadministration of Low Dose Cannabinoid Type 2 Receptor Agonist and Morphine on Vanilloid Receptor 1 Expression in a Rat Model of Cancer Pain. *Mol. Med. Rep.* **2017**, *16* (5), 7025–7031. <https://doi.org/10.3892/mmr.2017.7479>.
- (152) Ramsey, I. S.; Delling, M.; Clapham, D. E. AN INTRODUCTION TO TRP CHANNELS. *Annu. Rev. Physiol.* **2006**, *68* (1), 619–647. <https://doi.org/10.1146/annurev.physiol.68.040204.100431>.
- (153) Cao, E.; Liao, M.; Cheng, Y.; Julius, D. TRPV1 Structures in Distinct Conformations Reveal Activation Mechanisms. *Nature* **2013**, *504* (7478), 113–118. <https://doi.org/10.1038/nature12823>.
- (154) Mohapatra, D. P.; Nau, C. Regulation of Ca<sup>2+</sup>-Dependent Desensitization in the Vanilloid Receptor TRPV1 by Calcineurin and CAMP-Dependent Protein Kinase. *J. Biol. Chem.* **2005**, *280* (14), 13424–13432. <https://doi.org/10.1074/jbc.M410917200>.
- (155) Ross, R. A.; Gibson, T. M.; Brockie, H. C.; Leslie, M.; Pashmi, G.; Craib, S. J.; Di Marzo, V.; Pertwee, R. G. Structure-Activity Relationship for the Endogenous Cannabinoid, Anandamide, and Certain of Its Analogues at Vanilloid Receptors in Transfected Cells and Vas Deferens. *Br. J. Pharmacol.* **2001**, *132* (3), 631–640. <https://doi.org/10.1038/sj.bjp.0703850>.
- (156) Muller, C.; Lynch, D. L.; Hurst, D. P.; Reggio, P. H. A Closer Look at Anandamide Interaction With TRPV1. *Front. Mol. Biosci.* **2020**, *7* (July), 1–8. <https://doi.org/10.3389/fmolb.2020.00144>.
- (157) Hazan, A.; Kumar, R.; Matzner, H.; Priel, A. The Pain Receptor TRPV1 Displays Agonist-Dependent Activation Stoichiometry. *Sci. Rep.* **2015**, *5* (12278). <https://doi.org/10.1038/srep12278>.
- (158) Hui, K.; Liu, B.; Qin, F. Capsaicin Activation of the Pain Receptor, VR1: Multiple Open States from Both Partial and Full Binding. *Biophys. J.* **2003**, *84* (5), 2957–2968. [https://doi.org/10.1016/S0006-3495\(03\)70022-8](https://doi.org/10.1016/S0006-3495(03)70022-8).
- (159) Schrödinger 2018. *Schrodinger Release 2018-4 Maest*.
- (160) Lee, J.; Cheng, X.; Swails, J. M.; Yeom, M. S.; Eastman, P. K.; Lemkul, J. A.; Wei, S.; Buckner, J.; Jeong, J. C.; Qi, Y.; Jo, S.; Pande, V. S.; Case, D. A.; Brooks, C. L.; MacKerell, A. D.; Klauda, J. B.; Im, W. CHARMM-GUI Input Generator for NAMD, GROMACS, AMBER, OpenMM, and CHARMM/OpenMM Simulations Using the CHARMM36 Additive Force Field. *J. Chem. Theory Comput.* **2016**, *12* (1), 405–413. <https://doi.org/10.1021/acs.jctc.5b00935>.
- (161) Hurst, D. P.; Grossfield, A.; Lynch, D. L.; Feller, S.; Romo, T. D.; Gawrisch, K.; Pitman, M. C.; Reggio, P. H. A Lipid Pathway for Ligand Binding Is Necessary for a Cannabinoid

- G Protein-Coupled Receptor. *J. Biol. Chem.* **2010**, 285 (23), 17954–17964. <https://doi.org/10.1074/jbc.M109.041590>.
- (162) Malek, N.; Starowicz, K. Dual-Acting Compounds Targeting Endocannabinoid and Endovanilloid Systems-a Novel Treatment Option for Chronic Pain Management. *Front. Pharmacol.* **2016**, 7 (AUG), 1–9. <https://doi.org/10.3389/fphar.2016.00257>.
- (163) Assimakopoulou, M.; Pagoulatos, D.; Nterma, P.; Pharmakakis, N. Immunolocalization of Cannabinoid Receptor Type 1 and CB2 Cannabinoid Receptors, and Transient Receptor Potential Vanilloid Channels in Pterygium. *Mol. Med. Rep.* **2017**, 16 (4), 5285–5293. <https://doi.org/10.3892/mmr.2017.7246>.
- (164) Bellini, G.; Torella, M.; Manzo, I.; Tortora, C.; Luongo, L.; Punzo, F.; Colacurci, N.; Nobili, B.; Maione, S.; Rossi, F. PKC $\beta$ II-Mediated Cross-Talk of TRPV1/CB2 Modulates the Glucocorticoid-Induced Osteoclast Overactivity. *Pharmacol. Res.* **2017**, 115, 267–274. <https://doi.org/10.1016/j.phrs.2016.11.039>.
- (165) Punzo, F.; Manzo, I.; Tortora, C.; Pota, E.; D'Angelo, V.; Bellini, G.; Di Paola, A.; Verace, F.; Casale, F.; Rossi, F. Effects of CB2 and TRPV1 Receptors' Stimulation in Pediatric Acute T-Lymphoblastic Leukemia. *Oncotarget* **2018**, 9 (30), 21244–21258. <https://doi.org/10.18632/oncotarget.25052>.
- (166) Bhatta, P.; Dhukhwa, A.; Sheehan, K.; Al Aameri, R. F. H.; Borse, V.; Ghosh, S.; Sheth, S.; Mamillapalli, C.; Rybak, L.; Ramkumar, V.; Mukherjea, D. Capsaicin Protects Against Cisplatin Ototoxicity by Changing the STAT3/STAT1 Ratio and Activating Cannabinoid (CB2) Receptors in the Cochlea. *Sci. Rep.* **2019**, 9 (1), 1–16. <https://doi.org/10.1038/s41598-019-40425-9>.
- (167) Wi, R.; Chung, Y. C.; Jin, B. K. Functional Crosstalk between CB and TRPV1 Receptors Protects Nigrostriatal Dopaminergic Neurons in the MPTP Model of Parkinson's Disease. *J. Immunol. Res.* **2020**, 2020. <https://doi.org/10.1155/2020/5093493>.
- (168) Di Marzo, V.; Griffin, G.; De Petrocellis, L.; Brandi, I.; Bisogno, T.; Williams, W.; Grier, M. C.; Kulasegram, S.; Mahadevan, A. N. U.; Razdan, R. K.; Martin, B. R. A Structure/Activity Relationship Study on Arvanil, an Endocannabinoid and Vanilloid Hybrid. *J. Pharmacol. Exp. Ther.* **2002**, 300 (3), 984–991. <https://doi.org/10.1124/jpet.300.3.984>.
- (169) Lastres-Becker, I.; De Miguel, R.; De Petrocellis, L.; Makriyannis, A.; Di Marzo, V.; Fernández-Ruiz, J. Compounds Acting at the Endocannabinoid and/or Endovanilloid Systems Reduce Hyperkinesia in a Rat Model of Huntington's Disease. *J. Neurochem.* **2003**, 84 (5), 1097–1109. <https://doi.org/10.1046/j.1471-4159.2003.01595.x>.
- (170) Morgese, M. G.; Cassano, T.; Cuomo, V.; Giuffrida, A. Anti-Dyskinetic Effects of Cannabinoids in a Rat Model of Parkinson's Disease: Role of CB1 and TRPV1 Receptors. *Exp. Neurol.* **2007**, 208 (1), 110–119. <https://doi.org/10.1016/j.expneurol.2007.07.021>.

- (171) Avraham, Y.; Davidi, N.; Porat, M.; Chernoguz, D.; Magen, I.; Vorobeiv, L.; Berry, E. M.; Leker, R. R. *Leptin Reduces Infarct Size in Association with Enhanced Expression of CB2, TRPV1, SIRT-1 and Leptin Receptor*; 2010; Vol. 7.
- (172) Chávez, A. E.; Chiu, C. Q.; Castillo, P. E. TRPV1 Activation by Endogenous Anandamide Triggers Postsynaptic Long-Term Depression in Dentate Gyrus. *Nat. Neurosci.* **2010**, *13* (12), 1511–1519. <https://doi.org/10.1038/nm.2684>.
- (173) Adamczyk, P.; Miszkiet, J.; McCreary, A. C.; Filip, M.; Papp, M.; Przeglasiński, E. The Effects of Cannabinoid CB1, CB2 and Vanilloid TRPV1 Receptor Antagonists on Cocaine Addictive Behavior in Rats. *Brain Res.* **2012**, *1444*, 45–54. <https://doi.org/10.1016/j.brainres.2012.01.030>.
- (174) Arnold, J. C.; Hone, P.; Holland, M. L.; Allen, J. D. CB2 and TRPV1 Receptors Mediate Cannabinoid Actions on MDR1 Expression in Multidrug Resistant Cells. *Pharmacol. Reports* **2012**, *64* (3), 751–757. [https://doi.org/10.1016/S1734-1140\(12\)70871-X](https://doi.org/10.1016/S1734-1140(12)70871-X).
- (175) Rossi, F.; Bellini, G.; Tortora, C.; Bernardo, M. E.; Luongo, L.; Conforti, A.; Starc, N.; Manzo, I.; Nobili, B.; Locatelli, F.; Maione, S. CB2 and TRPV1 Receptors Oppositely Modulate in Vitro Human Osteoblast Activity. *Pharmacol. Res.* **2015**, *99*, 194–201. <https://doi.org/10.1016/j.phrs.2015.06.010>.
- (176) Cécyre, B.; Bachand, I.; Papineau, F.; Brochu, C.; Casanova, C.; Bouchard, J. F. Cannabinoids Affect the Mouse Visual Acuity via the Cannabinoid Receptor Type 2. *Sci. Rep.* **2020**, *10* (1), 1–13. <https://doi.org/10.1038/s41598-020-72553-y>.
- (177) Navarro, G.; Morales, P.; Rodríguez-Cueto, C.; Fernández-Ruiz, J.; Jagerovic, N.; Franco, R. Targeting Cannabinoid CB2 Receptors in the Central Nervous System. Medicinal Chemistry Approaches with Focus on Neurodegenerative Disorders. *Front. Neurosci.* **2016**, *10* (September), 1–11. <https://doi.org/10.3389/fnins.2016.00406>.
- (178) Aso, E.; Ferrer, I. CB2 Cannabinoid Receptor As Potential Target against Alzheimer's Disease. *Front. Neurosci.* **2016**, *10* (May), 1–10. <https://doi.org/10.3389/fnins.2016.00243>.
- (179) Javed, H.; Azimullah, S.; Haque, M. E.; Ojha, S. K. Cannabinoid Type 2 (CB2) Receptors Activation Protects against Oxidative Stress and Neuroinflammation Associated Dopaminergic Neurodegeneration in Rotenone Model of Parkinson's Disease. *Front. Neurosci.* **2016**, *10* (AUG), 1–14. <https://doi.org/10.3389/fnins.2016.00321>.
- (180) Cassano, T.; Calcagnini, S.; Pace, L.; Marco, F. De; Romano, A.; Gaetani, S. Cannabinoid Receptor 2 Signaling in Neurodegenerative Disorders: From Pathogenesis to a Promising Therapeutic Target. *Front. Neurosci.* **2017**, *11* (FEB), 1–10. <https://doi.org/10.3389/fnins.2017.00030>.

- (181) Behl, T.; Kaur, G.; Bungau, S.; Jhanji, R.; Kumar, A.; Mehta, V.; Zengin, G.; Brata, R.; Hassan, S. S. U.; Fratila, O. Distinctive Evidence Involved in the Role of Endocannabinoid Signalling in Parkinson's Disease: A Perspective on Associated Therapeutic Interventions. *Int. J. Mol. Sci.* **2020**, *21* (17), 1–27. <https://doi.org/10.3390/ijms21176235>.
- (182) Berry, A. J.; Zubko, O.; Reeves, S. J.; Howard, R. J. Endocannabinoid System Alterations in Alzheimer's Disease: A Systematic Review of Human Studies. *Brain Res.* **2020**, *1749*, 147135. <https://doi.org/10.1016/j.brainres.2020.147135>.
- (183) Uddin, M. S.; Al Mamun, A.; Sumsuzzman, D. M.; Ashraf, G. M.; Perveen, A.; Bungau, S. G.; Mousa, S. A.; El-Seedi, H. R.; Bin-Jumah, M. N.; Abdel-Daim, M. M. Emerging Promise of Cannabinoids for the Management of Pain and Associated Neuropathological Alterations in Alzheimer's Disease. *Frontiers in Pharmacology*. Frontiers Media S.A. 2020, pp 1–13. <https://doi.org/10.3389/fphar.2020.01097>.
- (184) Fowler, C. J. The Endocannabinoid System – Current Implications for Drug Development. *J. Intern. Med.* **2021**, *290* (1), 2–26. <https://doi.org/10.1111/joim.13229>.
- (185) Guindon, J.; Hohmann, A. G. Cannabinoid CB2 Receptors: A Therapeutic Target for the Treatment of Inflammatory and Neuropathic Pain. *Br. J. Pharmacol.* **2008**, *153* (2), 319–334. <https://doi.org/10.1038/sj.bjp.0707531>.
- (186) Anthony, A. T.; Rahmat, S.; Sangle, P.; Sandhu, O.; Khan, S. Cannabinoid Receptors and Their Relationship With Chronic Pain: A Narrative Review. *Cureus* **2020**, *12* (9). <https://doi.org/10.7759/cureus.10436>.
- (187) Aly, E.; Masocha, W. Targeting the Endocannabinoid System for Management of HIV-Associated Neuropathic Pain: A Systematic Review. *IBRO Neurosci. Reports* **2021**, *10* (September 2020), 109–118. <https://doi.org/10.1016/j.ibneur.2021.01.004>.
- (188) Bryk, M.; Starowicz, K. Cannabinoid-Based Therapy as a Future for Joint Degeneration. Focus on the Role of CB 2 Receptor in the Arthritis Progression and Pain: An Updated Review. *Pharmacol. Reports* **2021**, *73*, 681–699. <https://doi.org/10.1007/s43440-021-00270-y>.
- (189) Mlost, J.; Kostrzewa, M.; Borczyk, M.; Bryk, M.; Chwastek, J.; Korostyński, M.; Starowicz, K. CB2 Agonism Controls Pain and Subchondral Bone Degeneration Induced by Mono-Iodoacetate: Implications GPCR Functional Bias and Tolerance Development. *Biomed. Pharmacother.* **2021**, *136* (November 2020). <https://doi.org/10.1016/j.biopha.2021.111283>.
- (190) Ramírez-López, A.; Pastor, A.; de la Torre, R.; La Porta, C.; Ozaita, A.; Cabañero, D.; Maldonado, R. Role of the Endocannabinoid System in a Mouse Model of Fragile X Undergoing Neuropathic Pain. *Eur. J. Pain (United Kingdom)* **2021**, *25* (6), 1316–1328. <https://doi.org/10.1002/ejp.1753>.

- (191) Peppin, J. F.; Pappagallo, M. Capsaicinoids in the Treatment of Neuropathic Pain: A Review. *Ther. Adv. Neurol. Disord.* **2014**, *7* (1), 22–32. <https://doi.org/10.1177/1756285613501576>.
- (192) Shuba, Y. M. Beyond Neuronal Heat Sensing: Diversity of TRPV1 Heat-Capsaicin Receptor-Channel Functions. *Front. Cell. Neurosci.* **2021**, *14*, Article 612480. <https://doi.org/10.3389/fncel.2020.612480>.
- (193) Gibson, H. E.; Edwards, J. G.; Page, R. S.; Van Hook, M. J.; Kauer, J. A. TRPV1 Channels Mediate Long-Term Depression at Synapses on Hippocampal Interneurons. *Neuron* **2008**, *57* (5), 746–759. <https://doi.org/10.1016/j.neuron.2007.12.027>.
- (194) Ho, K. W.; Ward, N. J.; Calkins, D. J. TRPV1: A Stress Response Protein in the Central Nervous System. *American Journal of Neurodegenerative Diseases*. E-Century Publishing Corporation 2012, pp 1–14.
- (195) Sawamura, S.; Shirakawa, H.; Nakagawa, T.; Mori, Y.; Kaneko, S. TRP Channels in the Brain. In *Neurobiology of TRP Channels*; T. L. R. Emir, Ed.; CRC Press: Boca Raton : CRC Press, 2017., 2017; pp 295–322. <https://doi.org/10.4324/9781315152837-16>.
- (196) Martins, D.; Tavares, I.; Morgado, C. “hotheaded”: The Role of TRPV1 in Brain Functions. *Neuropharmacology* **2014**, *85*, 151–157. <https://doi.org/10.1016/j.neuropharm.2014.05.034>.
- (197) Marinelli, S.; Di Marzo, V.; Berretta, N.; Matias, I.; Maccarrone, M.; Bernardi, G.; Mercuri, N. B. Presynaptic Facilitation of Glutamatergic Synapses to Dopaminergic Neurons of the Rat Substantia Nigra by Endogenous Stimulation of Vanilloid Receptors. *J. Neurosci.* **2003**, *23* (8), 3136–3144. <https://doi.org/10.1523/jneurosci.23-08-03136.2003>.
- (198) Maione, S.; Cristino, L.; Migliozi, A. L.; Georgiou, A. L.; Starowicz, K.; Salt, T. E.; Di Marzo, V. TRPV1 Channels Control Synaptic Plasticity in the Developing Superior Colliculus. *J. Physiol.* **2009**, *587* (11), 2521–2535. <https://doi.org/10.1113/jphysiol.2009.171900>.
- (199) González-Aparicio, R.; Moratalla, R. Oleoylethanolamide Reduces L-DOPA-Induced Dyskinesia via TRPV1 Receptor in a Mouse Model of Parkinson’s Disease. *Neurobiol. Dis.* **2014**, *62*, 416–425. <https://doi.org/10.1016/j.nbd.2013.10.008>.
- (200) Kong, W.-L.; Peng, Y.-Y.; Peng, B.-W. Modulation of Neuroinflammation: Role and Therapeutic Potential of TRPV1 in the Neuro-Immune Axis. *Brain. Behav. Immun.* **2017**, *64*, 354–366. <https://doi.org/10.1016/j.bbi.2017.03.007>.
- (201) Nam, J. H.; Park, E. S.; Won, S. Y.; Lee, Y. A.; Kim, K. I.; Jeong, J. Y.; Baek, J. Y.; Cho, E. J.; Jin, M.; Chung, Y. C.; Lee, B. D.; Kim, S. H.; Kim, E. G.; Byun, K.; Lee, B.; Woo, D. H.; Lee, C. J.; Kim, S. R.; Bok, E.; Kim, Y. S.; Ahn, T. B.; Ko, H. W.; Brahmachari,

- S.; Pletinkova, O.; Troconso, J. C.; Dawson, V. L.; Dawson, T. M.; Jin, B. K. TRPV1 on Astrocytes Rescues Nigral Dopamine Neurons in Parkinson's Disease via CNTF. *Brain* **2015**, *138* (12), 3610–3622. <https://doi.org/10.1093/brain/awv297>.
- (202) Li, M.; Zhu, M.; Xu, Q.; Ding, F.; Tian, Y.; Zhang, M. Sensation of TRPV1 via 5-Hydroxytryptamine Signaling Modulates Pain Hypersensitivity in a 6-Hydroxydopamine Induced Mice Model of Parkinson's Disease. *Biochem. Biophys. Res. Commun.* **2019**. <https://doi.org/10.1016/j.bbrc.2019.10.204>.
- (203) Du, Y.; Fu, M.; Huang, Z.; Tian, X.; Li, J.; Pang, Y.; Song, W.; Tian Wang, Y.; Dong, Z.; Tian, | Xin; Li, | Junjie; Pang, Y.; Song, W.; Wang, Y. T.; Dong, Z. TRPV1 Activation Alleviates Cognitive and Synaptic Plasticity Impairments through Inhibiting AMPAR Endocytosis in APP23/PS45 Mouse Model of Alzheimer's Disease. *Aging Cell* **2020**, *19* (3), e13113. <https://doi.org/10.1111/accel.13113>.
- (204) Wilkerson, J. L.; Alberti, L. B.; Thakur, G. A.; Makriyannis, A.; Milligan, E. D. Peripherally Administered Cannabinoid Receptor 2 (CB2R) Agonists Lose Anti-Allodynic Effects in TRPV1 Knockout Mice, While Intrathecal Administration Leads to Anti-Allodynia and Reduced GFAP, CCL2 and TRPV1 Expression in the Dorsal Spinal Cord and DRG. *Brain Res.* **2021**, *1774* (November 2021), 147721. <https://doi.org/10.1016/j.brainres.2021.147721>.
- (205) Lowin, T.; Pongratz, G.; Straub, R. H. The Synthetic Cannabinoid WIN55,212-2 Mesylate Decreases the Production of Inflammatory Mediators in Rheumatoid Arthritis Synovial Fibroblasts by Activating CB2, TRPV1, TRPA1 and yet Unidentified Receptor Targets. *J. Inflamm. (United Kingdom)* **2016**, *13* (1), 1–10. <https://doi.org/10.1186/s12950-016-0114-7>.
- (206) Arnold, W. R.; Carnevale, L. N.; Xie, Z.; Baylon, J. L.; Tajkhorshid, E.; Hu, H.; Das, A. Anti-Inflammatory Dopamine- and Serotonin-Based Endocannabinoid Epoxides Reciprocally Regulate Cannabinoid Receptors and the TRPV1 Channel. *Nat. Commun.* **2021**, *12* (1). <https://doi.org/10.1038/s41467-021-20946-6>.
- (207) Di Marzo, V.; Bisogno, T.; De Petrocellis, L.; Brandi, I.; Jefferson, R. G.; Winckler, R. L.; Davis, J. B.; Dasse, O.; Mahadevan, A.; Razdan, R. K.; Martin, B. R. Highly Selective CB1cannabinoid Receptor Ligands and Novel CB1/VR1vanilloid Receptor 1hybrid Ligands. *Biochem. Biophys. Res. Commun.* **2001**, *281* (2), 444–451. <https://doi.org/10.1006/bbrc.2001.4354>.
- (208) Brooks, J. W.; Pryce, G.; Bisogno, T.; Jaggar, S. I.; Hankey, D. J. R.; Brown, P.; Bridges, D.; Ledent, C.; Bifulco, M.; Rice, A. S. C.; Di Marzo, V.; Baker, D. Arvanil-Induced Inhibition of Spasticity and Persistent Pain: Evidence for Therapeutic Sites of Action Different from the Vanilloid VR1 Receptor and Cannabinoid CB1/CB2 Receptors. *Eur. J. Pharmacol.* **2002**, *439* (1–3), 83–92. [https://doi.org/10.1016/S0014-2999\(02\)01369-9](https://doi.org/10.1016/S0014-2999(02)01369-9)

- (209) De Lago, E.; Urbani, P.; Ramos, J. A.; Di Marzo, V.; Fernández-Ruiz, J. Arvanil, a Hybrid Endocannabinoid and Vanilloid Compound, Behaves as an Antihyperkinetic Agent in a Rat Model of Huntington's Disease. *Brain Res.* **2005**, *1050* (1–2), 210–216. <https://doi.org/10.1016/j.brainres.2005.05.024>.
- (210) Cheong, S. L.; Federico, S.; Spalluto, G.; Klotz, K. N.; Pastorin, G. The Current Status of Pharmacotherapy for the Treatment of Parkinson's Disease: Transition from Single-Target to Multitarget Therapy. *Drug Discov. Today* **2019**, *24* (9), 1769–1783. <https://doi.org/10.1016/j.drudis.2019.05.003>.
- (211) Gontijo, V. S.; Viegas, F. P. D.; Ortiz, C. J. C.; de Freitas Silva, M.; Damasio, C. M.; Rosa, M. C.; Campos, T. G.; Couto, D. S.; Tranches Dias, K. S.; Viegas, C. Molecular Hybridization as a Tool in the Design of Multi-Target Directed Drug Candidates for Neurodegenerative Diseases. *Curr. Neuropharmacol.* **2019**, *18* (5), 348–407. <https://doi.org/10.2174/1385272823666191021124443>.
- (212) Maramai, S.; Benchekroun, M.; Gabr, M. T.; Yahiaoui, S. Multitarget Therapeutic Strategies for Alzheimer's Disease: Review on Emerging Target Combinations. **2020**. <https://doi.org/10.1155/2020/5120230>.
- (213) Hua, T.; Li, X.; Wu, L.; Iliopoulos-Tsoutsouvas, C.; Wang, Y.; Wu, M.; Shen, L.; Johnston, C. A.; Nikas, S. P.; Song, F.; Song, X.; Yuan, S.; Sun, Q.; Wu, Y.; Jiang, S.; Grim, T. W.; Benchama, O.; Stahl, E. L.; Zvonok, N.; Zhao, S.; Bohn, L. M.; Makriyannis, A.; Liu, Z.-J. Activation and Signaling Mechanism Revealed by Cannabinoid Receptor-Gi Complex Structures. *Cell* **2020**, *180* (4), 655–665.e18. <https://doi.org/10.1016/j.cell.2020.01.008>.
- (214) Baell, J. B.; Holloway, G. A. New Substructure Filters for Removal of Pan Assay Interference Compounds (PAINS) from Screening Libraries and for Their Exclusion in Bioassays. *J. Med. Chem.* **2010**, *53* (7), 2719–2740. <https://doi.org/10.1021/jm901137j>.
- (215) Capuzzi, S. J.; Muratov, E. N.; Tropsha, A. Phantom PAINS: Problems with the Utility of Alerts for P an- A Ssay in Terference Compound S. *J. Chem. Inf. Model.* **2017**, *57* (3), 417–427. <https://doi.org/10.1021/acs.jcim.6b00465>.
- (216) Daina, A.; Michielin, O.; Zoete, V. SwissADME: A Free Web Tool to Evaluate Pharmacokinetics, Drug-Likeness and Medicinal Chemistry Friendliness of Small Molecules. *Sci. Rep.* **2017**, *7*. <https://doi.org/10.1038/srep42717>.
- (217) Shao, Z.; Yin, J.; Chapman, K.; Grzemska, M.; Clark, L.; Wang, J.; Rosenbaum, D. M. High-Resolution Crystal Structure of the Human CB1 Cannabinoid Receptor. *Nature* **2016**, *540* (7634), 602–606. <https://doi.org/10.1038/nature20613>.
- (218) Kotsikorou, E.; Navas, F.; Roche, M. J.; Gilliam, A. F.; Thomas, B. F.; Seltzman, H. H.; Kumar, P.; Song, Z.-H.; Hurst, D. P.; Lynch, D. L.; Reggio, P. H. The Importance of Hydrogen Bonding and Aromatic Stacking to the Affinity and Efficacy of Cannabinoid



- Receptor CB 2 Antagonist, 5-(4-Chloro-3-Methylphenyl)-1-[(4-Methylphenyl)Methyl]- N-[(1 S ,2 S ,4 R )-1,3,3-Trimethylbicyclo[2.2.1]Hept-2-Yl]-1H-Pyrazole. *J. Med. Chem.* **2013**, *56* (17), 6593–6612. <https://doi.org/10.1021/jm400070u>.
- (219) Lingerfelt, M. A.; Zhao, P.; Sharir, H. P.; Hurst, D. P.; Reggio, P. H.; Abood, M. E. Identification of Crucial Amino Acid Residues Involved in Agonist Signaling at the GPR55 Receptor. *Biochemistry* **2017**, *56* (3), 473–486. <https://doi.org/10.1021/acs.biochem.6b01013>.
- (220) Sotudeh, N.; Morales, P.; Hurst, D. P.; Lynch, D. L.; Reggio, P. H. Towards a Molecular Understanding of the Cannabinoid Related Orphan Receptor Gpr18: A Focus on Its Constitutive Activity. *Int. J. Mol. Sci.* **2019**, *20* (9). <https://doi.org/10.3390/ijms20092300>.
- (221) Pumroy, R. A.; Samanta, A.; Liu, Y.; Hughes, T.; Zhao, S.; Yudin, Y.; Rohacs, T.; Han, S.; Moiseenkova-Bell, V. Y. Molecular Mechanism of TRPV2 Channel Modulation by Cannabidiol. **2019**. <https://doi.org/10.7554/eLife.48792.001>.
- (222) Singh, A. K.; McGoldrick, L. L.; Sobolevsky, A. I. Structure and Gating Mechanism of the Transient Receptor Potential Channel TRPV3. *Nat. Struct. Mol. Biol.* **2018**, *25* (9), 805–813. <https://doi.org/10.1038/s41594-018-0108-7>.
- (223) Zubcevic, L.; Herzik, M. A.; Wu, M.; Borschel, W. F.; Hirschi, M.; Song, A. S.; Lander, G. C.; Lee, S. Y. Conformational Ensemble of the Human TRPV3 Ion Channel. *Nat. Commun.* **2018**, *9* (1). <https://doi.org/10.1038/s41467-018-07117-w>.
- (224) Suo, Y.; Wang, Z.; Zubcevic, L.; Hsu, A. L.; He, Q.; Borgia, M. J.; Ji, R. R.; Lee, S. Y. Structural Insights into Electrophile Irritant Sensing by the Human TRPA1 Channel. *Neuron* **2020**, *105* (5), 882-894.e5. <https://doi.org/10.1016/j.neuron.2019.11.023>.
- (225) Zhao, J.; Lin King, J. V.; Paulsen, C. E.; Cheng, Y.; Julius, D. Irritant-Evoked Activation and Calcium Modulation of the TRPA1 Receptor. *Nature* **2020**, *585* (7823), 141–145. <https://doi.org/10.1038/s41586-020-2480-9>.
- (226) Diver, M. M.; Cheng, Y.; Julius, D. Structural Insights into TRPM8 Inhibition and Desensitization. *Science (80-. )*. **2019**, *365* (6460), 1434–1440. <https://doi.org/10.1126/science.aax6672>.
- (227) Yin, Y.; Le, S. C.; Hsu, A. L.; Borgia, M. J.; Yang, H.; Lee, S. Y. Structural Basis of Cooling Agent and Lipid Sensing by the Cold-Activated TRPM8 Channel. *Science (80-. )*. **2019**, *363* (6430). <https://doi.org/10.1126/science.aav9334>.
- (228) Fernandez-Fernandez, B.; Ortiz, A.; Gomez-Guerrero, C.; Egido, J. Therapeutic Approaches to Diabetic Nephropathy - beyond the RAS. *Nature Reviews Nephrology*. Nature Publishing Group 2014, pp 325–346. <https://doi.org/10.1038/nrneph.2014.74>.

- (229) Malek, N.; Starowicz, K. Dual-Acting Compounds Targeting Endocannabinoid and Endovanilloid Systems—A Novel Treatment Option for Chronic Pain Management. *Front. Pharmacol.* **2016**, 7 (AUG). <https://doi.org/10.3389/fphar.2016.00257>.
- (230) Barutta, F.; Grimaldi, S.; Gambino, R.; Vemuri, K.; Makriyannis, A.; Annaratone, L.; Di Marzo, V.; Bruno, G.; Gruden, G. Dual Therapy Targeting the Endocannabinoid System Prevents Experimental Diabetic Nephropathy. *Nephrol. Dial. Transplant.* **2017**, 32 (10), 1655–1665. <https://doi.org/10.1093/ndt/gfx010>.
- (231) Lago-Fernandez, A.; Zarzo-Arias, S.; Jagerovic, N.; Morales, P. Relevance of Peroxisome Proliferator Activated Receptors in Multitarget Paradigm Associated with the Endocannabinoid System. *Int. J. Mol. Sci.* **2021**, 22 (3), 1001. <https://doi.org/10.3390/ijms22031001>.
- (232) Morales, P.; Jagerovic, N. Advances Towards The Discovery of GPR55 Ligands. *Curr. Med. Chem.* **2016**, 23. <https://doi.org/10.2174/0929867323666160425113836>.
- (233) Morales, P.; Lago-Fernandez, A.; Hurst, D. P.; Sotudeh, N.; Brailoiu, E.; Reggio, P. H.; Abood, M. E.; Jagerovic, N. Therapeutic Exploitation of GPR18: Beyond the Cannabinoids? *J. Med. Chem.* **2020**, 63 (23), 14216–14227. <https://doi.org/10.1021/acs.jmedchem.0c00926>.
- (234) Appendino, G.; Ligresti, A.; Minassi, A.; Cascio, M. G.; Allarà, M.; Tagliatela-Scafati, O.; Pertwee, R. G.; De Petrocellis, L.; Di Marzo, V. Conformationally Constrained Fatty Acid Ethanolamides as Cannabinoid and Vanilloid Receptor Probes. *J. Med. Chem.* **2009**, 52 (9), 3001–3009. <https://doi.org/10.1021/jm900130m>.
- (235) Melck, D.; Bisogno, T.; De Petrocellis, L.; Chuang, H. H.; Julius, D.; Bifulco, M.; Di Marzo, V. Unsaturated Long-Chain N-Acyl-Vanillyl-Amides (N-AVAMs): Vanilloid Receptor Ligands That Inhibit Anandamide-Facilitated Transport and Bind to CB1 Cannabinoid Receptors. *Biochem. Biophys. Res. Commun.* **1999**, 262 (1), 275–284. <https://doi.org/10.1006/bbrc.1999.1105>.
- (236) Szallasi, A.; Di Marzo, V. New Perspectives on Enigmatic Vanilloid Receptors. *Trends Neurosci.* **2000**, 23 (10), 491–497. [https://doi.org/10.1016/S0166-2236\(00\)01630-1](https://doi.org/10.1016/S0166-2236(00)01630-1).
- (237) Appendino, G.; Cascio, M. G.; Bacchiega, S.; Moriello, A. S.; Minassi, A.; Thomas, A.; Ross, R.; Pertwee, R.; De Petrocellis, L.; Di Marzo, V. First “Hybrid” Ligands of Vanilloid TRPV1 and Cannabinoid CB2 Receptors and Non-Polyunsaturated Fatty Acid-Derived CB2-Selective Ligands. *FEBS Lett.* **2006**, 580 (2), 568–574. <https://doi.org/10.1016/j.febslet.2005.12.069>.
- (238) De Petrocellis, L.; Ligresti, A.; Moriello, A. S.; Allarà, M.; Bisogno, T.; Petrosino, S.; Stott, C. G.; Di Marzo, V. Effects of Cannabinoids and Cannabinoid-Enriched Cannabis Extracts on TRP Channels and Endocannabinoid Metabolic Enzymes. *Br. J. Pharmacol.* **2011**, 163 (7), 1479–1494. <https://doi.org/10.1111/j.1476-5381.2010.01166.x>.

- (239) Zagzoog, A.; Mohamed, K. A.; Kim, H. J. J.; Kim, E. D.; Frank, C. S.; Black, T.; Jadhav, P. D.; Holbrook, L. A.; Laprairie, R. B. In Vitro and in Vivo Pharmacological Activity of Minor Cannabinoids Isolated from Cannabis Sativa. *Sci. Rep.* **2020**, *10* (1). <https://doi.org/10.1038/s41598-020-77175-y>.
- (240) Tham, M.; Yilmaz, O.; Alaverdashvili, M.; M Kelly, M. E.; Denovan-Wright, E. M.; Laprairie, R. B. Allosteric and Orthosteric Pharmacology of Cannabidiol and Cannabidiol-Dimethylheptyl at the Type 1 and Type 2 Cannabinoid Receptors. *Cannabinoid Res. Br. J. Pharmacol. Br. J. Pharmacol.* **2019**, *176*, 1455. <https://doi.org/10.1111/bph.v176.10/issuetoc>.
- (241) Martínez-Pinilla, E.; Varani, K.; Reyes-Resina, I.; Angelats, E.; Vincenzi, F.; Ferreiro-Vera, C.; Oyarzabal, J.; Canela, E. I.; Lanciego, J. L.; Nadal, X.; Navarro, G.; Borea, P. A.; Franco, R. Binding and Signaling Studies Disclose a Potential Allosteric Site for Cannabidiol in Cannabinoid CB2 Receptors. *Front. Pharmacol.* **2017**, *8* (OCT). <https://doi.org/10.3389/fphar.2017.00744>.
- (242) Navarro, G.; Gonzalez, A.; Sánchez-Morales, A.; Casajuana-Martin, N.; Gómez-Ventura, M.; Cordoní, A.; Busqué, F.; Alibés, R.; Pardo, L.; Franco, R. Design of Negative and Positive Allosteric Modulators of the Cannabinoid CB2 Receptor Derived from the Natural Product Cannabidiol. *J. Med. Chem.* **2021**, *64* (13), 9354–9364. <https://doi.org/10.1021/acs.jmedchem.1c00561>.
- (243) Hashiesh, H. M.; Sharma, C.; Goyal, S. N.; Jha, N. K.; Ojha, S. Pharmacological Properties, Therapeutic Potential and Molecular Mechanisms of JWH133, a CB2 Receptor-Selective Agonist. *Front. Pharmacol.* **2021**, *12*. <https://doi.org/10.3389/fphar.2021.702675>.
- (244) Muller, C.; Reggio, P. H. An Analysis of the Putative CBD Binding Site in the Ionotropic Cannabinoid Receptors. *Front. Cell. Neurosci.* **2020**, *14*. <https://doi.org/10.3389/fncel.2020.615811>.
- (245) Huffman, J. W.; Hepburn, S. A.; Lyutenko, N.; Thompson, A. L. S.; Wiley, J. L.; Selley, D. E.; Martin, B. R. 1-Bromo-3-(1',1'-Dimethylalkyl)-1-Deoxy- $\Delta^8$ -Tetrahydrocannabinols: New Selective Ligands for the Cannabinoid CB2 Receptor. *Bioorganic Med. Chem.* **2010**, *18* (22), 7809–7815. <https://doi.org/10.1016/j.bmc.2010.09.061>.
- (246) Liu, J.; Wang, X.; Xu, L.; Hao, Z.; Wang, L.; Xiao, J. One Step Synthesis of 2-Alkenylchromanes via Inverse Electron-Demand Hetero-Diels–Alder Reaction of o-Quinone Methide with Unactivated Dienes. *Tetrahedron* **2016**, *72* (47), 7642–7649. <https://doi.org/10.1016/j.tet.2016.10.027>.
- (247) Sime, J. T.; Ainsworth, A. T. Aminomethyl Chromans. US4303656A, 1981.

- (248) Habi, A.; Gravel, D.; Villeneuve, L.; Su, H.; Vaillancourt, M. Halogenated Rhodamine Derivatives and Applications Thereof. US-2003212126-A1, 2001.
- (249) Kazuhiro, Y. ( 12 ) Patent Application Publication ( 10 ) Pub . No .: US 2008 / 0225123 A1 Patent Application Publication, 2008.
- (250) Kim, K.; Heo, P.; Pak, C.; Choi, S. EP 2 595 229 B1, 2013.
- (251) Wang, S.; Chen, J.; Collins, G.; Levant, B. WO 2010/025235 A1: SELECTIVE LIGANDS FOR THE DOPAMINE 3 (D 3 ) RECEPTOR AND METHODS OF USING THE SAME, 2010.
- (252) Carter, J. S.; William, A. K.; Brown, D. L.; Deprow, A.; Fletcher, T.; Hallinan, E. A.; Hamper, B. C.; Huff, R.; Kiefer, J. R. J.; Koszyk, F.; Kramer, S.; Liao, S.; Limburg, D. C.; Ludwig, C.; McCall, J. M.; Springer, J. R.; Talley, J. J.; Wang, L. J.; Xing, L.; Yu, Y. Benzopyran Compounds Useful for Treating Inflammatory Conditions. WO2004087686A2, 2004.
- (253) Razdan, R. K.; Dalzell, H. C. Benzopyrans Having an Unsaturated Side Chain. US4036857A, 1976.
- (254) Karsten, Mäder; Verena Weiss, Jörg Kressler, T. N. Cannabinoid Composition and Products Including Alpha-Tocopherol. WO2019074959, 2019.
- (255) Ghalili, B.; McGovern, K. CA2995418A1: Topical Compositions Comprising Hydroxy Acids and Cannabinoids for Skincare.
- (256) Viet Thang Vu, M.; Thacker Jr, L. N.; O'Malley, D. R.; Ogishi, T. Multi-Use Cartridge for Ingestion of Cannabis-Based Products. US20190275268A1, 2019.
- (257) Yong-Gang, W.; Guan-Peng, Q.; Bo-Lin, L.; Giu-Zhuan, S.; Guo-Zhi, Z.; Yong-Hua, L.; Hong-Zhu, C.; Guo-Fei, Q. Phosphonium Derivative, Preparation Method and Use Thereof. TW-I668224-B, 2019.
- (258) Funahashi, M.; Ito, M.; Kawamura, H. Organic Electroluminescent Element. EP1811585A1, 2007.
- (259) Byers, P. M.; Alabugin, I. V. Polyaromatic Ribbons from Oligo-Alkynes via Selective Radical Cascade: Stitching Aromatic Rings with Polyacetylene Bridges. *J. Am. Chem. Soc.* **2012**, *134* (23), 9609–9614. <https://doi.org/10.1021/ja3023626>.
- (260) Alabugin, I. V.; Byers, P. M. US 2013/0109855 A1: Electrophile-Induced Cyclization Cyclodehydrogenation of Polyphenylenes, 2013.
- (261) Winn, M. Heterocyclic Esters of Alkylphenyl Benzopyrans. CA1038383A, 1974.

- (262) Koji, M.; Hiroyasu, O. New 4,4''-Substituted Oxy-p-Terphenyl Compounds. JP2005145820A, 2005.
- (263) Ying-Ji, W.; Bo-Yuan, C. Preparation Method for 2-Substituted 3-Arylmethylbenzofuran. TW201339145A, 2013.
- (264) McPartland, J. M.; Glass, M.; Pertwee, R. G. Meta-Analysis of Cannabinoid Ligand Binding Affinity and Receptor Distribution: Interspecies Differences. *Br. J. Pharmacol.* **2007**, *152* (5), 583–593. <https://doi.org/10.1038/sj.bjp.0707399>.
- (265) Osman, N. A.; Mahmoud, A. H.; Allar, M.; Niess, R.; Abouzid, K. A.; Marzo, V. Di; Abadi, A. H. Synthesis, Binding Studies and Molecular Modeling of Novel Cannabinoid Receptor Ligands. *Bioorganic Med. Chem.* **2010**, *18* (24), 8463–8477. <https://doi.org/10.1016/j.bmc.2010.10.050>.
- (266) Saari, R.; Törmä, J. C.; Nevalainen, T. Microwave-Assisted Synthesis of Quinoline, Isoquinoline, Quinoxaline and Quinazoline Derivatives as CB2 Receptor Agonists. *Bioorganic Med. Chem.* **2011**, *19* (2), 939–950. <https://doi.org/10.1016/j.bmc.2010.11.059>.
- (267) Nanda, K. K.; Henze, D. A.; Della Penna, K.; Desai, R.; Leidl, M.; Lemaire, W.; White, R. B.; Yeh, S.; Brouillette, J. N.; Hartman, G. D.; Bilodeau, M. T.; Trotter, B. W. Benzimidazole CB2 Agonists: Design, Synthesis and SAR. *Bioorganic Med. Chem. Lett.* **2014**, *24* (4), 1218–1221. <https://doi.org/10.1016/j.bmcl.2013.12.068>.
- (268) Brown, D. C. Resiniferatoxin: The Evolution of the “Molecular Scalpel” for Chronic Pain Relief. *Pharmaceuticals* **2016**, *9* (3), 1–11. <https://doi.org/10.3390/ph9030047>.
- (269) Gianella-Borradori, M.; Christou, I.; Bataille, C. J. R.; Cross, R. L.; Wynne, G. M.; Greaves, D. R.; Russell, A. J. Ligand-Based Virtual Screening Identifies a Family of Selective Cannabinoid Receptor 2 Agonists. *Bioorganic Med. Chem.* **2015**, *23* (1), 241–263. <https://doi.org/10.1016/j.bmc.2014.11.002>.
- (270) Muller, C.; Lynch, D. L.; Hurst, D. P.; Reggio, P. H. TRPV1 Activation by Anandamide via a Unique Lipid Pathway. *J. Chem. Inf. Model.* **2021**, *61* (12), 5742–5746. <https://doi.org/10.1021/acs.jcim.1c00893>.
- (271) Pharmaceuticals, E. H. *Evaluation of Safety, Tolerability and Preliminary Efficacy of EHP-101 in Relapsing Forms of Multiple Sclerosis*; 2021.
- (272) Palomares, B.; Ruiz-Pino, F.; Navarrete, C.; Velasco, I.; Sánchez-Garrido, M. A.; Jimenez-Jimenez, C.; Pavicic, C.; Vazquez, M. J.; Appendino, G.; Bellido, M. L.; Calzado, M. A.; Tena-Sempere, M.; Muñoz, E. VCE-004.8, A Multitarget Cannabinoquinone, Attenuates Adipogenesis and Prevents Diet-Induced Obesity. *Sci. Rep.* **2018**, *8* (1). <https://doi.org/10.1038/s41598-018-34259-0>.

- (273) Hanuš, L.; Breuer, A.; Tchilibon, S.; Shiloah, S.; Goldenberg, D.; Horowitz, M.; Pertwee, R. G.; Ross, R. A.; Mechoulam, R.; Fride, E. HU-308: A Specific Agonist for CB2, a Peripheral Cannabinoid Receptor. *Proc. Natl. Acad. Sci. U. S. A.* **1999**, *96* (25), 14228–14233. <https://doi.org/10.1073/pnas.96.25.14228>.
- (274) Shao, Z.; Yin, J.; Chapman, K.; Grzemska, M.; Clark, L.; Wang, J.; Rosenbaum, D. M. High-Resolution Crystal Structure of the Human CB1 Cannabinoid Receptor. *Nature* **2016**, *540* (7634), 602–606. <https://doi.org/10.1038/nature20613>.
- (275) Kotsikorou, E.; Sharir, H.; Shore, D.; Hurst, D. P.; Lynch, D. L.; Madrigal, K. E.; Heynen-Genel, S.; Milan, L. B.; Chung, T. D. Y.; Seltzman, H. H.; Bai, Y.; Caron, M. G.; Barak, L.; Croatt, M. P.; Abood, M. E.; Reggio, P. H. Identification of the GPR55 Antagonist Binding Site Using a Novel Set of High-Potency GPR55 Selective Ligands. *Biochemistry* **2013**, *52*, 9456–9469.
- (276) Jagerovic, N.; Lago-Fernandez, A.; Morales, P.; Abood, M. E.; Brailoiu, E.; Leo, L. M.; Zhao, P.; Reggio, P. H.; Hurst, D. P.; Chafi, N. Pyrazolylbenzene-1,3-Diols for Diseases Associated with G Protein-Coupled Receptor 18 and in Combination with Transient Receptor Potential Vanilloid 1. European Patent Application EP20382324. Apr 22, 2020, 2020.
- (277) Rempel, V.; Atzler, K.; Behrenswerth, A.; Karcz, T.; Schoeder, C.; Hinz, S.; Kaleta, M.; Thimm, D.; Kiec-Kononowicz, K.; Müller, C. E. Bicyclic Imidazole-4-One Derivatives: A New Class of Antagonists for the Orphan G Protein-Coupled Receptors GPR18 and GPR55. *Medchemcomm* **2014**, *5* (5), 632–649. <https://doi.org/10.1039/c3md00394a>.